UNIVERSITY OF HAWAII
LIBRARY
MAY 29 '61

The Philosophical Magazine

FIRST PUBLISHED IN 1798

A Journal of Theoretical Experimental and Applied Physics

Vol. 6 March 1961 No. 63
Eighth Series

25s. 0d., plus postage
Annual Subscription £13 10s. 0d., payable in advance

Printed and Published by
TAYLOR & FRANCIS LTD
RED LION COURT, FLEET STREET, LONDON, E.C.4

THE PHILOSOPHICAL MAGAZINE

Editor

Professor N. F. MOTT, M.A., D.Sc., F.R.S.

Editorial Board

Sir LAWRENCE BRAGG, O.B.E., M.C., M.A., D.Sc., F.R.S.

Sir GEORGE THOMSON, M.A., D.Sc., F.R.S.

Professor A. M. TYNDALL, C.B.E., D.Sc., F.R.S.

AUTHORS wishing to submit papers for publication in the Journal should send manuscripts directly to the Publishers.

Manuscripts should be typed in *double* spacing on one side of quarto (8×10 in.) paper, and authors are urged to aim at absolute clarity of meaning and an attractive presentation of their texts.

References should be listed at the end in alphabetical order of authors and should be cited in the text in terms of author's name and date. Diagrams should normally be in Indian ink on white card, with lettering in soft pencil, the captions being typed on a separate sheet.

A leaflet giving detailed instructions to authors on the preparation of papers is available on request from the Publishers.

Authors are entitled to receive 25 offprints of a paper in the Journal free of charge, and additional offprints can be obtained from the Publishers.

The *Philosophical Magazine* and its companion journal, *Advances in Physics*, will accept papers for publication in experimental and theoretical physics. The *Philosophical Magazine* publishes contributions describing new results, letters to the editor and book reviews. *Advances in Physics* publishes articles surveying the present state of knowledge in any branch of the science in which recent progress has been made. The editors welcome contributions from overseas as well as from the United Kingdom, and papers may be published in English, French and German.

The Theory of Transition-Metal Ions

J. S. GRIFFITH

An account of the theory of the physical properties of the ions of metals having partially filled *d* shells in their compounds. For mathematical and theoretical chemists and a reference book for inorganic and physical chemists, biochemists and experimental physicists. 95*s. net*

Radio Waves in the Ionosphere

K. G. BUDDEN

This book gives the full mathematical theory of the propagation of radio waves in the ionosphere and their reflection from it. A reference work for engineers and a text-book for final-year students.

566 *pages.* 95*s. net*

CAMBRIDGE UNIVERSITY PRESS

Immediate and Low Level Effects of Ionizing Radiations

Edited by A. A. Buzzati-Traverso

Proceedings of The Symposium held at Venice in June 1959 under the joint sponsorship of U.N.E.S.C.O., I.A.E.A. and C.N.R.N. and published as a supplement to the International Journal of Radiation Biology

The effects of low level radiation, from a biological point of view, have received relatively little attention during many meetings on radiobiology held in the past years. The subject, however, appears of primary significance at this time, in view of the widespread use of radiation sources for scientific, medical, industrial and military purposes. For this reason a symposium exclusively devoted to the subject was called for. Thanks to the financial support of U.N.E.S.C.O., I.A.E.A. and the Italian Atomic Energy Agency (C.N.R.N.) and the hospitality of the Fondazione Giorgio Cini, Z. M. Bacq (Belgium), E. Boeri (Italy), A. A. Buzzati-Traverso (Italy) and A. Hollaender (U.S.A.) organized an international symposium on " The Immediate and Low Level Effects of Ionizing Radiations " which has been held at Venice in June 1959. The meeting was attended by some 120 specialists from many countries.

Price—£2 15*s.* 0*d.* ($8.00) plus postage

Printed and Published by

TAYLOR & FRANCIS LTD

RED LION COURT, FLEET STREET, LONDON, E.C.4

REVISED CHEAPER EDITION FOR LIBRARIES AND SCHOOLS

A History of Mathematics

From antiquity to the early nineteenth century

By J. F. SCOTT, B.A., D.Sc., Ph.D.

Vice-Principal of St. Mary's College, Strawberry Hill, Twickenham, Middlesex

Author of *The Scientific Work of René Descartes* (1596–1650), *Mathematical Work of John Wallis, D.D., F.R.S.* (1616–1703), and other works

CONTENTS: Mathematics in Antiquity—Greek Mathematics—The Invention of Trigonometry—Decline of Alexandrian Science and the Revival in Europe—Mathematics in the Orient—Progress of Mathematics during the Renaissance—New Methods in Geometry—The Rise of Mechanics—The Invention of Decimal Fractions and of Logarithms—Newton and the Calculus—Taylor and Maclaurin, the Bernoullis and Euler, Related Advances—The Calculus of Variations, Probability, Projective Geometry, Non-Euclidean Geometry—Theory of Numbers—Lagrange, Legendre, Laplace, Gauss. This volume is intended primarily to help students who desire to have a knowledge of the development of the subject but who have too little leisure to consult works and documents. The author has availed himself of the facilities afforded by the Royal Society and other learned Societies to reproduce extracts from manuscripts and many scarce works.

Size $9\frac{3}{4}'' \times 6\frac{3}{4}''$. 266 pp. **Price 27s. 6d.** plus postage and packing 2*s.* 0*d.*

Some Reviews of the First Edition

" The invention of trigonometry, decimal fractions, logarithms and the calculus are each discussed clearly and concisely. The book is easy to read for anybody who knows the elements of mathematics and, although not free from minor errors, can be strongly recommended."—*British Book News*, April 1958.

" Physicists will find that the development in applied mathematics are clearly set out, from ancient times, through that of Archimedes, to the mechanics of the sixteenth century when interest was revived. Significant advances made by Stevin, Galileo, Descartes, Huygens and others are stressed, and help the reader to appreciate what Newton achieved. There are useful appendices giving brief biographical notes on mathematical topics and terminology, followed by a bibliography."—*Proceedings of The Physical Society*, September 1958.

" . . . it has been written with clarity and balance, and the excellent printing helps to make it a pleasure to read."—*The Times Educational Supplement*, 21 March 1958.

" . . . his (Dr. Scott's) wide knowledge of the material, his careful description of methods combine to provide an account which at times gives a sense of the excitement of discovery."—*Nature*, 26 July 1958.

" The printers and publishers are to be congratulated upon having produced such an attractive volume, ... We feel sure the book will be received with delight by all those interested in mathematical histories."—*BEAMA Journal*, August 1958.

" The work comes to life mainly because of his admirable use of the writings of mathematicians themselves, which vividly illustrates the great difficulties under which many of them laboured. This is not a book for the layman but both the student and anyone to whom figures are a fascination, will find the subject clearly and pleasantly presented."—*Technical Bookguide*, March 1958.

Printed and Published by

TAYLOR & FRANCIS LTD

RED LION COURT, FLEET STREET, LONDON, E.C.4

The Distribution of Deformation in Lead Fatigued *in vacuo*†

By K. U. Snowden‡
The Baillieu Laboratory, University of Melbourne, Victoria, Australia

[Received July 27, 1960 ; and in revised form October 20, 1960]

Abstract

Observations have been made on the nature of the deformation, hardening, and recrystallization in polycrystalline specimens of high-purity lead fatigued in reverse-plane bending *in vacuo* (approx. 5×10^{-3} or 2×10^{-6} mm Hg).

Fatigue straining induced slip, and grain boundaries to migrate to more stable positions at ± 45 degrees to the principal stress axis.

The early distribution of slip-trace angles was in good agreement with the angular distribution which Hedgepeth (1952) predicted on a basis of the maximum shear stress criterion and by neglecting the slip and grain-boundary interaction. Evidence for this latter interaction was found as hard zones up to 100 microns wide near grain boundaries. These zones were the sites for recrystallization and grain growth.

§ 1. Introduction

The fatigue strengths of a number of metals have long been known to be affected by the presence of the atmosphere during cyclic straining (Haigh and Jones 1930, Gough and Sopwith 1932, 1935). More recently, in postulating and evaluating theories of fatigue in terms of fundamental concepts, such as dislocations and lattice defects, it has become important to separate the part played by the alternating strain from that by the attack of atmospheric gases. Moreover, Wood (1959), and Segal and Partridge (1959) have shown that the difference between unidirectional and fatigue deformation becomes more distinct at small alternating strains, and Wood considers that it is the deformation at small alternating strains which is typical of fatigue damage. It therefore seems likely that under these conditions of strain with the associated long life, the attack by atmospheric gases may have sufficient time to contribute significantly to the fatigue damage.

Recent investigators have examined the effect of atmosphere on fatigue life and deformation (Thompson *et al.* 1956, Wadsworth and Hutchings 1958, Snowden and Greenwood 1958 b, and Hempel 1959). These have shown that the lives of copper, aluminium and lead are affected by the presence of the atmosphere whereas the lives of gold and steel are not. The observations on copper and aluminium suggest that the initial crack formation is much the same in air as in vacuum but that the rate of crack growth is accelerated by the presence of the atmosphere. On the other

† Communicated by Professor J. Neill Greenwood.
‡ On the staff of the Broken Hill Associated Smelters Pty. Ltd.

hand, the early observations of Gough and Sopwith (1935) indicate that the manner of fatigue failure of lead in air is different from that in vacuum. These observations are supported by more recent work (Snowden and Greenwood 1958 b) which shows that lead fatigued in vacuum (about 5×10^{-3} mm Hg) is more severely distorted than lead fatigued in air for the same number of cycles.

High-purity lead specimens have been fatigued at an air pressure of either $\approx 5 \times 10^{-3}$ or $\approx 2 \times 10^{-6}$ mm Hg, and the nature of the deformation and hardening is examined in more detail below. It has been shown (Snowden 1959, 1961) that at about 5×10^{-3} mm Hg, the fatigue deformation and life of lead at 500 cycles per min is no longer affected by further reduction of air pressure. The observed changes are therefore thought to be due almost entirely to the alternating strain. It is hoped to publish observations on the influence of air pressure on fatigue life at a later date.

§ 2. Experimental Method

Specimens of the shape shown in fig. 1 were tested in a reverse-plane bending machine at the rate of 500 cycles per min. The specimens were prepared from lead strip (99·999% pure), 0·160 in. thick, rolled from rectangular ingots $1 \times 1 \times 9$ in. cast at 400°C. Prior to fatigue, specimens were cleaned with benzene, placed on flat steel plates, annealed in air at 100°C for 24 hrs, and chemically polished in a 70 : 30 mixture of glacial acetic acid hydrogen peroxide (Worner and Worner 1940). The specimen shape was designed to produce a uniform macroscopic strain over the test length, which is indicated by the shaded area in fig. 1.

Fig. 1

Specimen shape.

For the present observations, specimens were fatigued either at 'high' or 'low' alternating strains which were arbitrarily chosen as: $\leqslant 0{\cdot}140\%$ to $\geqslant 0{\cdot}075\%$ for the high strains and 0·034% for the low strain. The endurance corresponding to these strains was from $1{\cdot}50 \times 10^6$ to 25×10^6 cycles, and $\geqslant 2 \times 10^7$ cycles respectively.

§ 3. Experimental Results

3.1. *Grain-boundary Migration and Slip Formation*

As described in a previous paper (Snowden 1958), the initial effect of the alternating strain was shown by the appearance of slip traces and grain-boundary migration. The rate of migration increased with

increasing strain and was highest in the early part of the life, i.e. in the first 10^4 to 10^5 cycles. At the low strain, figs. 4 and 5, the grain structure tended to stabilize, except for the sporadic migration mentioned below. Boundary displacements of one or two hundred microns, such as those shown in fig. 4, were found to be common. However, some boundaries including coherent twin boundaries, did not move.

A striking feature of the migration at both high and low strains was that boundaries tended to migrate to positions at ± 45 degrees to the specimen axis (figs. 4 and 5) as in lead fatigued in air (Snowden and Greenwood 1958 a). However, in specimens fatigued in vacuum there was no sign of the intercrystalline cracks that formed in the specimens fatigued in air. This type of boundary migration resulted in the formation of an orthogonal grain structure which was better developed at the higher strains, fig. 2†.

Fig. 3

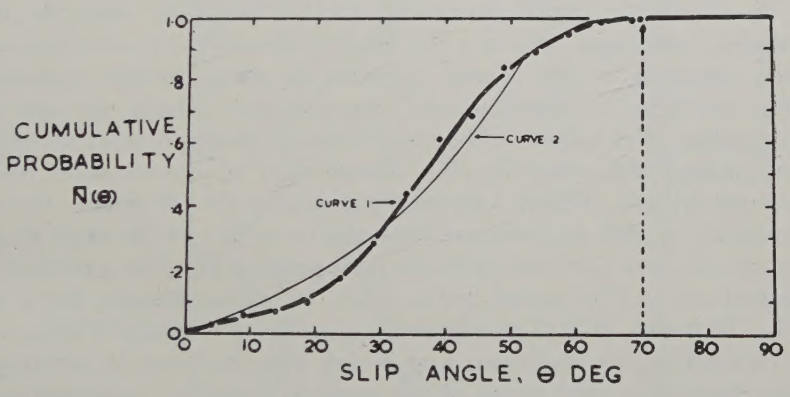

Theoretical and experimental slip-angle distribution for a specimen fatigued to 10^5 cycles at a strain of $\pm 0{\cdot}092\%$. Theoretical distribution, curve 2, after Hedgepeth (1952).

In view of the above tendency for boundaries to align themselves at ± 45 degrees to the specimen axis, the angular distribution of slip traces was examined to see if a similar relation existed for slip. The angular distribution of 289 traces was determined on the surface of a specimen fatigued to 10^5 cycles at a strain of $\pm 0{\cdot}092\%$. The result is shown in fig. 3, curve 1, in the form of a cumulative frequency diagram plotted at 5 degree intervals. The ordinate $\overline{N}(\theta)$ is the sum of frequencies of angles up to and including a given angle θ, where θ is the angle between the slip trace and the transverse specimen axis. The curve shows that approximately 65% of traces made angles between 30 and 60 degrees with the transverse axis of the specimen. This suggests that there is a tendency

† Figures 2, 4, 5, 6, 7, 8, 10 and 11 are shown as plates.

for traces to occur at angles near the ± 45 degree positions although the trend is not as clear-cut as that shown by the boundaries at the higher strains.

A further feature of curve 1 is that no slip traces were found which made angles greater than 70 degrees with the transverse axis of the specimen. This feature and the shape of curve 1 are in accord with the theoretical slip-angle distribution, curve 2, which Hedgepeth (1952) predicted for unidirectional straining on the basis of the maximum shear-stress criterion and by neglecting slip and grain-boundary interaction. The agreement suggests that the crystal aggregate deforms initially as if each crystal were free to deform independently of the other crystals. However, Taylor (1938) and others have pointed out that, for unidirectional deformation (at high strain rates and normal temperature), grains remain continuous at the boundary with their neighbours during deformation, i.e. there is an absence of cavities. Evidence for this latter restriction in fatigue at the low strain is provided by the series of micrographs shown in figs. 4 to 6, in which the initial slip distribution is modified near the grain boundaries, although the slip systems (indicated by double-headed arrows) operating in the central portions of grains remain unchanged. In order to bring out the structural changes more clearly, the specimen was repolished after various amounts of fatigue, thereby removing previous fatigue traces and observing the distribution of deformation due to subsequent fatigue. Figure 4 shows the area after 5×10^4 cycles. Previous observations on this area showed that the boundary of the central grain had migrated from the trace A to the final position B. The specimen was repolished at $7{\cdot}5 \times 10^5$ cycles, given $4{\cdot}55 \times 10^6$ cycles further, i.e. a total of $5{\cdot}3 \times 10^6$ cycles, and photographed again, fig. 5. Figure 5 shows that after repolishing, the deformed area which was produced by subsequent fatigue, tended to stop short of the grain boundaries. Approximately 80% of boundaries showed zones of low slip density of up to 100 or so microns wide. The slip density in the boundary zones tended to increase slightly with increasing number of cycles; however, after an intermediate polish at $5{\cdot}3 \times 10^6$ cycles and further fatigue the zones reformed and tended to be wider than before repolishing. This can be seen by comparing figs. 5 and 6.

Finally, examination of the area at 8×10^6 cycles showed that the zones of low-slip density underwent deformation on a new slip system not previously evident in the adjoining grains, fig. 7. This behaviour was the result of local recrystallization which produced a new grain along the original grain-boundary zones. The strip of new material readily deformed and built up its own zones of low-slip density as was shown by repolishing and further fatigue, fig. 8. The relative positions of boundaries before and after recrystallization are illustrated in fig. 9 which shows that the new grain in fig. 8 straddled the original orthogonal grain boundary.

Although the zones of low-slip density showed a steady development at low strains, the onset of localized recrystallization occurred spontaneously and irregularly after lengthy periods of cyclic straining. At the

higher strains, however, similar structural instability near grain boundaries was detected earlier and at a strain of $\pm 0{\cdot}092\%$ was even found during the initial period of rapid grain-boundary migration, i.e. in the first 10^4 to 10^5 cycles. An example of this is shown in figs. 10 and 11 in which the migrating boundary moved from positions A to B between 10^3 and 2×10^4 cycles. In this case the specimen was not given intermediate polishes.

Fig. 9

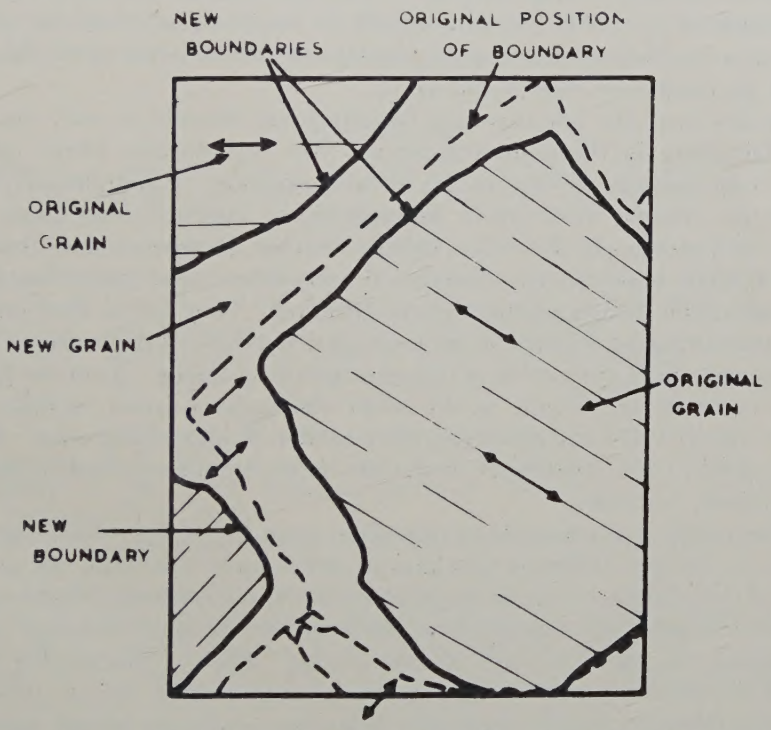

Diagram shows position of recrystallized grain (figs. 7 and 8) with respect to original grain boundary.

Recent observations by de Fouquet (1958) have suggested that an analogous process of grain growth along the intergranular regions may occur during the fatigue of iron in argon at 700°C. This kind of effect has also been found under other conditions of stressing by Brinson and Hargreaves (1958).

§ 4. Discussion

The observations described above throw some light on the nature of the slip deformation and of the process of work-hardening near grain boundaries in fatigue. The early stages of the deformation suggest that dislocations are set in motion on octahedral planes of high resolved shear stress, i.e. on the so-called 'natural' systems (Hargreaves 1956), as in unidirectional straining. During the first half cycle, some of these dislocations would

interact with grain boundaries and form pile-ups there or be transmitted to adjoining grains according to the orientation difference. However, if interactions were limited to simple pile-ups, then during stress reversal these dislocations would tend to run back on their glide plane so that the hardening would be dispersed after each half cycle. Evidence for this type of reversed movement during a partly-reversed stress cycle has been found by Takamura and Mura (1958) in the case of an α-brass bicrystal. Nevertheless, the present results indicate that when the strain is cycled for a large number of times, some of the boundary hardness, as indicated by the decreased tendency of the boundary zone to undergo slip after repolishing and fatigue, persists and in fact tends to extend away from the boundary (figs. 5 and 6).

In this case, the pile-ups at a boundary are thought to activate, near the boundary in the adjoining grain, extra slip systems which interact and form barriers to slip on the natural systems. Examples of slip on multiple systems near grain boundaries in fatigued lead have been described previously (Snowden 1958). Further, Berghezan and Fourdeux (1959) have observed the dislocation interaction near grain boundaries in aluminium during unidirectional straining. They found that multiple slip operated and resulted in an entangled network of dislocations which contained a high proportion of jogged screw dislocations. A similar process may occur during fatigue as the latter dislocations would be difficult to move (Read 1953) and could therefore harden the boundary zone. Gough *et al.* (1923, 1934, 1936) have observed similar boundary zones in fatigued aluminium and steel.

The initial grain-boundary migration may be explained on the basis that, in general, different amounts of deformation are built up on each side of boundaries so that, as Forsyth (1953–54) and Lücke and Detert (1957) have proposed, the migration is produced by unequal numbers of dislocations on opposite sides of boundaries. Such a mechanism would indicate that the diminished rate of migration after 10^4 to 10^5 cycles results from an almost complete balancing of forces across migrating boundaries. A further possible reason for the diminished rate is suggested by the tendency for boundaries to align themselves in the directions of maximum shear stress. This suggests that the diminished rate is associated with enhanced grain-boundary sliding at orientations in the shear directions, i.e. at ± 45 degrees to the specimen axis.

The observed features of the boundary zones and the intergranular grain growth are in accord with the model for recrystallization of a cold-worked metal proposed by Gay *et al.* (1954). In this model the onset of recrystallization is associated with the tilting in excess of a limiting angle of a 'particle' in a region of high dislocation density. The present results suggest that the tilting process, which evidently occurs more rapidly at high strains (figs. 10 and 11), takes place in the heavily strained boundary regions where the driving force for growth would be provided by absorption of the disoriented material.

Acknowledgments

This work forms part of the programme of research on the properties of lead being carried on by the Broken Hill Associated Smelters in the Baillieu Laboratory, University of Melbourne. The work is being done under the direction of Professor J. Neill Greenwood to whom thanks are due for many valuable discussions. The author wishes to thank Mr. R. J. Hopkins and Mr. R. S. Russell of the Broken Hill Associated Smelters for their interest and encouragement. The author is also indebted to Mr. R. C. Gifkins and colleagues in the Baillieu Laboratory and in the Research Division of the Broken Hill Associated Smelters Pty. Ltd. for many stimulating discussions.

References

Berghezan, A., and Fourdeux, A., 1959, *J. appl. Phys.*, **30,** 1913.
Brinson, G., and Hargreaves, M. E., 1958, *J. Inst. Met.*, **87,** 112.
De Fouquet, J., 1958, *Rev. Métall.*, **55,** 1133.
Forsyth, P. J. E., 1953–54, *J. Inst. Met.*, **82,** 449.
Gay, P., Hirsch, P. B., and Kelly, A., 1954, *Acta cryst., Camb.*, **7,** 41.
Gough, H. J., Cox, H. L., and Sopwith, D. G., 1934, *J. Inst. Met.*, **54,** 193.
Gough, H. J., and Forrest, G., 1936, *J. Inst. Met.*, **58,** 97.
Gough, H. J., and Hanson, D., 1923, *Proc. roy. Soc.* A, **104,** 539.
Gough, H. J., and Sopwith, D. G., 1932, *J. Inst. Met.*, **49,** 93; 1935, *Ibid.*, **56**. 55.
Haigh, B. P., and Jones, B., 1930, *J. Inst. Met.*, **43,** 271.
Hargreaves, M. E., 1956, *J. Aust. Inst. Met.*, **1,** 125.
Hedgepeth, J. M., 1952, National Advisory Committee for Aeronautics Technical Note 2777.
Hempel, M. R., 1959, *Conference on Fracture* (New York : Technology Press of M.I.T. and John Wiley & Sons, Inc.), p. 376.
Lücke, K., and Detert, K., 1957, *Acta Met.*, **5,** 628.
Read, W. T., 1953, *Dislocations in Crystals* (New York : McGraw-Hill), p. 80.
Segall, R. L., and Partridge, P. G., 1959, *Phil. Mag.*, **4,** 912.
Snowden, K. U., 1958, *Phil. Mag.*, **3,** 1411 ; 1959, Ph.D. Thesis, Melbourne University ; 1961, *Nature, Lond.*, **189**, 53.
Snowden, K. U., and Greenwood, J. N., 1958 a, *Trans. Amer. Inst. min. (metall.) Engrs*, **212,** 91 ; 1958 b, *Ibid.*, **212,** 626.
Takamura, Jin-Ichi, and Mura, Sei, 1958, *J. phys. Soc. Japan*, **13,** 1421.
Taylor, G. I., 1938, *Stephen Timoshenko 60th Anniversary Volume* (New York : Macmillan Co.), p. 218.
Thompson, N., Wadsworth, N. J., and Louat, N., 1956, *Phil. Mag.*, **1,** 113.
Wadsworth, N. J., and Hutchings, J., 1958, *Phil. Mag.*, **3,** 1154.
Wood, W. A., 1959, *Conference on Fracture* (New York : Technology Press of M.I.T. and John Wiley & Sons, Inc.), p. 412.
Worner, H. K., and Worner, H. W., 1940, *J. Inst. Met.*, **66**, 45.

Some New Habit Features in Crystals of Long Chain Compounds† Part I. Paraffins

By A. Keller
H. H. Wills Physics Laboratory, University of Bristol, Bristol, 8

[Received July 20, 1960]

Abstract

Habits of paraffin crystals were examined with the optical and electron microscope. In particular striations along different crystallographic directions were noticed which could be produced systematically by heat treatment. It was found that such striations often corresponded to geometrically regular ridges. It is proposed that these ridges represent different phases within the crystals corresponding to structures of differing obliquities all based on the same subcell. Accordingly a variety of structures can be realized within the same crystal by different amounts of simple shear on different planes along the **c** direction where the shear, while regular, need not be uniform. A number of other less regular morphological features are also described.

§ 1. Introduction

Crystals of paraffins have been studied extensively in the past by various methods (e.g. Müller 1927, Dawson and Vand 1951, Teare 1959). Our own interest in these crystals originates from the recently discovered similarity between the crystal habits of paraffins and polymers, polyethylene in particular (Keller 1959). Accordingly, crystals of polyethylene and those of paraffins can have identical habits. Further research on polyethylene crystals has revealed a number of additional morphological details. In view of the hitherto unsuspected close connection between paraffins and polymers it has become important to separate those features which can be explained on the basis of the crystallography of paraffins, from those where the long chain nature of the polymers has to be specifically invoked. Consequently, the question arises how far the more detailed morphological features in polymer crystals have corresponding counterparts in paraffins. In particular, we were interested in the origin of certain striations which frequently appeared in polymer single crystals. These were very elusive and there appeared to be little hope to clarify their nature by the continued study of polymers only. Therefore we turned to paraffins where evidence of similar morphological effects was found which appeared more readily interpretable. The present paper will deal with these investigations on paraffins, at this

† Communicated by Professor F. C. Frank, F.R.S.

stage with the morphological aspects, although it is hoped that these investigations will be supplemented later with diffraction results. In the following paper of this series the results obtained with paraffins will be utilized in the elucidation of morphological features in polymers.

§ 2. Experimental

2.1. *Materials and Techniques*

The majority of the investigations were carried out on $n C_{36}H_{74}$. All the figures and illustrations in the present publication refer to this latter paraffin except one photograph (fig. 9†) which is of $n C_{30}H_{62}$. The phenomena under discussion, however, are quite general and were found to occur also in all the other normal paraffins, namely, $C_{29}H_{61}$, $C_{30}H_{62}$, $C_{31}H_{69}$, $C_{32}H_{66}$, $C_{34}H_{70}$, handled by us in the course of this work. The paraffins were dissolved in low boiling petroleum ether (b.p. 40–60°c) or occasionally in benzene. On prolonged standing, or on cooling the originally warmed up solution, crystals precipitated forming a suspension.

The crystals were deposited on a microscope slide by evaporation of the solvent and examined first by the optical microscope. Most of the crystals of interest for this work were thin enough to profit from phase contrast illumination. All optical microscopy was restricted to the powers of dry objectives as the crystals could not be immersed in a mounting medium.

The crystals, selected under the optical microscope, could also be examined with the electron microscope either by precipitating them originally on a slide coated with carbon, or by carbon coating the crystals subsequently. If diffraction patterns were required or effects due to diffraction (Bragg fringes, etc.) were to be examined in the image, very weak beam intensities had to be used in order to minimize the effect of the beam. We found that the beam destroyed the crystallinity without affecting the crystal shapes, an effect which has already been known in the case of polythene (Agar *et al.* 1959). This restricts the working to lowest powers, unless the double condenser technique can be applied (see reference above), which was not possible on the instrument available for this work.

Transmission electron microscopy was only possible on the thinnest crystals. In the case of thicker crystals replication techniques had to be resorted to. For this purpose the crystals were first metal shadowed, coated with a moderately thick layer of carbon and the films were floated off in water and picked up on grids. By bringing the films in contact with xylene the paraffins were dissolved and the replicas were ready for examination.

In most cases the crystals were heat treated for these studies. This was done by placing the microscope slide with the crystals on them on a temperature gradient bar. The seemingly irreversible changes happening

† Figures 1–13 are shown as plates.

at different temperatures could be examined subsequently after the removal of the slide from the bar. The changes on heating could also be followed *in situ* with the help of a hot stage, both under the optical and electron microscope. Hot stage work in the electron microscope was necessarily restricted to transmission, hence to the thinnest crystals. Even so, it was made very difficult by the beam damage which was more severe at the elevated temperatures.

2.2. *Observations*

The crystals were the usual lozenge-shaped tablets ranging from macroscopic dimensions (1 mm or more) to a few microns). As already stated, some crystals grew while in suspension on standing or cooling. Further crystals formed when the solvent evaporated on the slide. The crystals grown in suspension were usually larger than the ones formed on evaporation. The acute angles of the lozenges could be either in the range of 75° or 67°. The former corresponds to the monoclinic, the latter to the orthorhombic variety (Dawson and Vand 1951, Schearer and Vand 1956, Teare 1959). Crystals of $C_{36}H_{74}$ grown from benzene were always monoclinic while both orthorhombic and monoclinic crystals were obtained from petroleum ether which was the most frequently used mode of preparation for this work. It was found in the course of a systematic study of habits carried out by Baltá-Calleja in this laboratory (details to be reported later) that the crystals which grew while in suspension were always monoclinic while those which formed on evaporation were orthorhombic, consequently the two could be separated by filtration. Besides regular lozenges many other habit modifications like twins, dendrites, lath-shaped crystals, etc., could be observed, many of which have been reported in the literature earlier and will not be itemized any further here.

Electron microscope examinations revealed that the crystals thickened through spiral terraces indicative of the screw dislocation mechanism in line with earlier findings (Dawson and Vand 1951). It may be noteworthy to point out that all transmission electron microscopy so far has been carried out on specimens, the crystallinity of which was destroyed by the electron beam. Whenever the damage could be avoided, by means already referred to, a variety of extinction effects were obtained in the image. Figure 1 shows one example. The crystals in this photograph being unshadowed, would have appeared practically structureless—as in fact they did become after electron bombardment—without the Bragg fringes. The Bragg fringes correspond to those parts of the crystals which are in a suitable orientation to diffract electrons. These electrons will be screened off by the microscope aperture and thus will be absent from the corresponding parts of the image. Consequently the existence of Bragg fringes implies that the structure within the crystal is not uniform. The fringes can be indexed, i.e. the reflections producing them can be determined by taking dark ground photographs

through chosen reflections or by the ghost image method (Agar *et al.* 1959), and with this information it should be possible to map the lattice orientation within the whole crystal. It was found, however, that the fringe pattern was changing in the electron beam—in addition to the trend of disappearing gradually—consequently it could not be readily assessed how far the fringe patterns which could be photographed reflected the original characteristics of the lattice and how far they were conditioned by beam effects. For this reason this particular line was not pursued any further.

When scanning extended areas of the preparations under the optical microscope occasionally straight lines could be seen in the crystals along one or the other lozenge diagonal. These were rare in $C_{36}H_{74}$ but in some of the other paraffins, particularly in $C_{32}H_{64}$ (studied by Baltá-Calleja) lines along the short lozenge diagonals could be very frequent. It is the study of these lines which forms the main part of the present investigation. In the following some of the most typical observations will be enumerated.

It was found that the lines in question could be produced systematically by heat treatment. If $C_{36}H_{74}$ crystals as grown from petroleum ether were heated to temperatures between 45–60°C lines which were readily visible under the optical microscope (fig. 2) formed along the long lozenge diagonals (to be referred to as **a** lines). In the region of 60°C and above, these lines receded and the crystals could become quite structureless optically. Above 65°C striations appear again but this time parallel to the short diagonal (to be referred to as **b** lines). There was a considerable variability as regards the temperatures. It could happen that the **b** striations appeared while some **a** lines were still present. As the melting point 76°C was approached the **b** striation pervaded the whole crystal. Near the melting point striations could also develop along other directions, e.g. parallel or occasionally approximately perpendicular to the lozenge faces (⟨110⟩ and ⟨130⟩ directions by the orthorhombic subcell structure; see later) the former being illustrated by fig. 3. As seen, the lozenge in this photograph also contains **b** lines.

The present account will be restricted to the striations of the kind just described. It will only be mentioned that in the immediate vicinity of the melting point even more drastic changes happened to the crystals which were still unfused. Thus the **b** striations, while becoming more pronounced, also became less regular and the crystals could buckle, fold or even crack, usually along their short diagonal. When the melting point was exceeded the crystals fused into blobs which, on cooling, recrystallized in a strongly striated form. It is hoped to illustrate these effects in a later publication.

The regular **a** or **b** striations appeared in the orthorhombic form only. Whenever they were found in preparations which originally contained monoclinic crystals it could be assessed from the lozenge angles that the crystals have become orthorhombic by the time the striations appeared. Whenever striations of the kind as in fig. 3 were seen the crystal (or part of the crystal) had become hexagonal (interfacial angle $\sim 60°$).

All these effects were in first approximation irreversible, shown by the fact that they could be observed after the specimens had cooled to room temperature. However, the **a** lines which formed at the lowest temperatures were sometimes observed to recede slowly over a period of days.

Optical observations of the effect of heating *in situ* with the hot stage revealed that the ridges appeared suddenly as short lines which then grew lengthwise across the crystal. In the course of the same experiments changes of the lozenge shapes could also be directly observed. Those corresponding to the monoclinic habit (interfacial angle 75°) were sometimes seem to change into the orthorhombic (angle 67°) and later into the hexagonal macroscopic shape. A transformation front was seen to sweep over the whole crystal. All these changes were irreversible, no reversion to the original form being seen on cooling.

A solid substrate was not essential for the striations to form ; they also appeared when the crystals were floating on the surface of water which was heated to the desired temperature.

The crystals which showed the striations best, were usually too thick for direct transmission electron microscopy, therefore they were examined by replication. Figures 4–9 show some examples of these investigations. As seen, the striations detected first by the light microscope are really regular ridges or roofs. Figures 4 and 5 show examples of **a** lines which were usually the largest and most regular. They are mostly roof-shaped. Figures 6 and 7 contain **b** lines in addition to some **a** lines which have still not fully receded. The **b** lines formed at these lower temperatures, where they may exist together with **a** lines, are flat topped. When formed at higher temperatures also the **b** ridges are roof-shaped but on a smaller scale than the **a** roofs. The **b** roofs are usually close together giving a corrugated appearance to the whole crystal. This state has already set in on the top right of the crystal in fig. 7. This crystal was evidently in the process of transformation. In crystals, as in figs. 6 and 7, the **b** ridges continue along the same straight line even when intersected by **a** lines. This is rather remarkable in view of the fact that they developed when the **a** ridges were already present. Figure 8 shows the centre of a crystal containing both **b** ridges and ridges parallel to the lozenge faces (⟨110⟩). Lines along ⟨110⟩ are also visible in fig. 9, where otherwise regular roof-shaped ridges perpendicular to the crystal face (⟨130⟩ in the case of a hexagonal subcell in terms of orthorhombic indices) represent the dominating feature. Here, as seen from the shadowing, some of the ridges are reversed, i.e. they correspond to grooves and not to protrusions. This makes it plausible that the ridges even when seen as protrusions are in fact hollow in their interior.

Even if crystals, as in figs. 4–9, were too thick for good transmission electron micrographs it was possible to obtain some kind of image in transmission before the crystallinity was destroyed by the beam. The images were necessarily very weak on the negatives and were consequently of poor pictorial quality. Figure 10 shows **a** lines in such a

transmission picture. It can be seen that some lines reveal diffraction contrast as one side of such ridges could be darker than the other in unshadowed specimens. In the case of really thin crystals suited for transmission work, the regularity of the striations was not so obvious. Such crystals could crack along the ridges, as shown by fig. 11, which was taken with a heating stage within the electron microscope. In spite of the difficulties encountered in such hot stage work, referred to earlier, it was possible to observe the formation of these cracks *in situ*. In other cases of such thin crystals, the striation showed up as pleats, particularly those along the **b** direction (fig. 12), which in the earlier stages became apparent through Bragg extinction fringes (fig. 13). In some cases it could be established from the corresponding diffraction patterns that in the course of this pleating the lattice is tilted around the short lozenge diagonal (**b** axis).

§ 3. Discussion

The main part of this discussion will be confined to the regular ridges. It will be attempted to relate these ridges to the arrangements of the paraffin chains in the crystals. In view of the ever-increasing complexity of the literature on paraffin crystals it may not be superfluous to lay down a few basic principles first.

In the crystals of paraffins the molecular chains are in a parallel packing. The question of the details of this packing can be resolved into three parts: (1) the lateral packing of the CH_2 groups, that is the main body of the chains, (2) the packing of CH_3 groups, that is the relative position of the chain ends, in adjacent chains, (3) the end-to-end arrangement of consecutive chains. As the normal habit is of the layer type, with the layers consisting of parallel stacks of paraffin molecules, the above three points correspond to the structure within the interior of an individual layer, to that at the surface of an individual layer and to the mode of packing of subsequent layers respectively.

(1) The paraffin chain consists of a repetition of CH_2 groups which defines a small repeating unit, the subcell with edges a_s, b_s, c_s within the true unit cell a, b, c, the latter comprising the full length of the chain or possibly several chains (Vand 1951, v. Sydow 1956). One of the subcell edges corresponds to the repeating CH_2 groups (two CH_2 per repeat) along the chain, the other two edges being determined by the relative positions of adjacent chains. Accordingly, the subcell structure defines the lateral packing of the chains. Two kinds of subcell are known to exist in paraffins. One, the more general orthorhombic, contains two molecular repeats, the other of triclinic symmetry contains only one (see e.g. v. Sydow 1956). Only the orthorhombic subcell is relevant to the crystals to be discussed here. For the case of an infinite paraffin chain (polyethylene, where the subcell is usually regarded as the true unit cell) it is shown by fig. 14. At high temperatures the orthorhombic

subcell can acquire higher symmetry and become hexagonal in which case $a = 3/\sqrt{3}b$ in fig. 14.

Fig. 14

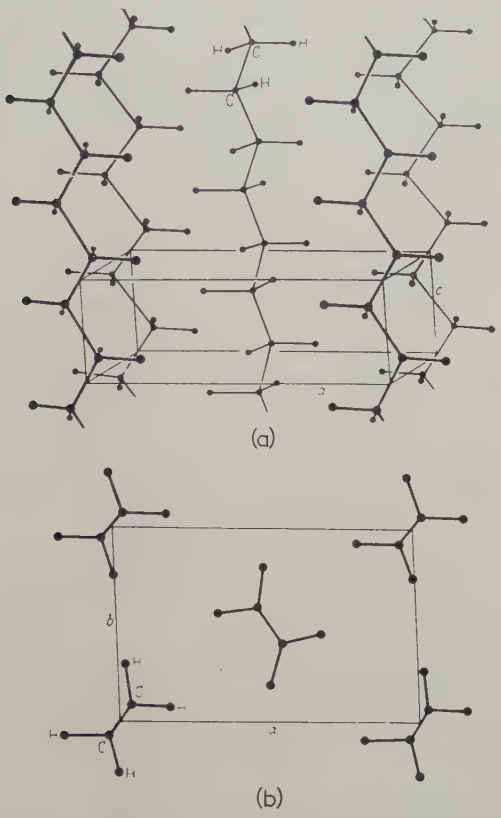

Orthorhombic subcell structure of a paraffin of infinite chain length (polyethylene, after Bunn), (*a*) perspective view; (*b*) projection along the **c** axis (molecular chain).

(2) If the adjacent chains are displaced lengthwise with respect to each other by an amount corresponding to the subcell edge along the chain direction the subcell structure is maintained unaltered except that the terminal CH_2 groups will be at altered levels. If they are all in one level the planes defined by them will be perpendicular to the chains (fig. 15 *a*), otherwise they will be oblique (fig. 15 *b*). In the first case the structure may be orthorhombic, in the latter always monoclinic or triclinic (see below). Clearly a large number of obliquities can be realized by shearing the structures along the **c** direction on different shear planes through different amounts. The basic requirement is that the terminal planes must be indexable in terms of the subcell. Thus in fig. 15 *a*, the terminal plane is $(001)_s$, while in fig. 15 *b* it is $(h, k, l)_s$ where at least one of h and k is not zero. The suffix s is used here and

subsequently to denote subcell indices. While this scheme for generating paraffin structures was implied in some of the early works on paraffinoid substances, it was Müller (1927) who first stated explicitly that the cross-sectional area of the unit cell projected on a plane perpendicular to **c** was identical for different monoclinic angles. The relation between different oblique structures having the same chain packing was systematized by Schoon (1938). The subcell concept was first introduced by Müller (1928), without actually naming it as such, in order to facilitate

Fig. 15

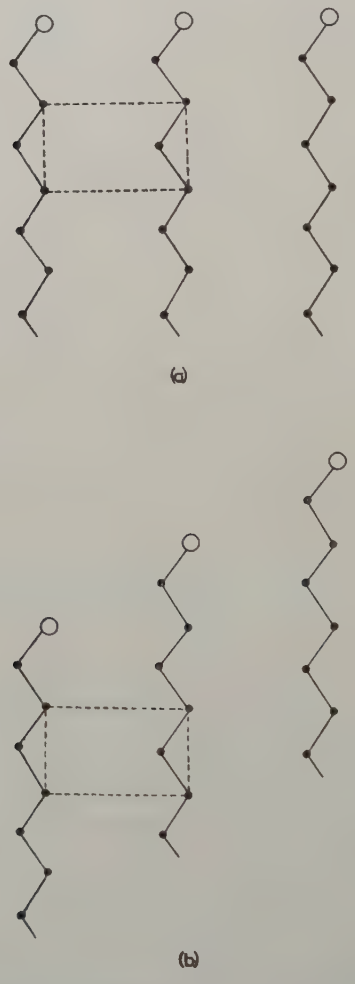

Simplified two-dimensional representation of the arrangement of the paraffin chains. (*a*) in a vertical stucture; (*b*) in an oblique structure. Solid circles are CH_2, open circles are CH_3 groups. The small parallelepipeds indicate the subcell.

structure determinations, and was utilized later under this name by Vand (1951), followed by v. Sydow (1956) to simplify the classification of paraffinoid structures in the way presented in this paper.

(3) The fitting of consecutive chains end to end is of lesser importance for the present discussion. It will be added here for completeness. Here we have the possibility of distinguishing between the structure of odd and even paraffins. Figures 16 (*a* and *b*) shows the same kind of end-to-end relation for odd and even paraffins. In both cases the planes containing the terminal groups are perpendicular to the chains, nevertheless (*a*) is orthorhombic while (*b*) is monoclinic.

Fig. 16

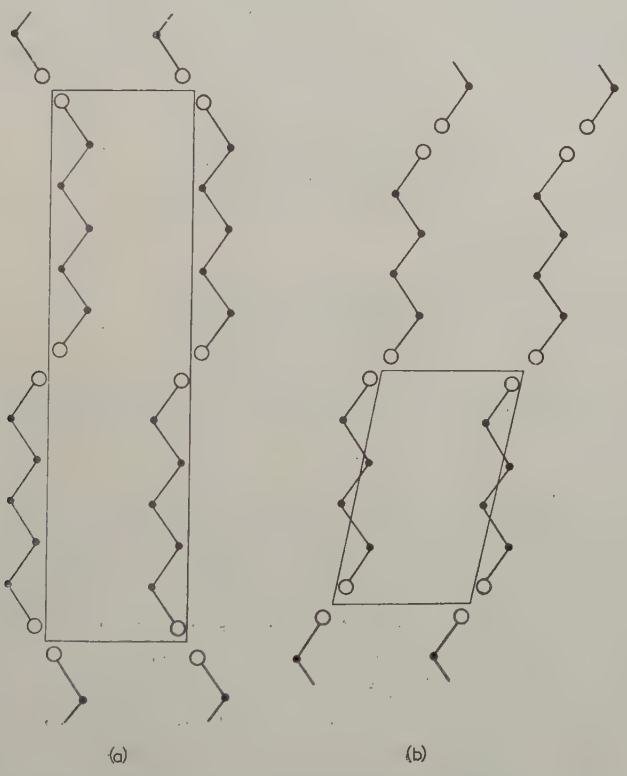

Simplified two-dimensional representation of the unit cell in a vertical structure for the case of (*a*) odd; (*b*) even paraffins. Solid circles are CH_2, open circles are CH_3 groups.

When determining the symmetry different criteria are used by different investigators. It is customary to distinguish between the orthorhombic and monoclinic forms on the basis of the **c** repeat directly derivable from the 00*l* reflections. While this would give the correct answer for cases like fig. 15 (*a* and *b*), fig. 16 *b* would be classed as orthorhombic on this

basis because with sufficiently long chains the shortening of the **c** period may not be normally noticeable.

As structures in fig. 16 (*a* and *b*) are clearly distinct from that in fig. 15 *b* we propose the distinction of vertical structures (which would also include fig. 16 *b*) and oblique structures (fig. 15 *b*) in addition to the strict classification by lattice symmetry. In the vertical structures, the planes containing the CH_3 groups should be indexable as $00l_s$ (in terms of the subcell), while in the oblique structures h_s and k_s would not be both identically zero. In the literature hexagonal phases are also referred to. Evidence for this is usually obtained from the $hk0$ reflections which show that $a = 3/\sqrt{3}b$. However, this only gives the subcell structure. The scheme outlined above (fig. 15) could still be operative also with a hexagonal subcell. Thus many oblique structures could correspond to a hexagonal subcell. Whether the structure is truly hexagonal or not can only be determined from hkl reflections.

Fig. 17

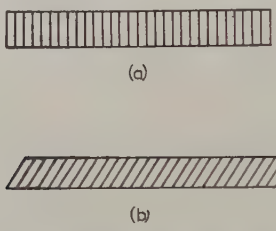

Schematic representation of a crystal layer having (*a*) a vertical structure; (*b*) an oblique structure.

The lozenge-shaped paraffin crystal layers consist of parallel stacks of molecules. In the case of the vertical structure the molecules are perpendicular to the crystal planes (fig. 17 *a*), in the oblique case (fig. 17 *b*) they are not. Since molecular packing requires shears by discrete amounts, and intermediate amounts of shear involve higher free energies, transition should not occur simultaneously over the whole crystal but spread out from wherever it was first initiated. It will now be proposed that such a progressive transformation could occur by the molecules slipping past each other while maintaining their original orientation with respect to the geometrical outlines of the crystal. The result will be a sloping basal plane which could lead to a ridge as in fig. 18 *a*. It is propsed further that the ridges observed in the crystal are of this origin. Accordingly, **a** striations would arise through a simple shear on (010) planes, **b** striations by simple shear on (100) planes and other striation directions would have their corresponding shear planes. Consequently in single crystals like the ones in figs. 6–9 several oblique structures differing by the amount of shear and by the plane of shear are represented.

It will be assumed that the orthorhombic or, if at high temperatures, hexagonal subcell is preserved during this transformation. Subcell theory requires that the planes containing the end groups, hence the planes of the ridges, should be defineable in terms of rational subcell indices. We shall now proceed to index some of these planes from the electron micrographs. The **a** ridges were the most suitable for this purpose, being the largest and most regular, being clearly separated by flat areas of the unaltered crystal. These ridges are terminated by oblique faces or by a sequence of such faces (fig. 5). These terminating faces must have originated through a shear on (100) planes, hence must have the same origin as the **b** ridges, consequently they should also be indexable with reference to the subcell coordinates.

Fig. 18

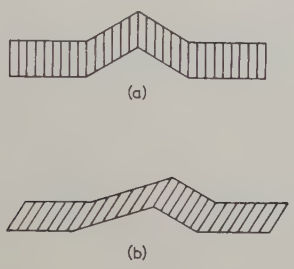

Schematic representation of a crystal layer with a localized transformation. (*a*) from a vertical to an oblique structure; (*b*) from an oblique structure to one with a larger obliquity.

While without further information the indices themselves cannot be assigned, the ratio of the indices of planes meeting along a line can. The subcell indices of the sides of the ridges are $(0kl)_s$, those of the terminal planes are $(h0l)_s$. The line along which they meet is the axis of the zone to which both belong. By measuring the angle enclosed by this edge in projection and a given crystal axis the component of this zone axis in the (001) plane, hence the U and V zone coordinates and thus h/k can be determined.

The angles between these interplane edges and the **a** axis (the direction of the ridges were measured in several cases. Most of the figures obtained fell in two main groups. Those which were the most regular, hence most accurately measurable, were between 50 and 56°. A number of measurements gave figures 17–23°. However, other values were also obtained. Such were 24–28°, and much smaller angles like 10–11°, and $< 5°$ possibly 3°. The angle 53° corresponds to $h/k = 2$, which clearly defines the first group. The angle of 20° gives $h/k = 1/2$ which defines the second group. 24° gives $h/k = 2/3$, 28° 3/4, 10–11° 1/3 or 1/4 and an angle less than 5° would require at least $h/k = 1/10$ or possibly a still smaller ratio.

For obtaining the indices themselves the heights of the ridges are required. These were obtained by shadowing the specimens at an angle of 10° and by measuring length of the shadows cast by suitably oriented ridges. From this and from the ridge width the slope of the planes could be directly assessed.

It was found that the inclinations of the side faces of the **a** ridges were mainly of two kinds. One corresponded to the range of 25–29° while the other to that of 15–18°. Intermediate values such as 19°, 22° were also measured ; in fact the slope could vary along the same ridge and could also be somewhat different on both sides of the same ridge, although in general, the ridges were symmetrical.

The slope of 27° corresponds to a shear on (010) by 2·5 Å per unit cell, i.e. by c_s/a_s. Accordingly the basal planes would be $(011)_s$. The slope of 15° requires a shear of $\frac{1}{2}c_s$ per unit cell, the corresponding subcell index being $(012)_s$. We conclude that these indices define the planes of the corresponding ridges in the crystals. Intermediate values would correspond to indices like, e.g. $(023)_s$. Knowing the ratio h/k from the interplane edge directions the terminal faces could also be similarly indexed once the side planes of the ridges were known. In suitable photographs, indices of the terminal planes could also be determined directly from the ridge height. The indices of the terminal faces found by the above methods were $(201)_s$; $(101)_s$; $(102)_s$; $(104)_s$ or $(103)_s$; $(203)_s$ or $(304)_s$, $\sim(1, 0, 10)$. In the case where alternatives are given both types of planes are permissible within the accuracy of our measurements.

One may now consider the structures giving basal planes as determined from the electron micrographs. With (010) or (100) as shear planes, and with a homogeneous shear, preserving the same subcell structure, the displacement of successive planes of molecules must either be a multiple of c_s, or an odd multiple of $\frac{1}{2}c_s$. accompanied by a rotation through 180° about c_s of the molecules in every second plane. The largest shear observed in fact corresponds to the latter case, with displacements of $\frac{1}{2}c_s$ between successive planes.

We must infer either that the rotations through 180° of half the molecules occur, or that the shears are not homogeneous (rejecting as improbable the change of subcell structure from Pnam to Pbnm known as a paraffinoid subcell structure only in 2D, methyloctadecanoic acid, Abrahamson 1959). The smaller observed shears cannot be homogeneous, but appear to be regular, with displacements between every second, or every third plane, etc., since the inhomogeneity is not resolved in the electron microscope, and a principle of rational indices does seem to apply.

In general, let $(hkl)_s$ be the basal plane and h_s be expressed as nH and k_s as nK, where n is the largest common factor of h_s and k_s. Then the molecules within every l_sth $hk0$ plane will need displacing by $n \,.\, c_s/2$ along the c-axis. Clearly a very large number of oblique structures can

be realized in this way for any particular shear plane. Such possibilities were not included in earlier schemes for generating paraffin structures.

High index planes implying long-range order would not be expected. Nevertheless, such are occasionally seen to exist amongst the terminal planes of the ridges where slopes so low that they could not be accurately measured any longer on our photographs could be observed corresponding to l_S indices at least as high as 10. The terminal parts are really accommodation structures forced into being by the main body of the ridges, consequently they can be far removed from equilibrium structures. The existence of very high index planes is therefore not surprising, neither is the occasionally observed curved boundaries of the terminal faces indicative of a continuous variation of the slopes. Nevertheless, there is a tendency towards equilibrium structures even within the terminal parts, as indicated by the frequent occurrence of the low index faces like $(101)_S$ and $(102)_S$.

The foregoing implies that the molecular direction remains unaffected in all these ridges, consequently the same $hk0$ reflections should be either in or out of reflecting position within the different structures in the same crystal. This follows from the fact that in first approximation the $hk0$ reflections are determined by the subcell which should be identical in all the structures, and should also retain the same orientation in these transformations. As with paraffins, the diffraction contrast in electron micrographs is predominantly due to $hk0$ reflections one would not expect such a contrast in the image of the ridges. However, near diffracting position only a very small tilt, let us say 1°, towards or away from diffracting position would already be sufficient to produce a strong contrast effect. Such small deformations could occur if only for reasons of mechanical rigidity in the ridges. Also it has to be remembered that though the molecular displacements in a transformation of crystal structure are well described, within a layer, as simple shear displacements along the axes of the chains, the resulting changes of structure at the surfaces of the layers are likely to cause small readjustments in the stacking of one layer on another, the consequence of which will be small rotations of the subcell structure, which can well suffice to account for the observed diffraction contrast between the two sides of a roof. This might be the case in some of the ridges in fig. 10 where one side of some of the roofs is darker than the other. That the difference in orientation can only be slight, and consequently does not invalidate our interpretation of the roof structures is shown by the fact that in some ridges the dark zone is in the centre of the roof and in others it is absent altogether. Also the dark sides can be opposite ones in the different ridges. This would not happen if the different parts of the ridges were associated with distinct molecular orientations which differ from that in the untransformed crystal and also differ for the two sides of the ridges.

In none of these cases did we consider the change in the subcell structure due to the change of temperature. It was mentioned that the ridges

were unambiguously observed in the orthorhombic (vertical) crystals. In principle, it is not excluded that crystals with an oblique structure as in fig. 17 *b* should form ridges. Such ridges would have to be asymmetrical (fig. 18 *b*).

The regular ridges were most readily observed in crystals about twenty–forty layers thick. In thinner crystals, more suited for transmission electron microscopy, the striations lacked the geometrical regularity. It is to be expected that thin layers will not be able to form large regular ridges, if merely for lack of rigidity. As the shear spreads the crystals could eventually split along the shear planes. Apparently this has occurred in the crystal of fig. 11. The thinness of the crystals would also lead more readily to bending or pleating of the layers (fig. 12). which would also cause noticeable disorientation to show up in the diffraction patterns, also revealed by the corresponding Bragg fringes in fig. 13. Nevertheless, there appears something systematic in the pleating along the **b** direction which is noticeable also in thicker crystals. This can correspond to a tilt of the unit cell around **b**. as indicated by some of our experiments. The large expansion along **a** might be partly responsible for this effect but there is evidence that this could not account for it fully. Transitions from vertical to oblique structures, such as in fig. 17 *b*, involving a tilt of the molecule cannot be excluded. This would increase the surface area and if it occurred in parts or progressively it could push up the material in the form of pleats. While such less regular morphological features have been mentioned here, a more detailed discussion or description would be beyond the scope of the present paper.

Besides the purely structural implications, the present observations raise a number of further questions. A few of them will just be mentioned without attempting an explanation at this stage. The formation of ridges implies a change from the vertical to an oblique structure, that is from a system of higher to lower symmetry on raising the temperature. This is contrary to the usual trend in crystal transformations. Similarly puzzling is the behaviour that such structures should become vertical again and change into ones of a different kind of obliquity. Further, the structural changes in question are essentially irreversible. Crystallographic changes in paraffins below the melting point are usually referred to as reversible in the literature, both as regards the changes confined to the true unit cell (monoclinic–orthorhombic, or rather oblique and vertical in the present nomenclature) and as regards the changes also occurring in the subcell (orthorhombic–hexagonal). Clearly the thermodynamics of these systems is still largely obscure. Finally, the conditions under which the present effects appear are very sensitive to a number of variables. Besides the generally recognized criterion of purity (e.g. Shearer and Vand 1956, Teare 1959), the size and thickness of the crystals, the rate of heating, substrate, etc., are apparently important factors.

It will be seen from the next paper of the series that the effects described and discussed here have their counterparts in polymer crystals, which without this background with paraffins could hardly have been interpreted or even followed up effectively experimentally.

Acknowledgments

I wish to thank Dr. J. M. Goppel, of the Shell Laboratories, Amsterdam, for the supply of paraffin samples, Mr. D. C. Bassett for a number of valuable suggestions, and Mr. F. Balta-Calleja for contributing to the growing of crystals as mentioned in the text. I am specially indebted to Professor F. C. Frank for his interest and guidance throughout this work.

References

Abrahamson, S., 1959, *Acta cryst., Camb.*, **12,** 304.
Agar, A. W., Frank, F. C., and Keller, A., 1959, *Phil. Mag.*, **4,** 32.
Dawson, I. M., and Vand, V., 1951, *Proc. roy. Soc.* A, **206,** 555.
Keller, A., 1959, *Makromol. Chem.*, **34,** 1.
Muller, A., 1927, *Proc. roy. Soc.* A, **114,** 542; 1928, *Ibid.*, A, **120,** 437.
Schoon, Th., 1938, *Z. phys. Chem.* B, **39**, 385.
Shearer, H. H. M., and Vand, V., *Acta cryst., Camb.*, **9,** 379.
Sydow, E. v., 1956, *Ark. Kemi*, **9,** 231.
Teare, P. W., 1959, *Acta cryst., Camb.*, **12**, 294.
Vand, V., 1951, *Acta cryst., Camb.*, **4,** 104.

Some New Habit Features in Crystals of Long Chain Compounds† Part II. Polymers

By D. C. Bassett and A. Keller
H. H. Wills Physics Laboratory, University of Bristol, Royal Fort, Bristol, 8

[Received July 20, 1960]

Abstract

The morphology underlying the characteristic striations observed in polymer crystals has been examined in more detail than hitherto. The striations were found to correspond to corrugations in the crystal layers. Both pleat and roof-ridge corrugations were observed in polyethylene crystals. These latter are pictorially similar to those in paraffin crystals discussed in Part I. The analogy between the two cases is pursued with the folds replacing the end groups in the polyethylene case. A possible common origin for both types of corrugation is proposed to be the collapse of non-planar crystals. A particular non-flat-based pyramidal model is proposed. Evidence for the existence of such crystals is presented. A variety of observations, including the non-planar crystals, is shown to be explainable in terms of a particular type of packing of the folded molecular chains. Further, it is suggested that if folding also occurs in the bulk polymer, then roof ridges of the type discussed might account for its well-known four-point low-angle x-ray pattern.

§ 1. Introduction

The first observations on polymer single crystals showed that they consisted of flat plates growing perpendicular to themselves by screw dislocation mechanisms (e.g. Keller 1957). Polyethylene single crystals, in particular, have similar habits to those of the orthorhombic *n*-paraffins. Both the electron microscopic images and the diffraction patterns were at first sight indistinguishable for crystals of the two materials. Thus in polyethylene, also, the molecular chains were perpendicular (or nearly so) to the crystal layers. As these polyethylene layers are only 80 to 160 Å thick and the molecules microns long, it was necessary to postulate that a regularly and sharply folded molecular configuration existed within them (Keller 1957). More detailed examination of polymer single crystals has revealed a number of new features, in particular characteristic striations (e.g. Agar *et al.* 1959). As described in Part I, striations were, in fact, also found in paraffins, of which at least the most regular could be given a satisfactory interpretation. The present paper considers some examples of striations in polymer crystals and draws parallels with paraffins as far as is possible.

† Communicated by Professor F. C. Frank, F.R.S.

§ 2. Experimental

2.1. *Materials and Specimens*

The experimental material was mainly the linear polyethylene, Marlex 50, but reference will also be made to polyoxymethylene $(CH_2O)_n$. In all cases, the polymers were dissolved in hot solvents and crystallized by cooling these solutions. In this way a suspension of single crystals formed which could be examined after drying down on a microscope slide. By using carbon-coated slides, and subsequently floating the film off on water the crystals could be examined electron microscopically. The illustrations shown here were selected from a body of material which has accumulated whilst following several different lines of research. Because of this, to detail the various preparative methods used would take too long here and we shall merely quote the types of specimens used. For polyethylene, these were four.

(1) Crystals which were truly lozenge-shaped, obtained by various methods of crystallization at temperatures below 80°C.

(2) Truncated lozenge crystals, formed at slightly higher temperatures (the relative size of the truncating faces {100} increasing, for a given solvent, with the temperature of crystallization). Those mostly referred to were formed at 90°C and were filtered off at that temperature before cooling.

(3) Crystals heated above their original crystallization temperature while still in suspension and subsequently subjected to various conditions of cooling.

(4) Crystals heated dry on a microscope slide and examined after re-cooling.

The polyoxymethylene crystals referred to were formed as a solution cooled to room temperature.

2.2. *Some New Observations*

As first observed, the striations in polyethylene crystals of type (1) were irregular, wavy lines, approximately perpendicular to the faces of adjacent crystal quadrants (Keller and O'Connor 1958, Agar *et al.* 1959). These were observed as Bragg fringes in suitably taken electron micrographs, but were later found to correspond to an actual morphology (see, e.g. Keller and Bassett 1960). These physical corrugations were, for the most part, transient and largely disappeared soon after drying the crystals down. When the regular roof-shaped ridges were recognized in paraffins (Part I), the possibility of drawing a parallel between these and the polymer striations presented itself. For this, a clear pictorial evidence was required. The experimentation which followed aimed at obtaining such evidence by improving the methods of specimen preparation and observation. In the course of this work, the regularity of the striations became increasingly apparent. In the first instance,

the regularity was observed in the Bragg fringes described above, which could take the forms of straight lines or bands (figs. 1, 2†). These were seen best in specimens examined immediately after drying down. Moreover, the regularity and definition of these fringes deteriorated continuously on exposure to the electron beam. The underlying morphology, however, could be preserved at least partially by shadowing the specimens more heavily than is usual, immediately on drying down. This makes the structures more permanent and also more resistant to electron damage. Using this method photographs at higher magnification could be obtained. Figure 3 shows a central part of a crystal obtained in this way. As seen there is a line structure corresponding to the direction of the extinction fringes in figs. 1 and 2. The most pronounced lines appear to be pleats, but others parallel to them, regular ridges as best recognizable from fig. 4 which is an enlarged detail of such a crystal. As seen from figs. 3 and 4 such ridges are crossed obliquely by another striation. This second striation direction is best visible where it passes through the first-mentioned ridges but can also appear alone in other parts of the crystal. In some other photographs this latter feature could be seen more prominently. Figure 5 is an example of a multilayer crystal, with a few striations on the top layers only. It has been a general experience that the striations on the higher layers were progressively more permanent. The decorating effect of small latex-type particles of unknown origin along the crystal edges may be noteworthy.

The regular roof-shaped nature of the striations is also evident in the truncated lozenges of type (2). Here they are usually most pronounced in the sector bounded by the truncating face where they are parallel to the short diagonal of the crystal (fig. 6). The detail in fig. 7 reveals the geometrical regularity of these ridges. (The overgrowth corresponds to crystals formed at a lower temperature (see Keller and Bassett 1960, fig. 31); the study of such effects is part of another programme of work and will not be commented on further here.) There are usually signs of the ridges continuing beyond the sector boundary changing their direction to that of the kind found in the true lozenges described above. This effect became more pronounced when the suspension containing such crystals was heated above 90°c in which case these ridges could be observed to extend further into the adjacent sectors until eventually they pervaded them entirely (Keller and Bassett 1960, figs. 28, 29). In these latter cases the direction of the lines in the adjacent sectors could change somewhat so as to become more nearly parallel to the short crystal diagonal.

The transient nature of the striations has already been mentioned. These previous comments referred to the disappearance of the lines after drying down. The suspensions themselves did not alter. On drying down the same kind of crystals were obtained even after the suspension had been kept for months. However, those striations which appeared in

† With the exception of fig. 12, all figures are shown as plates.

the truncated lozenges on heating the suspension could only be observed if the crystals were deposited within a very few hours of the end of the heat treatment.

Apart from such rather special effects, in general the effect of heating was to enhance the striated appearance of the crystals. Here again the striations could be either pleats or regular roof-shaped ridges or stages between these two, even within the same crystal.

As reported elsewhere (Bassett and Keller 1959, Keller and Bassett 1960) striations could also appear on heating the dry crystals on a microscope slide. On the first layer, in contact with the substrate, the lines were either perpendicular to the lozenge faces or parallel to the short diagonal; on the higher layers they were always of the latter type. While these usually manifested themselves as pleats, in the early stages they showed a definite geometrical regularity. In all the heating experiments, in suspension or dry, the striations formed first on the top layer of the crystals.

Observations of pleats are not new. These have been reported in polymer crystals under a variety of circumstances. In some truly lozenge-shaped crystals they outline a small lozenge at the centre similar in shape to the main crystal, but rotated through 90° with respect to it. In most other cases these pleats lie along the short crystal diagonal, though occasionally they are found also along other directions. These latter pleats are usually triangular in shape and amongst our preparations could be most clearly seen in the truncated lozenges (fig. 8).

Striations and a corresponding morphology do not appear only in polyethylene, but may well be a general phenomenon in long chain crystals. Polyoxymethylene, for example, forms large, rather irregular, crumpled hexagonal crystals often containing radial pleats or thickenings. Electronmicrographs revealed regular striations which were shown up best by diffraction contrast (fig. 10) but there is evidence for an underlying morphology (fig. 11).

For the sake of continuity the description of a number of further observations will be included in the appropriate part of the Discussion.

§ 3. Discussion

At first the basic structural data will be briefly recapitulated. The subcell (often called the unit cell) of polyethylene is orthorhombic (Bunn 1939, see fig. 1, Part I). In the crystals the long lozenge diagonal is along the **a**, the short along the **b** axis. The prism faces always present are {110}. The truncating prism faces present in crystals grown at higher temperatures are {100}. The **c** direction, that of the chains, is approximately perpendicular to the lamellae. The molecules are expected to fold along the boundary prism faces of the crystals. This implies that the crystal consists of as many distinct sectors as there are prism faces, the sectors being defined by the direction of the folds within them (Keller and O'Connor 1958, Bassett *et al.* 1959).

The striations provide a clear example of sectorization. Thus, they change in direction at the sector boundaries (figs. 1, 2, 6) and the different sectors are distinguished by the different directions of the striations within them. The existence of distinct sectors is confirmed by diffraction effects since different diffraction conditions may be satisfied in the different sectors (Agar *et al.* 1959, Bassett *et al.* 1959). This selective diffraction allows different sectors to be brought into Bragg extinction positions in different orientations to the electron beam. The crystal in fig. 8 has two {110} sectors in Bragg contrast; we have other micrographs with the {100} sectors alone diffracting—see e.g. fig. 2 in Bassett *et al.* (1959). Figure 1, with opposite pairs of quadrants in different contrast, illustrates the same effect.

Until recently striations were only mentioned as far as they served to confirm the hypothesis of sectorization. The nature and origin of these lines was left unexplained. The transient and rather irregular line structure did not lend itself to further interpretation. The present results (figs. 4, 7) have revealed an unmistakable similarity between these lines and the paraffin ridges reported earlier. In paraffins these ridges were interpreted as resulting from new phases, the different parts of the ridges containing structures with different obliquities, the sloping planes of the ridges being the planes containing the end groups. In the case of polymers consisting of folded chains there are no end groups, but the folds should play a similar part. They define a basal plane which should be indexable in terms of the subcell (Part I), and accordingly could give rise to vertical and oblique structures (figs. 2, 3 in Part I). By geometrical arguments alone all the possibilities discussed in connection with the paraffins should be realizable.

Having obtained photographs with more regular striations than before the directions could be more accurately measured. They were found, in contradiction to earlier reports, to be always crystallographic. In the true lozenges they were either $\langle 130 \rangle_s$, $\langle 250 \rangle_s$ or $\langle 120 \rangle_s$ where the suffix s refers to the subcell. The common feature of all these is that they are nearly perpendicular to the {110} faces bounding the adjacent sectors. The second kind of striation sometimes seen to cross the ones mentioned above (figs. 3 and 4) is $\langle 230 \rangle_s$. This is distinguished by the fact that $[230]_s$ and $[\bar{2}30]_s$ are almost at right angles to each other, the corresponding lines in the different sectors defining a square. In the {100} sectors of the truncated lozenges the lines were along **b**, [010]. While the above directions were the principal ones they are by no means unique as less frequently others were also observed. Such were the ones parallel to **a**, [100], and in one instance along the lozenge faces, i.e. $\langle 110 \rangle$.

The lines along $\langle 130 \rangle_s$, $\langle 250 \rangle_s$, $\langle 120 \rangle_s$ define the sectors by changing directions at the boundaries. The **b** lines in the truncated lozenges define the {100} sectors by being confined to them. (The sectors are often also delineated by elevations along the boundaries (fig. 6)). Sometimes, however, the **b** just as the rare **a** lines may pass through the whole

crystal. A possible reason for the particular choice of shear planes in the different sectors will be given later. In the {100} sectors of truncated lozenges they are parallel to the assumed fold plane; accordingly layers of folded molecules would only need to stack differently without any need to change the arrangement of the folds within the layers. In other cases, however, the shear plane would have to pass through folded layers which would affect the folding of the molecules themselves. In the case of paraffins the ridges formed mainly on heating. There is a parallel in polymers where heating enhanced the striated effect.

Regular striations are not restricted to polyethylene, as shown by our observations on polyoxymethylene (figs. 10, 11). It is possible, therefore, that the same explanation as above would also be valid for other polymers, polyoxymethylene in particular.

One may enquire about the origin of the ridges formed in untreated crystals. One possibility is that in analogy with paraffins they represent phases stabler at the higher temperatures where the crystal originally formed. When the crystals cool to room temperature, while still in suspension, parts of them might change into the modification stabler at the lower temperature. This issue could only be decided if the crystals could be examined at the temperature at which they were grown.

The ridges and pleats would also originate from a dished pyramidal habit of the crystal layers. That polymer crystals may indeed be non-planar was inferred from the triangular pleats seen in crystals as in fig. 8 (Bassett *et al.* 1959, Niegisch 1959). These pleats, it was suggested, were formed by the regular flattening of a hollow pyramidal crystal as it dried down on a substrate, the pleat accommodating the excess material. Alternatively, the crystal could crack, which has also been observed (both pleats and cracks are seen simultaneously in fig. 5). Other kinds of pleats, e.g. the square, round, or fourfold star-shaped ones in poly-4-methyl-pentene-1 (Frank *et al.* 1959) and the six-fold stars in polyoxymethylene reported here are equally compatible with the idea of a collapsed pyramid. There were, in fact, some theoretical reasons which gave support to this suggestion. Accordingly the dished pyramidal habit could be a conceivable consequence of the sectorization of the crystals (Bassett *et al.* 1959). Consider a crystal consisting of four {110} sectors (true lozenges). The existence of folds along {110} planes would lower the symmetry of the lattice in a sector because the two ⟨110⟩ directions would not be equivalent any longer as in the truly orthorhombic cell. In case the diagonal containing the fold became shorter this could make the central angle by which the quadrants meet less than 90°. Consequently the four quadrants would not join while staying in a plane and a ' dished ' pyramid would result. The hollow pyramidal habit could also be arrived at by considering the possible modes of packing of the layers containing the folded molecules. The folds need not define a basal plane normal to the chains but could form a staggered configuration. This would lead to oblique basal planes with different directions of obliquity in the different

quadrants and thus to hollow pyramids. This explanation suggested to us by Reneker and Geil (private communication) is, in fact, an extension of the ideas underlying the formation of ridges.

However, such theoretical considerations, while very attractive cannot be considered as compelling unless backed by unambiguous experimental evidence. The triangular central fold was certainly a strong indication, but was not in itself decisive evidence as it was conceivable to account for it otherwise. Clearly direct observation of the pyramid in its uncollapsed state was required. This was achieved by the following experiment. To eliminate the effect of a possible flattening a drop of suspension containing the same kind of crystals as in fig. 8 was placed on the surface of a viscous solution of polyvinyl alcohol. After evaporation of the xylene, crystals could be seen floating on the polyvinyl alcohol solution with the optical microscope. It was noticed that the different sectors could appear bright or dark even as seen optically (see fig. 20, Keller and Bassett 1960). This effect was preserved after the polyvinyl alcohol solution had solidified. At this stage the surface was metal shadowed, coated with a thick layer of carbon, and the polyvinyl alcohol dissolved in water. It was assumed that the heavily carbon-coated crystals examined electronmicroscopically would retain the configuration they had when deposited on the liquid surface originally. In fig. 9 one of the first photographs taken of this subject is seen. The central fold is absent and the different sectors are in different contrast near the centre as required for a pyramid. The observation that the different sectors could be brighter or darker as seen with the light microscope would follow from the fact that such sectors together with the underlying substrate material would be prisms which deviate light so as to increase or decrease the corresponding image intensity in the microscope.

Hollow pyramids could flatten in two distinct ways. In one case, if all the molecules are parallel to the pyramidal axis, they could slide past each other as visualized in the ridge formation. If the sliding past of molecules is not uniform over the whole crystal and the flattening is not complete, elevated regions, ridges in particular, could form in the course of collapsing. Accordingly, a ridged structure could be an intermediate one between a pyramidal and a flat crystal. In fact it has been observed that ridges disappear rapidly on standing after the drying down of the crystals which accordingly could represent the final stage in the collapse of the pyramid. No definite change of area on the substrate was observed on the disappearance of the ridges in agreement with these ideas. In contrast to the regular striations, the pleats do not disappear in time.

Alternatively, one could consider the molecules in the crystal layers as fixed. In this case the layer would tilt as a whole when the pyramid collapses. This, in fact, would lead to excess material within the basal area of the collapsed pyramid, which would result in folds as, e.g., in fig. 8 being pushed up. These folds would be associated with a tilt of the molecules which should be noticeable from the diffraction patterns. This,

in fact, was confirmed both by x-ray and electron diffraction. X-ray patterns were taken of aggregates obtained by sedimentation where the crystals sedimented horizontally (Keller and O'Connor 1957). Such aggregates formed oriented thin films. As reported previously, the molecules were approximately perpendicular to the film planes. The x-ray patterns obtained with the beam parallel to the film plane were essentially fibre photographs with all $\{hk0\}$ reflections on the equator. The present experiments on aggregates of crystals like those in fig. 8 revealed that the $\{200\}$ reflection was split azimuthally by some 20°. The $\{020\}$ was not split while in the $\{110\}$ the presence of a smaller split was possible but could not be ascertained with certainty owing to the large inherent disorientations of the arcs. For similar reasons, the interpretation of the patterns is necessarily imprecise. It is clear, however, that the b_s* axis lies essentially in the specimen plane while a_s* is rotated out of it. (The asterisk denotes a quantity in reciprocal space.) This implies that the molecules are now inclined to the fibre axis. In terms of the single crystals forming our specimens this would involve crystal layers tilted to the specimen plane for a vertical structure (fig. 15 *a*, Part I). For an oblique structure the molecules would be tilted within the layers which could themselves be lying flat. Physically, we expect the hollow pyramids to collapse during the formation of the x-ray specimen. This and other reasons which will shortly become obvious, lead us to prefer the latter alternative.

The main features of the electron diffraction patterns from crystals as in fig. 8 were consistent with the x-ray evidence. It was reported previously (Bassett *et al.* 1959) that diffraction was selective, different sectors adding different reflections to the pattern given by the crystal as a whole. The details are as follows: with the beam normal to the crystal, the $\{110\}$ reflections were by far the most prominent. They originated primarily from the $\{110\}$ sectors, each sector producing only that pair of $\{110\}$ reflections, from planes parallel to the faces of adjacent sectors. The (020) reflections were mostly present in strengths, which varied from crystal to crystal. The $\{200\}$ reflections, though, were either absent or very weak, in the latter case split azimuthally into two or sometimes three spots. The narrow $\{100\}$ sectors were also diffracting selectively as seen from the Bragg fringes (Bassett *et al.* 1959) but the reflecting conditions could not be determined with greater accuracy.

The observed selection is what one would expect from the collapse of a hollow pyramidal crystal containing triclinic $\{110\}$ sectors with chains parallel to the pyramidal axis; (the existence of $\{100\}$ sectors will be disregarded for the moment). We shall assume that the pyramid is not flat-based (fig. 12). Such a pyramid can be characterized by the direction of the lines along which a plane normal to the pyramid axis intersects the pyramid. We shall refer to the contiguous pyramid based on these lines as the equivalent flat-based pyramid. We shall assume further, that in our case these lines are $\langle 130 \rangle_s$ (or some nearby direction such as $\langle 250 \rangle_s$ or

$\langle 120 \rangle_S$ (see Keller and Bassett 1960)). It will be demonstrated that a number of observations can be accounted for on this basis.

If a pyramid is to be flattened without plastic deformation, its faces must be tilted as unaltered structural entities. For a non-flat-based pyramid in which the surfaces containing the folds are $\{hkl\}_S$, then a condition of flattening is that the new orientation of a sector can be

Fig. 12

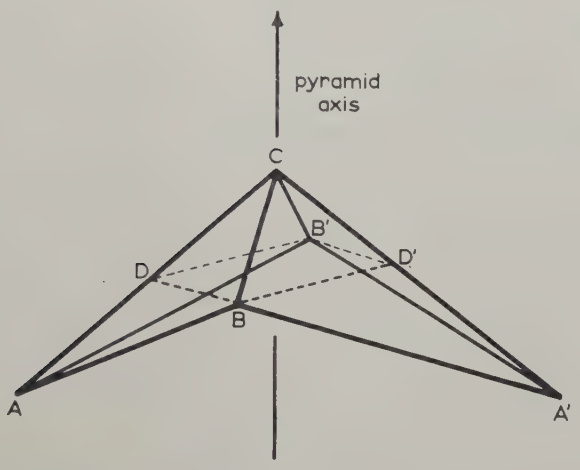

Diagram of the non-flat-based hollow pyramid. The four basal apices A, A′, B, B′ are not coplanar. The lines connecting A and A′, and B and B′, are perpendicular to the pyramid axis but are on different levels. Lines BD, DB′, B′D′ and D′B define the directions along which planes normal to the pyramid axis intersect the pyramid. It is postulated that the crystals are pyramids of this kind where these directions are $\langle 130 \rangle_S$. The base BDB′D′ and apex C define the equivalent flat based pyramid.

related to the old by a single rotation about an axis near to one of the $\langle kh0 \rangle_S$ directions. In our case, these directions would be of $\langle 130 \rangle_S$ type which would account for the observed selection of the $\{110\}$ reflections and with a suitable choice of planes $\{31l\}_S$, for the observed tipping of approximately 20° of the $\{200\}$ reflection out of the specimen plane in the x-ray patterns mentioned previously. Planes of the type $\{312\}_S$ and $\{313\}_S$ give the best fit with the experimental results here and elsewhere. The presence of the $\{020\}$ reflection is not explained on this model, however, as it would still be tipped at least 10° out of the specimen plane, i.e. out of reflecting position (cf. Agar *et al.* 1959) but not so far as is (200). Its presence could be due to misalignments within the crystal, formed possibly as irregularities in the collapse of the pyramid or by the electron beam. This is consistent with the variable intensity which may well be indicative of its accidental origin. In any case, the orientation of the $\{020\}$ planes in a $\{110\}$ sector is intermediate between that set of $\{110\}$

planes which remains essentially untipped and the {200} plus the other set of {110} planes. Thus the indecisive behaviour of the {020} reflection compared with the clear cut extremes of {110} and {200} is at least broadly compatible with the picture proposed.

The above mode of collapse would push up excess material, i.e. would produce pleats, along the corresponding $\langle 130 \rangle_s$ directions. Such lines are seen sometimes in the truncated lozenges (e.g. fig. 6) and are systematic features in the large non-truncated lozenges (figs. 3, 5). If the postulated pyramid collapses through the sliding past of molecules and the formation of roof ridges as discussed previously, these ridges would have to be along $\langle 130 \rangle_s$ directions, and along different ones in different sectors, which is again the observed fact (figs. 3, 5). (For a flat-based pyramid, these directions would be $\langle 110 \rangle_s$.) Thus the hitherto puzzling direction of the striations appears to be accounted for. The choice of pyramid assumed can, moreover, be based on considerations of molecular packing.

We have made three assumptions in our consideration of polyethylene lozenges so far. (1) That the molecules fold along the growing faces, i.e. {110} planes in the {110} sectors. (2) That the lozenges are pyramids with the chain direction parallel to the pyramid axis. (3) That the pyramid is not flat-based but has an equivalent flat-based pyramid bounded by $\{310\}_s$ prism faces. These three requirements are incompatible with a vertical structure in the folded molecular ribbons lying in the {110} growing surfaces. The structure in the ribbon must, in fact, be oblique and the adjacent ribbons must pack obliquely, too. For a pyramid whose faces are $\{311\}_s$, $\{312\}_s$, $\{313\}_s$ etc. adjacent chain segments within a ribbon ({110} prism faces) must be displaced vertically by c_s, $\frac{1}{2}c_s$, $\frac{1}{3}c_s$ and so on respectively. The staggered stacking of adjacent ribbons requires the same segment displacements respectively between successive segments along (**b**). The displacements of contiguous chain folds within each ribbon are twice these amounts. The first two of these pyramids can be achieved uniformly with each fold displaced in the same way relative to its neighbours, the third requires non-uniform displacements (see the discussion for paraffins in Part I). As already mentioned, the planes $\{312\}_s$ and $\{313\}_s$ agree best with the experimental evidence. Of the two, $\{312\}_s$ would give the simpler packing. As, however, the detailed crystallography of the folds is not known, $\{313\}_s$ cannot be ruled out *a priori* on this basis. In these ways it seems we can account for the characteristic striation directions in the {110} sectors in terms of a particular packing of the folds in those sectors. Similar considerations apply to the **b** striations in the {100} sectors, when considering a corresponding six-sided pyramid. In addition, the experimental observation of the striations developed on flattening in crystals heated in suspension being nearer to **b** than are the $\langle 130 \rangle_s$ directions would be accounted for if the pyramids became steeper on heating (by a suitable change in fold packing).

When ridges and pleats are both present, the two modes of collapse could be operative simultaneously. The regular ridges would not

produce appreciable changes in the diffraction conditions, consequently crystals in which the ridge structure is preponderant are not expected to reveal appreciable selection in the diffraction pattern. This is largely in agreement with electron diffraction results on crystals of the kind in figs. 1–5. One would, however, expect selection around the localities of the pleats and the fact that selection of the expected type exists in zones parallel to the appropriate directions (i.e. $\sim \langle 130 \rangle_s$) in the different sectors has already been reported (Agar *et al.* 1959).

The most definite observations on selective diffraction were made on the $\{110\}$ sectors of truncated lozenges; these were the results referred to previously. In these crystals, however, a triangular pleat along **b** is the dominant morphological feature (fig. 8). This is a more complicated type of collapse than that previously dealt with and requires a rotation around $[001]_s$ as well as about a particular $\langle 130 \rangle_s$ direction to relate the sector orientations before and after collapse. The reason for adopting this method of collapse rather than that referred to earlier is not obvious. In our experience, however, the central fold is most regular in the truncated lozenges, though it also appears in some true lozenges, particularly those grown at higher temperatures (cf. figs. 2 and 8). Crystals which collapse in this way to give a well-developed central fold show few, if any, other pleats in the $\{110\}$ sectors. This is to be expected as the excess material in a sector is already taken up in the central fold. The angle of the triangular fold (about 5° in practice) can be calculated subject to the assumptions (2) and (3) above. The best fit is given by assuming planes $\{312\}_s$ and $\{313\}_s$ for the pyramidal surfaces, the former giving $6\frac{1}{2}°$, the latter 3°. These are the two planes which agreed best with the x-ray evidence mentioned previously, which gives confidence in the argument developed here.

In the foregoing, the chains were assumed to lie along the axis of the uncollapsed pyramid. If this condition is relaxed, a variety of other mechanisms could be constructed. However, as seen, the simplest assumption suffices to explain the experimental observations.

It needs pointing out that diffraction effects in the crystals undergo pronounced changes during electron irradiation apart from their tendency to disappear altogether. The sequence will not be described here, it will only be mentioned that the selectivity, where it is originally present, gradually decreases and the crystal becomes uniformly diffracting. One characteristic stage, frequently encountered unless great precautions are taken to minimize the beam damage, is when all $\{hk0\}$ reflections are present, with (200), still very weak, split azimuthally, while other reflections are split both azimuthally and radially (corresponding to a change both in orientation and spacing). This split decreases towards b_s^* in the diffraction pattern, (020) being single. Such a pattern was first brought to our notice by Mitsuhashi (private communication) and was quoted as evidence for a sheared, non-orthorhombic subcell due to the presence of the fold along one of the cell diagonals (Bassett *et al.* 1959). The existence

of the pyramid alone with the chains parallel to the pyramid axis (originating in a way such as that proposed by Reneker and Geil, see above) requires merely that the true unit cell should be of lower symmetry than orthorhombic, i.e. that it should possess an oblique structure. The departure from exact orthorhombic symmetry of the subcell itself must be inferred from splittings of diffraction spots like those just quoted. This splitting is particularly apparent in such patterns. As the selectivity is much reduced, each sector contributes with every main $\{hk0\}$ reflection, consequently, the non-equivalence of $(hk0)$ and $(\bar{h}k0)$ is apparent by inspection. More complex splittings have also been observed during electron bombardment. In particular, triple $\{h00\}$ reflections are characteristic of truncated lozenges. The third spot is probably due to the $\{100\}$ sectors. The detailed effect of electron bombardment, though, will neither be described nor discussed further here.

According to the above explanation of the roof ridges, the molecular orientation should be preserved in them and no essential change in the diffraction conditions for the strongest $\{hk0\}$ reflections and hence no Bragg fringes would be expected. As pointed out in Part I, however, a small disorientation, of order 1°, would be sufficient to produce such fringes if the crystal as a whole is near diffracting position. It was shown that such small disorientations should occur particularly if the crystals are thin which is always the case with the single layer polymer crystals. Also, slight changes, in the chain orientations due to possible molecular readjustments within the ridges (see Part I) may occur. Thus the appearance of extinction fringes in the ridged crystals is not incompatible with the basic mechanism proposed in this paper. Large disorientations, however, would certainly not be expected. Whenever these accompany the striations as, for example, the rotations around the **b** axis in the diffraction patterns of heat treated crystals (Bassett and Keller 1959) the present explanations cannot suffice any longer. It will be recalled that similarly to the analogous cases in paraffins (Part I) in such cases definite pleats are seen in the crystals, which are different from the regular ridges although they might be initiated by them. This folding of the crystals and the accompanying diffraction phenomena promise to be of significance in connection with spherulite formation and the heat relaxation of oriented systems (Bassett and Keller 1959) but is beyond the scope of the present discussion.

The interpretation of the ridges was based on the idea that different crystal phases with the same subcell can exist in polymers. This situation has been well known in paraffins even if the morphological consequences in question have not been pointed out previously. In polymers, however, such a concept was of no meaning while the chemical repeat unit, which is defined as the subcell in the present discussion, was considered as the true unit cell. It becomes meaningful only with the introduction of chain folding. This makes the crystallography of polymers, polyethylene in particular, analogous to that of paraffins, the folds in the

former corresponding to the end groups in the latter. There is a distinction though: the length of the paraffin chain is invariable, while the fold length in polymers can be changed by physical factors How far this difference may affect the phase changes in question still remains to be seen.

In paraffins the existence of different phases is normally assessed by diffraction methods. In principle, this should also be possible with polymers. The fold length can, in fact, be assessed from x-ray diagrams, the corresponding periodicity showing in discrete low-angle reflections when aggregates of single crystals are examined (Keller and O'Connor 1957). Such reflections at low angles have been known to exist in bulk polymers, particularly in drawn fibres, for a long time (e.g. Hess and Kiessig 1944) where they correspond to a periodicity along the fibre axis, i.e. along the chain direction. These are not normally considered as belonging to the crystal structure and are usually believed to be due to an alternation of amorphous and crystalline regions. Such explanations are by no means completely satisfactory and we are under the impression that the whole phenomenon is even qualitatively still unexplained. Once, however, such large periods have been associated with chain folding in the particular case of single crystals it seemed to be natural for us to look for a similar explanation also in other cases where such low angle reflections were found. This view, however, is not generally shared, and owing to the difficulty of obtaining morphological evidence from bulk samples it cannot readily be put to test. Keller and O'Connor (1957) found that a film of sedimented single crystals of polyethylene gave a ' fibre-diagram ' corresponding to a chain orientation normal to the film, and small angle reflections on the meridian when the x-ray beam was parallel to the plane of the film, as would be expected for a vertical structure. If the structure became oblique through the formation of ridges each single low-angle diffraction maximum would be expected to split into two spots along a layer line, the separation of the spots becoming larger with the increasing obliquity of the structure. It would be difficult to test this directly as individual crystal layers cannot be used and in the case of aggregates the nature of the individual crystals is not under control. However, analogous effects are well known in the case of oriented fibres. Here, under the effect of various physical treatments, the meridional low-angle reflections can split along the layer lines while the chains remain parallel to the fibre axis. The nature of this so-called ' four point diagram ' (Meibohm and Smith 1951) is still quite unexplained apart from the recognition that an oblique arrangement of large periodicities is required (Statton 1959). It is tempting to suggest therefore that vertical and oblique phases in the sense discussed in these papers might exist in the fibres and would gives rise to these low angle diagrams. This would naturally imply that the folded configuration would be present in the bulk specimen, a conclusion which is suggested by other morphological evidence (Fischer 1957).

To summarize, it has been shown how very few assumptions, about the packing of the folded chains, namely the simplest modes of staggerings within and between the ribbons within the crystal sectors, are sufficient to relate a great diversity of experimental observations on polymer single crystals.

Acknowledgment

We are indebted to Professor F. C. Frank, F.R.S., for much helpful discussion.

Note added in proof.—Since this paper has been submitted further confirmatory evidence for the model proposed here has been obtained. This together with some additional information will form the subject of a third paper in this series.

References

Agar, A. W., Frank, F. C., and Keller, A., 1959, *Phil. Mag.*, **4,** 32.
Bassett, D. C., Frank, F. C., and Keller, A., 1959, *Nature, Lond.*, **184,** 810.
Bassett, D. C., and Keller, A., 1959, *J. Polym. Sci.*, **40,** 565.
Bunn, C. W., 1939, *Trans. Faraday Soc.*, **35,** 482.
Fischer, E. W., 1957, *Z. Naturf.* A, **12,** 753.
Frank, F. C., Keller, A., and O'Connor, A., 1959, *Phil. Mag.*, **4,** 200.
Hess, K., and Kiessig, H., 1944, *Z. phys. Chem.*, **193,** 196.
Keller, A., 1957, *Phil. Mag.*, **2,** 1171; 1959, *J. Polym. Sci.*, **36,** 361.
Keller, A., and Bassett, D. C., 1960, *J. R. micr. Soc.*, **79,** 243.
Keller, A., and O'Connor, A., 1957, *Nature, Lond.*, **180,** 1289; 1958, *Disc. Faraday Soc.*, **25,** 114.
Meibohm, E. P. H., and Smith, A. F., 1951, *J. Polym. Sci.*, **7,** 449.
Niegisch, W. D., 1959, *J. Polym. Sci.*, **40,** 263.
Statton, W. O., 1959, *J. Polym. Sci.*, **41,** 143.

Charge Effects during Inhomogeneous Deformation of Rocksalt†

By F. Rueda† and W. Dekeyser
Laboratorium voor Kristallografie, Rozier 6, Ghent, Belgium

[Received September 8, 1960]

Abstract

The electrical charge flow associated with an inhomogeneous plastic deformation, as first described by Fishbach and Nowick, was further investigated. Microindentations were made in order to localize the deformation to a single small volume. In these conditions the observed effect corresponds qualitatively to a transport of negative charge by moving dislocations. Small additions of cadmium ions enhance the effect slightly. Flexion gives strong but non-reproducible signals.

§ 1. Introduction

Fishbach and Nowick observed an electrical signal when rocksalt crystals were indented. i.e. inhomogeneously deformed (Fishbach and Nowick 1955, 1958). We examined this effect further in relation to experiments carried out in this laboratory about charged dislocations (Amelinckx *et al.* 1959, Remaut *et al.* 1960, Remaut and Vennik 1961. Pure and doped rocksalt crystals, grown in the laboratory, have been used and some tests with crystals submitted to flexion were also performed. As far as pure crystals are concerned, our observations are different from those of Fishbach and Nowick; the origin of this discrepancy could be found. In this paper, we describe some of the results which have been obtained so far.

§ 2. Experimental

Two Leitz microindentation hardness testers were used. The first was a standard type instrument, the second had some special features. It had a stainless steel point indenter which was electrically insulated from the rest of the instrument and could be connected to an outside circuit without hampering its movement. The shape of this steel point was similar to that of the diamond identer of the current type apparatus. Both instruments allowed controlled loading of the indenter and microscopic observation of the produced pattern. In most of the experiments the applied weight was 100 g, the indentation process slow and of the order of 10 μ/min. By indenting etched crystals, which were

† Communicated by the Authors.
‡ On leave from Instituto de Fisica ' Alonso Santa Cruz ', Madrid.

etched again afterwards, we made sure that only the typical rosette patterns were produced. The set-up and the electrical circuit is shown in fig. 1. Two alternative arrangements were used. In one a gold film, evaporated on one of the faces of the crystal, was connected to the grid, and through *Rg* to the earth. In the other, the probe was the brass holder of the diamond point, or the steel point.

Fig. 1

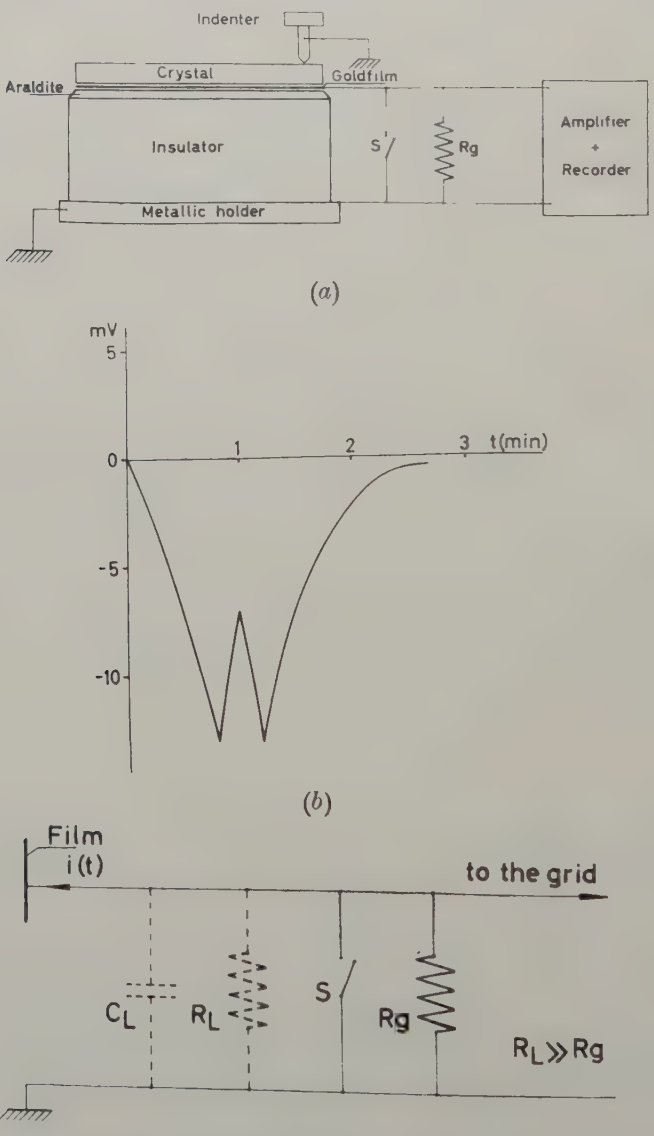

(*a*) Electrical circuit; (*b*) recorded signal; (*c*) equivalent circuit.

The crystal was fixed with araldite to a rigidly mounted insulator. All necessary precautions to avoid effects of humidity and other possibilities of disturbance were taken. The experiments were performed in a small dry box, which also acted as a Faraday cage.

§ 3. Results

3.1. *Pure Crystals*

A considerable number of experiments were made to ascertain that the signal was not due to other causes than the plastic deformation. The gold film was evaporated on different faces of the crystal and the distance of the indentation point varied with respect to it. In this way a variety of signals was recorded; a typical one and the arrangement used are shown in fig. 1. This type of signal is reproducible in the stated conditions, provided that the distance of the indenter to the edge of the

Fig. 2

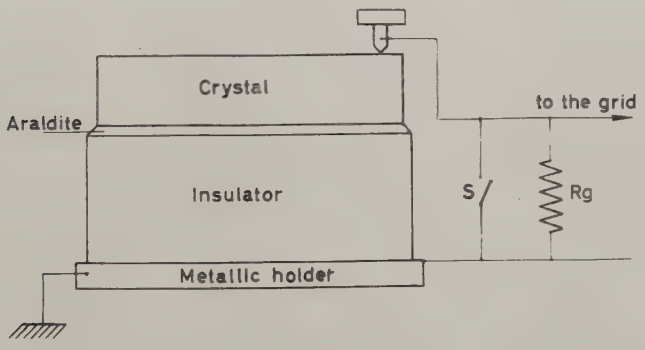

(*a*)

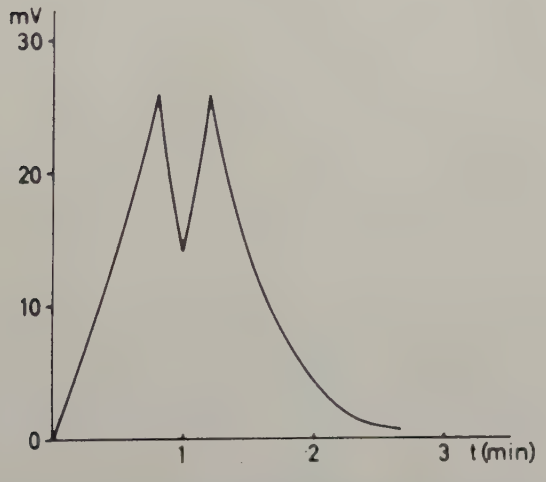

(*b*)

(*a*) Alternative arrangement ; (*b*) recorded signal.

crystal is greater than 0·5 mm. In principle, the indentations were always made near the centre of sub-grains. The M shape is due to a slowing down of the indenter. This only happens when the overall speed of penetration of the point is slow, otherwise no bump is observed. That the M shape is due to this could be checked by performing a similar indentation test on an Instron machine. The recorded 'stress–strain' type curve showed two sharp changes of slope corresponding to the

Fig. 3

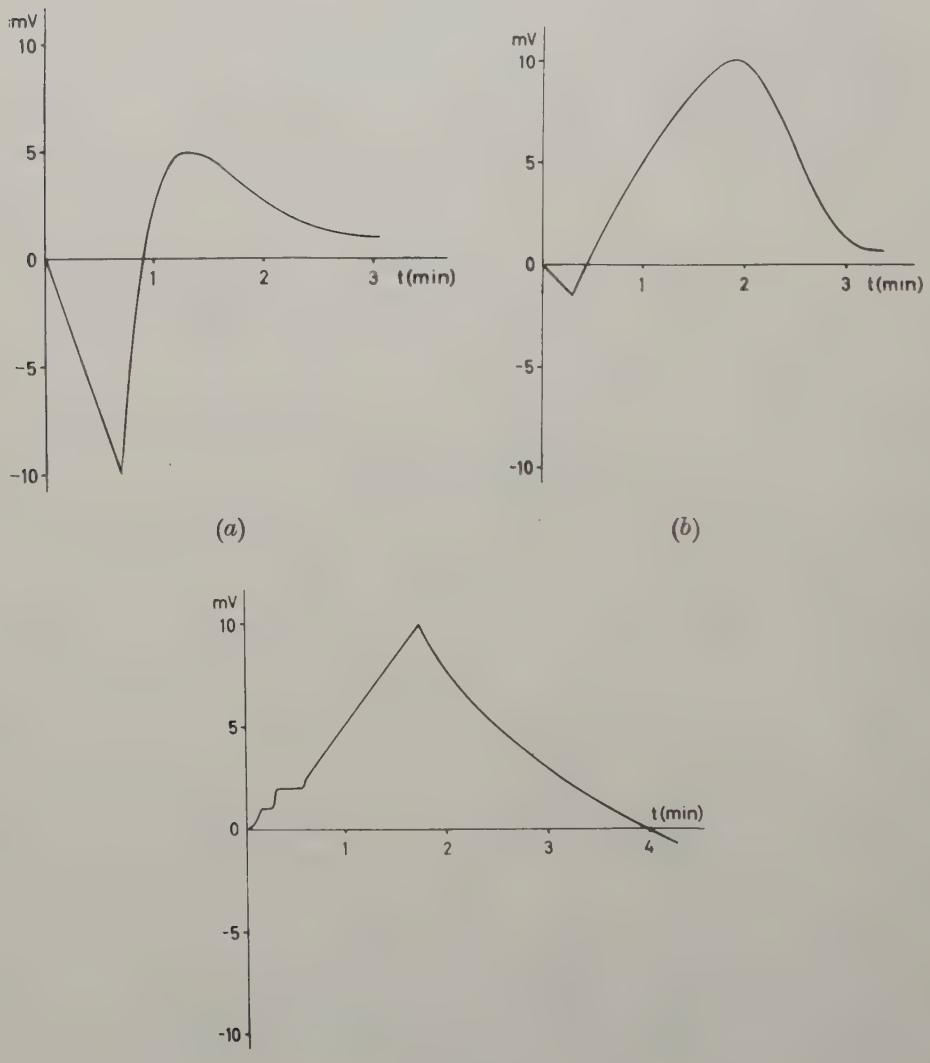

(*a*) Sharp indenter, crystal deposited on a flat base; (*b*) flat indenter, crystal deposited on a flat base; (*c*) flat indenter, crystal deposited on a rough base.

decrease and further increase of the electrical signal. A similar M-shaped signal is recorded when the indenter is the probe (fig. 2). However, the sign of the induced charge is now reversed and its magnitude somewhat greater. As seen in fig. 1, the signal is always negative when the indenter is not the electrode. This is opposite to what Fishbach and Nowick observed. In order to trace back the origin of this, we tried to reproduce their arrangement. The crystal (thickness 2 mm) was deposited on a flat steel base acting as probe (fig. 3 (*a*)). A flat indenter ($\phi = 2$ mm), connected to the earth was used, the applied load was 200 g (fig. 3 (*b*)).

As we presumed that the deformation was not localized around the indenter in this case, the crystal was placed on a rougher base (a grid as used in electron microscopy) in order to enhance this effect. Figure 3 (*c*) shows that the signal is now completely reversed.

3.2. *Doped Crystals*

A number of crystals, grown from melts to which quantities ranging from 0·09% to 0·6% of $CdCl_2$ were added have also been examined. The charge flow, obtained in similar conditions and normalized for indentations of equal sizes, rises with the cadmium content; the increase is however small. As an example we quote the values, obtained for pure rocksalt and the crystals containing the highest percentage of cadmium. They are respectively $1{\cdot}39 \pm 0{\cdot}13$ and $1{\cdot}66 \pm 0{\cdot}05$ c 10^{-11}.

3.3. *Bending*

As a complement to these experiments, several bars of NaCl with a thin film of gold deposited on one face acting as active electrode have been bent. Very strong signals have been observed of positive and negative sign. The magnitude of the signal changes from experiment to experiment. When the bar is deformed slowly and the deformation stopped when the electrical effect starts, new slip bands are always observed. When deformation was stopped before an electrical signal could be observed, no movement of dislocations or creation of new slip bands could be found on subsequent etching.

§ 4. Conclusions

From the described experiments we can deduce that :

(i) A negative charge flow is observed when dislocations, formed on one side of the crystal, move towards the probe. Expanding loops thus disturb the electric field in the swept area. Whether the dislocations become charged during their motion or not, needs further investigation.

(ii) The results of Fishbach and Nowick are due to a deformation involving creation of dislocations on opposite faces of the crystal. In this way, a mixed effect is observed, the dislocations running in opposite

direction to those formed around the indenter play a more prominent rôle, because they are nearer the probe (cf. figs. 1 and 3).

(iii) Addition of very small quantities of divalent ions influences the effects.

Experiments, now in progress, concerning the effect of temperature, and simultaneous measurements of ionic conductivity may allow the interpretation of the described results.

Acknowledgments

We are much indebted to E.R.A. (European Research Associates) Brussels for their support. In particular, one of us (R.F.) expresses his gratitude for a research fellowship. We also thank the Leitz works, Wetzlar, Germany, who were willing to modify considerably the standard apparatus.

References

Amelinckx, S., Vennik, J., and Remaut, G., 1959, *J. Phys. Chem. Solids*, **11**, 170.

Fishbach, D. B., and Nowick, A. J., 1955, *Phys. Rev.*, **99**, 1333; 1958, *J. Phys. Chem. Solids*, **5**, 302.

Remaut, G., Vennik, J., and Amelinckx, S., 1960, *J. Phys. Chem. Solids*. (in the press).

Remaut, G., and Vennik, J., 1961, *Phil. Mag.*, **6**, 1.

The Soft X-Ray Emission Spectra of Sodium, Beryllium, Boron Silicon, and Lithium†

By R. S. Crisp‡ and S. E. Williams
Department of Physics, University of Western Australia, Nedlands, W.A.

[Received September 5, 1960]

Abstract

Emission band forms of several elements obtained with a photon-counting spectrometer are compared with previously published spectra. The sodium $L_{23}I(E)$ vs λ curve departs from the free electron parabola at energies less than about 1 ev from the Fermi limit in accord with the theoretical form. The sodium extrapolated band width is $2{\cdot}6 \pm 0{\cdot}3$ ev. In beryllium K there is no contribution of p states from the bottom of the overlapping second zone. Zone overlap is estimated at 1–2 ev. The extrapolated band width for boron K is estimated at $14{\cdot}1 \pm 0{\cdot}8$ ev. The L_{23} band of silicon differs from those previously published but is apparently not affected by the temperature or the purity of the silicon. The extrapolated width is $13{\cdot}4 \pm 0{\cdot}8$ ev. A strong line at 253 Å and a blue fluorescence which accompanies the lithium K spectrum are shown to be connected with the reaction with lithium of hydrocarbon molecules not condensed by the cold trap.

§ 1. Introduction

In addition to the material already published on the soft x-ray emission spectra of Li, Al, Mg and K (Crisp and Williams 1960 a, b, Crisp 1960) the photon-counting spectrometer (Fisher *et al.* 1958) has provided new information about the band forms of the K or L_{23} spectra of several other elements of low atomic number. The direct registration of intensities, the use of low-beam currents to reduce the power dissipated in the target to a few watts, and the ability of the photon-counting instrument to follow changes of intensity with time have made possible confirmation of features not always detectable photographically, as well as corrections to some of the band forms obtained previously by photographic photometry. The instrumental window, or resolution, in all cases was 0·9 Å on the previously adopted criterion (Fisher 1954). All the spectra reproduced here, except those for Li, were obtained with a glass grating. The pressure in the target chamber was $1\text{–}2 \times 10^{-6}$ mm Hg and the target was almost surrounded by a copper baffle cooled to about $-110°$C by external conduction to a liquid air reservoir.

† Communicated by the Authors.
‡ Now at National Research Council, Ottawa, Canada.

§ 2. Sodium

The L_{23} spectrum of Na at 110°K, published by Skinner (1940), shows a departure from the free electron parabola just before the high-energy limit is reached. Skinner attributed this feature to zone overlap, but could not observe it at 300°K. The Na spectrum published by Tomboulian (1957) does not show this feature, and it has been tacitly assumed that there is no departure from the free electron shape. Figure 1† shows a sodium L_{23} spectrum with a distinct departure from the free electron shape near the high-energy limit. This feature can always be obtained from a fresh target cooled to about 300°K, but is less apparent when the target surface is contaminated.

A curve of $I(E) \propto E^{1/2}$ has been fitted on a wavelength scale to the middle portion of the spectrum to indicate the extrapolated band width, $2{\cdot}6 \pm 0{\cdot}3$ ev. To the high-energy side of about 420 Å the spectrum diverges from the $E^{1/2}$ curve, following the trend of the theoretical $N(E)$ vs E curve proposed by Jones and Mott (1937). Their curve is included in the diagram, with a broken vertical line indicating the approximate position of the Fermi limit. This interpretation accords with other evidence that the Fermi surface in Na is nearly spherical and that as a consequence the occupied states do not come closer than about 1 ev to the nearest zone boundary.

§ 3. Beryllium

Measurements on fourth-order K spectra of Be show that the metal edge extends to between 25 and 30% of the intensity at the peak. The width of this edge estimated from measurements on second, third and fourth order spectra is about 0·2 ev which agrees with Skinner's (1940) result since the temperature of the surface of a solid Be target is probably appreciably higher than that of the cooling water. According to Skinner the contribution of states in the second Brillouin zone " can just be detected as a slight upward curvature at the edge ". None of our Be K spectra show any such upward curvature, though the upper limit of the metal edge is quite clearly marked. This is taken as evidence that there are no low lying p states in the second zone. The prominent spike in the MgL_{23} spectrum shows that s states are present in the bottom of the second zone, and this can be assumed to hold for Be. By extrapolating the $I(E)$ vs λ curve of Be past the metal edge, the area corresponding to the unoccupied part of the zone can be estimated approximately. This part of the zone is not filled because s states in the overlapping second zone are occupied. If a hypothetical $I(E)$ vs λ curve is drawn (with $I(E) \propto E^{3/2}$) for these s states, having the same area up to the metal edge, the amount of zone overlap can be estimated as between 1 and 2 ev.

† All figures are shown as plates.

§ 4. Boron

A fourth-order boron K spectrum is reproduced in fig. 2. The points shown have ordinates proportional to $I(E)^{2/3}$, so if for the bottom of the band $I(E) \propto E^{3/2}$, the intersection of the straight line fit with the axis should define the lower band limit. The 'band end' recorded by Skinner (1940) on the high-energy side involves intensities less than 1% of those at the peak and the existence and extent of this 'band end' are both uncertain in our spectra. Assuming that the band end extends to 65·5 Å, the extrapolated width of the boron K band is then $14{\cdot}1 \pm 0{\cdot}8$ ev. This is comparable with the 17 ev obtained by Coster and Hof (1940), but is much less than Skinner's estimate of 30 ± 2 ev which included a long tail as well as the 'band end'. The short-wavelength fall of the band shown in fig. 2 is distrinctly concave towards high energies, not straight as other published spectra show. Its width is 2·6 ev (instrumental width 0·6 ev) which is consistent with emission involving the valence band of a semi-conductor.

§ 5. Silicon

Silicon L_{23} spectra from evaporated Si have been published by Skinner (1940) and from solid crystalline Si by Coster and Hof (1940). The Si spectrum in fig. 3. was obtained from a target of powdered AR grade Si which glowed red-hot under the action of the electron beam. An identical spectrum was obtained from a single crystal of 30-ohm cm p-type Si. The temperature of the crystalline Si varied from about 100°c for the lowest target powers (2 w) to possibly several hundred degrees for the spectrum of fig. 3, but no changes with temperature have been observed. The spectrum of fig. 3 resembles that of Coster and Hof (1940) in that the maxima are the same in number and position, but the indication is that in the photograph taken by these authors the emulsion was seriously saturated. Skinner's spectrum, which closely resembles the SiO_2 spectrum of Coster and Hof, shows a single broad maximum which cannot be explained by saturation of the emulsion.

The points plotted are proportional to $I(E)^2$, assuming $I(E) \propto E^{1/2}$ for the bottom of the band so the intersection of the line with the axis gives the lower band limit. The extrapolated width of the band is then $13{\cdot}4 \pm 0{\cdot}8$ ev in agreement with Skinner's 14 ev.

§ 6. Lithium

A strong line at 253 Å accompanying the Li K spectrum was attributed in an earlier paper (Fisher *et al.* 1958) to contamination by kerosene in which the solid Li had been stored. Subsequently it has been found that the line was produced from an evaporated Li target, when the Li had previously been vacuum melted and the target was nearly surrounded by a copper baffle cooled to about −110°c. A blue fluorescence is closely associated with the appearance of the line and both, needless to say, develop only on a lithium surface. A strong evaporation of Li which coats the baffle as well as

the target is found to prevent the appearance of either fluorescence or line (Crisp and Williams 1960 b).

Figure 4 (*a*) shows the decrease with time of the peak intensity of Li K, and also, since the band shape does not change, of the intensity in the tail of the Li band at 253 A. The decrease is roughly exponential, the intensity falling to half in about $1\frac{1}{4}$ min. The variation with time of the intensity at 253 A is shown in fig. 4 (*b*). When the exponential decrease is subtracted, there is left a component whose intensity increases roughly as $[1-\exp(-xt)]$ which represents the growth of the Li line. A continuous chart record showing successive traversals of the Li K band and Li line for 60 min following the recording of fig. 4 (*c*) showed that after reaching an equilibrium value the line intensity remained constant, while the Li K peak intensity fell by 90%.

The fall in intensity of the Li K band is mainly caused by the deposit of a layer of carbon on the target following decomposition of condensed hydrocarbon molecules by the electron beam. The exponential fall indicates that the carbon film thickness grows at a constant rate. Carbon contamination of Mg (Crisp 1958) was almost eliminated when the baffle was cooled below a critical temperature of -90°C, indicating that a substantial proportion of the hydrocarbon molecules were removed by condensation on the cooled surfaces. However, fluorescence, carbon contamination, and growth of the Li line were still observed for Li targets. While it is possible that Li_2O and Li_3N could be formed on the target, both would be decomposed by electron bombardment, and Catterall and Trotter (1959) have observed this for Li_2O. It seems more probable that hydrocarbon molecules which do not condense on the cooled surfaces react with Li, but not with Mg.

The discovery that a heavy evaporation of Li inhibited development of the Li line supports this explanation. When the baffle surfaces surrounding the target are coated with Li this will help remove hydrocarbons from the residual vacuum and less of these will be available with the Li on the target to produce fluorescence and the Li line. There is no marked decrease in pressure which would be expected if nitrogen were the reactant, but there is a marked slowing of the rate of decrease in intensity of the Li K band, indicating a much slower rate of deposition of carbon. Figure 4 (*d*) shows a lithium K spectrum in which no line has appeared a few minutes after a heavy evaporation of Li. A continuous record of the Li K band and the region of the Li line for 100 min following this evaporation showed that no line developed and that the Li K peak intensity decreased by only 33%. This is one-quarter of the contamination rate for the conditions of fig. 4 (*c*).

It is concluded therefore, that removal of hydrocarbons by the widely spread Li film, decreases the thickness of the hydrocarbon layer reacting with lithium on the target surface to an extent that makes the line undetectable and the associated fluorescence invisible, and consequently lowers the rate of decomposition of hydrocarbon molecules on the target by the electron beam so reducing the rate at which the Li K band intensity drops.

Acknowledgments

We are indebted to Dr. N. H. Fletcher, formerly of the C.S.I.R.O. Radiophysics Laboratory, Sydney, for the samples of single crystal Silicon. R.S.C. desires to acknowledge a grant from the Australian Atomic Energy Commission, during tenure of which this work was done. It is a pleasure to record the continued interest and encouragement of Professor C. J. Birkett Clews.

References

Catterall, J. A., and Trotter, J., 1959, *Phil. Mag.*, **4,** 1164.
Coster, D., and Hof, S., 1940, *Physica*, **7,** 655.
Crisp, R. S., 1958, *Aust. J. Phys.*, **11,** 449.
Crisp, R. S., and Williams, S. E., 1960 a, *Phil. Mag.*, **3,** 525; 1960 b, *Ibid.*, **5,** 1205.
Fisher, P., 1954, *J. opt. Soc. Amer.*, **44,** 665.
Fisher, P., Crisp, R. S., and Williams, S. E., 1958, *Opt. Acta*, **5,** 31.
Jones, H., and Mott, N. F., 1937, *Proc. roy. Soc.* A, **162,** 49.
Skinner, H. W. B., 1940, *Phil. Trans.*, **239,** 95.
Tomboulian, D. H., 1957, *Handb. Phys.*, **30,** 246 (Berlin: Springer).

A Variational Approach to Correlation in an Electron Gas†

By W. H. Young
Department of Physics, The University, Sheffield

[Received July 21, 1960]

Abstract

A method is proposed for calculating correlation energies and pair functions associated with an electron gas at any density. Upper bounds to the exact energy, lying however at least as low as the corresponding plane wave results are guaranteed and exact solutions are obtained in the high- and low-density limits. The technique used is that of allowing a periodic electron density and a proof emerges of the recent conjecture of Overhauser that there exist one-particle states energetically more favourable than the usual plane wave orbitals. It is concluded that in the ground state a single-particle approximation implies static spin density waves of wavelength proportional to the usual separation electron parameter r_s, at least for r_s sufficiently large.

§ 1. Introduction

The modern theories of the electron gas, for example those of Wigner (1938), Bohm and Pines (1953), Gell-Mann and Brueckner (1957) and Cowan and Kirkwood (1958), have proved to be illuminating and valuable within their own restricted domains of validity. However, each has its own peculiar difficulties and it seems fair to say that there does not appear to be a simple, reliable method applicable over a wide density range. It is therefore of considerable interest to note the recent speculation of Overhauser (1960 a, b), and of Gross (1960) that the Hartree equations appropriate to an electron gas have solutions of a periodic nature corresponding to a total energy below that of the usual plane wave solutions. In the following we will prove the latter assertion, show that the periodic orbitals are related to Wigner's lattice and demonstrate that the Hartree–Fock method promises to give accurate information for an electron gas below a certain density. In particular we show that exact results are forthcoming in the limits of very high and very low densities.

The technique used is the variational principle employing a Slater determinant of orbitals corresponding to the von Weizsäcker approximation (March and Young 1958). The latter orbitals are capable of achieving the high and low density results mentioned in the previous paragraph. Should it prove necessary, a discussion using more general orbitals is entirely possible but it is much easier to follow the behaviour of the various dynamical functions as the density is widely varied in the present approximation. The use of the von Weizsäcker orbitals

† Communicated by the Author.

also reveals an interesting relation with the results of Young and March (1960) (subsequently referred to as YM) from which indeed, the following work stemmed. YM used a method suggested by Mayer (1951) and specified a second-order density matrix characterizing the system. The advantage of the method was its wide applicability, its disadvantage was that the density matrix was not obviously derivable from a many-body wave function. In this respect the following constitutes an improvement over the YM investigation.

The work is divided into two parts, § 2 dealing with a one-spin and § 3 dealing with a two-spin electron gas. It has been thought worth while to present the ferromagnetic theory since the effect of allowing a periodic electron density alone may thereby be studied. In § 3, the additional complication of the juxtaposition of the two kinds of spin density waves is resolved.

§ 2. The One-spin Gas

It has been shown (Mayer 1955) that the investigation of a degenerate electron gas for all densities $3/4\pi r_s^3$ is equivalent to considering the ground state of the Hamiltonian

$$H = -\frac{1}{2\lambda}\sum_1^N \nabla_{\mathbf{r}_i}^2 + \frac{1}{\lambda}\left\{\sum_{i<j}\frac{1}{|\mathbf{r}_i' - \mathbf{r}_j'|} - \sum_1^N \int \frac{d\mathbf{r}_0}{|\mathbf{r}_i' - \mathbf{r}_0|} + \tfrac{1}{2}\int\int \frac{d\mathbf{r}_0 d\mathbf{r}_1}{|\mathbf{r}_0 - \mathbf{r}_1|}\right\} \quad (1)$$

of a plasma of N particles in a volume $\mathcal{N}$ for all values of the coupling parameter $\lambda = (4\pi/3)^{1/3} r_s$. The appropriate energy (in atomic units) is then

$$\epsilon = -\frac{1}{2\lambda^2}\int [\nabla_{\mathbf{r}}^2 \gamma(\mathbf{r}' \mid \mathbf{r})]_{\mathbf{r}'=\mathbf{r}}\, d\mathbf{r} - \frac{1}{2\lambda}\int\int \frac{[1 - 2P(\mathbf{r}'\mathbf{r})]}{|\mathbf{r}' - \mathbf{r}|}\, d\mathbf{r}'\, d\mathbf{r}, \quad (2)$$

where γ and P are respectively the usual first-order spinless density matrix and pair function (for precise definitions see YM). For further details of the density matrix formalism reference may be made to Löwdin (1955), Mayer (1955) and Koppe (1957). Formula (2) has been used previously by Mayer and YM under the usual Sommerfeld condition of constant particle density but it is readily seen to retain its validity under the more general periodic conditions.

We now recognize the desired density periodicity in the following way. Suppose we consider the high coupling limit $\lambda \to \infty$. Then by an argument of Wigner (1938) the potential energy becomes all-important and the particles take up positions on a body-centred cubic lattice. On relaxing the coupling we obtain a periodic particle density and we are now free to employ the conventional methods available for such problems. Strictly the particular choice of lattice should be chosen on energy grounds at any given coupling, but as this seems impracticable we will restrict our considerations to the body-centred cubic case. It should be remembered, however, that an upper bound to the energy below the plane wave value is obtained whatever lattice is used.

We now choose as trial wave function the single Slater determinant of Bloch orbitals

$$\phi_{\mathbf{k}}(\mathbf{r}) = \frac{J^{1/2}}{N^{1/2}} \exp(2\pi i) \frac{\mathbf{k} \cdot \mathbf{R}}{N^{1/3}}, \quad . \quad . \quad . \quad . \quad . \quad . \quad (3)$$

which have been discussed by March (to be published). Here the $\mathbf{k}$ are the N vectors of least moduli having integer coordinates and J is the Jacobian of $\mathbf{R}(\mathbf{r})$, the latter having the properties

$$\mathbf{R}(\mathbf{r}+\boldsymbol{\mu}) = \mathbf{R}(\mathbf{r}) + \boldsymbol{\mu}, \quad \mathbf{R}(-\mathbf{r}) = -\mathbf{R}(\mathbf{r}), \quad . \quad . \quad . \quad . \quad (4)$$

$\boldsymbol{\mu}$ being any translation vector between equivalent lattice points. $\mathbf{R}$ is now available for energy minimization using the variational principle. Computing matrices in the usual way we obtain

$$\gamma(\mathbf{r}' \mid \mathbf{r}) = [J(\mathbf{r}')\, J(\mathbf{r})]^{1/2}\, l\{\mathbf{R}(\mathbf{r}') - \mathbf{R}(\mathbf{r})\} \quad . \quad . \quad . \quad . \quad . \quad (5)$$

and

$$2P(\mathbf{r}'\, \mathbf{r}) = J(\mathbf{r}')\, J(\mathbf{r})\, [1 - l^2\{\mathbf{R}(\mathbf{r}') - \mathbf{R}(\mathbf{r})\}] \quad . \quad . \quad . \quad . \quad (6)$$

where

$$l(\mathbf{r}) = 3\zeta^{-3}(\sin\zeta - \zeta\cos\zeta), \quad \zeta = (6\pi^2)^{1/3} r. \quad . \quad . \quad . \quad . \quad (7)$$

Hence, using the periodicity condition (4) we obtain from (2),

$$\frac{\epsilon}{N} = \frac{1}{\lambda^2}\int_C \left[\frac{(6\pi^2)^{2\,3}}{10} J \sum_1^3 (\nabla R_i)^2 + \tfrac{1}{8}\frac{(\nabla J)^2}{J}\right] d\mathbf{r} - \frac{1}{2\lambda}\int_{\text{All space}} \frac{[1 - F(\xi)]}{\xi} d\boldsymbol{\xi} \quad (8)$$

where

$$F(\boldsymbol{\xi}) = \int_C 2P(\mathbf{r} + \boldsymbol{\xi}\, \mathbf{r}) d\mathbf{r} = \int_C J(\mathbf{r} + \boldsymbol{\xi})\, J(\mathbf{r})\, [1 - l^2\{\mathbf{R}(\mathbf{r} + \boldsymbol{\xi}) - \mathbf{R}(\mathbf{r})\}]\, d\mathbf{r}, \quad (9)$$

C denoting a unit volume Wigner–Seitz cell defined by the body-centred cubic lattice. From (5) we see J plays the rôle of the particle density.

It is now possible to see that exact descriptions are possible in the two density limits using (8). When $\lambda \to 0$ only kinetic energy is important and $\mathbf{R} = \mathbf{r}$ gives the usual plane wave result. When $\lambda \to \infty$ only potential energy is important and the Wigner lattice of point charges is given by

$$J = \sum_i \delta(\mathbf{r} - \mathbf{X}_i), \quad . \quad . \quad . \quad . \quad . \quad . \quad . \quad . \quad (10)$$

the $\mathbf{X}_i$ denoting all the lattice points. (To obtain (10), one defines $\mathbf{R}(\mathbf{r})$ within C by the coordinates of the point where the straight line from the centre of the cell to $\mathbf{r}$ meets the cell boundary, (4) being used to extend the definition to all space.) The average pair function then becomes

$$F(\mathbf{r}) = J - \delta(\mathbf{r}), \quad . \quad . \quad . \quad . \quad . \quad . \quad . \quad . \quad (11)$$

the exchange term cancelling the charge at the origin since $\mathbf{R}(0) = 0$. Use of (11) in (8) then gives the exact energy per particle in this limit of

$$-\frac{1}{2\lambda}\left(\int_{\text{All space}} \frac{d\boldsymbol{\xi}}{\xi} - \sum_{X_i \neq 0} \frac{1}{X_i}\right) = -\frac{0{\cdot}896}{r_s}, \quad . \quad . \quad . \quad . \quad (12)$$

the latter following from a Madelung calculation (see Wigner 1938).

Since, for large r_s, (12) is lower than the plane wave result, we have proved Overhauser's conjecture for the ferromagnetic gas, at least for sufficiently low densities.

§ 3. The Two-spin Case

In setting up this case we must consider the way in which the two kinds of particles are to be associated with the Wigner lattice. In order to obtain the desired results, it seems necessary to consider the body-centred cubic lattice as consisting of two interpenetrating simple cubic sub-lattices, each associated with a given spin. In coming to this conclusion the results of § 8 of YM were particularly useful and reference to fig. 4 of that article should prove helpful to the reader.

Accordingly we describe the situation by a determinantal wave function of $N/2$ orbitals $J^{1/2}/N^{1/2}\exp(2\pi i)(\mathbf{k}\,.\,\mathbf{R}/N^{1/3})$ associated with one spin and $N/2$ orbitals $K^{1/2}/N^{1/2}\exp(2\pi i)(\mathbf{k}\,.\,\mathbf{S}/N^{1/3})$ associated with the other, the $\mathbf{k}$ consisting of the $N/2$ vectors of smallest moduli having integer coordinates and J and K being the Jacobians of $\mathbf{R}$ and $\mathbf{S}$ respectively. We also require the periodicity conditions

$$\mathbf{R}(\mathbf{r}+\boldsymbol{\mu}_1)=\mathbf{S}(\mathbf{r})+\boldsymbol{\mu}_1 \quad . \quad . \quad . \quad . \quad . \quad . \quad . \quad . \quad (13)$$

and

$$\mathbf{R}(\mathbf{r}+\boldsymbol{\mu}_2)=\mathbf{R}(\mathbf{r})+\boldsymbol{\mu}_2, \quad \mathbf{R}(-\mathbf{r})=-\mathbf{R}(\mathbf{r}) \quad . \quad . \quad . \quad . \quad (14)$$

where $\boldsymbol{\mu}_1$ and $\boldsymbol{\mu}_2$ are translation vectors between equivalent points in the body-centred and either simple cubic lattice respectively. The spin densities are $\frac{1}{2}J$ and $\frac{1}{2}K$, the total density being $\frac{1}{2}(J+K)$. We obtain in a straightforward manner

$$\gamma(\mathbf{r}'\,|\,\mathbf{r})=\tfrac{1}{2}\{J(\mathbf{r}')J(\mathbf{r})\}^{1/2}\,l\{\mathbf{R}(\mathbf{r}')-\mathbf{R}(\mathbf{r})\}+\tfrac{1}{2}\{K(\mathbf{r}')K(\mathbf{r})\}^{1/2}\,l\{\mathbf{S}(\mathbf{r}')-\mathbf{S}(\mathbf{r})\} \quad . \quad . \quad . \quad (15)$$

and

$$2P(\mathbf{r}'\mathbf{r})=\tfrac{1}{4}\{J(\mathbf{r}')+K(\mathbf{r}')\}\,\{J(\mathbf{r})+K(\mathbf{r})\}-\tfrac{1}{4}J(\mathbf{r}')J(\mathbf{r})l^2\{\mathbf{R}(\mathbf{r}')-\mathbf{R}(\mathbf{r})\} \\ -\tfrac{1}{4}K(\mathbf{r}')K(\mathbf{r})l^2\{\mathbf{S}(\mathbf{r}')-\mathbf{S}(\mathbf{r})\} \quad (16)$$

where here

$$l(\mathbf{r})=3\zeta^{-3}(\sin\zeta-\zeta\cos\zeta), \quad \zeta=(3\pi^2)^{1/3}r. \quad . \quad . \quad . \quad . \quad (17)$$

Equation (2) is again applicable to give

$$\frac{\epsilon}{N}=\frac{1}{\lambda^2}\int_D\left\{\frac{(3\pi^2)^{2/3}}{20}J\sum_1^3(\nabla R_i)^2+\frac{1}{16}\frac{(\nabla J)^2}{J}\right\}d\mathbf{r}-\frac{1}{2\lambda}\int_{\text{All space}}\frac{\{1-F(\boldsymbol{\xi})\}}{\xi}d\boldsymbol{\xi} \quad (18)$$

where

$$F(\boldsymbol{\xi})=\int_D P(\mathbf{r}+\boldsymbol{\xi}\,\mathbf{r})d\mathbf{r}=\tfrac{1}{4}\int_D\{J(\mathbf{r}+\boldsymbol{\xi})J(\mathbf{r})[1-l^2\{\mathbf{R}(\mathbf{r}+\boldsymbol{\xi})-\mathbf{R}(\mathbf{r})\}] \\ +J(\mathbf{r})K(\mathbf{r}+\boldsymbol{\xi})\}\,d\mathbf{r}, \quad . \quad . \quad . \quad . \quad . \quad . \quad . \quad (19)$$

D denoting two adjacent Wigner–Seitz cells defined by the body-centred cubic lattice. The apparent lack of symmetry with respect to $\mathbf{R}$ and $\mathbf{S}$ in (19) is due to the use of (13).

At high densities $\mathbf{R} = \mathbf{r}$ gives the plane wave results, while at low densities a suitably defined step function for $\mathbf{R}$ leads to a distribution of point charges on one of the simple cubic structures for $\frac{1}{2}J$. An analysis somewhat similar to the one-spin case then reproduces the Wigner result (12).

§ 4. Discussion

We have seen above how one may profitably modify the usual one-particle model of an electron gas to obtain a scheme which is rigorously based on the variational principle in such a way that at all densities an upper bound to the exact energy at least as low as the plane wave value is assured. This upper bound property is by no means a trivial consequence of the use of the variational principle, as it is well known that a trial wave function chosen without due regard to the physical conditions of the problem can lead to energies which are too low. Since furthermore it has been shown that exact results are obtained in the high- and low-density limits, one might hope for accuracy at intermediate densities†. While detailed numerical calculations in the region corresponding to real metallic densities are not as yet available, work is currently being undertaken in this Department in which the aim is to obtain the accurate predictions of this approach and that of YM over a wide density range.

A point of interest implied by the results of § 3 is the form of the spin density waves in the ground state. It is felt that by relating them to the Wigner lattice, as described above, we obtain a more accurate description within a one-body framework than that of Overhauser (1960 a, b), useful though the latter was in demonstrating the existence of new low-energy states. The existence of such spin density waves in the ground-state electron gas would appear to lend support to the theory of antiferromagnetism proposed by Overhauser (1959), although clearly the quantitative predictions of this theory will have to be reworked‡. It is hoped to report further on this at a later date.

The connection of the present approach with the conventional philosophy of the Sommerfeld model also merits attention. The Sommerfeld method may be summarized as saying that since we have a translationally invariant Hamiltonian we may suppose all points in the gas to be equivalent in the sense that the wave functions differ by at most a trivial phase factor independent of the electron coordinates. It follows that the Nth order and all reduced matrices are translationally invariant within the Sommerfeld framework. If we consider for notational convenience the ferromagnetic case, it is readily seen that eqn. (8) results fom the use of the translationally invariant Nth-order trial density matrix

$$\frac{1}{N}\int_{\text{Volume } N} \psi^*(\mathbf{r}_1' + \xi\ \mathbf{r}_2' + \xi \ldots \mathbf{r}_N' + \xi)\psi(\mathbf{r}_1 + \xi\ \mathbf{r}_2 + \xi \ldots \mathbf{r}_N + \xi)\, d\xi, \quad (20)$$

† See, however, the recent work of Kohn, W., and Nettel, S. J., 1960, *Phys. Rev. Letters*, **5**, 8.

‡ See, however, Marshall, W., 1960, *Phys. Rev.*, **118**, 1519.

where ψ is the Slater determinant of the orbitals (3). Thus while many methods (for example Jastrow (1955) and Clarke and Feenberg (1959)) use variationally trial wave functions which are translationally invariant, we have seen it is permissible to use the Nth-order matrix (20). The mathematical simplicity thereby introduced is in marked contrast with the method based on wave functions. The interpretation of the matrix elements will however be different in the two cases. For example, the Sommerfeld second order matrix based on the use of (20) is

$$\frac{1}{N}\int_{\text{Volume } N} \begin{vmatrix} \gamma(\mathbf{r}_1'+\xi\,|\,\mathbf{r}_1+\xi) & \gamma(\mathbf{r}_1'+\xi\,|\,\mathbf{r}_2+\xi) \\ \gamma(\mathbf{r}_2'+\xi\,|\,\mathbf{r}_1+\xi) & \gamma(\mathbf{r}_2'+\xi\,|\,\mathbf{r}_2+\xi) \end{vmatrix} d\xi, \quad . \quad . \quad (21)$$

γ being defined by (5), the pair function thus being

$$\frac{1}{N}\int_{\text{Volume } N} 2P(\xi+\eta\,\eta)\,d\eta = \int_C 2P(\xi+\eta\,\eta)\,d\eta.$$

More generally, diagonal elements of matrices on the Sommerfeld model are obtained by averaging the corresponding periodic elements. This is in accord with the essential distinction between the methods, the one placing all points on an equal footing, the other inducing a periodicity by reformulating the problem.

Finally, it is interesting to note the degree of similarity between the results presented here and those of YM despite the use of fundamentally different approaches. This is perhaps best illustrated by an examination of the pair functions. From (6), for example, we may say

$$J(\mathbf{r}+\xi)J(\mathbf{r})[1-l^2\{\mathbf{R}(\mathbf{r}+\xi)-\mathbf{R}(\mathbf{r})\}]$$

is the probability that there are simultaneously particles at $\mathbf{r}$ and $\mathbf{r}+\xi$. Since $J(\mathbf{r})$ is the particle density, $J(\mathbf{r}+\xi)[1-l^2\{\mathbf{R}(\mathbf{r}+\xi)-\mathbf{R}(\mathbf{r})\}]$ is the probability that there is a particle at $\mathbf{r}+\xi$ when there is a particle at $\mathbf{r}$. Since J is greatest at the lattice points, the most likely value of

$$J(\mathbf{r}+\xi)[1-l^2\{\mathbf{R}(\mathbf{r}+\xi)-\mathbf{R}(\mathbf{r})\}] \quad \text{is} \quad J(\xi)[1-l^2\{\mathbf{R}(\xi)\}]$$

and this is just the YM Sommerfeld pair function. Clearly a complete elucidation of the connection between the methods would be of interest.

Acknowledgments

It is a pleasure to thank Dr. N. H. March for many helpful discussions relating to the above work.

References

Bohm, D., and Pines, D., 1953, *Phys. Rev.*, **92,** 609.
Clark, J. W., and Feenberg, E., 1959, *Phys. Rev.*, **113,** 388.
Cowan, R. D., and Kirkwood, J. G., 1958, *Phys. Rev.*, **111,** 1460.
Gell-Mann, M., and Brueckner, K. A., 1957, *Phys. Rev.*, **106,** 364.
Gross, E. P., 1960, *Phys. Rev. Letters*, **4,** 599.
Jastrow, R., 1955, *Phys. Rev.*, **98,** 1479.

Koppe, H., 1957, *Z. Phys.*, **148,** 135.
Löwdin, P. O., 1955, *Phys. Rev.*, **97,** 1474, 1490, 1509.
March, N. H., and Young, W. H., 1958, *Proc. phys. Soc. Lond.*, **72,** 182.
Mayer, J. E., 1955, *Phys. Rev.*, **100,** 1579.
Overhauser, A. W., 1959, *Phys. Rev. Letters*, **3,** 414 ; 1960 a, *Ibid.*, **4,** 462 ; 1960 b, *Ibid.*, **4,** 415.
Wigner, E. P., 1938, *Trans. Faraday Soc.*, **34,** 678.
Young, W. H., and March, N. H., 1960, *Proc. roy. Soc.* A, **256,** 62.

Deformation Twinning in Face-centred Cubic Metals†

By J. A. Venables
Cavendish Laboratory, University of Cambridge

[Received August 22, 1960]

Abstract

The principal features of the experimental results of Blewitt *et al.* (1957) and of Suzuki and Barrett (1958) on deformation twinning in face-centred cubic metals are explained in terms of an extension of the ' prismatic ' source mechanism of Cottrell and Bilby (1951). Suitable prismatic dislocation sources are thought to be long jogs in the dislocations of the two conjugate slip systems in a work-hardened metal and prismatic dislocation loops produced by vacancy condensation in a neutron-irradiated metal. The dissociation of slip dislocations is also considered and is found to be an unlikely mechanism for the production of deformation twins in copper, silver or gold.

§ 1. Introduction

Blewitt *et. al.* (1957) have observed twinning as a mode of deformation of copper single crystals in low-temperature tensile tests. Suzuki and Barrett (1958) have made similar observations on a series of silver–gold alloys.

Figure 1 indicates the principal features of the results on copper of Blewitt *et al.* (1957). Twinning, when observed on the principal slip plane $(11\bar{1})$, took place by shear in the [112] direction and not by shear in the $[2\bar{1}1]$ direction. Twinning was not observed at 4·2°K when the tensile axis was between [311] and [100], and was confined to a small range of orientations near [111] at 77°K. In specimens which had been neutron-irradiated to an integrated flux of $1{\cdot}5 \times 10^{20}$ nvt at 80°C, twinning at 4·2°K occurred on the secondary slip plane (111), although the stress on the primary twin system $(11\bar{1})[112]$ was higher than on the conjugate system $(1\bar{1}1)[121]$‡. Specimens which had been irradiated to lower fluxes at 30°C twinned at 77°K in a similar manner to work-hardened crystals at the same stress. Similar results were obtained for work-hardened silver–gold alloys by Suzuki and Barrett though twinning often occurred on both the conjugate slip planes $(11\bar{1})$ and $(1\bar{1}1)$.

The resolved shear stress for twinning is high, typically $\sim 15\,\mathrm{kg/mm^2}$ for Cu and ~ 6–$10\,\mathrm{kg/mm^2}$ for the Ag–Au alloys. The onset of twinning is

† Communicated by the Author.

‡ Blewitt *et al.* (1957) state that for crystal 416, whose tensile axis had not rotated to the dodecahedral plane when twinning began, the stress is higher on the secondary slip plane. This is not so for the two twin systems quoted above.

accompanied by a load drop of about 10% of the applied load, but as the area of the twinned region is typically about 10% less than that of the non-twinned region of the specimen, the shear stress for the propagation of twinning throughout the crystal is about the same as that for twin initiation.

Fig. 1

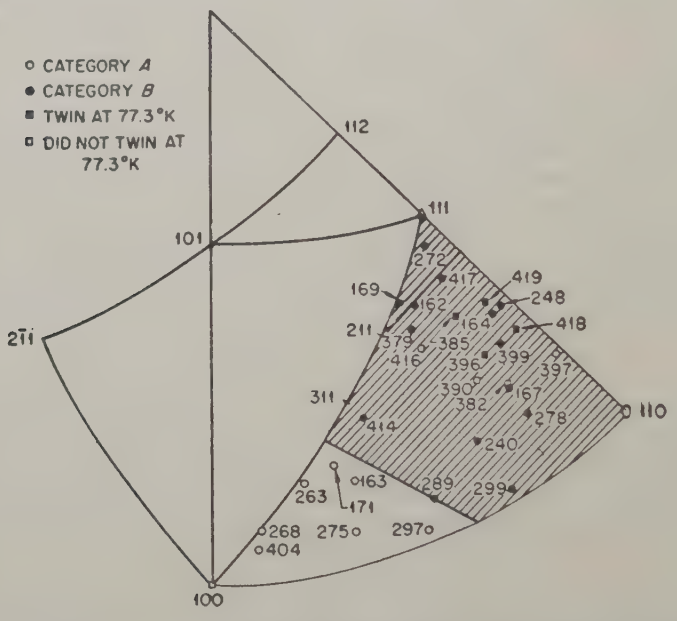

(Reproduced by courtesy of the American Institute of Physics.)

Stereographic projection showing the tensile axes of the copper crystals tested by Blewitt *et al.* (1957). Crystals of class B twinned in tensile tests at 4·2°K whereas those of class A did not. The shaded area of the stereogram contains those tensile axes which had rotated to between [311] and [111] after 50% extension of the crystals.

Any model of deformation twinning must account for the above results, in particular for the twin systems observed and the orientations of the tensile axis necessary for twinning to occur. In this paper a dislocation model of the production of deformation twins is proposed and the results of Blewitt *et al.* (1957) and of Suzuki and Barrett (1958) are interpreted in terms of the proposed model.

§ 2. Possible Models of Twinning in F.C.C. Metals

If a twin is generated by the spiralling of a twinning dislocation around a suitable pole, then sources of the twinning dislocation, and a pole dislocation, whose component Burgers vector perpendicular to the {111} twin plane is equal to the spacing of these {111} planes, must be present in the metal.

It is convenient to use the reference tetrahedron of Thompson (1953) to designate the slip planes and Burgers vectors in the f.c.c. lattice. The orientation of the tetrahedron is shown in fig. 2. In work hardened copper, with the tensile axes of fig. 1, the principal slip and twin plane is (a) and the observed twin direction **αC**. The twinning dislocation **αC** can be produced in the dissociations of the whole dislocations **BC**, **DC** and **AC**. **BC** and **DC** may be called 'glide' sources, as they are glissile in (a), and **AC** a 'prismatic' source as it cannot glide in the twin plane. Suitable pole dislocations for twinning on (a) are **AB**, **AC** and **AD**.

Fig. 2

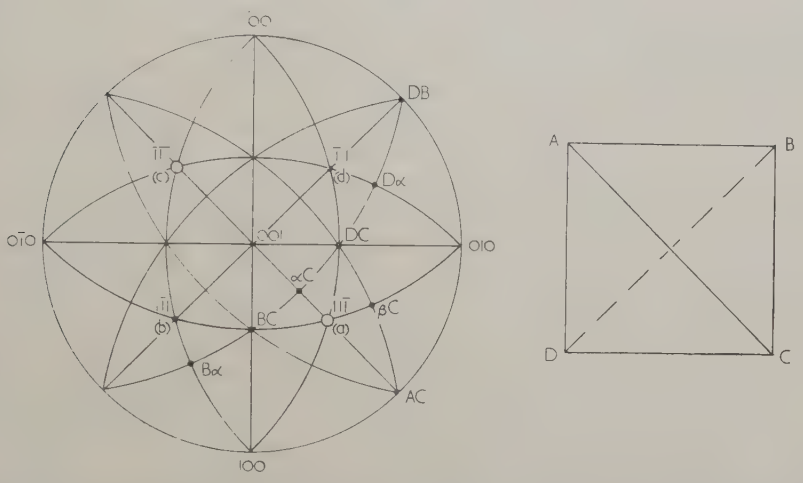

Thompson's notation for slip planes and Burgers vectors in a face-centred cubic crystal. Planes (a), (b), (c) and (d) (opposite corners A, B, C and D) of the reference tetrahedron correspond to $(11\bar{1})$, $(1\bar{1}1)$, $(\bar{1}11)$ and $(\bar{1}\bar{1}1)$. The mid-points of the faces (a), (b), (c) and (d) are denoted by α, β, γ and δ.

Cottrell and Bilby (1951) have considered the dissociation of the prismatic dislocation **AC** (fig. 3 (a)) on plane (a) into the Frank sessile **Aα** and the Shockley partial **αC**. Frank (1951), and Frank and Nicholas (1953) have designated the two possible types of stacking fault in face-centred cubic metals 'intrinsic' and 'extrinsic' fault. It will be assumed throughout, with Cottrell and Bilby, that intrinsic faults occur and that they have a much lower energy than extrinsic faults. There is now considerable experimental evidence that this is the case (Howie 1960). The stacking of $(11\bar{1})$ planes across the intrinsic fault behind **αC** has the sequence 231/312 (fig. 3 (b)). After one revolution around the pole dislocation, the **αC** dislocation meets the sessile **Aα** again (fig. 3 (c)), and, according to Cottrell and Bilby, cannot proceed further as the stacking sequence 231/123 would be produced, in which nearest-neighbour distances are not preserved. However, when **αC** meets **Aα**, we have the original dislocation **AC** and a sheet of stacking fault. If this dislocation **AC** glides prismatically along

the glide cylinder (G–G′, fig. 3 (*c*)) in either direction through a distance equal to the Burgers vector than the dissociation

$$\mathbf{AC} \rightarrow \mathbf{A}\alpha + \alpha\mathbf{C}$$

can take place again. This dissociation produces the double stacking fault sequence 231/3/23 or 23/2/123, depending on whether **AC** glides up (as in fig. 3 (*d*)) or down respectively. Repeated operation of this source then gives the required twin. The production and operation of such a source is considered in § 4 for work-hardened metals and in § 6 for neutron-irradiated metals.

Fig. 3

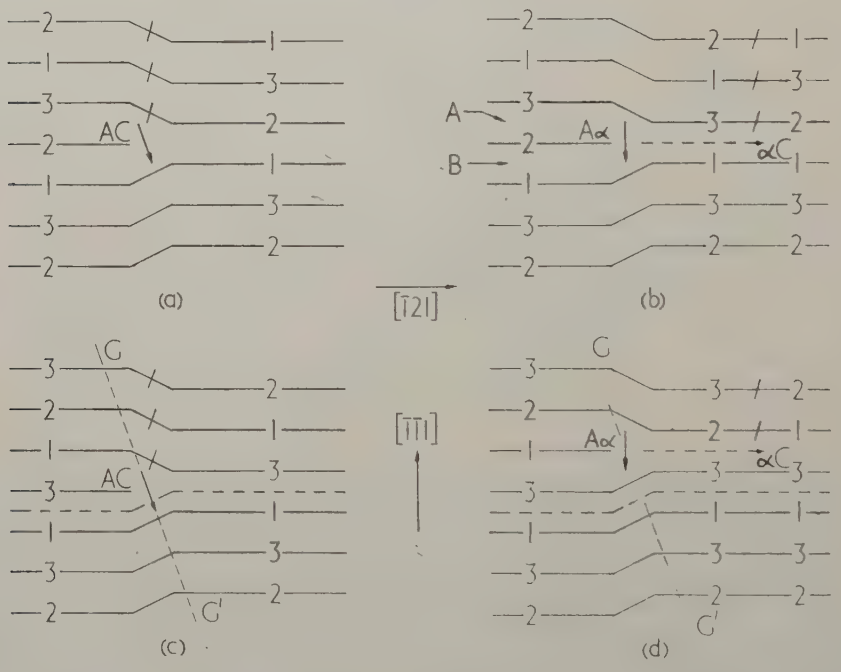

The extension of the mechanism of Cottrell and Bilby (1951).

(*a*) The unit dislocation **AC** lying in the (111)planes (*a*). The positive direction of the dislocation is into the paper, along **CB**.

(*b*) The dissociation $\mathbf{AC} \rightarrow \mathbf{A}\alpha + \alpha\mathbf{C}$, producing intrinsic stacking fault on plane (*a*).

(*c*) Recombination of the dislocations **A**α and α**C** after one revolution of the Shockley partial.

(*d*) Prismatic glide of **AC** along G–G′, followed by the dissociation (*b*) on the next atomic plane.

It is also conceivable that twinning could originate from the slip dislocations **BC** and **DC** by the normal splitting on plane (*a*) (Heidenrich and Shockley 1948),

$$\mathbf{BC} \rightarrow \mathbf{B}\alpha + \alpha\mathbf{C} \text{ and } \mathbf{DC} \rightarrow \mathbf{D}\alpha + \alpha\mathbf{C}.$$

Under certain conditions the dislocations **Bα** and **Dα** could be immobilized and these reactions are considered in § 3.

It will be shown below that the separation of glide sources into partials is unlikely to provide a suitable twinning mechanism, and that the facts recorded in the introduction can be understood in terms of the extension of the mechanism of Cottrell and Bilby given above.

§ 3. Operation of 'Glide' Sources

3.1. *General Considerations*

If a slip dislocation, Burgers vector **b**, which splits up into Shockley partial dislocations $\mathbf{b}_1$ and $\mathbf{b}_2$, is to be a twin source, a resolved shear stress on the slip plane, **σ**, must be applied which is sufficient to separate these partials. The configuration of the dislocation under stress may approximate to that of fig. 4 (*a*). The front partial is $\mathbf{b}_1$, which is bent to

Fig. 4

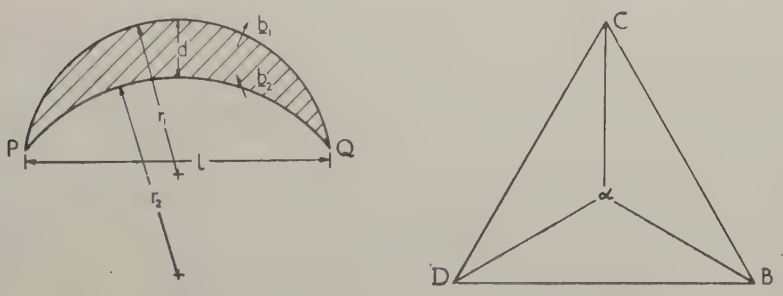

Glide sources.
(*a*) Configuration of a glide dislocation under stress.
(*b*) Burgers vectors of the dislocations which are glissile in plane (*a*).

a radius r_1 under the stress **σ**, and the back partial $\mathbf{b}_2$ has a radius of curvature r_2. The dislocations are pinned at the points P and Q, which are a distance l apart. Unit lengths of the two partial dislocations (in the centre of the arcs PQ) are in equilibrium if the following two equations are satisfied:

$$\boldsymbol{\sigma}.\mathbf{b}_1+F(d)-\gamma-\frac{\alpha\mu b_1^{\,2}}{2r_1}=0, \qquad \ldots\ldots \quad (3.1)$$

$$\boldsymbol{\sigma}.\mathbf{b}_2-F(d)+\gamma-\frac{\alpha\mu b_2^{\,2}}{2r_2}=0. \qquad \ldots\ldots \quad (3.2)$$

$F(d)$ is the repulsive force per unit length between the partials, which depends on their spacing d, and α is of order unity for large r. The stacking fault energy is γ and μ is the shear modulus. If the back partial $\mathbf{b}_2$ also operates as a Frank–Read source then slip occurs rather than twinning. The back partial cannot follow the front partial beyond the unstable

semicircular configuration, if eqn. (3.2) can still be satisfied when the front partial is at a large distance from the back partial. When the separation of the partials is large, $F(d)=0$, and eqn. (3.2) reads, since $2r_2 > l$,

$$\boldsymbol{\sigma}\,.\,\mathbf{b}_2+\gamma-\frac{\alpha\mu {b_2}^2}{l}<0. \qquad \ldots\ldots \quad (3.3)$$

Thus twinning may originate from a glide dislocation if eqns. (3.1) and (3.3) are satisfied and the dislocation can only be a source of slip if they are not satisfied.

The whole and partial dislocations which are glissile in (*a*) are shown in fig. 4(*b*), which is the face (*a*) of Thompson's tetrahedron. The dissociations are as follows:

$$(1) \qquad \mathbf{BC}\rightarrow \mathbf{B\alpha}+\boldsymbol{\alpha}\mathbf{C},$$
$$(2) \qquad \mathbf{DC}\rightarrow \mathbf{D\alpha}+\boldsymbol{\alpha}\mathbf{C},$$
$$(3) \qquad \mathbf{DB}\rightarrow \mathbf{D\alpha}+\boldsymbol{\alpha}\mathbf{B}.$$

The tensile axis is between [311] and [111] when twinning occurs, and hence the direction of greatest resolved shear stress on (*a*) is between **BC** and **αC**. By applying the conventions of Frank (1951) and Thompson (1953) it may be shown that **αC** is the front partial in both dissociations (1) and (2), given intrinsic stacking faults. The stress is such as to separate the partials, independent of the sign of the Burgers vector. The stress in case (3), although it tends to move the partials **Dα** and **αB** in opposite directions, tends to decrease the width of intrinsic stacking fault, and so the dislocation **DB** is not expected to be an important twin source. The operation of the sources **BC** and **DC** is considered in the next section.

3.2. *The Stresses Required to Operate 'Glide' Sources*

The eqns. (3.1) and (3.3) give the restrictions on the stress $\boldsymbol{\sigma}$ and source length l necessary for twin production from 'glide' sources. In order to obtain estimates for $\boldsymbol{\sigma}$ and l, the following simplifying assumptions will be made. It may be seen by more detailed calculations that these estimates are not in fact restrictive enough.

It will be assumed that $\boldsymbol{\sigma}$ can be represented by an effective local tensile stress τ. Thus $\boldsymbol{\sigma}\,.\,\mathbf{b}_1$ will be equated with $\tau b_1 \cos\chi\cos\lambda_1$, and $\tau b_2 \cos\chi\cos\lambda_2$ with $\boldsymbol{\sigma}\,.\,\mathbf{b}_2$, where χ and λ are the angles between the tensile axis and the glide plane normal, and the tensile axis and the glide direction respectively. Since the stress on the dislocation **BC** or **DC** under consideration tends to separate the partials, the separation of the partials, d, will be greater than the equilibrium value. Therefore $F(d)$ will be smaller than its equilibrium value, γ. If the value of $F(d)$ only varies slowly with r_1, then the front partial $\mathbf{b}_1$ will be unstable when $2r_1 = l$, in a similar manner to an ordinary

Frank–Read source. Thus eqn. (3.1) now reads, putting $F(d) \leqslant \gamma$,

$$\tau b_1 \cos\chi \cos\lambda_1 > \frac{\alpha\mu {b_1}^2}{l}, \quad \ldots\ldots\ldots (3.4)$$

and eqn. (3.3) reads

$$\tau b_1 \cos\chi \cos\lambda_2 < \frac{\alpha\mu {b_1}^2}{l} - \gamma, \quad \text{where } |b_2| = |b_1|. \quad \ldots (3.5)$$

These equations give the following condition on l when $\cos\lambda_1$ and $\cos\lambda_2$ are both positive:

$$l < \frac{\alpha\mu {b_1}^2}{\gamma}\left(1 - \frac{\cos\lambda_2}{\cos\lambda_1}\right). \quad \ldots\ldots\ldots (3.6)$$

Table 1 gives the minimum values of τ and the maximum values of l necessary to operate the twin sources **BC** and **DC**, as a function of tensile axis orientation.

Table 1. Values of the source length, l, and of tensile stress, τ, necessary for glide dislocations **BC** and **DC** to act as twin sources in copper. The observed tensile stress, τ_{obs}, when twinning occurs is $\sim 35\,kg/mm^2$ (Blewitt *et al.* 1957)

$[\gamma = 40\,erg\,cm^{-2}$, $\mu = 4{\cdot}2 \times 10^{11}\,dyne\,cm^{-2}$, $b_1 = 1{\cdot}5 \times 10^{-8}\,cm]$

Tensile axis	Restriction on l, eqn. (3.6) (Å)		Minimum tensile stress, τ, eqn. (3.4) (kg/mm^2)		Ratio (τ/τ_{obs})	
	BC	**DC**	**BC**	**DC**	**BC**	**DC**
[111]	115	115	190	190	5·5	5·5
[211]	45	180	340	85	10	2·5
[311]	0	225	∞	63	∞	1·8
[100]	†	∞	†	60‡	†	1·7

† A compressive stress is required to separate the partials.
‡ Value estimated from eqns. (3.1) and (3.2) with $F(d) = 0$.

The main feature of table 1 is that, whereas the **DC** dislocation source requires a lower shear stress than the **BC** source for operation, separation of the partials **Dα** and **αC** will be most easily effected with a tensile axis near [100], when twinning is not observed. The dislocations of the principal slip system have Burgers vector **BC**, and these dislocations may react with the few dislocations **CD** which are present to form **BD** dislocations. In this case only the **BC** dislocations will be available as glide sources, and these sources, while giving approximately the observed dependence of twinning frequency on tensile axis orientation, require very large stresses and prohibitively short source lengths.

Cottrell and Bilby (1951) pointed out that the pole dislocation, around which the twinning partial rotates, must not move under the stress necessary to move the twinning dislocation. It seems very unlikely that the dislocation network would stand the stresses given in table 1, and unless the back partial can be immobilized in some other way than by making the source length small, then it is doubtful whether glide sources can operate, except in metals of very low stacking-fault energy. The further difficulty of the partials overcoming their mutual stress field after one revolution of the twinning dislocation has been considered by Seeger (1956), for the case of generating a h.c.p. from a f.c.c. lattice using a pole mechanism, and will not be considered here.

3.3. *'Glide' and 'Prismatic' Twin Sources*

The back partial (**Bα** or **Dα**) may most effectively be immobilized by reacting with a dislocation which does not lie in (a), and which cannot glide in this plane. This limits the choice of the interacting dislocations to the possible pole dislocations **AB**, **AC** and **AD**. If the interactions with the sources **DC** and **BC** are to have sufficient stability, the Burgers vectors of the interacting dislocations must be at 120° to each other (Whelan 1958), and hence the total Burgers vectors of these new sources must be **BA**, **DA** or **AC**. These sources, however, are no longer glide sources but prismatic sources, as the total Burgers vectors do not lie in the twin plane (a).

Hence it appears that, on several counts, the slip dislocations are unlikely to be effective twin sources. Prismatic sources will be considered in the following sections.

§ 4. Prismatic Twin Sources in Work-hardened F.C.C. Metals

4.1. *Possible Prismatic Twin Sources*

Prismatic dislocations which lie in plane (a) may have Burgers vectors **AB**, **AC** or **AD**. These dislocations may become sources of twins on each of the three twin systems on plane (a) by dissociating in the manner considered by Cottrell and Bilby (1951):

$$\mathbf{AB} \rightarrow \mathbf{A\alpha} + \mathbf{\alpha B}, \quad (4)$$

$$\mathbf{AC} \rightarrow \mathbf{A\alpha} + \mathbf{\alpha C}, \quad (5)$$

$$\mathbf{AD} \rightarrow \mathbf{A\alpha} + \mathbf{\alpha D}. \quad (6)$$

These dissociations may take place when the stress on the twinning dislocations is high. For tensile axes between [100] and [111] the resolved shear stress on (a) is greatest between the **Bα** and **αC** directions, and is never high in the **αD** direction, so that the dissociation (6) is unimportant. If it is assumed, as before, that intrinsic faults have substantially lower energy than extrinsic faults, then the twinning dislocations **αB** and **αC** separate on one particular side of the Frank sessile **Aα** (see fig. 5). By using the convention of Thompson (1953) again, it can be seen that the stress is such as to expand the intrinsic fault behind

αC and contract the intrinsic fault behind **αB**. The expansion or contraction of the fault is independent of the sign of the Burgers vectors. (The difference between reactions (4) and (5) may be seen simply. The dislocations **αB** and **αC** are on the same side of **Aα**, but the stresses are high for the movement of **Bα** and **αC** dislocations in the same direction, and hence **αB** and **αC** must move in opposite directions (fig. 5).)

Fig. 5

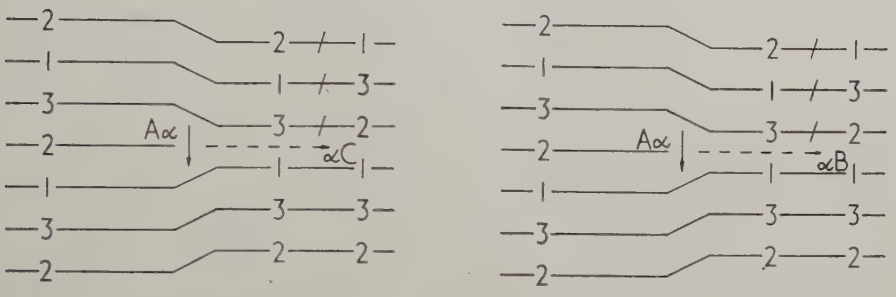

The dissociation of prismatic dislocations.

(*a*) **AC**→**Aα**+**αC**.

(*b*) **AB**→**Aα**+**αB**.

The positive direction of the dislocations is along **CB**, into the paper. Under the tensile stress **αB** will move to the left and **αC** to the right. The Burgers vector **αB** points into and **αC** points out of the plane of the paper.

Thus the **AC** dislocation is the only important source for twinning on plane (*a*) and twinning can only take place by shear in **αC** direction on this plane. The result of Blewitt *et al.* (1957), that twinning on the (11$\bar{1}$) plane takes place in the [112] direction only, can therefore be explained in terms of the geometry of the twin source dislocations, if only intrinsic stacking faults are produced.

4.2. *Production of Prismatic Dislocations in the Work-hardened Metal*

The dislocations of the secondary glide system have the Burgers vector **AC** and lie in plane (*b*). Lengths of these dislocations can be transferred to plane (*a*) by glide processes in three ways:

(1) The dislocations can lie along CD.

(2) They can cross-slip onto plane (*d*) and then lie along BC, the direction which is also in plane (*a*).

(3) They can be intersected by dislocations of the primary slip system. If Frank–Read sources of 'plane' type operate (Bilby 1955), repeated intersection of the dislocation **AC** will produce a long jog which lies along the primary slip direction **BC** in planes (*a*) and (*d*).

These three processes will be considered separately.

If the dislocations **AC** lie along CD they can react with the primary slip dislocations, Burgers vector **CB**, to form Lomer–Cottrell locks **AB**, lying along CD. It seems unlikely that considerable lengths of the dislocations will lie along CD unless they are part of Lomer–Cottrell locks (see Whelan 1958).

If process (2) is important then twinning cannot occur below the cross-slip stress. The beginning of stage III of the work-hardening curve has been associated with the onset of cross-slip by several authors, and the initial stage III stress, extrapolated to 0°K, τ_{III_0}, is above the twinning stress at 4·2°K (Seeger *et al.* 1959). The copper crystal which was typical of the crystals which twinned (Blewitt *et al.* 1957, fig. (3)) was work-hardening linearly at the twin stress, indicating that cross-slip is not important. Also as for process (1), there appears to be no special reason why the dislocations **AC**, on planes (*b*) or (*d*), should lie along that particular direction which is also in plane (*a*).

If process (3) occurs, then the long jog with Burgers vector **AC** is constrained to lie along BC and the dislocation is pinned where it leaves the plane (*b*). This source should withstand the high stresses needed for twinning as envisaged by Cottrell and Bilby (1951).

4.3. *Operation of the Prismatic Twin Source*

The operation of the long jog in **AC** as a twin source will now be considered in more detail. If the jog is formed by the motion of the slip dislocations, Burgers vector **BC** or **CB**, on the same atomic plane, the jogged dislocation **AC** (or **CA**) has the configuration of fig. 6 (*a*). The dissociation of the jog **AC** is shown in fig. 6 (*b*). The twinning dislocation **αC** rotates in opposite directions around the poles X and Y (fig. 6 (*b*)) until it meets the sessile **Aα** again. The partial **αC** approaches **Aα** between either the upper (A) or the lower (B) pair of atom planes which bound the core of the sessile dislocation, as shown in fig. 3 (*b*). The actual position of the partial dislocation **αC** (or **Cα**) is between that pair of planes which is further away from the pole dislocation, and hence the configuration after one revolution may be that of fig. 6 (*c*), if the twinning dislocation spirals round both poles X and Y. The partial **αC** which rotates round X and Y will meet one atomic plane apart along RS, as the pole dislocation has a component Burgers vector perpendicular to and equal to the spacing of the $(11\bar{1})$ planes (*a*).

Seeger (1956) has suggested that a dislocation such as the twinning partial **αC** may acquire sufficient kinetic energy as it rotates around the poles X and Y to overcome the stress field of the configuration RS (fig. 6 (*c*)) dynamically. If this very large stress field (resolved shear stress $\sigma \sim 180\,\mathrm{kg/mm^2}$) is overcome after one revolution of the twinning dislocation, then the partials comprising RS can rotate about the poles Y and X, generating a lenticular twin without further hindrance (see fig. 6 (*f*)). It is not, however, necessary that the twinning dislocation should

Fig. 6

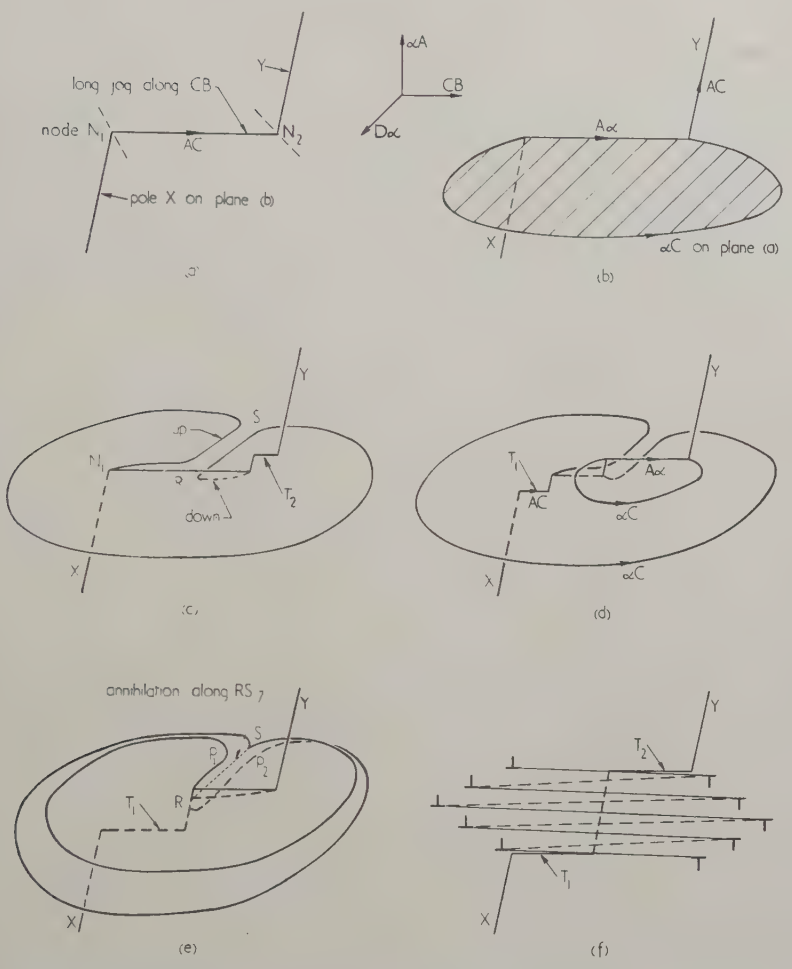

The operation of a long jog in the dislocation **AC** as a twin source.

(*a*) The dislocation **AC** which is jogged along **CB**.

(*b*) Dissociation of the jog, with the twinning dislocation **αC** rotating about the poles X and Y.

(*c*) After one revolution of the twinning dislocation. A unit jog has been created at N_2 and is moving along the long jog, reforming the twin source T_2.

(*d*) Operation of the twin source T_2, producing a second layer of fault above the first. A unit jog has been created at N_1 and is moving towards R, producing the source T_1, which will operate (see (*f*)) to continue the twin downwards.

(*e*) After a complete revolution of the twinning dislocation from T_2. Annihilation of twinning dislocations of opposite sign has taken place along RS, leaving a continuous helical layer of fault.

(*f*) The form of the twin after several operations of the sources T_1 and T_2. The twin is a continuous helical fault and has a biconvex lenticular shape. It is viewed along **αD** in this diagram.

travel fast enough to overcome this obstacle dynamically for twinning to occur from such a source. If a helical twin a few (~ 10) atomic planes thick can be formed by repeated operation of the twin source, as suggested in § 2, then the partials p_1 and p_2 (fig. 6 (*e*)) which bound the twin above and below are sufficiently far apart to overcome their mutual stress field statically under the applied stress alone. Once a twin this size has been formed it can grow by the rotation of the partials p_1 and p_2 around Y and X respectively. The final width of the twin will be limited by the back stress on the rotating partials and by the length of the pole dislocation.

The prismatic glide which is necessary for the first few repeated operations of the twin source may take place in one of several ways. The two mechanisms considered here are

(1) The passage along the long jog of a unit jog created at the node N_1 and/or at the node N_2. This mechanism will only be possible if the extended pole dislocation on plane (*b*) is constricted at the nodes.

(2) Reactions taking place along the length of the long jog. These may take place if the nodes N_1 and N_2 are stable pinning points for the twinning dislocation **αC**. It is not at present certain that the nodes N_1 and N_2 are stable in the configuration of fig. 6 (*c*).

If a pole dislocation (X or Y, fig. 6 (*c*)) is constricted at N where it is jogged, a unit jog can be formed which is glissile in the same surface (the plane (*d*)) as the long jog, thus moving the twin source through the required distance **AC**. Unit jogs (of length **AC**) will tend to be formed for two reasons. They are expected to have a lower energy than multiple jogs when the pole dislocation is not exactly in screw orientation; and the twin source which is reformed by the movement of a jog can split on plane (*a*) with lowest energy when the new stacking fault behind **αC** is on the next atomic plane to the old one (see fig. 3 (*d*)). Because the sessile **Aα** is split into the stair rod dislocation **δα** along BC and **Aδ** on plane (*d*) the dislocation configuration at the two nodes N_1 and N_2 is not symmetrical (see fig. 7 (*a*) and (*c*)). A unit jog created at N_2 will have a higher energy than one from N_1. Any shear stress concentration on plane (*a*) will force a jog from N_1 along the long jog and a jog from N_2 back to N_2. Hence the source T_1 (fig. 6 (*d*)) may be the only one which operates, but T_2 is shown operating in the sequence of fig. 6 for the sake of clarity. In any case, whether T_1 and/or T_2 operate as twin sources, more helical layers of fault, and a more extended composite dislocation line RS will be produced (fig. 6 (*e*)). The component partials **αC** of the dislocation RS which lie on the same atomic plane can annihilate in pairs, leaving only the top and bottom partials p_1 and p_2 and a single helical fault between them.

Reactions taking place along the length of the long jog are shown in fig. 7. The configurations (*a*) and (*b*) refer to lengths of the long jog near N_1 and (*c*) and (*d*) near N_2. Because there is a shear stress concentration on the (111) planes (see § 4.4), the **δC** dislocation produced by the

coalescence of **αC** and **δα** moves towards the **Aδ** dislocation on plane (*d*). It is energetically favourable for the reverse reaction

$$\delta\mathbf{C} \rightarrow \delta\alpha + \alpha\mathbf{C}$$

to take place on the next atomic plane because of the presence of the first fault. If the configuration of fig. 7 (*b*) and/or (*d*) occurs a twin is produced which is equivalent to the one obtained by generating unit jogs at N_1 only. It appears most likely that this is the twin produced from this source.

In all cases considered, this prismatic glide of the twin source can take place at a lower stress than is required to split **AC** dislocation on plane (*a*) initially. Therefore the critical stage for twin nucleation is the creation of the first ring of fault from this source. The stresses required for twin nucleation are considered in the next section.

Fig. 7

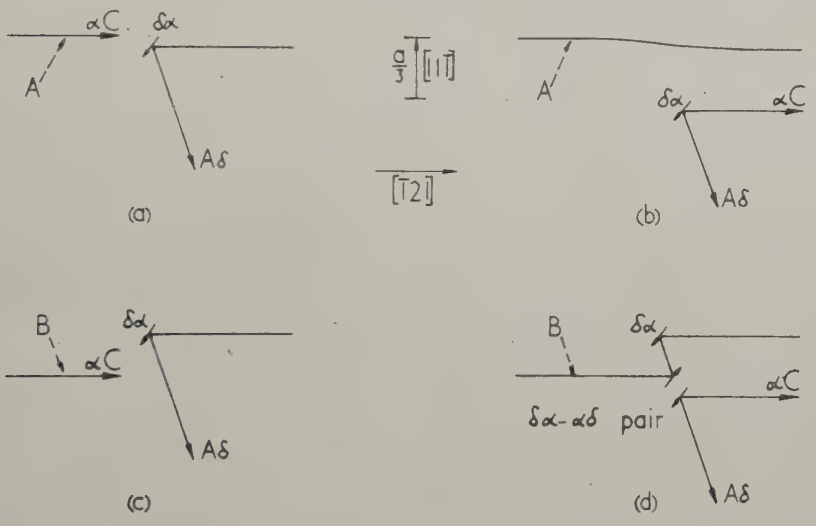

Prismatic glide of the twin source **AC**. The lines represent intrinsic stacking faults, and the letters A and B give the positions of the faults with respect to fig. 3, which is in the same orientation. The reaction (*a*) → (*b*) occurs near the node N_1 and (*c*) → (*d*) near N_2. See text for discussion.

4.4. *The Stress Required to Operate a Prismatic Twin Source*

The resolved shear stress on plane (*a*) required to operate this prismatic twin source **AC** may be given by the following equation:

$$\boldsymbol{\sigma} \cdot \mathbf{b}_1 = \gamma + \frac{\alpha \mu b_1^2}{l}. \quad . \quad . \quad . \quad . \quad . \quad . \quad . \quad (4.1)$$

where l is the length of the source and $\mathbf{b}_1 = \alpha\mathbf{C}$. This equation assumes that $\alpha\mu b_1^2/l$ is greater than the short range force needed to separate the **αC** and **Aα** dislocations. For a copper crystal with a [111] tensile axis, the stress required to operate this prismatic source will be less than that

for either slip source (table 1) if l is greater than about 50 Å. Thus 20 primary slip dislocations on one atomic plane intersecting a secondary slip dislocation produce a jog of sufficient length to make it the most favourable type of twin source in the work-hardened crystal. Since a stress equal to twice the observed twinning stress is needed to overcome the surface tension of the fault alone, some shear stress concentration on the twin plane is necessary for twinning to occur at all. The stress concentration factors required for the operation of this source range from about five for a 50 Å source to below three for a source which is longer than 200 Å. These shear stress concentrations could easily be produced in the neighbourhood of the jog by a small pile-up of primary slip dislocations which have not penetrated the twin source.

§ 5. Correlation of the Proposed Model with Experiments on Work-hardened Crystals

The most important result of considering the various types of twin sources is that the observed twin systems and the tensile axis orientation relationship of Blewitt *et al.* (1957) and of Suzuki and Barrett (1958) may be explained, if prismatic sources operate. Only the [112] twin direction (**αC**) is observed experimentally when twins are produced on the primary slip plane ($11\bar{1}$). Twins with a [$2\bar{1}1$] shear are not produced in tension tests and this is explained, by considering the stress acting on the **αB** twin source, and by assuming that extrinsic stacking faults have a high energy. Both 'glide' and prismatic sources will account for this distinction between the [112] and [$2\bar{1}1$] directions of twinning. Only the prismatic source **AC** will account satisfactorily, however, for the dependence of twinning on tensile axis orientation.

To satisfy eqn. (4.1) the resolved shear stress must be high along [112] and there must be some stress concentration on the primary slip plane. A high stress concentration can only be maintained if cross-slip is unfavourable and this is the case when the tensile axis is around [211]. (For a [211] tensile axis there is no stress on the cross-slip plane.) Therefore the tensile axes of the crystals which twin must be concentrated near [111] and away from [100]. The range of tensile axes for which twinning occurs must also decrease as the temperature is raised; i.e. the tensile axes must cluster around [111] as cross-slip becomes more prevalent. This is precisely what was observed by Blewitt *et al.* (1957). If the internal stress is considerably different from the external stress, the scatter in the values of the measured twin stress obtained by Blewitt *et al.* (1957) and by Suzuki and Barrett (1958) is easily accounted for.

In a copper sample (169) whose initial tensile axis was near the (100)–(111) zone (fig. 1), Blewitt *et al.* (1957) found twins on the two conjugate systems. Conjugate twinning was also a general feature of the twinning in the silver–gold alloys investigated by Suzuki and Barrett (1958). This may be simply explained on the proposed model. Just as jogs produced

by primary slip dislocations **BC** in **AC** dislocations are sources of twins on the primary twin plane (a), so the jogs produced in **BC** by the secondary slip dislocations **AC** are sources of twins on the secondary twin plane (b). Thus in conditions when the internal stress is the same on both systems or when there is local overshoot (Suzuki and Barrett 1958), conjugate twins will be formed.

The high shear stress for continued twinning may be explained if new sources are necessary to propagate the twin throughout the crystal. This is consistent with the width of each twin being limited to the length of the pole dislocation. If eqn. (4.1) is an adequate expression for the twin stress, the twin stress should not be strongly temperature dependent. This was observed over the temperature range 20–273°K by Suzuki and Barrett (1958) and between 4·2 and 77°K by Blewitt *et al.* (1957).

The prismatic source model will also account for the twinning behaviour of neutron-irradiated copper (Blewitt *et al.* 1957). The production of mechanical twins in neutron-irradiated f.c.c. metals is considered in the next section.

§ 6. The Effect of Neutron-irradiation on Twinning

Recently it has been discovered that neutron-irradiated copper contains prismatic dislocation loops (Silcox and Hirsch 1959) similar to those observed in quenched metals by the same authors. A summary of their results and the results of Blewitt *et al.* (1957) on the effect of neutron irradiation on the twinning properties of copper single crystals is given in table 2.

Table 2. Twinning in neutron-irradiated copper

From Silcox and Hirsch (1959)			
Irradiation temperature (°C)	30	30	80
Neutron flux (nvt)	$6{\cdot}7\times10^{17}$	$5{\cdot}6\times10^{18}$	$1{\cdot}4\times10^{20}$
Average loop size (Å)	75	150	300

From Blewitt *et al.* (1957)		
Irradiation temperature (°C)	30	80
Neutron flux (nvt)	1×10^{18}	$1{\cdot}5\times10^{20}$
Crystals investigated	396, 419	416
Twinning characteristics at 77°K	Twinned in a similar manner to work-hardened crystals	Did not twin as $\sigma < 13$ kg/mm^2
Twinning characteristics 4·2°K	Not reported	Twinned after small extension on secondary slip plane

When the irradiated crystals are strained, dislocations on the primary slip system (Burgers vector **BC** on plane (*a*)) will interact with the prismatic loops. Interaction of the glide dislocations with large loops may cause the loops to act as twin sources. In particular the annihilation reaction

$$\underset{\text{on } (a)}{\mathbf{BC}} - \underset{\text{on } (b)}{\text{loop } \mathbf{BC}} = 0$$

$$\underset{\text{on } (b)}{\text{loop } \mathbf{BC}} \rightarrow \underset{\text{on } (b)}{\mathbf{B\beta}} + \underset{\text{on } (b)}{\mathbf{\beta C}}$$

Fig. 8

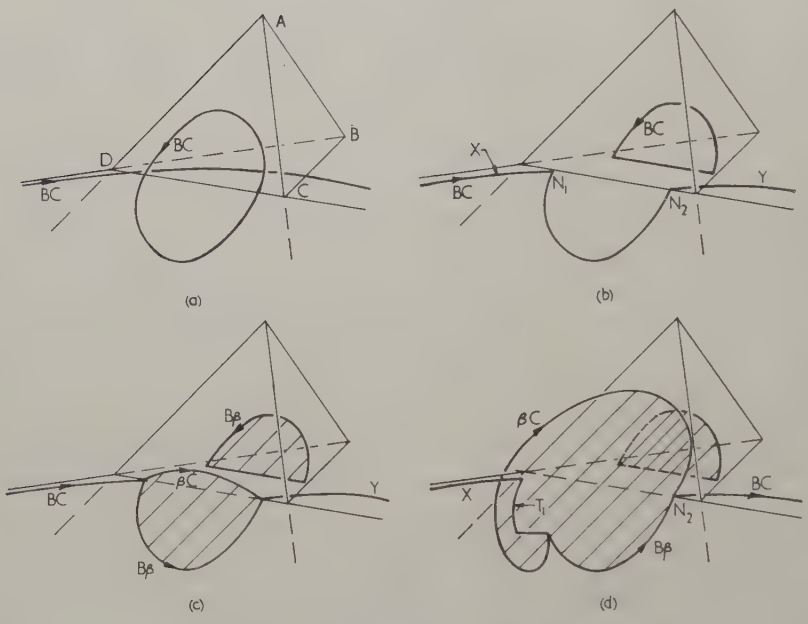

The twin source in neutron-irradiated metals.

(*a*) A dislocation of the primary slip system **BC** on plane (*a*) held up by a prismatic loop **BC** on plane (*b*).

(*b*) The slip dislocation intersects the loop by moving to the left and displaces the two halves of the loop by a Burgers vector **BC**. The slip dislocation is now continuous with the open half of the loop.

(*c*) When the stress on (*b*) is high enough the dissociation $\mathbf{BC} \rightarrow \mathbf{B\beta} + \mathbf{\beta C}$ occurs.

The twinning dislocation $\mathbf{\beta C}$ spirals round the pole X and creates a jog at N_1. The new twin source T_1 is formed by movements of this jog around the loop, and it can dissociate again producing a second layer of twin. The pole Y may be inoperative because of the presence of the sessile loop $\mathbf{B\beta}$. The growth of the twin is analogous to that described in fig. 6.

produces a source of secondary twins, as pictures in the sequence of fig. 8. Secondary twins were observed by Blewitt *et al.* (1957) in crystal 416 at 4·2°K.

If it is assumed, following Silcox and Hirsch (1959) that the prismatic loops are formed by the condensation of vacancies†, then the opening in the loop produced by the annihilation reaction enables the intrinsic stacking fault behind **βC** to expand freely (fig. 8 (*c*)). After the loop has been cut, and the fault expanded on plane (*b*), the twin can grow by prismatic glide of the loop, in a similar manner to the twins in the work-hardened crystals. If unit jogs are created at the nodes where the source dislocation changes from plane (*b*) to plane (*a*), the mechanisms for work-hardened and neutron-irradiated crystals are anologous.

If the stress concentration for twinning on the secondary system is small, the twin will only nucleate from large loops. In the case of crystal 416, the tensile axis had not rotated onto the (311)–(111) zone when twinning occurred and so the stress concentration on the secondary slip plane cannot have been large. Thus it is not to be expected that crystals containing small loops twin on the secondary slip plane. The crystals 396 and 419 (table 2) were observed to have similar twinning properties to the work-hardened crystals at 77°K, but their behaviour at 4·2°K has not yet been reported.

§ 7. Conclusions

The main conclusions of this paper are as follows:

1. Prismatic dislocations are the most likely source of mechanical twins in work-hardened and neutron-irradiated metals. These sources can operate by a modification of the mechanism of Cottrell and Bilby (1951).

2. The twin systems observed and the tensile axes necessary for twinning to occur in the experiments of Blewitt *et al.* (1957) and Suzuki and Barrett (1958) can be explained in terms of the operation of the 'prismatic' sources. The stress concentration factor required for their operation can be as low as 2 or 3, given a source length of about 200 Å.

3. Glide dislocations have been considered as twin sources. It is considered that the experimental results cannot be explained in terms of the operation of such sources.

4. It is thought that suitable prismatic dislocations are produced in the work-hardened material by the jogging of the dislocations of the two conjugate slip systems. A long jog ($\gtrsim 50$ Å) in a secondary slip dislocation is a source of twins on the primary slip plane.

† *Note added in proof.*—Since this paper was written, Barnes and Mazey (1960) have shown that the dislocation loops observed by Silcox and Hirsch (1959) are probably produced by the clustering of interstitial atoms. The model described here is also applicable to the case of interstitial loops, the fault (fig. 8 (*c*)) nucleating outside instead of inside the loop.

5. In the neutron-irradiated copper crystals, prismatic dislocation loops produced by the collapse of discs of vacancies are observed to be present (Silcox and Hirsch 1959). Certain prismatic loops on the secondary slip plane can act as sources for twinning on this plane when they are intersected by the primary slip dislocations. Twins were observed on the secondary slip plane by Blewitt *et al.* (1957) in some neutron-irradiated copper crystals strained at 4·2°K.

Acknowledgments

It is a pleasure to thank Professor N. F. Mott and Dr. W. H. Taylor for interest and encouragement, Drs. P. B. Hirsch and M. J. Whelan, Professor F. R. N. Nabarro and Dr. F. Kroupa for many helpful discussions, and for reading the manuscript, Mr. J. Silcox and Mr. A. Howie for access to information prior to publication, and Dr. T. H. Blewitt for helpful correspondence. The author is indebted to the D.S.I.R. for a maintenance grant.

References

Barnes, R. S., and Mazey, D. J., 1960, *Phil. Mag.*, **5**, 1247.
Bilby, B. A., 1955, *Report on Defects in Crystalline Solids* (London : Physical Society), p. 124.
Blewitt, T. H., Coltmann, R. R., and Redman, J. K., 1957, *J. appl. Phys.*, **28**, 651.
Cottrell, A. H., and Bilby, B. A., 1951, *Phil. Mag.*, **42**, 573.
Frank, F. C., 1951, *Phil. Mag.*, **42**, 809.
Frank, F. C., and Nicholas, J. F., 1953, *Phil. Mag.*, **44**, 1213.
Heidenreich, R. D., and Schockley, W., 1948, *Report on Strength of Solids* (London : Physical Society), p. 57.
Howie, A., 1960, Ph.D. Thesis, University of Cambridge.
Seeger, A., 1956, *Z. Metallk.*, **47**, 654.
Seeger, A., Berner, R., and Wolf, H., 1959, *Z. Phys.*, **155**, 247.
Silcox, J., and Hirsch, P. B., 1959, *Phil. Mag.*, **4**, 1356.
Suzuki, H., and Barrett, C. S., 1958, *Acta Met.*, **6**, 156.
Thompson, N., 1953, *Proc. phys. Soc. Lond.* B, **66**, 481.
Whelan, M. J., 1958, *Proc. roy. Soc.* A, **249**, 114.

The Influence of Atmospheric Corrosion on the Fatigue Limit of Iron–0·5% Carbon†

By N. J. Wadsworth
Metallurgy and Physics Department, Royal Aircraft Establishment, Farnborough, Hants

[Received August 18, 1960]

Abstract

Iron–0·5% carbon was fatigued in air and in vacuum. The knee in the S–N curve at the fatigue limit occurred at about the same number of cycles in vacuum as in air but at a higher strain. Above this strain specimens lasted about ten times as long in vacuum as in air. Slip occurred in a similar manner above and below the fatigue limit and cracks formed in the slip bands in both cases. Below the fatigue limit the cracks grew a few microns long.

§ 1. Introduction

Previous work (Gough and Sopwith 1932, 1935 and 1946, Wadsworth and Hutchings 1958, Wadsworth 1959 a) has shown that the presence of air can have a considerable effect on the fatigue life of various metals. The air increases the rate of growth of the cracks, apparently by some chemical action. All the experiments so far have been on metals without a fatigue limit in which presumably failure would occur eventually at all stresses. Steel, however, is peculiar in that it has a fatigue limit—that is a stress above which specimens fail in a finite number of cycles (usually $< 10^7$) and below which they apparently last for ever. There is inevitably some scatter in the behaviour of different, nominally identical, specimens but it is clear that there is some real physical discontinuity in behaviour at the fatigue limit (see for example Clayton-Cave *et al.* 1955). In view of the close connection between strain-ageing phenomena, yield points and fatigue limits one might expect that the fatigue limit would be the stress below which slip could not occur. Hempel (1956) has shown that this is not so. The discontinuity must occur later in the series slip→crack formation→failure. From the previous work, quoted above, one would expect that the presence of air would speed the spreading of cracks once they formed, but have little effect at stresses where cracks never form. Thus a comparison of the fatigue limit in air with that in vacuum would provide further evidence about the nature of the fatigue limit.

† Communicated by the Author.

This paper describes the results of some experiments allowing such a comparison, together with the results of metallographic examination of specimens stressed above and below the fatigue limit.

§ 2. Material

The tests were made on a high purity iron with about 0·5% carbon added. The carbon was distributed uniformly throughout the specimen. Figure 1† shows a typical microstructure.

§ 3. Apparatus and Method of Test

The specimens were fatigued in reversed bending between constant strain limits in the apparatus previously described (Wadsworth 1959 b). The frequency was 100 c/s and the amplitude was built up to its maximum value in a few thousand cycles. The tests were run to completion without interruption unless otherwise stated.

§ 4. Results

The specimens were fatigued at various strains in laboratory air or in vacuum. The results are shown in fig. 2. In the higher strain range the life in vacuum was about ten times that in air. At lower strains there appeared to be a fairly well-defined fatigue limit both in air and in vacuum. The two limits occurred at approximately the same number of cycles but at different strains. There was a range of strain in which specimens would break in air but not in vacuum.

The specimens were examined microscopically at the end of the test. The amount of slip visible was smaller on specimens subjected to smaller strains but some slip was visible on all specimens. There was no qualitative difference between the appearance of specimens fatigued just above and just below the fatigue limit. Etching specimens after fatiguing showed that the slip occurred in the ferrite grains and not in the pearlite, as shown in fig. 3.

Some specimens (not shown on fig. 2) were examined at intervals during the test. As any one test progressed the slip became more pronounced and obvious cracks appeared towards the end of the test. However, cracks were present in some slip bands earlier in the test and could be detected by extending the specimen thus causing the cracks to open. A number of specimens fatigued at a strain of $1{\cdot}34 \times 10^{-3}$ were examined. The life in vacuum was about 10^7 cycles and in air about 10^6 cycles. Cracks could not be detected in specimens fatigued for 10^5 cycles either in air or in vacuum but there were many present after 10^6 cycles in vacuum. Typically the larger of these cracks were 50–100 μ long and 5 μ deep.

Specimens fatigued for between 5×10^7 and 7×10^7 cycles below the fatigue limit in air or in vacuum were examined after extension. In all

† Figures 1, 3, 4 and 5 are shown as plates.

cases small cracks were found in a few slip bands. (A control test on an unfatigued specimen showed no similar cracks.) Those in the specimens fatigued in vacuum just below the fatigue limit were in general larger than those in specimens fatigued in air at a corresponding stress. Figures 4 and 5 show an example of each.

Fig. 2

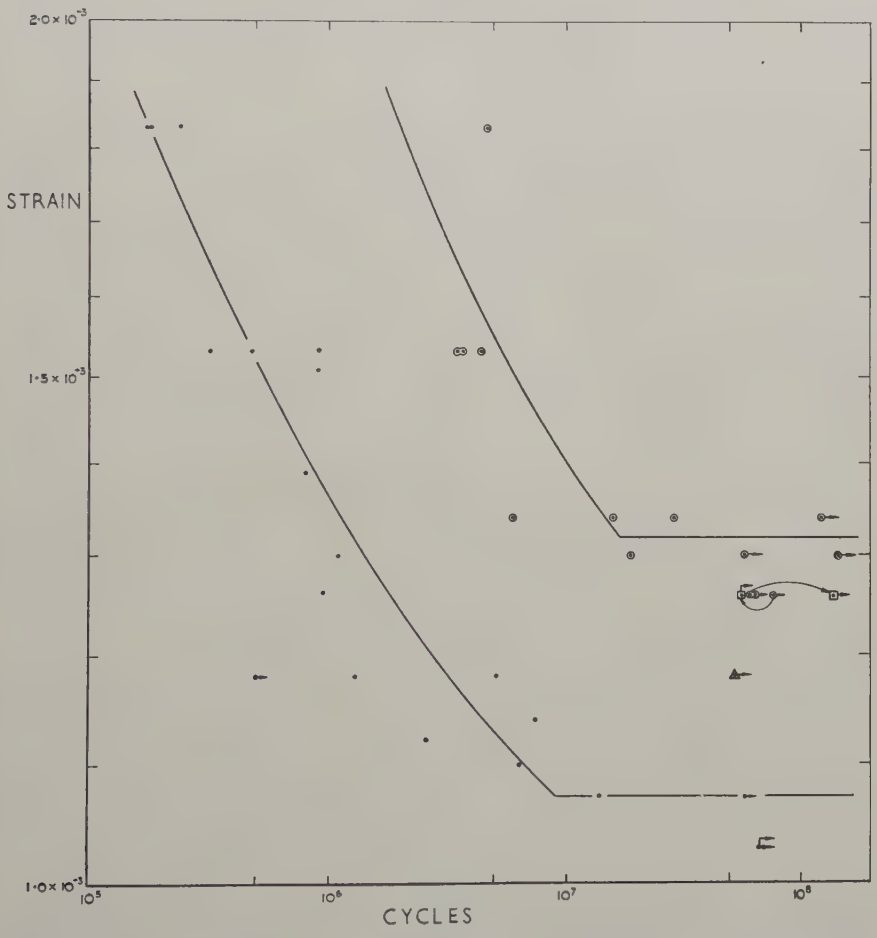

S–N Diagram. ●test in air; ⊙test in vacuum; △test in vacuum after fatiguing in air; ⊡ test in air after fatiguing in vacuum.

One specimen was fatigued for $7{\cdot}5 \times 10^7$ cycles at a strain of $1{\cdot}26 \times 10^{-3}$ in vacuum and then the test was continued in air. The specimen was still unbroken after a further $5{\cdot}6 \times 10^7$ cycles although the life of fresh specimens strained at this level in air is only about 10^6 cycles. Two other specimens were fatigued for about 10% and 15% of their expected life in air at a strain of $1{\cdot}18 \times 10^{-3}$ and the test continued in vacuum. The first

was unbroken after $3{\cdot}3 \times 10^7$ cycles and the second survived until 3×10^7 cycles when it broke possibly due to an equipment failure.

§ 5. Discussion

The results shown in fig. 2 show that the lives of specimens fatigued at high strains are about ten times longer in vacuum than in air. This factor is similar to those found for copper and aluminium (Wadsworth and Hutchings 1958). The interesting point, however, is that the fatigue limit occurred at approximately the same number of cycles in air as in vacuum but at a different strain. Thus there is a range of strains in which the specimens break after a few million cycles in air but seemingly last for ever in vacuum. It appears that fatigue cracks form in the slip bands at all the strains used in these experiments but that they can become non-propagating if the conditions are such as to give sufficiently slow initial growth. These conditions may be either a low strain ($1{\cdot}05 \times 10^{-3}$) in the presence of air or a higher strain ($1{\cdot}3 \times 10^{-3}$) without air. Once the crack has stopped propagating it is difficult to start again. Thus specimens fatigued below their fatigue limit in vacuum have small cracks in them but these do not propagate if the test is continued in air although fresh specimens would break at this strain. Presumably this difficulty in restarting a crack (or starting a new one) is also responsible for 'coaxing' (the increase of fatigue strength produced by prefatiguing below the fatigue limit) (Sinclair 1952). Coaxing and the fatigue limit appear to occur only together and with strain ageing.

It is interesting to consider if it is necessary for there to be continuing reversed plastic flow at the tip of a non-propagating crack or whether it is possible for the deformation at the tip to be elastic.

The theoretical elastic stress concentration factor at the tip of a crack of depth d (small compared with the specimen diameter) and tip radius ρ is $K_t = 1 + 2\sqrt{(d/p)}$ (Neuber 1946).

The maximum strain occurs over a very small region at the tip of the crack which may be very work hardened. Even so an elastic strain there of more than 1 or 2% is unlikely so K_t cannot be more than 10 or 20 on these assumptions. For cracks $3\,\mu$ deep these correspond to root radii of about 1500 Å and 300 Å respectively which are not impossible. It is very doubtful however if the strains can be wholly elastic in the case of larger non-propagating cracks such as those formed at the root of sharp notches in mild steel. Frost (1959) summarizes the evidence on these and shows photographs of cracks whose depth including the notches, is 1·3 mm and whose tip radius is less than $0{\cdot}4\,\mu$. This indicates $K_t > 100$. These cracks did not spread under a nominal stress of YM/2000 which would produce a strain of 5% at the crack tip. This is improbably high and it seems almost certain that reversed plastic flow must have occurred in each cycle without the crack spreading; it is quite possible that the same occurred in the tests described here.

If we assume that the crack was sufficiently sharp for plastic flow to be necessary it is of interest to calculate the order of magnitude of the flow involved. The depth of the plastic region at the bottom on the crack depends on the depth of the crack, the applied stress and the yield stress of the work hardened metal under the triaxial stress conditions at the tip of the crack. Lack of knowledge of the last factor precludes exact calculation but clearly the depth of the plastic region will be of the same order as the crack depth. The local plastic strain in the zone varies from zero at the inner edge to a large value in a small region at the tip of the crack. However, the whole region is surrounded by elastic material and the average plastic strain in it must be comparable with the elastic strain. Thus the total flow in the plastic zone is of the order of the crack depth multiplied by the maximum elastic strain. This is of the order of 100 Å. In other words in these specimens stressed just below their fatigue limit there was probably a region at the tip of each crack where some tens of dislocations move distances of perhaps half a micron each half cycle without producing further spreading of the crack.

It seems from this work that the fatigue limit is the strain below which cracks cannot propagate rather than the stress at which they cannot form, but more work is needed before the mechanism by which they are stopped is clear.

References

Clayton-Cave, J., Taylor, R. J., and Ineson, E., 1955, *J. Iron St. Inst.*, **180**, 161.

Frost, N. E., 1959, *Proc. Instn. mech. Engrs, Lond.*, **173**, 811.

Gough, H. J., and Sopwith, D. G., 1932, *J. Inst. Met.*, **49**, 93; 1935, *Ibid.*, **56**, 55; 1946, *Ibid.*, **72**, 415.

Hempel, M., 1956, *Fatigue in Aircraft Structures* (New York: Academic Press).

Neuber, H., 1946, *Theory of Notch Stresses* (Ann Arbor, Michigan, U.S.A.: Edwards Bros. Inc.).

Sinclair, G. M., 1952, *Proc. Amer. Soc. Test. Mater.*, **52**, 743.

Wadsworth, N. J., and Hutchings, J., 1958, *Phil. Mag.*, **3**, 1154.

Wadsworth, N. J., 1959 a, *Internal Stresses and Fatigue in Metals* (Elsevier Pub. Co.), p. 382; 1959 b, *J. sci. Instrum.*, **36**, 274.

The Kinetics of Impurity Precipitation on Dislocations Small Drift Theory†

By R. Bullough and R. C. Newman
Research Laboratory, Associated Electrical Industries,
Aldermaston Court, Aldermaston, Berkshire

[Received August 8, 1960]

Abstract

A perturbation solution of the differential equation controlling the migration of impurity atoms to a dislocation is given and boundary conditions appropriate to precipitation on the dislocation are derived. Numerical results within the range of validity of the perturbation analysis are obtained and used to discuss the ageing of carbon and nitrogen in iron.

§ 1. Introduction

It is now well established that there is a strong interaction between impurity atoms and dislocations. We envisage two distinct situations at the dislocation cores; either (*a*) some of the impurities there are rendered immobile and effectively removed from solid solution, that is, local precipitation is occurring on the dislocations (Bullough, Newman and Wakefield 1959, Bullough, Newman, Wakefield and Willis 1959, 1960, Ham 1959); or (*b*) the impurities all remain mobile and the equilibrium state is a Maxwellian concentration distribution (Bullough and Newman 1959): this will be referred to as an impurity atmosphere. Situation (*a*) could arise if either the local impurity concentration exceeds the equilibrium solid solubility or two impurities with a strong chemical affinity for each other are present in the core, since this provides an ideal site for nucleation of a second phase. (*b*) will arise if the impurities are chemically inert and if the final concentration in the core region is still sufficiently small for the probability of occupation of sites to be controlled by Boltzmann statistics; it is also necessary that this final concentration should be less than the equilibrium solid solubility of the impurity.

In the present treatment we shall consider a crystal initially containing a uniform concentration of impurities and investigate the kinetics of their migration. This is controlled by two processes, namely, diffusion and drift flow (Ham 1959, Bullough and Newman 1959). The solutions obtained of the differential equation take full account of the diffusion flow while a perturbation technique has been used to obtain the contribution of the drift flow when this is small. Boundary conditions at the dislocation cores are taken appropriate to either (*a*) or (*b*), and allowance is

† Communicated by the Authors.

made for a finite dislocation density. Also in the treatment of (a) due allowance is made for the possibility of a rate-limiting process occurring at the precipitate-matrix interface. This treatment therefore is essentially an extension of the previous theoretical analyses (Ham 1959, Bullough and Newman 1959, Cottrell and Bilby 1949, Harper 1951, Bilby 1955), each of which ignored at least one of the above factors. The general solution of the governing partial differential equation and a detailed formulation of the relevant boundary conditions are given in §§ 2 and 3 respectively. The required solutions satisfying the precipitation boundary conditions are derived in § 4 where the atmosphere solutions appear as a special limiting case. The solutions have been computed for various values of the parameters involved and are illustrated graphically in § 5. Finally, the theory is discussed with reference to some experiments of Thomas and Leak (1955) on the ageing of steel.

§ 2. The General Solution of the Differential Equation Governing the Migration of Impurities near a Dislocation

The governing differential equation for the flow of impurities in the neighbourhood of a dislocation, where the interaction potential has the form

$$\phi(r) = -A/r \qquad . \; . \; . \; . \; . \; . \; . \; (1)$$

has been shown to be (Bullough and Newman 1959)

$$\frac{1}{D}\frac{\partial c(r,t)}{\partial t} = \frac{\partial^2 c(r,t)}{\partial r^2} + \frac{1}{r}\frac{\partial c(r,t)}{\partial r} + \frac{L}{r}\left[\frac{1}{r}\frac{\partial c(r,t)}{\partial r} - \frac{1}{r^2}c(r,t)\right] \qquad (2)$$

where $L = A/kT$. Attempts to obtain an exact closed solution of (2) have been unsuccessful and recourse has been made to the following approximate analytic technique. The terms in (2) not involving L constitute the well-known radial diffusion equation for which the general solution is known. We therefore look for a solution consisting of the diffusion solution plus additional terms of order L/r. Such a solution will, of course, only be valid if $L/r \lesssim 0{\cdot}2$. For carbon in iron the value of L is about 40 Å (Cottrell 1953); however, much smaller values may be expected when the ionic radius of the impurity is similar to that of the atoms forming the parent lattice and where these impurities occupy substitutional sites. It is reasonable to associate the minimum value of r with the radius of the region at the centre of the dislocation inside which linear elasticity is not valid; this radius is probably less than about 10 Å. Thus, it is clear that our first order solution† in L/r will not be directly applicable to the case of carbon in iron. But nevertheless it should indicate the relative importance of the diffusion and drift flows at various stages in the ageing process in iron and may well be directly applicable to other systems.

† The second-order perturbation has been carried through and it is found that the coefficient of $(L/r)^2$ cannot be expressed in closed form.

Transforming eqn. (2) by means of a Laplace transform, and writing

$$\bar{c}(r, \lambda) = \int_0^\infty c(r, t) \exp(-qt)\, dt \quad (\text{where } q = D\lambda^2)$$

we obtain the ordinary differential equation for $\bar{c}(r, \lambda)$:

$$\frac{d^2\bar{c}(r, \lambda)}{dr^2} + \left[\frac{1}{r} + \frac{L}{r^2}\right]\frac{d\bar{c}(r, \lambda)}{dr} - \left[\frac{L}{r^3} + \lambda^2\right]\bar{c}(r, \lambda) = -c_0/D \quad . \quad . \quad (3)$$

where c_0 is the initial uniform concentration and D is the diffusion coefficient. The general solution of (3), correct to order L/r, must have the form:

$$\bar{c}(r, \lambda) = A(\lambda)K_0(\lambda r)[1 + Lg(r, \lambda)] + B(\lambda)I_0(\lambda r)[1 + Lh(r, \lambda)] + \frac{c_0}{D\lambda^2} + Lf(r, \lambda) \quad . \quad . \quad . \quad . \quad . \quad . \quad . \quad (4)$$

where A and B are arbitrary functions of λ to be determined from the boundary conditions; (4), with $L = 0$, is the well-known solution of Bessel's equation to which (3) reduces when $L = 0$. Substituting (4) into (3) leads to three elementary second-order differential equations from which the functions g, h and f can easily be deduced:

$$g(r, \lambda) = -\frac{\lambda}{K_0(\lambda r)}\left\{I_0(\lambda r)\int_\infty^r \frac{K_0(\lambda t)K_1(\lambda t)}{t}\, dt + K_0(\lambda r)\int_0^r \frac{K_0(\lambda t)I_1(\lambda t)}{t}\, dt\right\}, \quad . \quad . \quad . \quad . \quad . \quad (5)$$

$$h(r, \lambda) = -\frac{\lambda}{I_0(\lambda r)}\left\{K_0(\lambda r)\int_0^r \frac{I_0(\lambda t)I_1(\lambda t)}{t}\, dt + I_0(\lambda r)\int_\infty^r \frac{K_1(\lambda t)I_0(\lambda t)}{t}\, dt\right\}, \quad . \quad . \quad . \quad . \quad . \quad (6)$$

$$f(r, \lambda) = \frac{c_0}{D\lambda^2 r} + \frac{c_0}{D}\left\{I_0(\lambda r)\int_\infty^r K_0(\lambda t)dt - K_0(\lambda r)\int_0^r I_0(\lambda t)\, dt\right\} \quad . \quad (7)$$

The arbitrary constants associated with the subsidiary differential equations for g and h have been compounded into the A and B of the complete solution (4) and it can be shown that

$$g(r, \lambda) = \frac{1}{r} - \frac{\lambda K_1(\lambda r)}{K_0(\lambda r)}, \quad . \quad . \quad . \quad . \quad . \quad . \quad . \quad (8)$$

$$h(r, \lambda) = \frac{1}{r} + \frac{\lambda I_1(\lambda r)}{I_0(\lambda r)}, \quad . \quad . \quad . \quad . \quad . \quad . \quad . \quad (9)$$

$$f(r, \lambda) = \frac{c_0}{D\lambda^2}\left\{\frac{1}{r} + \frac{\pi\lambda}{2}[L_0(r\lambda) - I_0(r\lambda)]\right\} \quad . \quad . \quad . \quad (10)$$

where L_ν is a Struve function of imaginary argument (see Watson 1952, p. 329). However, because of the complexity of the boundary conditions, it was convenient to leave g, h and f in the integral form (5)–(7) until after inversion of the Laplace transform.

§ 3. The Boundary Conditions

The model of the core is similar to that used in our previous treatment for the growth of an impurity atmosphere (Bullough and Newman 1959). We surround the dislocation line by a virtual cylindrical surface of radius r_0 inside which the impurity atoms have very high mobility (in this region we designate an infinite value for D). Observations indicate that the precipitates nucleate and grow at discrete points along the dislocation. The basic feature of the model is that the rate of growth of these particles is assumed to be proportional to the concentration of impurity in the core region. The constant of proportionality will be varied between infinity, the fastest possible rate of precipitation and zero, corresponding to the formation of an atmosphere with no precipitation.

In the derivation of this boundary condition, we shall neglect any back flow from the precipitate particles; such a flow would lead to a non-zero equilibrium distribution of impurity in the crystal. If, however, the equilibrium surface concentration at the precipitate matrix interface is small compared with the initial concentration c_0 then omission of this term is not important. We write the core boundary condition:

$$c(r_0, t) = c_g(t) \qquad (11)$$

where $c_g(t)$ is the concentration of mobile impurities within the region $r < r_0$. $c_g(t)$ may be determined since its rate of change is simply the difference between the net flow of impurities into the core region $F(r_0, t)$ and their simultaneous removal as a result of the precipitation; thus

$$\pi r_0^2 \frac{dc_g(t)}{dt} = 2\pi r_0 F(r_0, t) - \pi r_0^2 c_g(t) P \qquad (12)$$

where P is the rate-limiting constant governing precipitation and

$$F(r_0, t) = D\left[\frac{L}{r_0^2} c(r_0, t) + \frac{\partial c}{\partial r}(r_0, t)\right]. \qquad (13)$$

Integrating (12) with the initial condition

$$c_g(0) = c_0 \qquad (14)$$

we obtain, with the aid of (11), the general core boundary condition:

$$c(r_0, t) = c_0 \exp[-Pt] + \frac{2}{r_0} \exp[-Pt] \int_0^t \exp[Pt] F(r_0, t)\, dt. \qquad (15)$$

If $P = 0$, (15) becomes:

$$c(r_0, t) = c_0 + \frac{2}{r_0} \int_0^t F(r_0, t)\, dt. \qquad (16)$$

which is the core boundary condition for the growth of an impurity atmosphere. Similarly, if $P \to \infty$, (15) becomes:

$$c(r_0, t) = 0 \qquad (17)$$

which is the core boundary condition (Ham 1959) appropriate to precipitation without rate limitation at the precipitate matrix interface.

In a real crystal there will be a finite dislocation density ρ and we may associate with each dislocation a cylindrical surface of radius $R=(\pi\rho)^{-1/2}$. The second boundary condition is simply that there should be zero net flow across this surface; thus

$$\frac{L}{R^2}c(R,t)+\frac{\partial c}{\partial r}(R,t)=0. \quad . \quad . \quad . \quad . \quad . \quad (18)$$

For an isolated dislocation, $\rho\to 0$, (18) leads to the boundary condition $c(r,t)\to c_0$, when $r\to\infty$.

The quantity eventually required is the number of impurities $W(t)$ precipitated in time t per unit length of a dislocation, which is given by

$$W(t)=\pi r_0^2 P\int_0^t c_g(t')\,dt' \quad . \quad . \quad . \quad . \quad . \quad . \quad (19)$$

where $c_g(t)$ is defined by (11) and (15). It is not convenient to obtain W directly, and we first evaluate the number of impurities $V(t)$ which have entered unit length of the core region $r<r_0$ in time t. We have, from (13),

$$V(t)=2\pi r_0 D\int_0^t\left[\frac{L}{r_0^2}c(r_0,t)+\frac{\partial c}{\partial r}(r_0,t)\right]dt. \quad . \quad . \quad . \quad (20)$$

This quantity rather than (19) is required for the case of the growth of an impurity atmosphere (Bullough and Newman 1959). By differentiating eqn. (20) and making use of (13), the relationship between W and V follows:

$$W(t)=\pi r_0^2 c_0[1-\exp(-Pt)]+P\int_0^t\exp(-Pt')\,dt'\int_0^{t'}\exp(Px)\frac{dV(x)}{dx}dx.$$
$$. \quad . \quad . \quad (21)$$

The Laplace transforms of the boundary conditions and the quantity $V(t)$ are: from (15) and (13):

$$\bar{c}(r_0,\lambda)=\frac{c_0 r_0^2}{D(r_0^2\lambda^2+\alpha^2)}+\frac{2r_0}{(r_0^2\lambda^2+\alpha^2)}\left[\frac{L}{r_0^2}\bar{c}(r_0,\lambda)+\frac{d\bar{c}}{dr}(r_0,\lambda)\right] \quad (22)$$

where the dimensionless parameter α^2 is given by $\alpha^2=r_0^2P/D$; (18) becomes:

$$\frac{L}{R^2}\bar{c}(R,\lambda)+\frac{d\bar{c}}{dr}(R,\lambda)=0 \quad . \quad . \quad . \quad . \quad . \quad . \quad (23)$$

and

$$\bar{V}(\lambda)=\frac{2\pi r_0}{\lambda^2}\left[\frac{L}{r_0^2}\bar{c}(r_0,\lambda)+\frac{d\bar{c}}{dr}(r_0,\lambda)\right] \quad . \quad . \quad . \quad . \quad (24)$$

§ 4. The Required Solutions

The two arbitrary functions $A(\lambda)$ and $B(\lambda)$ in the general solution (4), with g, h and f given by (5), (6) and (7) respectively are obtained by satisfying the boundary conditions (22) and (23). The resulting expressions†

† In the analysis L/r_0 is treated as a small quantity and only terms of this and zero order are conserved.

for $\bar{c}(r_0, \lambda)$ and $d\bar{c}(r_0, \lambda)/dr$, are then substituted into eqn. (24) for $\bar{V}(\lambda)$. After considerable algebraic manipulation it can be shown that:

$$\frac{\bar{\Gamma}(\lambda)}{2\pi r_0 c_0} = \frac{\alpha^2 w_{11}(r_0)}{D\lambda^3[\alpha^2 w_{10}(r_0) + \lambda^2 r_0^2 w_{12}(r_0)]} + \frac{L}{r_0} \frac{(r_0^2\lambda^2 + \alpha^2)}{D\lambda^3[\alpha^2 w_{10}(r_0) + \lambda^2 r_0^2 w_{12}(r_0)]^2} \int_{r_0}^{R} w_{11}(y)[\alpha^2(w_{10}(r_0) - w_{10}(y)) + \lambda^2 r_0^2 w_{12}(r_0)]\, dy/y \quad . \quad . \quad . \quad . \quad . \quad . \quad . \quad . \quad (25)$$

where $w_{ij}(x) = I_i(R\lambda)K_j(x\lambda) + (-1)^j K_i(R\lambda)I_j(x\lambda)$.

The quantity $V(t)$ is now given by the inverse Laplace transformation:

$$V(t) = \frac{1}{2\pi i}\int_{c-i\infty}^{c+i\infty} \bar{V}(\lambda) \exp(qt)\, dq \quad . \quad . \quad . \quad . \quad . \quad . \quad (26)$$

where $\lambda = \sqrt{(q/D)}$, and the Bromwich contour appropriate for a single valued function of q is used; an unusual feature of this inverse Laplace transformation is the evaluation of the residues at the double poles of $\bar{V}(\lambda)$. The integration over y is then performed; we obtain after considerable reduction:

$$\frac{V(t)}{V(\infty)} = 1 - \frac{4\alpha^2 K}{1-K^2} \sum_{n=0}^{\infty} \frac{\exp(-\lambda_n^2 M) v_{11}(\lambda_n)}{\lambda_n^2 A_n} + \frac{4K}{1-K^2} \cdot \frac{L}{r_0} \times \sum_{n=0}^{\infty} \frac{\exp(-\lambda_n^2 M)}{\lambda^2{}_n A_n{}^2} [\alpha^2(\alpha^2 - K^2\lambda_n^2) C_n M + \alpha^2 D_n - (\alpha^2 - K^2\lambda_n^2) A_n B_n] \quad . \quad . \quad . \quad (27)$$

where $V(\infty) = \pi c_0(R^2 - r_0^2)$, $M = Dt/R^2$, $K = r_0/R$ and λ_n are the positive roots of

$$Y_1(\lambda)[\alpha^2 J_0(K\lambda) + K^2\lambda^2 J_2(K\lambda)] - J_1(\lambda)[\alpha^2 Y_0(K\lambda) + K^2\lambda^2 Y_2(K\lambda)] = 0. \quad (28)$$

The quantities A_n, B_n, C_n and D_n are given by:

$$A_n = (\alpha^2 - K^2\lambda_n^2)(v_{00} - Kv_{11}) + 2K\lambda_n v_{01},$$

$$B_n = -\frac{2}{\pi} + H_1(\lambda_n) - K\lambda_n v_{10} + v_{11} - \frac{\pi K\lambda_n}{2}[v_{11}H_0(K\lambda_n) - v_{10}H_1(K\lambda_n)],$$

$$C_n = -\frac{8}{\pi^2} + 2\lambda_n[K\lambda_n(v_{11}^2 + v_{10}^2) - v_{11}v_{10}],$$

$$D_n = -\frac{8\alpha^2}{\pi^2\lambda_n^2} + \alpha^2 K[3v_{11}^2 + 3v_{10}^2 - 2\lambda_n(v_{01}v_{11} + v_{00}v_{10})] - \alpha^2[v_{11}v_{20} + v_{10}v_{21}] + K^2\lambda_n^2[v_{10}v_{21} - v_{00}v_{11}] - K^3\lambda_n^2[v_{11}^2 + v_{10}^2 - 2\lambda_n(v_{01}v_{11} + v_{10}v_{00})] \quad . \quad . \quad . \quad . \quad . \quad (29)$$

where $$v_{ij} = v_{ij}(\lambda_n) = Y_i(\lambda_n)J_j(K\lambda_n) - J_i(\lambda_n)Y_j(K\lambda_n). \quad . \quad . \quad . \quad (30)$$

$W(t)$, the number of impurities precipitated in time t per unit length of the dislocation, can now be obtained by differentiating (27) term by

term with respect to t and then substituting the result in (21), and performing the elementary repeated (term by term) integration. If we write $V(t)/V(\infty)$ in the symbolic form:

$$V(t)/V(\infty)=1+\sum_{n=0}^{\infty}X_n\exp(-\lambda_n{}^2M)+\frac{L}{r_0}\sum_{n=0}^{\infty}(Y_nM+Z_n)\exp(-\lambda_n{}^2M) \quad . \quad . \quad . \quad (31)$$

where the values of X_n, Y_n and Z_n follow from (27) we obtain

$$\frac{W(t)}{W(\infty)}=1-\exp(-\alpha^2m)+\frac{\alpha^2}{K^2}(1-K^2)\sum_{n=0}^{\infty}\frac{X_n}{(\alpha^2/K^2-\lambda^2{}_n)}[\exp(-\lambda^2{}_nM)-\exp(-\alpha^2m)]+\frac{L}{r_0}\frac{\alpha^2}{K^2}(1-K^2)$$

$$\times\left\{\sum_{n=0}^{\infty}\frac{[\exp(-\alpha^2m)-\exp(-\lambda_n{}^2M)][Y_n-Z_n(\alpha^2/K^2-\lambda_n{}^2)]}{(\alpha^2/K^2-\lambda_n{}^2)^2}+\frac{(\alpha^2/K^2-\lambda_n{}^2)Y_nM\exp(-\lambda_n{}^2M)}{(\alpha^2/K^2-\lambda_n{}^2)^2}\right\} \quad . \quad . \quad . \quad . \quad . \quad . \quad (32)$$

where $W(\infty)=\pi R^2c_0$ and $m=Dt/r_0{}^2$.

If $\alpha\to 0$ in (27), that is precipitation is inhibited and an impurity atmosphere forms round the dislocation, then $V(t)\to N(t)$ given by eqn. (49) of our previous atmosphere calculation (Bullough and Newman 1959). It should be noted that when taking the limit as α tends to zero in (27) the first root λ_0 of (28) also tends to zero; in fact $\lambda_0\to\alpha\to 0$. In the present notation we have for the number $N(t)$ of impurities having entered the core region $r<r_0$ in time t:

$$\frac{N(t)}{N(\infty)}=1-\frac{4}{(1-K)^2}\sum_{n=0}^{\infty}\exp(-\lambda_n{}^2M)E_n \quad . \quad . \quad . \quad (33)$$

where

$$\delta_nE_n=v_{11}\left[-1+\frac{2}{\pi}\left(1-\frac{\pi}{2}H_1(\lambda_n)\right)+\frac{\pi}{2}\left(2H_1(K\lambda_n)-K\lambda_nH_0(K\lambda_n)\right)\right],$$

$\delta_n=K\lambda_n{}^2[v_{22}-Kv_{11}]$ and λ_n are the positive roots of

$$J_1(\lambda)Y_2(K\lambda)-J_2(K\lambda)Y_1(\lambda)=0. \quad . \quad . \quad . \quad . \quad . \quad (34)$$

$N(\infty)$ in eqn. (32) is given by

$$N(\infty)=\pi Lr_0c_0(1-K)^2. \quad . \quad . \quad . \quad . \quad . \quad . \quad (35)$$

If the dislocation density is sufficiently low, any interaction between adjacent dislocations will be negligible and the kinetics of precipitation and atmosphere formation on such dislocations may be obtained by considering an isolated dislocation in an infinite medium. The required expression for $\bar{V}(\lambda)$ is again obtained by substituting $\bar{c}(r_0,\lambda)$ and $d\bar{c}(r_0,\lambda)/dr$ into (24). In this case, however, the arbitrary function $B(\lambda)$ is set equal to zero; that is there is only one arbitrary function $A(\lambda)$ in what is now

the *bounded* general solution. $A(\lambda)$ is determined from the core boundary condition (22). The final result is:

$$\frac{\bar{V}(\lambda)}{2\pi r_0 c_0} = \frac{\alpha^2 K_1(r_0\lambda)\Phi(\lambda)}{D\lambda^3} + \frac{L}{r_0}\frac{(r_0^2\lambda^2+\alpha^2)}{D\lambda^3}\Phi(\lambda) \times\left\{\alpha^2\Phi(\lambda)\int_\infty^{r_0}\frac{K_0(\lambda y)K_1(\lambda y)}{y}dy - \int_\infty^{r_0}\frac{K_1(\lambda y)}{y}dy\right\} \quad . \quad . \quad . \quad (36)$$

where

$$\Phi(\lambda) = [\alpha^2 K_0(r_0\lambda) + r_0^2\lambda^2 K_2(r_0\lambda)]^{-1}. \quad . \quad . \quad . \quad . \quad (37)$$

$V(t)$ is given by the inverse Laplace transform using a 'cut' Bromwich contour appropriate for a multi-valued function, the only residue being at $\lambda=0$. After performing the integration over y we obtain for the number of impurities $V(t)$ which have entered unit length of the core in time t:

$$\frac{V(t)}{4r_0^2c_0} = \frac{2\alpha^2}{\pi}\int_0^\infty \frac{[1-\exp(-mx^2)]}{x^3}\left\{\frac{\alpha^2-x^2}{\Delta_1^2(x)+\Delta_2^2(x)}\right\}dx + \frac{L}{r_0}\int_0^\infty [1-\exp(-mx^2)](x^2-\alpha^2)\left\{\alpha^2\left[H_0(x)-Y_0(x)-\frac{2}{\pi x}\right] + x^2\left[H_2(x)-Y_2(x)-\frac{2}{\pi x}\left(1+\frac{x^2}{3}\right)\right]\right\}dx$$

$$\frac{}{x^2[\Delta_1^2(x)+\Delta_2^2(x)]}$$

$$+\frac{L}{r_0}\alpha^2\int_0^\infty \frac{[1-\exp(-mx^2)](\alpha^2-x^2)\{R(x)[\Delta_1^2(x)-\Delta_2^2(x)]+2S(x)\Delta_1(x)\Delta_2(x)\}}{x^2[\Delta_1^2(x)+\Delta_2^2(x)]^2}dx \quad . \quad . \quad . \quad (38)$$

where $m = Dt/r_0^2$, $\Delta_1(x) = \alpha^2 Y_0(x) + x^2 Y_2(x)$ and $\Delta_2(x) = \alpha^2 J_0(x) + x^2 J_2(x)$. The quantities $R(x)$ and $S(x)$ are given by:

$$\left.\begin{aligned} R(x) &= 2x[J_1(x)Y_1(x)+J_0(x)Y_0(x)] - [J_0(x)Y_1(x)+Y_0(x)J_1(x)], \\ S(x) &= x[J_1^2(x)+J_0^2(x)-Y_1^2(x)-Y_0^2(x)] - J_0(x)J_1(x) \\ &\quad + Y_0(x)Y_1(x). \end{aligned}\right\} \quad (39)$$

$W(t)$ can be obtained directly from (38) by following the procedure given above.

α^2 can be set equal to zero in (38) and we get

$$\frac{V(t)}{\pi r_0 c_0 L} = 1 - \frac{4}{\pi}\int_0^\infty \frac{\exp(-mx^2)}{x^2}\frac{\{H_2(x)-Y_2(x)-(2/\pi x)[1+x^2/3]\}}{J_2^2(x)+Y_2^2(x)}dx \quad . \quad . \quad . \quad (40)$$

for the growth of an impurity atmosphere round an isolated dislocation†.

† In our previous treatment for the growth of an impurity atmosphere (Bullough and Newman 1959) the term $J_2(x)$ in the numerator of the solution (eqn. (43)) should be $Y_2(x)$ as shown in (40) above. The correct term was, however, included for the numerical computation described in this previous work.

§ 5. Numerical Results

The expressions (27), (32) and (38) have been computed for various values of the parameters. In order to compute (27) and (32), we have first to determine the positive roots of (28). At this stage we must allocate numerical values to the parameters α^2 and $K = r_0/R$. We choose an arbitrarily large value of 60 Å for r_0, which for a dislocation density of 3×10^{10} lines/sq. cm leads to the value of K of 0·1838; by a reduction of r_0, the same K would, of course be applicable to a greater dislocation density. The values of α^2 taken were:

0·03, 0·1, 0·3, 1·0, 3·0, 10·0 and 1000,

the final value corresponding approximately to no rate limitation ($\alpha^2 = \infty$) at the precipitate matrix interface. The roots of (28), for the above values of K and α^2, were obtained by an iteration procedure involving the use of a high speed digital computer. The first four roots were found for each α^2 value and are given in the table. These roots were used to sum the first four terms of (27) and (32) for the range of $M = 2^n$ where n runs

First four roots of expression (28) with $K = 0{\cdot}1838$

α^2	λ_0	λ_1	λ_2	λ_3
0·03	0·172100	3·871807	7·196025	10·675518
0·1	0·308740	3·914209	7·221338	10·688623
0·3	0·511182	4·028760	7·293896	10·727002
1·0	0·815088	4·353662	7·546533	10·870264
3·0	1·082666	4·861475	8·161279	11·331201
10·0	1·258545	5·308838	9·005615	12·525635
1000	1·359912	5·569385	9·491260	13·372607

from -7 to $+9$ in unit steps. The constant factor between successive values of M was taken to provide a uniform spacing of points when M is plotted on a logarithmic scale. Clearly, for $M > 1$, only the first term in (27) or (32) is required while for $M \lesssim 0{\cdot}1$, more terms in the series will be necessary. The error introduced by restricting the series to four terms was determined by computing (38) since, by suitable normalization (see ordinate scale of fig. 3), this solution for an infinite body becomes identical to the early stage solution (small values of M) for a finite body; for

$$1 > M > 0{\cdot}01,$$

the error was, in fact, negligible.

Figure 1 shows the variation of the precipitated fraction with time (expression (32)), in the absence of any drift flow ($L = 0$). The expression has also been computed assuming $L/r_0 = 0{\cdot}2$, which is a value consistent with the first-order perturbation solution. On the scale used in fig. 1, it is found that inclusion of the drift terms leads to no significant increase in the precipitated fraction at any time for any of the values of α^2 adopted.

Fig. 1

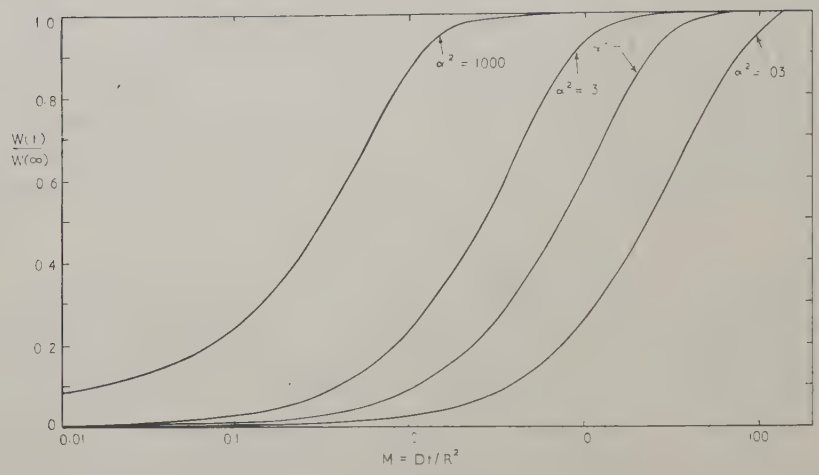

The precipitated fraction of solute as a function of reduced time $M = Dt/R^2$; pure diffusion flow ($L=0$).

Fig. 2

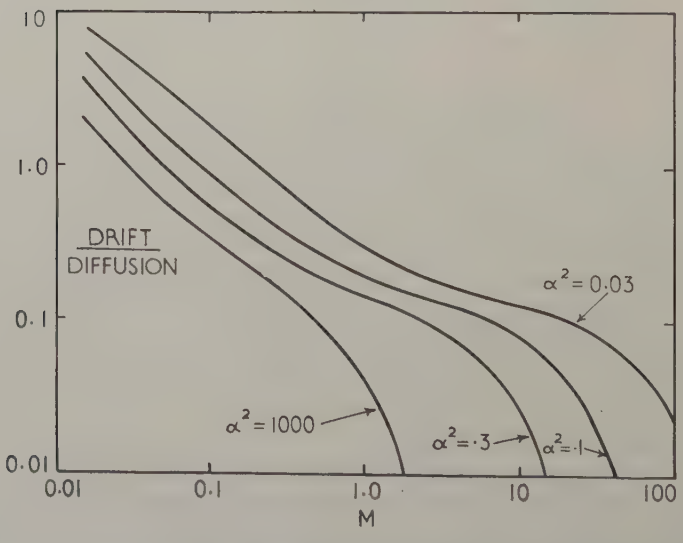

Ratio of drift contribution to diffusion contribution as a function of reduced time and $\alpha^2(L/r_0=0{\cdot}2)$.

However, as one might expect, the relative contribution of drift to diffusion can be quite large in the early stages of precipitation as illustrated in fig. 2, where the ratio of the drift and diffusion contribution from eqn. (32) has been plotted against M.

$V(t)/V(\infty)$ from expression (31) has also been computed and shows no significant difference from $W(t)/W(\infty)$ shown in fig. 1.

Fig. 3

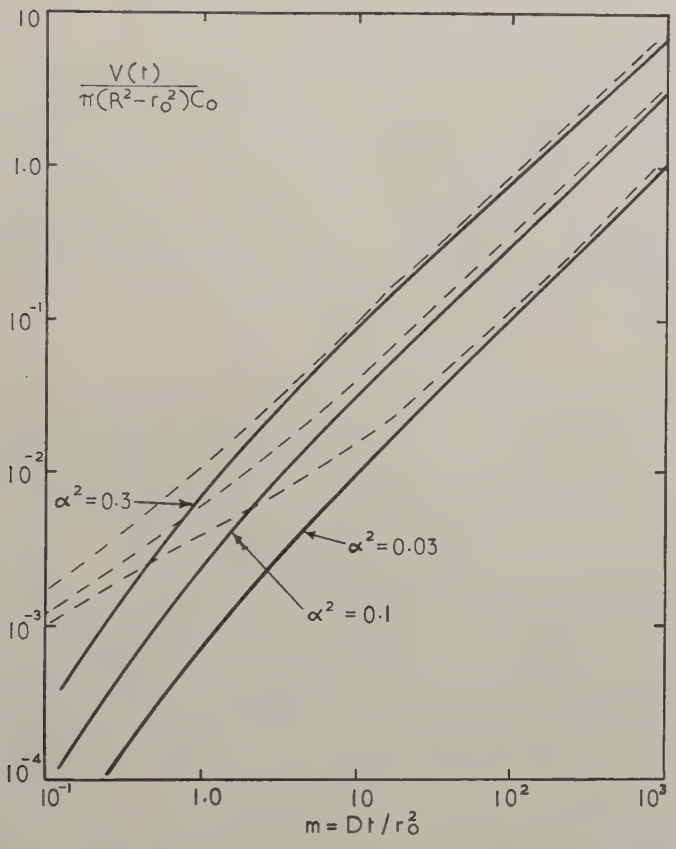

Quantity of solute entering isolated dislocation, normalized for link up procedure.

———— Diffusion flow only ($L=0$).

– – – – Diffusion plus drift ($L=0{\cdot}2$).

For very low dislocation densities, we require the solution (38) for an isolated dislocation and also for the small M values shown in fig. 1 (after suitable normalization). Figure 3 shows expression (38) with $L/r_0=0$ and 0·2 respectively; from these curves it is again apparent that the drift contribution is important during the early stages.

It is important to know the sensitivity of the curves in fig. 1 to possible variations in the dislocation density, specified by the ratio K. The three curves shown in fig. 1 for the low α^2 values may be closely approximated to by the first term in the infinite series (32) since most of the variation shown by these curves is over the range $M > 1$. In fact, for $\alpha^2 \lesssim 0{\cdot}1$ we may write

$$\left.\begin{aligned} \frac{W(t)}{W(\infty)} &= 1 - \exp\left[-\lambda_0{}^2 M\right] \\ \text{where } \lambda_0{}^2 \text{ is given by} & \\ \lambda_0{}^2 &\approx 2[\ln(1/K) - \tfrac{1}{2} + 2/\alpha^2]^{-1}. \end{aligned}\right\} \quad \ldots\ldots \quad (41)$$

It is clear that for the above small values of α^2, $\lambda_0{}^2$ is not very sensitive to variations in K; however, when α^2 is very large, variations of K will have a much greater effect on the values of $\lambda_0{}^2$ and hence on the value of M for which $W(t)/W(\infty)$ attains a given value. This latter result, for infinite α^2, has been discussed previously by Ham (1959). It is also worth noting that if the dislocation density is reduced then because the value of $W(\infty)$ is increased, the ratio of the drift to diffusion contributions, as shown in fig. 2, will also be reduced at a given M value.

§ 6. Discussion

We now consider briefly some of the available experimental results for quench and strain ageing in relation to the above theoretical treatment.

The quench ageing results obtained by Thomas and Leak (1955) have been replotted in figs. 4 and 5 where the vertical scale has been renormalized for all the curves such that the variation is between one and zero. The necessity for such renormalization indicates that there is a measurable non-zero equilibrium solubility of the impurity at these high temperatures. In these figures an arbitrary time scale has been used since a plot against reduced time (proportional to Dt where D has been given by Wert (1950) for carbon in iron, and Thomas and Leak (1954) for nitrogen in iron) does not bring the various curves into coincidence; in fact, the relative separation of the curves as a function of temperature is much less than it would be if the ageing were a simple diffusion limited process. If the precipitation were controlled by a single mechanism, then the experimental results would indicate much reduced activation energies compared with those of the diffusion coefficients. A possible conclusion is that a finite rate limiting process occurs at the precipitate matrix-interface. That this is so can be seen from eqn (41) since for small values of α^2 the explicit dependence of $W(t)/W(\infty)$ on D disappears.

For nitrogen in iron (fig. 4) the results at 98°C lie on a very good straight line while the results at 84°C deviate somewhat from a straight line. For carbon in iron (fig. 5) the results at 109°C, 300°C and 397°C all lie on straight lines; the latter two show a small zero error on the time scale of about 30 sec. Such small time errors have been observed by Wert (1949) in similar experiments when high annealing temperatures are involved.

The curious behaviour at 200°C is completely inexplicable and is quite out of keeping with the results at the other temperatures.

The linear variations found for the experimental results shown in figs. 4 and 5 are consistent with the form of the theoretical curves in fig. 1 for small α^2; the curves for $\alpha^2 = 0{\cdot}1$ and $0{\cdot}03$ have been replotted in fig. 4. To compare theory and experiment, it is necessary to know either the dislocation density or α^2 to determine the other uniquely, since both these factors are directly involved in the evaluation of the controlling first root of (28).

Fig. 4

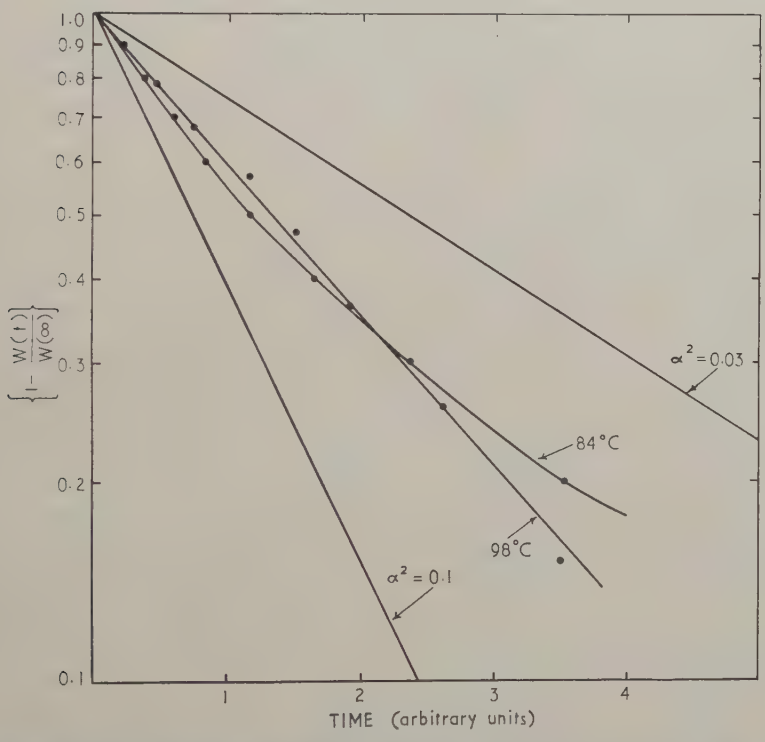

Experimentally observed kinetics of formation of nitride precipitates in iron (Thomas and Leak 1955).

In this discussion of quench ageing, we have assumed, by our adoption of cylindrical geometry, that all the precipitates are nucleated on the dislocations. However, if the dislocation density is very low, then it is probable that a significant proportion of precipitate nuclei form at random sites throughout the crystal. This could provide an explanation for the different precipitation kinetics, more characteristic of spherical rather than cylindrical geometry, observed in the quench ageing experiments of Wert (1949).

The kinetics of impurity depletion during strain ageing experiments do not have the form of the curves given in fig. 1 but are better represented by the semi-empirical formula proposed by Harper (1951):

$$\frac{W(t)}{W(\infty)} = 1 - \exp\left[-3\rho(\pi/2)^{1/3}(LDt)^{2/3}\right]$$

where ρ is the dislocation density. Any explanation of this variation must still await a treatment which incorporates a large drift potential or a transient variation in the value of the rate-limiting parameter or possibly both these factors. Such a treatment requires a completely numerical approach and will be presented in a subsequent paper.

Fig. 5

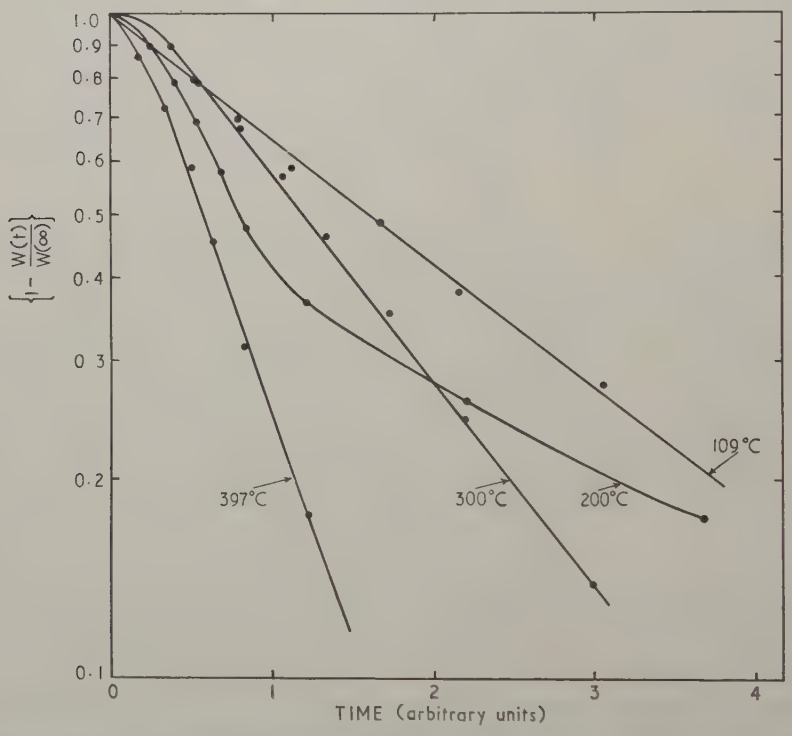

Experimentally observed kinetics of formation of carbide precipitates in iron (Thomas and Leak 1955).

Acknowledgments

The authors wish to thank Mr. D. P. R. Petrie and Mr. R. L. Rouse for their encouragement and useful comments on the manuscript and also Mr. P. Redman for assistance with the numerical work. Thanks are due to Dr. T. E. Allibone, F.R.S., Director of the Laboratory, for permission to publish this paper.

References

Bilby, B. A., 1955, *J. phys. Soc. Japan*, **10,** 673.
Bullough, R., and Newman, R. C., 1959, *Proc. Roy. Soc.* A, **249,** 427.
Bullough, R., Newman, R. C., and Wakefield, J., 1959, *Proc. Inst. elect. Engrs*, B, **106,** 277.
Bullough, R., Newman, R. C., Wakefield, J., and Willis, J. B., 1959, *Nature, Lond.*, **183,** 34; 1960, *J. appl. Phys.*, **31,** 707.
Cottrell, A. H., 1953, *Dislocations and Plastic Flow in Crystals* (Oxford: University Press).
Cottrell, A. H., and Bilby, B. A., 1949, *Proc. phys. Soc. Lond.*, **62,** 49.
Ham, F. S., 1959, *J. appl. Phys.*, **30,** 915.
Harper, S., 1951, *Phys. Rev.*, **83,** 709.
Thomas, W. R., and Leak, G. M., 1954, *Phil. Mag.*, **45,** 656; 1955, *J. Iron St. Inst.*, **180,** 155.
Watson, G. N., 1952, *The Theory of Bessel Functions* (Cambridge: University Press).
Wert, C. A., 1949, *J. appl. Phys.*, **20,** 943; 1950, *Phys. Rev.*, **79,** 601.

The Hall Coefficient of Liquid Mercury †

By N. Cusack and P. Kendall
Department of Physics, Birkbeck College, London

[Received September 13, 1960]

Abstract

A technique for measuring the Hall coefficient of liquid metals is described. Results for solid and liquid mercury are presented and discussed. The Hall coefficient for liquid mercury is found to be -75×10^{-5} e.m.u. over the temperature range $-38{\cdot}9$°c to $+100$°c.

§ 1. Introduction

On both the experimental and theoretical sides, knowledge of electrical properties is far less complete for liquid than for solid metals. Observations of de Haas–van Alphen effect or other properties which have been significant for the understanding of electronic states in solids are not possible for liquids, while theoretical accounts of the change (if any) in electronic states at and above the melting point are still undeveloped.

Although observations of resistivity, thermoelectric power, and galvanomagnetic coefficients cannot by themselves provide detailed information about electronic states, there are certain qualitative questions which should be answerable by observation of the Hall coefficient in liquid metals. These are: do the conduction electron states change significantly at the melting point? and do they vary with temperature in the liquid state? These questions are suggested by (i) the occurrence of the volume and structure change at the melting point; (ii) the possibility of progressive structural change in the liquid state as the temperature rises (Bernal 1959); (iii) the fact that the rate of increase of resitivity with temperature is frequently smaller in the liquid than in the solid and, though often constant, is much less than would correspond to $\rho\propto T$°k; (iv) the fact that the absolute thermoelectric power often changes considerably at the melting point, e.g. in Li, Cs, Cu, Hg, Zn, Bi amongst others.

Observation (iii), which has never been satisfactorily explained, can be exemplified as follows. Let α be the observed $(\partial\rho/\partial T)_p$ and let α' be the hypothetical value of α if, above the melting point, ρ were proportional to T°k. Then some values of α'/α are: Na, K, Rb, 0·7; Cu, Ag, Au, 1·6; Al, 1·8; In, Sn, Pb, 3 to 4; Hg, Ga, Tl, Sb, Bi, 4 to 5. The proportionality of ρ to T in the solid state, for $T>\Theta$, is inferred

† Communicated by the Authors.

from the theory of electron–phonon interaction on the assumption of constant volume, and some observed departures from it have been attributed to thermal expansion. It is therefore reasonable to consider $(\partial\rho/\partial T)_v$ where that is possible. For a few liquid metals the variation of ρ with pressure is known and this enables $(\partial\rho/\partial T)_v$ to be calculated. At constant volume, α'/α is greater than stated above. In particular for the alkali metals it becomes approximately 1·0. (Lithium is exceptional in that ρ increases with increased pressure in the liquid and solid states.) The most striking example of observation (iii) is in the Zn, Cd, Hg group in which $(\partial\rho/\partial T)_p$ is negative for some way above the melting point in Zn and Cd (Scala and Robertson 1953). This is also true of $(\partial\rho/\partial T)_v$ in Hg (see fig. 1).

Fig. 1

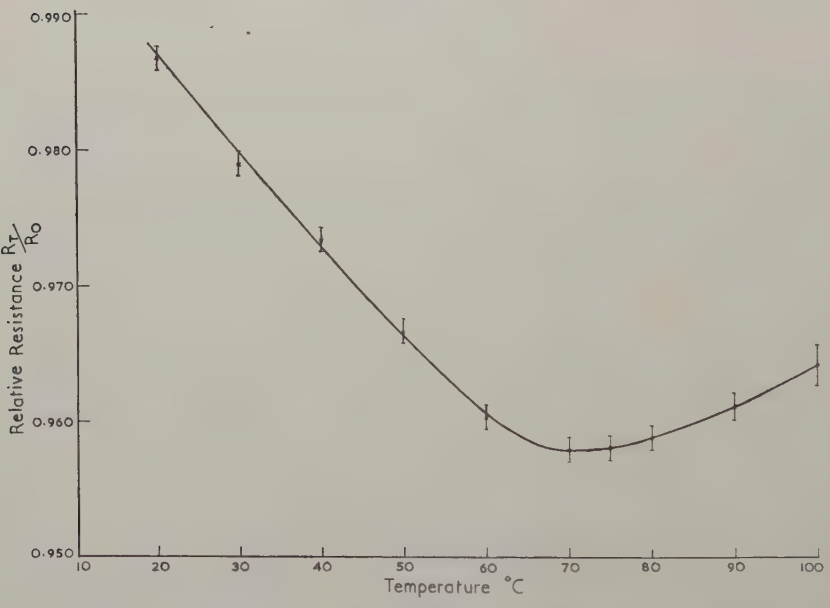

The variation of resistivity of liquid Hg with temperature at constant volume relative to that at 0°c, zero pressure, calculated from the results of Birch (1932) and Bett *et al.* (1954).

When $\partial\rho/\partial T$ is abnormally low it has been supposed that the effective number of free electrons is increasing, possibly as a result of some change in bonding, to counteract the simultaneous increase of scattering with temperature (Mott 1934, Regel 1958). It would therefore be of interest to measure the Hall coefficient of Zn, Cd, and Hg at and above the melting point to see whether this property reflects any such change. The present paper is concerned with the method of measurement and its application to Hg. A preliminary statement of results has already appeared (Kendall and Cusack 1960).

§ 2. Method of Measurement

The measurement of the Hall coefficient in solids is so well known that it is only worth mentioning here the additional difficulties presented by liquids. These are : (i) definition of the shape and size of the specimen; (ii) the possible occurrence of magnetohydrodynamic effects.

Since a very thin parallel-sided layer of metal is required, several methods of constructing glass cells were tried. For Hg, a suitable method was to bond flat pyrex plates with hot-setting epoxy-resin. During the setting, the separation of the plates was kept under observation by forming interference fringes in the air-film between them and corrections made to the parellelism when necessary. After setting, and before and after the electrical measurements, the separation of the plates was measured by means of Edser–Butler fringes. In this way, rectangular cells of well-defined thickness in the range 20 to 100 microns were obtained (see fig. 2).

Fig. 2

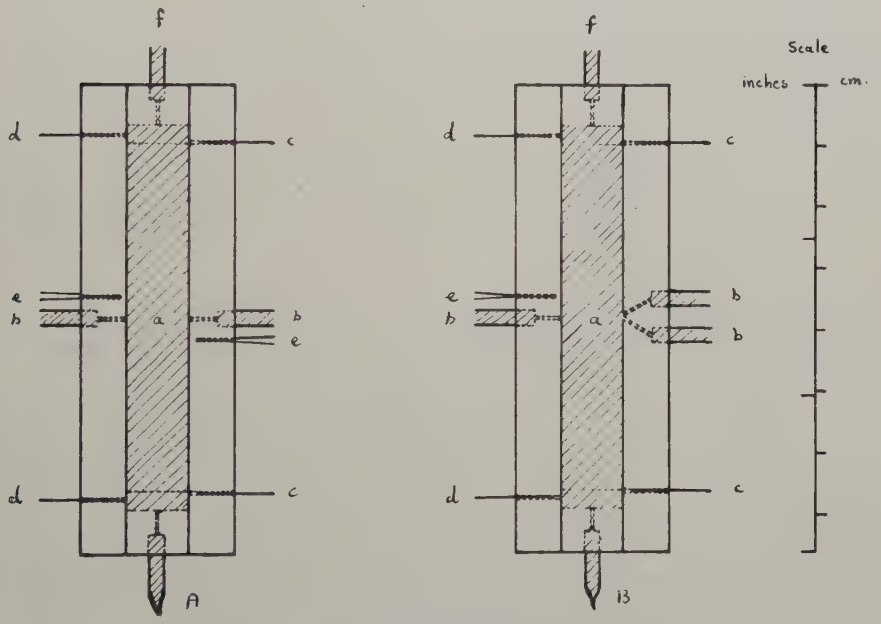

Glass Hall cells.

A. Two-probe cell. B. Three-probe cell. (*a*) Mercury specimen ; (*b*) Hall probe ; (*c*) resistivity probe ; (*d*) current lead ; (*e*) thermocouple ; (*f*) filling tube.

Current leads to the cells were of tungsten wire or foil and the Hall probes were columns of mercury in glass capillaries cemented into the cells. Both 2- and 3-probe methods were used. The ends of the Hall probes remote from the specimen were sealed off with tungsten electrodes, brought close together, and kept in a Dewar vessel; this is desirable to eliminate voltages from the Ettingshausen and thermoelectric effects.

The cells were filled under vacuum with purified Hg and encased in a thick copper box through whose walls passed tubes for circulating heating or cooling fluids. The whole assembly was mounted between the pole pieces of an electromagnet.

Careful filling is of considerable importance because voids in the Hg film will permit irreversible movements under electro-dynamic forces thus changing the current flow lines. The absence of voids was indicated by visual inspection and by reproducibility of the readings after reversals of current or field.

The Hall coefficient was obtained by the standard d.c. method described by Lindberg (1952), the voltages being measured to about $\pm 0{\cdot}02\,\mu$v with a constant resistance potentiometer based on the design of Teele and Schulman (1939). The whole measuring apparatus was tested by measuring known voltages from calibrated standards and by measuring the Hall coefficient of pure solid copper with good agreement with currently accepted values.

Fig. 3

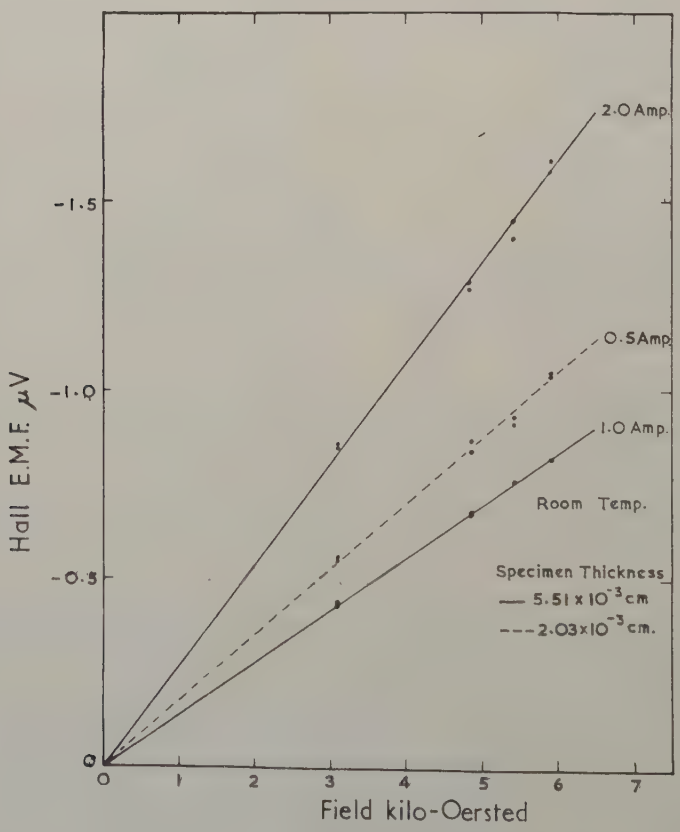

Liquid mercury : Hall e.m.f. *vs* magnetic field.
The dots indicate independent measurements.

It is possible that the voltages at the Hall probes of a cell contain a component due to magnetohydrodynamic effects. It was found too difficult to estimate its value from magnetohydrodynamic theory and some empirical checks on its importance were made. The general problem was first discussed by Williams (1925) from whose work it can be inferred that the magnetohydrodynamic effect will be (i) present only in so far as the current density and magnetic field vary over the specimen; (ii) proportional to H^2 for constant specimen current, I; (iii) proportional to the linear dimensions of the specimen. The Hall effect on the other hand is proportional to H and inversely proportional to the linear dimensions. H here refers to the total field which means in practice the applied field since the field of the specimen current is negligible by comparison. Since it is only inhomogeneities in H and I that produce the undesired effects, it was thought that the best check would be to perform the experiment with several cells of different thicknesses. Other things being equal, the ratio of Hall voltage to spurious voltage should have varied by a factor of 25 from the thinnest to the thickest cell. In one experiment the pole separation and therefore, probably, the field inhomogeneity was varied, and different geometries of the current electrodes were also tried. Inhomogeneities of current density, though bound to exist to some extent, are certain to vary from cell to cell and the observed agreement of the results from cell to cell was regarded as good evidence that magnetohydrodynamic effects, if present, were not serious. It was also confirmed that the Hall voltage varied linearly with H for constant I and vice versa (see fig. 3).

§ 3. Results and Comparison with other Experiments

Figure 3 shows a typical result for liquid Hg. The average value of the Hall coefficient from many measurements on four cells of thicknesses 2·03, 4·17, 5·51, $10{\cdot}5 \times 10^{-3}$ cm was $74{\cdot}6 \times 10^{-5} \pm 4\%$ e.m.u. The variation with temperature is shown in fig. 4.

Some measurements on solid Hg were also made. After each freezing, the readings were internally very consistent, somewhat more so than on a liquid specimen, but the Hall coefficient changed when the specimen was melted and refrozen. In this way, values ranging from -87 to -101×10^{-5} e.m.u. were observed. This is probably due to the lack of control over the crystallization; very likely the orientation of the crystals varied from specimen to specimen and it is highly probable that the Hall coefficient of solid Hg is anisotropic. This deserves a separate study. The suspected anisotropy makes it difficult to compare the present results with those of Jaggi and Sommerfelder (1959; table) especially as they worked at 4·17°K. The Hall coefficient may very well vary with temperature between the freezing point and 4·17° and the variation will not necessarily be the same for all orientations; such phenomena have been demonstrated in gallium (Yahia and Marcus 1959).

Only a few measurements of the Hall coefficient of liquids have been made before but naturally Hg features in these. The table shows the unsatisfactory state of the subject†.

Fig. 4

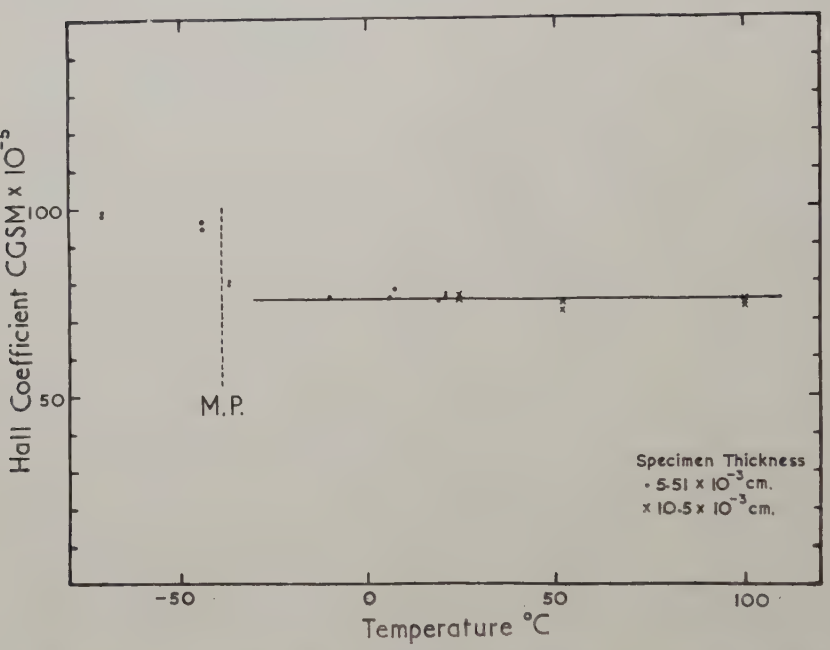

Hall coefficient of mercury as a function of temperature. Its sign is negative.

Value of 10^5R (in e.m.u.) for mercury

Author	R solid	R liquid
des Coudres 1901	—	−52
Fenninger 1914	0·0	0·0
Serduke and Fisher 1932	−72 to −88 (at m.p.)	—
Kikoin and Fakidow 1931	—	0·0
Jaggi and Sommerfelder 1959	−200 (at 4·17°K)	—
Present work	−87 to −101 (near m.p.)	−75

Measurements on solids are less subject to error than those on liquids and the agreement between the present results and those of Serduke and Fisher is satisfactory for solid Hg. The authors therefore agree with Serduke and Fisher in regarding the results of Fenninger with some

† *Note added in proof.*—Satisfactory confirmation of the values in the present paper has now been given by G. Wilson (private communication) and Y. Tièche, *Helv. phys. Acta*, 33, 963, 1960.

suspicion. Kikoin and Fakidow did not measure solid Hg and could not detect a Hall effect in the liquid. It is difficult to discuss this result without detailed knowledge of the apparatus, but it seems likely that their specimen thickness was greater than those of the present experiments—a circumstance tending to greater inaccuracy. Their stated error in the Hall coefficient of liquid Na–K alloy was $\pm 10\%$ and the voltage from a mercury specimen of similar size would be only 17% of that from Na–K—if the present result for Hg is correct.

The early work by des Coudres (1901) agrees with this paper in that a definite negative effect was found. There is no point in discussing the magnitude because other of des Coudres' results, on solid materials, are now known to be very inaccurate quantitatively.

The present experiments have the advantages that the specimens were thinner and of more accurately determined thickness, that more than one cell was used, and that the temperature was varied. In view of the disagreements in the table, it would be desirable to repeat the measurements using an a.c. technique which, though involving difficulties of its own, offers another way of minimizing the specific disadvantages of working with liquids.

§ 4. Discussion

The sign of the Hall coefficient in solid Hg is negative. In the course of discussing the bonding of Group IIB elements, Wallace (1955) put the hypothesis that 0·67 valence electrons per atom participate in covalent bonds in the basal planes, leaving 1·33 electrons per atom as conduction electrons contributing to metallic binding. It was subsequently inferred that the Hall coefficient would be positive, in agreement with experiment for Zn and Cd. The negative value for Hg, while by no means sufficient in itself to disprove this theory of bonding, certainly casts some doubt on it.

The small change in the Hall coefficient at the melting point is consistent with the constancy of the Knight shift across the melting point, since the latter argues that the electron states cannot alter much on melting (Knight *et al.* 1959).

In a solid metal the 'free electron value', $-1/n|e|c$, of the Hall coefficient obtains if (i) the Fermi surface is spherical and (ii) the electron scattering is independent of $\mathbf{k}$ for a given energy. Naïve considerations of the structural disorder in a liquid metal might encourage the expectation that these conditions should be fulfilled, since their contravention in solids arises from the crystal structure. However, it is not yet clear whether liquids are sufficiently like solids for similar electronic terminology to be used, e.g. it is not certain whether it is permissible to speak of a Fermi surface. Assuming that it is, one may ask to what extent the electronic properties of liquid mercury are accounted for by a free electron model with two electrons per atom.

On this model, the Hall coefficient would be $-77{\cdot}4 \times 10^{-5}$ e.m.u. which agrees within experimental error with the observed one. The

electron mean free path at the melting point would have to be 7·4 Å which is smaller than in many other metals but not of a different order. The Lorenz number would be $2{\cdot}25 \times 10^{-8}$ watt ohm deg^{-1} and independent of temperature, whereas the observed value is $2{\cdot}62 \pm 0{\cdot}03 \times 10^{-8}$ from 100 to 300°c (Ewing *et al.* 1955). The absolute thermoelectric power should be negative and proportional to the absolute temperature with an approximate value of $-2{\cdot}9\,\mu\mathrm{v}\,\mathrm{deg}^{-1}$ at 0°c; the observed values vary approximately linearly with, but not proportionally to, the absolute temperature and the 0°c value is $-4{\cdot}4\,\mu\mathrm{v}\,\mathrm{deg}^{-1}$ (Gehlhoff and Neumeier 1919). According to Schulz (1957), though not according to Hodgson (1959), the optical properties of liquid Hg are also very well accounted for by the Drude free electron theory with two electrons per atom. It seems therefore that liquid Hg shows free electron behaviour to a considerable degree.

However, between the melting point and 100°c, the observed resistivity of Hg increases by a factor 1·14; if the resistivity were roughly proportional to absolute temperature, as occurs commonly in solid metals (including Hg) and also in liquid Na and K, the factor would be about 1·59. To attribute the difference to a rise in the effective number of free electrons requires the latter to increase by 40% in 140°c. As is clear from fig. 4, the present experiments fail to reveal any comparable variation in the Hall coefficient which remains at about the 'free electron' value throughout. It would be of interest to know if similar constancy characterizes the Knight shift. Thus either the effective number of free electrons must increase considerably without alteration in the Hall coefficient or the scattering of electrons by the disordered structure is sufficiently different from ordinary electron–phonon interaction for a much smaller rate of increase with temperature to be possible. The first alternative, though not impossible, is less attractive because both quantities depend on the Fermi surface. The second is in line with the view that liquid metal resistivity has much in common with a residual resistance created by lattice defects, this disorder entering at the melting point (MacDonald 1959, Cusack and Enderby 1960). It remains of interest to find whether the Hall coefficient is also constant when the resistivity actually decreases with rising temperature as in Zn. Such work is in progress but the higher melting point considerably increases the technical difficulty.

If the resistivity increment, $\Delta\rho$, on melting of Hg is of the 'residual' type, the abnormally large ratio of resistivities, ρ_L/ρ_S, at the melting point (~ 4 instead of ~ 2) is a simple consequence of the abnormally low melting point. For if the solid state were to persist to ~ 500°c, ρ_S would be trebled and $\Delta\rho$ remain about the same. However, other explanations of the high ρ_L/ρ_S have been offered, e.g. a decrease in the effective number of free electrons on melting (Mott and Jones 1936), extra scattering mechanisms in the liquid state (Wallace 1955) and it is not possible to decide certainly between them.

Acknowledgments

The authors are indebted to Professor Bernal for facilities in his department; to the Central Research Fund of the University of London for a grant, to Mr. I. Harris for calculations concerned with fig. 1, and to Mr. J. Enderby for useful discussions.

References

Bernal, J. D., 1959, *Nature, Lond.*, **183,** 141.
Bett, K. E., Weale, K. E., and Newitt, D. M., 1954, *Brit. J. appl. Phys.*, **5,** 243.
Birch, F., 1932, *Phys. Rev.*, **41,** 641.
des Coudres, T., 1901, *Phys. Z.*, **2,** 586.
Cusack, N., and Enderby, J., 1960, *Proc. phys. Soc. Lond.*, **75,** 395.
Ewing, C. T., Seebold, R. E., Grand, J. A., and Miller, R. R., 1955, *J. phys. Chem.*, **59,** 524.
Fenninger, W. N., 1914, *Phil. Mag.*, **27,** 109.
Gehlhoff, G., and Neumeier, F., 1919, *Verh. für. Phys. Ges.*, **21,** 201.
Hodgson, J. N., 1959, *Phil. Mag.*, **4,** 183.
Jaggi, R., and Sommerfelder, R., 1959, *Helv. phys. acta*, **32,** 167.
Kendall, P., and Cusack, N., 1960, *Phil. Mag.*, **5,** 100.
Kikoin, J., and Fakidow, I., 1931, *Z. Phys.*, **71,** 393.
Knight, W. D., Berger, A. G., and Heine, V., 1959, *Annals of Physics*, **8,** 173.
Lindberg, O., 1952, *Proc. Inst. Radio Engrs, N.Y.*, **40,** 1414.
MacDonald, D. K. C., 1959, *Phil. Mag.*, **4,** 1283.
Mott, N. F., 1934, *Proc. roy. Soc.* A, **146,** 465.
Mott, N. F., and Jones, H., 1936, *The Theory of the Properties of Metals and Alloys* (Oxford: Clarendon Press), p. 279.
Regel, A. R., 1958, *J. tech. Phys., Moscow*, 521.
Scala, E., and Robertson, W. D., 1953, *J. Metals, N.Y.*, **5,** 1141.
Schulz, L. G., 1957, *Advanc. Phys.*, **6,** 102.
Serduke, J. T., and Fisher, T. F., 1932, *Phys. Rev.*, **39,** 1932.
Teele, R. P., Schulman, S., 1939, *Bur. Stand. J. Res., Wash.*, **22,** 431.
Wallace, W. E., 1955, *J. chem. Phys.*, **23,** 2281.
Williams, E. J., 1925, *Phil. Mag.*, **50,** 27.
Yahia, J., and Marcus, J. A., 1959, *Phys. Rev.*, **113,** 137.

Etching of Diamond Surfaces with Gases†

By T. Evans and D. H. Sauter
J. J. Thomson Physical Laboratory, University of Reading

[Received August 15, 1960]

Abstract

Etching experiments are described in which diamonds showing octahedral, cubic and dodecahedral faces are heated in air within the temperature range of 800°c to 1400°c. A change in the etch pit orientations of the characteristic etch pits for these faces has been found as the temperature of etching is raised. Etching with mixtures of gases has led to the conclusion that oxygen and water vapour are the relevant constituents of air in the formation of well-defined etch pits. Surface graphite formation at temperatures below 1400°c is considered and it is proposed that the mechanism of formation is essentially a chemical reaction and not connected with a purely physical phase change.

§ 1. Introduction

Most of the previous work on the etching of diamond surfaces has been done with fused potassium nitrate or sodium carbonate as the etchant (see, for instance, Williams 1932, Omar *et al.* 1954, Patel and Tolansky 1957) in which characteristic etch pit shapes for the octahedral, cubic and dodecahedral faces have been produced. Omar and Kenawi (1957) however formed well-defined pits of triangular outline by heating an octahedron on a molybdenum strip to about 1000°c in the presence of air at 2·5 microns Hg pressure. Using the nomenclature of Frank *et al.* (1958), these pits were in the positive orientation, that is, in the same orientation as the octahedral face which is opposite to the negatively oriented natural 'trigons'. On an attempt to produce negatively oriented etch pits, Frank and Puttick (1958) heated octahedra in steam, chlorine and wet hydrogen at 800°c but did not succeed in doing so. They did however, produce such pits by heating in fused kimberlite at about 1450°c.

In the experiments to be described, the above work has been extended by etching diamonds in air at reduced and at atmospheric pressure in the temperature range of 800°c to 1400°c. As the temperature of etching is raised, the etch pit orientations have been found to change on the octahedral, cubic and dodecahedral faces. In an attempt to determine which of the constituents of the air are responsible for the observed etch pits, octahedra have been etched by heating in various combinations of the gases found in the atmosphere.

† Communicated by the Authors.

§ 2. Experimental Procedure

The diamonds primarily used in the etching experiments were 0·1 carat octahedra which were selected for their surface perfection. The cleaning procedure prior to etching consisted of immersing the diamond in boiling concentrated nitric acid, washing in distilled water and refluxing in ethyl alcohol. The stones were handled throughout with glass tweezers to avoid contamination. For etching experiments at temperatures less than 1000°c the specimen was placed in a silica tube, closed at one end, which was evacuated to 10^{-6} mm Hg after flushing with argon. At temperatures greater than 1000°c alumina tubes were used. The stone was heated to the etching temperature in this vacuum which served to complete the cleaning procedure. Control experiments showed that this heating operation did not result in any detectable etching of the surfaces. The air was then bled into the tube at a controlled rate so as to maintain the required etching pressure whilst continuously pumping. On completion of the run the tube was again evacuated to 10^{-6} mm Hg and the specimen allowed to cool. An optical microscope examination was then made of the surfaces.

The main constituents of air are approximately 78% by volume of nitrogen and 21% by volume of oxygen. Water vapour is also present at concentrations usually less than 1%. The inert gases and the trace quantities of hydrogen and carbon dioxide have been found not to influence the etching significantly. In experiments on etching with mixtures of gases, two flasks were evacuated to 10^{-6} mm Hg, one filled with nitrogen to atmospheric pressure, and the other with oxygen to the same pressure. The volumes of the flasks were in the ratio of 4 : 1 so as to simulate the nitrogen/oxygen ratio in air. The flasks were interconnected and the mixture fed into the heated silica or alumina tube, which had previously been evacuated and isolated from the pumping unit. After the required etching time, the tube was again evacuated to 10^{-6} mm Hg and allowed to cool. In this case, the mixture in the tube was at approximately atmospheric pressure during the etching. With this system it was possible to etch separately with oxygen, nitrogen, water vapour, oxygen and nitrogen mixtures, oxygen, nitrogen and water vapour mixtures at the partial pressures at which these gases were found in air. In some experiments it was desirable to substitute an inert gas in place of the nitrogen, and argon was used. The nitrogen, argon and oxygen were obtained from cylinders, and these gases were separately dried and impurities removed before admission into the flasks by passing the gases through:

(1) a horizontal column designed for turbulent flow containing soda lime to remove carbon dioxide;
(2) heated palladized asbestos for removal of hydrogen;
(3) a horizontal tube containing coarse silica gel which removed most of the water vapour;
(4) a heat exchanger type of cooling trap at −80°c;
(5) a cold trap at −80°c filled with fine silica gel to remove organic matter and water vapour;

(6) a turbulent flow tube containing magnesium perchlorate for the final drying.

When the gases were required to be saturated with water vapour, they were subjected to the above sequence and then finally passed through two water bubblers.

At etching temperatures of 900°C and above, the diamond surfaces were covered with a layer of graphite which was removed by heating for 10 min in a mixture of perchloric, nitric and sulphuric acids before the surfaces were examined.

Although most of the experiments were done with octahedral stones, cubes with {100} surfaces and also, cubes with a mixture of {100} and {110} surfaces were investigated.

§ 3. Results

In the first series of experiments octahedra were etched at temperatures between 800°C and 900°C in air at pressure ranging from 10^{-3} mm to atmospheric pressure. The severity of the attack increased with increasing pressure, temperature and time, but the sequence of etching appeared to be the same at these ranges of pressure and temperature. First of all, the microcracks and edges were attacked more vigorously than the rest of the surface, but at a later stage the surface became covered with etch pits of triangular outline in the positive orientation. Figure 1† shows such pits on an octahedron which had been etched for 15 min at 850°C at an air pressure of 760 mm Hg.

When the same experiments were repeated at temperatures in excess of 1000°C, the stones were covered with a layer of graphite. Removal of the graphite and examination showed that the same sequence of etching occurred as before except that the pits were now in the negative orientation, i.e. the same as for natural 'trigons'. Figure 2 shows these pits on an octahedron etched for 5 min at 1250°C at atmospheric pressure.

It was thus interesting to investigate the region between 900°C and 1000°C which would be the region where reversal of pit orientation occurs. An octahedron was etched for 1 hour at 950°C in air at a pressure of 10^{-1} mm of Hg, and the resultant etch pits are shown in fig. 3. They were primarily circular pits with a tendency towards the hexagonal outline which would be expected in an intermediate region where reversal of orientation of triangular etch pits takes place.

3.1. {100} *Surfaces*

The etching of these surfaces could not be investigated at various pressures and temperatures to the same extent as {111} surfaces, owing to the comparative scarcity of the polished cubes which would be necessary. However, a cube with {100} surfaces was heated at 775°C for 2 hours at an air pressure of 5×10^{-1} mm of Hg. The etch pits formed were of square

† Figures 1–7, 9, 10 and 11 are shown as plates.

outline such that the sides were in ⟨100⟩ directions. Figure 4 shows these pits. A second cube was heated at 1400°c in air for 6 min at atmospheric pressure and the surface graphite removed. Again there were pits of square outline on the surface but now the sides were parallel to ⟨110⟩, i.e. the high temperature square pits were rotated through 45° relative to the low temperature pits. The orientation of the high temperature pits was the same as those found on the untreated natural cubic crystals which occur in nature. Figure 5 shows the high temperature pits on a (100) surface.

3.2. {110} *Surfaces*

In the case of dodecahedral faces, difficulty was experienced in forming etch pits and prolonged etching times were required to obtain recognizable pits. However, by etching in air at atmospheric pressure for $2\frac{1}{2}$ hours at

Fig. 8

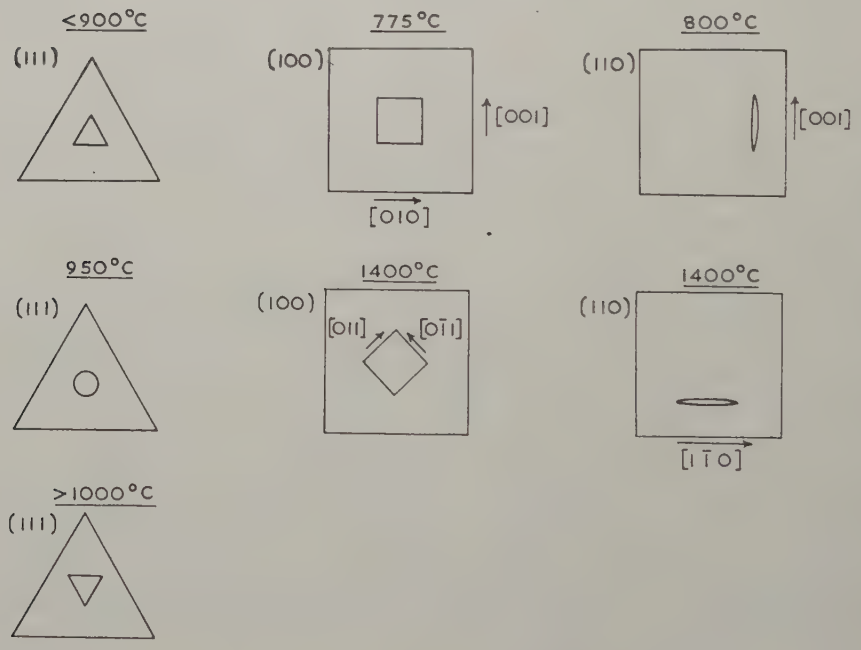

800°c 'boat-shaped' pits were formed such that on a (110) face, the keel of the boat was in the [001] direction (fig. 6). In the corresponding experiment at 1400°c, etching in air at atmospheric pressure for 10 min produced 'boat-shaped' pits with the keel in the [$\bar{1}$10] direction on the (110) face (fig. 7). A graphite layer had to be removed before the diamond surface was revealed for examination. Thus for the dodecahedral face as well, the high temperature pits were rotated relative to the low temperature pits: through 90° in this instance.

Summarizing these results, fig. 8 shows the etch pit orientations on the three faces which have been considered.

3.3. *Graphite Formation*

The etching experiments at 900°c and above with octahedral stones showed that the formation of graphite on the surface depended, not only on the temperature, but also upon the pressure of the air surrounding the diamond. Heating for 16 hours at an air pressure of 10^{-6} mm of Hg resulted in a faint grey graphite layer with slight attack at microcracks and edges of the underlying surface. However, heating for 5 min in air at atmospheric pressure provided an appreciable opaque black layer of surface graphite at 900°c and above, with a corresponding heavy attack of the diamond surface. Reflection electron diffraction revealed that the crystallite size varied from less than 50 Å in the case of rapid graphite formation, to greater than 200 Å when formed at 1400°c at 10^{-6} mm air pressure. In the cases examined, namely octahedral surfaces, oriented growth of the graphite had occurred with the graphite layers lying parallel to the puckered (111) surface.

Heating octahedra in an atmosphere of carbon dioxide also produced surface graphite at temperatures in excess of 900°c with heavy attack of the underlying diamond surface. Carbon monoxide however, did not alter the surface of the diamond appreciably, even after heating for 45 min at 1400°c at atmospheric pressure.

3.4. *Etching with Mixtures of Gases*

The use of air as the etchant has been seen to produce well defined etch pits on the three surfaces considered. It cannot be assumed that the oxygen in the air was solely responsible for the etch pit formation as current theories (Frank 1958, Cabrera and Vermilyea 1958, and Gilman *et al.* 1958) postulate that an etchant which produces well-defined etch pits has at least two consituents, namely the substance which attacks the surface and an inhibitor which modifies the attack so that pits are formed instead of, for instance, surface polishing occurring. In order to separate the roles of the constituents of air in the etching process on octahedral surfaces of diamond, stones were etched in different mixtures of the gases found in air. The pressures of the constituents in these mixtures were the same as the partial pressures of the same gases in air.

3.4.1. *Low-temperature etching with gas mixtures*

In all these experiments, the etching time was 12 min at 850°c.

(*a*) Etching at atmospheric pressure in a mixture of 4 parts nitrogen plus 1 part oxygen plus water vapour, produced positively oriented triangular pits over the surface as in fig. 9. These showed all the characteristics of etch pits formed in the previous experiments with air.

(*b*) Etching with dry oxygen at 170 mm of Hg pressure resulted in a rough matt-type surface with no triangular pits (fig. 10). An important and significant observation however, was that the microcracks had been widened by etching to form large deep positively oriented pits of triangular outline. Etching at atmospheric pressure in a dry mixture of 4 parts argon plus 1 part oxygen gave essentially the same result. Thus the pits formed by air etching could not have been due to the action of oxygen alone.

(*c*) Etching in wet oxygen at 170 mm of Hg pressure produced well-defined positively oriented etch pits and these could not be differentiated from those produced in air. The same type of etch pits were obtained by etching in 4 parts argon plus 1 part oxygen plus water vapour at atmospheric pressure.

(*d*) To determine the effect of nitrogen, an octahedron was etched in a dry mixture of 4 parts nitrogen plus 1 part oxygen. No etch pits were formed and the surface was roughened in the same manner as when dry oxygen was used as the etchant.

Control experiments were done on the etching effect of nitrogen and water vapour separately. Treatment with nitrogen alone at 590 mm of Hg pressure did not produce any detectable attack on the diamond surface; neither did water vapour at 18 mm of Hg pressure under similar conditions to the etching experiments described in this section.

3.4.2. *High-temperature etching with gas mixtures*

The above experiments in the previous section were repeated at 1250°c with an etching time of 5 min. Surface graphite had to be removed before the surface could be examined.

(*a*) The wet nitrogen and oxygen mixtures produced well-defined triangular etch pits in the negative orientation (fig. 11), which were indistinguishable from those obtained by air etching.

(*b*) The dry oxygen and also the dry nitrogen and oxygen mixture resulted in rough pitting with no crystallographically oriented etch pits.

(*c*) Wet oxygen produced well-defined etch pits in the negative orientation, similar to those formed in (*a*) above.

The experiments in the previous two sections showed that the oxygen and the water vapour were the constituents responsible for the etch pit formation observed when diamonds were heated in air.

3.5. *Etch Rates*

The effect of water vapour on the etch rate of oxygen on octahedral diamond surfaces was determined by measuring the rate of attack in both dry and wet oxygen in the closed system used in the mixture experiments. The presence of water vapour reduced the rate of oxygen attack by approximately four times. This result is at variance with the work of

Hennig (1960) who found that water vapour acted as a catalyst to the reaction of oxygen with the surface of single crystals of graphite. Work done on the etch rates of diamonds in a fast-flowing stream of oxygen also showed that under these conditions water vapour acted in such a way as to double the etch rate with wet oxygen over that of dry oxygen (Evans and Phaal, to be published). This apparent contradiction in results can be explained by assuming that water vapour accelerates the oxygen–carbon reaction, but that one or more of the products of the reaction acts as an inhibitor. In the case of flow experiments, the gaseous products of the primary reaction tend to be swept from the surface as they are formed, whereas in the closed system, secondary surface reactions take place resulting in inhibition to the oxygen–carbon reaction.

§ 4. Discussion

Frank (1958) and Cabrera and Vermilyea (1958) ascribe the growth of crystals from solution to the movement of atomic steps over the surface. They also apply the theory to dissolution and propose that in formation of well-defined etch pits, the etching solution contains a solvent and also an impurity which inhibits the movement of steps, causing 'bunching' of steps to occur. The results of Gilman *et al.* (1958) confirm this theory for the etching of lithium fluoride in which they used water as the solvent and ferric ions as the inhibitor in the formation of well-defined etch pits. The experiments described have shown that the theory can also be applied to etching by gaseous mixtures. In the case of air etching on diamond surfaces, the carbon atoms are removed by the oxygen–carbon reaction which is accelerated by the presence of water vapour on the surface. However, one or more of the primary products of the water–carbon reaction, if it is not removed, can accumulate on the surface and act as inhibitor to the oxygen–carbon reaction, resulting in well-defined etch pits. This also explains the difficulty which we have found in forming good etch pits in a flow type experiment. Extensive work has been done on the steam–carbon reaction, and most investigators agree that the primary reaction is $H_2O + C \longrightarrow H_2 + CO$ (see for instance Binford and Eyring 1956); Long and Sykes (1948) consider that hydrogen molecules retard the steam–carbon reaction by being strongly adsorbed on the surface. Key, quoted by Strickland-Constable (1950), on the other hand, considers the retardation as due to the reaction of hydrogen gas with surface oxide to give H_2O gas. Whatever the details of the surface reactions, it is probable that in the air etching experiments on diamond surfaces, the primary reaction product which acts as an inhibitor to the oxygen–carbon reaction is associated with the hydrogen. Experiments on etching with dry hydrogen and oxygen mixtures have failed to produce well-defined etch-pits on octahedral surfaces, but it was not possible to vary the hydrogen concentration widely owing to the explosive nature of the mixture at elevated temperatures.

4.1. *Etch Pit Formation*

If an etch pit is considered as being formed by the movement of atomic steps over the surface, the resultant pit is outlined by the steps moving at the slowest rate. Thus the observed change in etch pit orientation can be explained by a change in the relative velocities of different types of steps, under the varying experimental conditions. Consider the etching of an octahedral face where, of course, the triangular {111} faces are outlined by ⟨110⟩ directions. Frank, Puttick and Wilks (1958) describe the atomic structure of steps formed in the ⟨110⟩ directions. Take, for the sake of illustration, an etch pit as in fig. 12—which is initially hexagonal in outline and bounded by ⟨110⟩ directions. Steps 1 are atomically identical as are steps 2, and Frank *et al.* (1958) point out that the edges of steps 1 consist of atoms which are trebly bonded to the lattice, whereas atoms at steps 2

Fig. 12

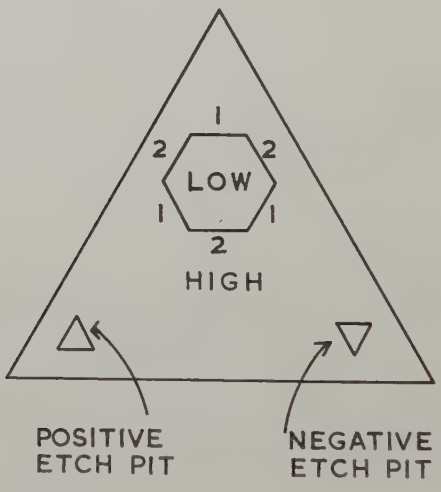

are doubly bonded to the lattice. When steps 1 move at a higher velocity than steps 2, positive etch pits result, whereas when the reverse is the case, negative pits are formed. The observation that oxygen attack alone opened microcracks to form deep pits of positive orientation at 850°C, indicates that the relative step velocities are determined by the relative stabilities of the different oxygen–carbon complexes at the steps and is distinct from the action of the inhibitor. Information is lacking about the type of complexes formed between oxygen and carbon on diamond surfaces, but steps 2 must be more strongly stabilized by oxygen than steps 1 at temperatures below 900°C. The tentative explanation by Frank *et al.* that steps 2 are strongly stabilized by oxygen atoms forming bridges between carbon atoms as in a lactone, appears reasonable by our experiments. No similar stabilization is possible on steps 1 as the free bonds are

not favourably oriented for bridge formation. At temperatures exceeding 1000°c, the observation of negative pit formation can be explained by a reduction in the stabilization by bridge formation at these temperatures such that the lifetime of the oxygen–carbon complex on steps 2 is less than the different type of complex formed on steps 1. At temperatures between 900°c and 1000°c the lifetimes of the complexes at the two types of step are the same and circular pits result.

Now the (100) surface will be considered. It is not possible to describe the results by considering that the kinetics of dissolution is determined by the number of bonds per carbon atom which has to be broken during dissolution. If the diamond structure is considered in terms of (400) planes, the (100) surface consists of atoms which are doubly bonded to the

Fig. 13

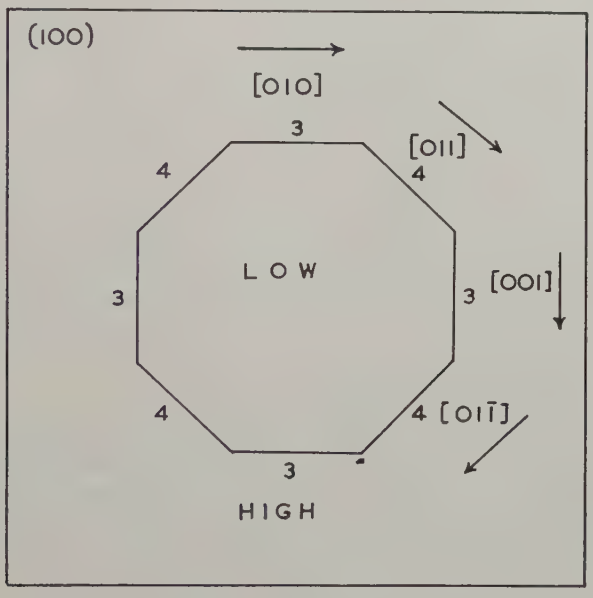

lattice. Removal of these atoms reveals a plane at distance $\frac{1}{4}a[100]$ below the original surface which again consists of doubly bonded atoms and so on. Step formation and also kink formation at steps on such a surface do not produce favoured sites for dissolution as the terminal atoms are also doubly bonded to the lattice. To account for the fact that etch pit formation is readily obtainable on {100} diamond surfaces, it is necessary to postulate that the flat surface is strongly stabilized by adsorbed atoms so that sites which are kinetically favoured can be formed at steps. Examination of the free bonds on a flat (100) surface, shows that bridge formation by adsorbed oxygen atoms between carbon atoms is possible because the free carbon bonds are favourably oriented and spaced for the

formation of such a complex. Thus a flat (100) surface can be stabilized in the same way as steps of type 2 on octahedral surfaces since the free carbon bond configurations are similar in both cases. If the flat (100) surface is assumed to be strongly stabilized by bridge formation of oxygen atoms between carbon atoms, steps can again be considered as positions where it is kinetically favourable for etching to occur. Consider the initial etch pit to be bounded by steps of height $\frac{1}{2}a[100]$ and in directions shown in fig. 13. Steps 3 are identical atomically as are steps 4. Low temperature pits will form if steps 3 have a lower velocity over the surface than steps 4, and high temperature pits will be produced when the reverse is the case. Examination of the atomic configurations at these steps shows that if the rates of step movement are determined by the number of bonds per carbon atom which have to be broken during dissolution, then steps 3 and 4 would move with the same velocity. This is clearly not so by the experimental evidence. The relevant asymmetry in the two types of steps is the distribution of free bonds at the terminal atoms. These free bonds determine the type of oxygen–carbon complexes which form at the steps. It is postulated that the complexes on steps 3 are more stable than those formed on steps 4 at low temperatures (i.e. less than 900°C) and the reverse occurs at temperatures greater than 1000°C. This could then account for the change in etch pit orientation as the temperature is raised.

As mentioned before, difficulty was found in forming boat-shaped pits on {110} surfaces, and considerable roughening of the surface was necessary before they developed. Williams (1932) in his book also states that the boat-shaped etch features are sometimes raised hillocks on the dodecahedral face. It is considered that the boat-shaped pits are not formed as a result of step movement over the surface, but are due to the tendency for depressions formed during roughening by etching to stabilize themselves by assuming a shape bounded by surfaces with the slowest etch rates. This necessitates that there is a change in the relative etch rates of different diamond surfaces as the temperature is raised, and experiments are being done to test this.

4.2. *Graphite Formation*

As stated in the results, diamond octahedra which had been heated in air between 900°C and 1400°C had a carbon layer on the surface. The structure of the layer varied from effectively amorphous carbon to an oriented layer of graphite with a crystallite size of greater than 200 Å. The presence of this layer depended markedly upon the atmosphere surrounding the stone during the heating operation. In a high vacuum (10^{-6} mm of Hg) very little formation of surface carbon resulted, whereas heating in air at atmospheric pressure caused the stone to be covered with an opaque carbon layer at 900°C. This has led to the conclusion that in the temperature range of 900°C to 1400°C the formation of surface graphite is due to the deposition of carbon on the diamond surface as a result of

surface chemical reactions and the effect of a purely physical phase change is not evident. Work on graphite, summarized by Nelson Smith (1959) has shown it is possible to deposit carbon on the surface by a secondary surface reaction in which carbon monoxide reacts with a surface oxide complex to form carbon dioxide and carbon, i.e.

$$CO + (CO) \rightarrow CO_2 + C.$$

This is consistent with our results, as the primary reaction product of the oxygen–carbon reaction is presumably CO which at a sufficiently high temperature can react with the (CO) surface complexes (Nelson Smith 1959). Also no graphite formation would be expected by heating in carbon monoxide alone as no surface oxide complexes would be formed with which it could react. The graphite formation as a result of heating diamonds in carbon dioxide can also be explained by the same mechanism following the primary reaction

$$CO_2 + C \longrightarrow CO + (CO).$$

The thickness of the carbon layer under particular experimental conditions would be an equilibrium thickness determined by the rate of formation of the deposited carbon as a result of these secondary surface reactions and the rate of removal of the layer by oxidation. It would be expected that the structure of the layer would play an important role in the equilibrium thickness as this would determine the effectiveness of the layer in protecting the underlying diamond surface from the surrounding oxidizing atmosphere. It must be emphasized that the experiments were done at 1400°C and below and the interpretation does not necessarily hold for temperatures in excess of 1400°C.

Acknowledgments

The authors wish to thank Professor R. W. Ditchburn for his interest throughout this work. Thanks are also due to Dr. J. F. H. Custers, Director of the Diamond Research Laboratory, Johannesburg, for the liberal supply of stones with low index faces and also for his interest. The reflection electron diffraction was done by Dr. R. C. Newman of Associated Electrical Industries, Aldermaston Court, to whom thanks is given. The work has been financed by a grant from Industrial Distributors (1946) Limited which is gratefully acknowledged.

References

Binford, J. S., and Eyring, H., 1956, *J. phys. Chem.*, **60**, 486.
Cabrera, N., and Vermilyea, D. A., 1958, *Growth and Perfection of Crystals*, Cooperstown Conference (New York: J. Wiley & Sons Inc.).
Frank, F. C., 1958, *Growth and Perfection of Crystals*, Cooperstown Conference (New York: J. Wiley & Sons Inc.).
Frank, F. C., and Puttick, K. E., 1958, *Phil. Mag.*, **3**, 1273.
Frank, F. C., Puttick, K. E., and Wilks, E. M., 1958, *Phil. Mag.*, **3**, 1262.
Gilman, J. J., Johnson, W. G., and Sears, G. W., 1958, *J. appl. Phys.*, **29**, 747.

Hennig, G. R., 1960, 10th Réunion annuelle de la Société de Chimie Physique, Paris, June 1960.
Long, F. J., and Sykes, K. W., 1948, *Proc. roy. Soc.* A, **193,** 377.
Nelson Smith, R., 1959, *Quart. Rev.*, **13,** 287.
Omar, M., and Kenawi, M., 1957, *Phil. Mag.*, **2,** 859.
Omar, M., Pandya, N. S., and Tolansky, S., 1954, *Proc. roy. Soc.* A, **225,** 33.
Patel, A. R., and Tolansky, S., 1957, *Proc. roy. Soc.* A, **243,** 41.
Strickland-Constable, R. F., 1950, *J. Chim. phys.*, **47,** 356.
Williams, A. F., 1932, *Genesis of the Diamond* (London: Ernest Benn).

Etch Pits and Dehydration Nuclei on Crystals of Gypsum†

By J. E. Bright and M. J. Ridge
Division of Building Research, Commonwealth Scientific and Industrial Research Organization, Melbourne, Australia

[Received September 5, 1960]

Abstract

A study has been made of the development of etch pits and dehydration nuclei on the (010) face of crystals of gypsum. The etch pits marked the sites of features that extended into the crystals. Dehydration nuclei in general did not occur at the same sites as etch pits. The nature of the sites favourable for the formation of etch pits and of dehydration nuclei is discussed.

Chemical reactions and phase changes in solids are likely to be initiated at particular sites such as lattice imperfections. This applies also to the dissolution of crystals, which probably begins at unit pits nucleated preferentially at the points of emergence of dislocation lines, with removal of the matter of the crystal proceeding by movement of monomolecular steps across the surface.

This note presents the results of a study of dissolution and thermal decomposition at the (010) face of naturally occurring, high quality crystals of gypsum. When the faces, which were produced by cleaving, were washed with distilled water etch pits were formed on parts of the surface. Some of these pits occurred in rows (cf. Grengg 1914, Viola 1897). Washing the crystal with a 1% solution of sodium hexametaphosphate, which is known to have a marked effect on the crystallization of gypsum (Ridge and Surkevicius 1960), made the pits more pronounced and somewhat increased their number. It also brought about the formation of geometric features on the parts of the surface free from etch pits. In general, the full crop of pits appeared within a minute or two and was not greatly increased by further washing, showing that the probability of forming a pit was high over the population of sites favourable for the formation of pits.

It was found that if a thickness of 10 μ, the approximate depth of the largest pits, was removed from the surface by grinding, rewashing frequently produced the original pattern of pits. Indeed, even after the removal of 60 μ some of the features of the original pattern of pits could often be distinguished. This shows that the pits occur at fixed sites

† Communicated by the Authors.

which extend into the crystal. In a particular case the x-ray technique devised by Schulz (1954) revealed a sub-grain boundary at which the change in orientation was about 1°; on etching this boundary was marked by a dense line of pits. These facts suggest that in the crystals examined the etch pits do mark the points of emergence of dislocation lines, and the rows of pits the positions of sub-grain boundaries, although some of the observations are difficult to reconcile with this view. The pits show a density of about 10^5 per cm^2, which is probably several orders of magnitude less than the density of dislocations in such crystals. Furthermore, examination of the crystals by the Schulz x-ray technique revealed sub-grain boundaries in parts of the crystals where the etch pits did not form rows. Some of the rows of etch pits terminated at the edge of the crystal or at junctions with other rows of pits. On the other hand some rows terminate in the crystal, as is shown in figs. 1 to 4†. These facts show that etching did not reveal all dislocations cut by the surface. Breaks in rows of etch pits often occur in the region of cleavage steps (see fig. 5), and demonstrate that some parts of the features promoting the formation of rows of pits are immune to etching. It is possible that such effects may be due to variations in the distribution of impurities in the crystal, or to the capacity of dislocation lines to produce pits depending upon their direction.

Focusing below the surface of the crystal showed that some, but by no means all, of the rows of etch pits were associated with walls of crystal-like inclusions. No tubular features suggesting hollow dislocations (Verma 1953) were seen.

Substances promoting the formation of etch pits probably act by being adsorbed on the edges of the receding sheets of ions, and hinder horizontal dissolution (Gilman *et al.* 1958). For this reason substances that modify habit seem likely to promote the formation of etch pits. Other habit modifiers for gypsum were tried, including acetates, citrates and borates, but sodium hexametaphosphate was the most effective. No reagent tried was effective in filling in the gaps in the rows of pits. The relative effectiveness of distilled water suggests that the crystals had grown in an environment in which substances capable of adsorption on the growing surface were present.

Holding crystals at 98°c for a few hours in an air oven resulted in the formation of areas of slow decomposition which began as rectangular nuclei, the sites of which did not generally coincide with those of etch pits, although some cases of coincidence were observed. Unlike the etch pits, further treatment (heating) caused the dehydration nuclei to grow and new ones to appear continuously in the empty parts of the crystal. When the nuclei had grown sufficiently to begin to overlap they were about two orders of magnitude less numerous than the etch pits. The nuclei were not of quite the same shape as those obtained by

† All figures are shown as plates.

Zolotov (1958) on cleaved, unwashed surfaces, and the appearance varied a little in crystals from different sources. Re-etching the surface after formation of the dehydration nuclei did not result in the formation of a new pattern of etch pits. If 60 μ were ground off the surface to remove the nuclei and the crystal reheated, new dehydration nuclei were formed but not in the same position as the previous ones.

The behaviour of the surfaces on etching and on dehydration is illustrated in figs. 1 to 4. Figure 1 shows the surface after washing with a solution of sodium hexametaphosphate, the field containing a row of pits which ends abruptly. Figure 2 shows the same field after heating at 98°C for several hours. A row of dehydration nuclei have formed and do not correspond with the row of etch pits. Figure 3 shows the same field after 60 μ has been ground off and the surface washed with distilled water. The etch pits are fewer in number than in fig. 1, but the rows of pits can still be distinguished.

If dehydration tends to occur at the points of emergence of dislocation lines, the facts covering dehydration could be explained on the ground that the probability of the formation of a dehydration nucleus at a dislocation line at 98°C is low. In this way the dehydration nuclei would be unlikely to coincide with etch pits, since the pits mark the site of no more than some of the dislocations. It is also possible that the dislocations that readily nucleate etch pits are not favourable sites for dehydration. This may be due to the type or direction of the dislocation or to the segregation of impurities. The facts are also in accord with the view that dehydration begins at sites other than dislocations.

The shapes of dehydration nuclei like those of etch pits are affected by the presence of materials adsorbed on the surface. When the surface had been washed with water well defined rectangular nuclei were formed, as is seen from fig. 4, which shows the field of fig. 3 after heating at 98°C for several hours. When the surface had been treated with sodium hexametaphosphate the nuclei were less clearly defined, and were not of the same apparent orientation as those formed on water-washed surfaces (see figs. 2 and 4). The nuclei formed on water-washed surfaces showed the ' hour glass ' structure observed by previous authors (Zolotov 1958), whereas those formed on surfaces treated with sodium hexametaphosphate did not. This effect is not very clear in figs. 2 and 4, but was quite distinct when lower magnifications were used. The nuclei on surfaces treated with sodium hexametaphosphate showed a marked tendency to occur in rows.

Acknowledgments

Thanks are due to Messrs. J. H. Auld and R. A. Coyle of the Aeronautical Research Laboratories, Department of Supply, for the Schulz photographs.

This investigation forms part of the programme of work carried out within the Division of Building Research and sponsored by Australian Plaster Industries Ltd. and the Colonial Sugar Refining Company Ltd.

References

Gilman, J. J., Johnston, W. G., and Sears, G. W., 1958, *J. appl. Phys.*, **29,** 747.
Grengg, R., 1914, *Miner. petrogr. Mitt.*, **33,** 201.
Ridge, M. J., and Surkevicius, H., 1960, *Aust. J. appl. Sci.*, **11,** 355.
Schulz, L. G., 1954, *Amer. Inst. min. (metall.) Engrs*, **200,** 1082.
Verma, A. R., 1953, *Crystal Growth and Dislocations* (London: Butterworths).
Viola, C., 1897, *Z. Kristallogr.*, **28,** 573.
Zolotov, V. A., 1958, *Kristallografiya*, **3,** 237.

Observation of de Haas–van Alphen Type Oscillation in the Acoustomagnetic Attenuation of Zinc†

By D. F. Gibbons
Bell Telephone Laboratories, Incorporated, Murray Hill, New Jersey

[Received August 22, 1960]

Abstract

de Haas–van Alphen type oscillations have been observed in the acoustomagnetic attenuation of zinc. The oscillations were observed only for specific modes and direction of propagation with a field strength greater than 20·0 k oersteds. Periods in $\Delta(1/H)$ of $2{\cdot}1 \pm 0{\cdot}05$, $0{\cdot}3 \pm 0{\cdot}1$ and $7{\cdot}0 \pm 1{\cdot}0 \times 10^{-6}$ oersteds^{-1} were measured; these data are in excellent agreement with the magnetic data of Verkin and Dmitrenko (1955).

The purpose of this note is to report upon the observation of de Hass–van Alphen (dHvA) type oscillations in zinc single crystals in magnetic fields of 20–70 k oersteds. The ultrasonic losses in metals when $ql \geqslant 10$, where q is the sound wave vector $(2\pi/\lambda)$ and l the mean free path of the electrons, have been shown (Cohen *et al.* 1960) to originate in the interaction of the acoustic wave with the conduction electrons. Any changes in the conductivity tensor produced by the application of a magnetic field should in principle result in changes in the ultrasonic attenuation. Oscillations in components of the conductivity tensor with applied field have been seen to give rise to oscillations in the acoustic attenuation, and the maxima in the attenuation can be shown to occur where $qR = n\pi$ for small magnetic fields; R is the cyclotron orbit radius. These oscillations are the so-called geometric resonances which have been observed by many workers (Morse and Gavenda 1959, Reneker 1959). The period of these resonances will scale with λ, the acoustic wavelength. However, when $R < \lambda/2$ and the separation between the Landau levels $\hbar\omega_c$, where ω_c is the cyclotron frequency, is comparable to kT, the semi-classical arguments used to describe geometrical resonances breakdown and dHvA type oscillations may occur just as in the case of magnetic susceptibility (Shoenberg 1959) and Hall coefficient (Bergeran *et al.* 1960). This assumes that there is sufficient coupling between the acoustic field and the electrons for the phenomena to be observed. The period of these oscillations is independent of λ. This type of oscillation in the acoustic attenuation has until now only been observed in the semi-metal Bi (Reneker 1959).

† Communicated by the Author.

Many geometrical resonances have been observed in zinc single crystals grown from zone refined material, these crystals have a residual resistance ratio $R_{RT}/R_{4\,2°K} \sim 30 \times 10^3$ which gives a mean free path ~ 1–2 mm (Gibbons 1959). These geometrical oscillations occur in magnetic fields ~ 100–1000 oersteds. Using a Bitter type solenoid magnet dHvA oscillations have been observed in some directions of these crystals in fields ~ 20–70 k oersteds. The figure shows the data from a zinc crystal for a shear wave propagated along $\langle 10\bar{1}0 \rangle$ with the particle motion $\boldsymbol{u}$ along $\langle 0001 \rangle$ and the field perpendicular to $\boldsymbol{u}$ (i.e. along $\langle 11\bar{2}0 \rangle$) at a temperature of $1{\cdot}0°$K. Less pronounced oscillations have also been observed for the orientation, $\boldsymbol{q}$ along $\langle 11\bar{2}0 \rangle$, $\boldsymbol{u}$, $\langle 0001 \rangle$ and $\boldsymbol{H}$, $\langle 10\bar{1}0 \rangle$. So far, no dHvA oscillations have been observed for other directions or modes of propagation of the acoustic wave. The temperature dependence of the amplitude of the oscillations was measured for the orientation of the figure, and found to be $0{\cdot}25$ dB/°K between $4{\cdot}2$°K and $1{\cdot}0$°K. At the present time this temperature dependence data cannot be used to determine the effective mass of the carriers as the coupling coefficient between the acoustic wave and the carriers is unknown.

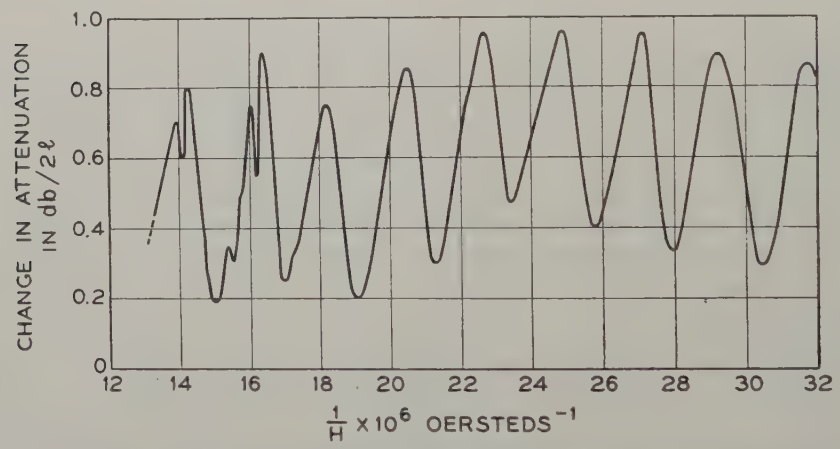

The change in attenuation of a shear wave, propagated along $\langle 10\bar{1}0 \rangle$ with particle motion along $\langle 0001 \rangle$, as a function of $1/H$, where H is along $\langle 11\bar{2}0 \rangle$, at a temperature $1{\cdot}0$°K ($2l = 1{\cdot}573$ cm).

In the data of the figure the main period exhibited $\Delta(1/H)$ is

$$2{\cdot}1 \pm 0{\cdot}05 \times 10^{-6}\ \text{oersteds}^{-1}.$$

This value is in excellent agreement with the magnetic susceptibility data of Verkin and Dmitrenko (1955), (their orientation No. 1 with $\theta = 90°$). Below approximately 28 k oersteds the amplitude of these oscillations becomes too small to resolve accurately with the techniques availabe at present. In fields greater than 59 k oersteds a fine structure becomes discernible with a period of $0{\cdot}3 \pm 0{\cdot}1 \times 10^{-6}$ oersteds^{-1} which is in agreement with Verkin and Dmitrenko (their curve No. 3); however, they did not

observe this period for $\theta > 50°$, whereas these present data are for $\theta = 90°$. Both of these components appear to be superimposed upon a considerably smaller amplitude low-frequency component with a period

$$\sim 7{\cdot}0 \pm 1{\cdot}0 \times 10^{-6}\,\text{oersteds}^{-1}.$$

The small amplitude of this component results in the low precision with which this period can be measured. However, this value is in good agreement with the value of $6{\cdot}0 \times 10^{-6}\,\text{oersteds}^{-1}$ observed by Verkin and Dmitrenko. This latter period is the main oscillation seen in their work. This branch of carriers, but with $\theta = 0°$ where the period becomes $60{\cdot}0 \times 10^{-6}\,\text{oersteds}^{-1}$, has also been seen in Hall coefficient measurements (Bergeran *et al.* 1960).

Harrison (1960) has attributed the main period observed in this work ($2{\cdot}1 \times 10^{-6}\,\text{oersteds}^{-1}$) to the horizontal arms (i.e. normal to the C axis) of the Fermi surface in the first and second bands of zinc. The geometry used in this investigation would be the optimum to observe such segments of the Fermi surface. Harrison attributes the smallest period observed to the diagonal arms (lying in $\{10\bar{1}0\}$ planes) of the Fermi surface. The geometrical resonances observed for this orientation indicate that the wave vector of the carriers in this orientation is $k' = 0{\cdot}25 \times 10^{8}\,\text{cm}^{-1}$. The effective mass is $0{\cdot}03m_0$, which would correspond to the horizontal arms.

Acknowledgments

I would like to thank V. G. Chirba and H. Dail for their help in making these experiments, J. Wernick for zone refining the zinc and P. H. Schmidt who grew the single crystals.

References

Bergeran, C. J., Grenier, C. G., and Reynolds, J. M., 1960, *Phys. Rev.*, **119,** 925.

Cohen, M. H., Harrison, M. J., and Harrison, W. A., 1960, *Phys. Rev.*, **117,** 937.

Gibbons, D., 1959, *Interaction of Acoustic Waves with Conduction Electrons*, A. S. M. Seminar on Resonances and Relaxations in Metals, Chicago, 1960 (American Society for Metals).

Harrison, W. A., 1960, *Phys. Rev.*, **118,** 1190.

Morse, R. W., and Gavenda, S. D., 1959, *Phys. Rev. Letters*, **2,** 250.

Reneker, D. H., 1959, *Phys. Rev.*, **115,** 303.

Shoenberg, D., 1959, *Progress in Low Temperature Physics*, Vol. II (New York: Interscience Publishers).

Verkin, B. I., and Dmitrenko, I. M., 1955, *Izv. Akad. Nauk. USSR.*, **19,** 409, English translation p. 365.

On Dislocation Loops Formed in Zinc Crystals During Low Temperature Pyramidal Glide†

By P. B. Price‡
Physics and Chemistry of Solids, Cavendish Laboratory, Cambridge

[Received August 2, 1960]

Recently electron transmission observations have been reported (Price 1960) of $(11\bar{2}2)[\bar{1}\bar{1}23]$ pyramidal glide in thin vapour-grown zinc crystals which were strained in tension inside an electron microscope. The orientation of these platelet crystals was such that the dislocations with a $\frac{1}{3}[\bar{1}\bar{1}23]$ Burgers vector were of predominantly screw orientation, and it was frequently observed that in the path of one of these gliding dislocations a long, narrow dislocation loop was left behind on a basal plane, presumably as a result of the formation of a multiple jog on the screw by cross-glide to enable it to avoid an obstacle. This long loop was unstable and was able to lower its energy by splitting up into a row of circular loops. It was shown that some of these loops had a $\frac{1}{3}[\bar{1}\bar{1}23]$ Burgers vector and others had a [0001] Burgers vector. Both types were sessile but were observed to shrink slowly by climb at room temperature and eventually to disappear.

The intermediate stage of splitting up of a long, narrow loop was rapid (1 to 5 sec) and it was impossible to take photographs, but it appeared that the total area of the circular loops was about the same as the area of the elongated loop and therefore that the process took place without a net flow of vacancies to or from the loop. The redistribution of the area inside the long loop clearly could only take place at a temperature at which jogs could easily be formed. It was therefore predicted that if the deformation were done at low temperature, this process should not be able to occur and the crystal should contain elongated loops instead of circular loops.

The purpose of this note is to describe some electron microscope observations, made during straining at low temperature, which confirmed this prediction. Figure 1 shows a low temperature micro-tensile device which was designed for use inside the Siemens Elmiskop 1. It was similar to one designed by Forsyth and Wilson (1960) except that the bimetal strips were arranged to stretch the specimen when the temperature was lowered instead of raised. The strips, which were made of aluminium and molybdenum, were fixed at one end to a phosphor–bronze body

† Communicated by the Author.

‡ U.S. National Science Foundation Post-Doctoral Fellow, 1959–60. Present address: General Electric Research Laboratory, Schenectady, New York, U.S.A.

which was thermally insulated from the rest of the microscope by a teflon collar but electrically connected by a small wire to prevent the specimen from charging up during examination. The strips and specimen were cooled by bringing into contact with the body of the device a thermally insulated finger, which was connected through the microscope column to a low temperature bath. By changing the level of liquid nitrogen in the bath the temperature of the bimetal strips, as determined by a contact thermocouple, could be lowered from 20°c to −150°c and the tensile strain increased to a maximum of 8%. A specimen was always mounted in a sagging position so that the slack was not taken up and deformation started until it was considerably below room temperature.

Fig. 1

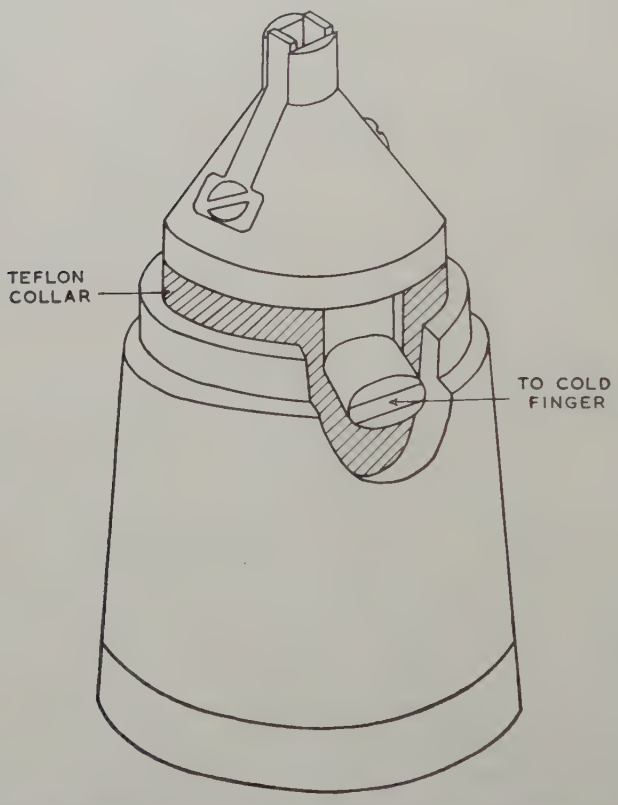

Low temperature straining stage for Siemens Elmiskop 1.

As was expected, it was found that loops produced at low temperature were elongated. Figure 2† is a series of six transmission electron micrographs of the same set of loops taken at intervals of about 20 sec when the recorded temperature was −60°c. As long as the electron

† Figure 2 is shown as a plate.

beam was off, the loops were stable and showed no tendency to split up at this temperature. During observation, the local temperature was raised enough (probably by at least 10 to 20°C) to allow the middle one of the three long loops to split into a row of circular loops. By proper adjustment of the beam current, the process could be made to occur slowly enough to photograph, and fig. 2 shows the various stages in the formation of the second circular loop in a row which eventually comprised six loops. These stages are exactly the same as those which occurred at room temperature (but at a different rate) and which are depicted in the drawing, fig. 8, of the paper by Price (1960). The elongated loops to either side of the centre one (fig. 2) did not change their shape, presumably because they were not in the centre of the illuminated region and were therefore at a lower temperature.

It was verified by direct measurement that the total area of the six circular loops was the same, to within 10%, as that of the parent loop and therefore that there was no net flow of vacancies to or from the loop. Measurements also showed that the criterion for loop splitting (Price 1960) was satisfied and that the energy, as calculated from the geometry of the loops, was lowered by $\sim 25\%$ by splitting.

Further studies of low temperature deformation are in progress ; the results will be reported later.

Acknowledgment

I am indebted to J. A. Venables for the original idea for the low temperature straining stage.

References

Forsyth, P. J. E., and Wilson, R. N., 1960, *J. sci. Instrum.*, **37**, 37.
Price, P. B., 1960, *Phil. Mag.*, **5**, 873.

CORRESPONDENCE

The Cooperative Movement of Dislocations in Very Pure Aluminium Foil

By R. N. Wilson and P. J. E. Forsyth
Metallurgy and Physics Department, Royal Aircraft Establishment, Farnborough, Hants

[Received September 29, 1960]

Dislocation sub-boundaries in aluminium have been shown to be essentially of two types: (*a*) tilt boundaries consisting of arrays of edge dislocations formed by thermally activated dislocation climb and elastic interaction with like dislocations on parallel planes, and (*b*) twist boundaries formed by the cross slipping and arraying of screw dislocations.

Tilt boundaries in aluminium have been studied by Cahn (1949) who showed they could be produced in a single crystal by light deformation followed by an annealing treatment. He called this phenomenon polygonization. Hirsch *et al.* (1956) and Hirsch *et al.* (1958) have studied dislocation sub-boundaries formed by heavy cold-working. They have used transmission electron metallography for direct observation and have shown many of these boundaries to be chiefly composed of screw dislocations.

The authors have studied the movement of dislocations in foils of aluminium using transmission electron microscopy with a straining device described elsewhere (Forsyth and Wilson 1960). As part of this work, a study was made of the influence of impurity level upon dislocation motion and the mode of fracture of the foils. Thin foils were prepared from super purity aluminium (99·99% Al) and zone refined aluminium (99·9999% Al). It was found that whereas deformation in the super pure aluminium was by the independent movement of dislocations, those in the zone refined metal moved in a cooperative manner as shown in the plate. The axis of tension in the foil is vertical in the micrograph and dislocations, believed to be essentially screw in character, can be seen to have been moving from right to left before the photograph was taken. It can be seen that many dislocations are in the process of moving in formation as well defined arrays of several dislocations, i.e. they are not only being influenced by the repulsive forces from like dislocations on their slip planes but also by the attractive forces of dislocations on parallel slip planes. Wilsdorf (1959), discussing the frictional force influencing dislocation movement in thin foils of stainless steel, has suggested two factors may be operative. The first is the presence of a surface oxide film anchoring the ends of the dislocation. This could account for the

convex bowing of dislocations under stress. The second factor is the pinning of a dislocation by atmospheres of point defects or impurity atoms along its length. This he suggests could account for the great variation in width of stacking fault in stainless steel and also be one cause of the jerky dislocations observed in metals of higher stacking fault energy such as aluminium. These frictional forces may also retard one dislocation with respect to its neighbours due to the variation in degree of locking of the dislocations as they move through the lattice.

In aluminium of very high purity the latter frictional force might be expected to be low. Also the absence from solid solution of such foreign atoms as magnesium and copper, which have a tendency to associate with vacancies, might reduce the number of vacancies present and increase the mobility of those remaining. It is suggested that it is this reduction of lattice friction which increases the effectiveness of the attractive forces between like dislocations on neighbouring planes causing this cooperative movement of dislocations. By this process small angle arrays can move unbroken through the lattice.

Acknowledgment

This letter is published by permission of the Controller, H.M. Stationery Office. Crown Copyright reserved.

References

Cahn, R. W., 1949, *J. Inst. Met.*, **76**, 121.
Forsyth, P. J. E., and Wilson, R. N., 1960, *J. sci. Instrum.*, **37**, 37.
Hirsch, P. B., Horne, R. W., and Whelan, M. J., 1956, *Phil. Mag.*, **1**, 677.
Hirsch, P. B., Partridge, P. G., and Tomlinson, H., 1958, *Fourth International Conference on Electron Microscopy*, p. 536.
Wilsdorf, H. G. F., 1959, *Structure and Properties of Thin Films* (New York: Wiley & Sons), p. 151.

Correlation between Magnetic Susceptibility and Hydrogen Solubility in Alloys of Early Transition Elements

By D. W. Jones, N. Pessall and A. D. McQuillan
Department of Physical Metallurgy, University of Birmingham

[Received December 1, 1960]

The elements of groups IVA and VA of the periodic table share with palladium the ability to take into solid-solution large quantities of hydrogen, but whereas in the case of palladium this type of behaviour can be explained in terms of an almost filled d-band, no explanation has yet been offered for the case of the early transition elements. As part of a general investigation of the physical properties of alloys of the early transition elements with each other, it was decided, therefore, to include hydrogen solubility as one of the properties to be examined. In the preliminary survey the elements chosen for study were titanium, niobium and molybdenum because these metals are from successive groups of the periodic table, and because they are completely miscible with each other in the body-centred cubic structure. It was possible, therefore, to follow continuously changes in physical properties in passing from one metal to the next. Since molybdenum, being in Group VIA, does not dissolve hydrogen, the systems containing molybdenum are of particular interest because in these systems hydrogen solubility must fall to zero with increasing molybdenum content.

Figure 1 shows the maximum amount of hydrogen which can be absorbed by alloys in the binary systems, titanium–niobium, and titanium–molybdenum. The alloy compositions have been plotted in terms of electron to atom ratio assuming the values 4, 5 and 6 for titanium, niobium and molybdenum respectively. With increasing electron/atom ratio, the capacity of the alloys to absorb hydrogen decreases continuously, and is effectively zero at about 5·6 electrons per atom. Because titanium-rich alloys form hydride phases with face-centred cubic structures, the crystal structure does not remain the same over the length of the curve shown in fig. 1. It is preferable, therefore, to measure not the total solubility of hydrogen in the alloys, but the heat of solution of a very small quantity of hydrogen in the alloys having a body-centred cubic form. Figure 2 shows the results of this type of investigation. As the electron/atom ratio approaches 5·6, the heat of solution decreases rapidly, passing through zero at 5·5 electrons per atom, and thereafter becoming endothermic. The zero value of heat of solution has little significance, being merely the point where the reaction with the metal changes from exothermic to endothermic with respect to gaseous molecular hydrogen.

The magnetic susceptibility at room temperature of alloys in the three binary systems titanium–niobium, niobium–molybdenum and titanium–molybdenum are plotted in fig. 3. The most characteristic features of the curves are the minimum points which occur in the systems titanium–molybdenum, and niobium–molybdenum at electron/atom ratios between

Fig. 1

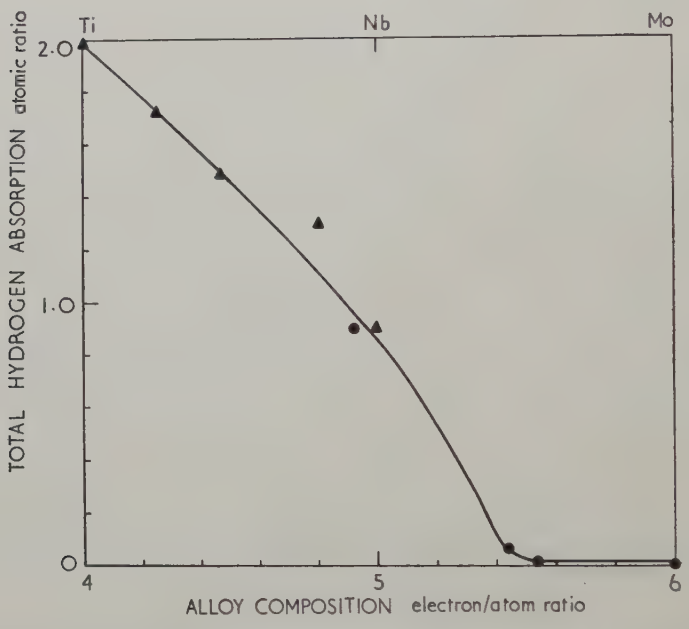

Total amount of hydrogen absorbed by alloys of titanium with niobium ▲, and titanium with molybdenum ●, as a function of alloy composition expressed in terms of electron/atom ratio.

5·6 and 5·7 and which correlate very well with the disappearance of hydrogen solubility in the alloys. There exists, furthermore, one other piece of evidence that a change in electronic structure occurs at this critical composition. Figure 4 gives results (Grum-Grzhimailo and Gromova 1956) on the Hall coefficient of body-centred cubic titanium–molybdenum alloys at room temperature. The Hall coefficient is positive throughout and reaches a maximum value at about 5·6 electrons/atom. The magnetic susceptibility and Hall coefficient curves taken together strongly suggest that, as the critical composition of 5·6 is approached, a sub-band is being filled, since the Pauli paramagnetism of the alloys, which is proportional to the density of states at the Fermi level is decreasing rapidly immediately before the critical composition is reached, and the Hall coefficient, as would be expected if the top of a band were being

Fig. 2

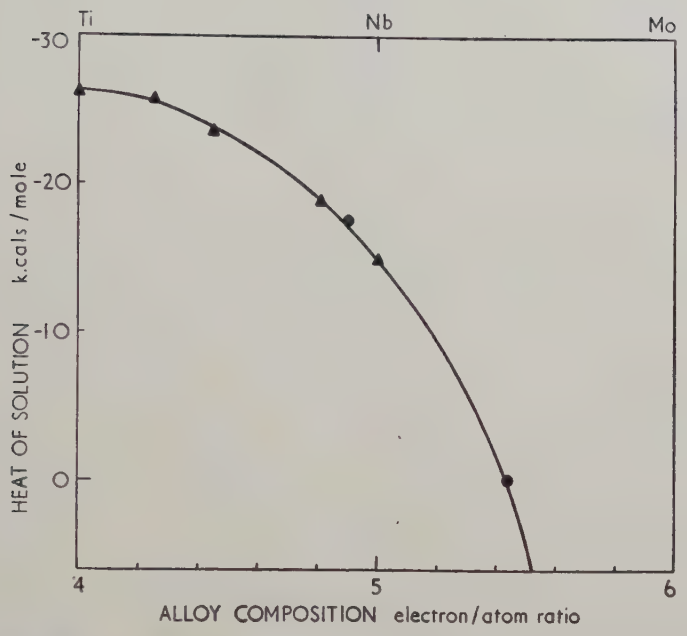

Heat of solution of molecular hydrogen in body-centred cubic alloys in the systems titanium–niobium ▲, and titanium–molybdenum ● in terms of electron/atom ratio.

Fig. 3

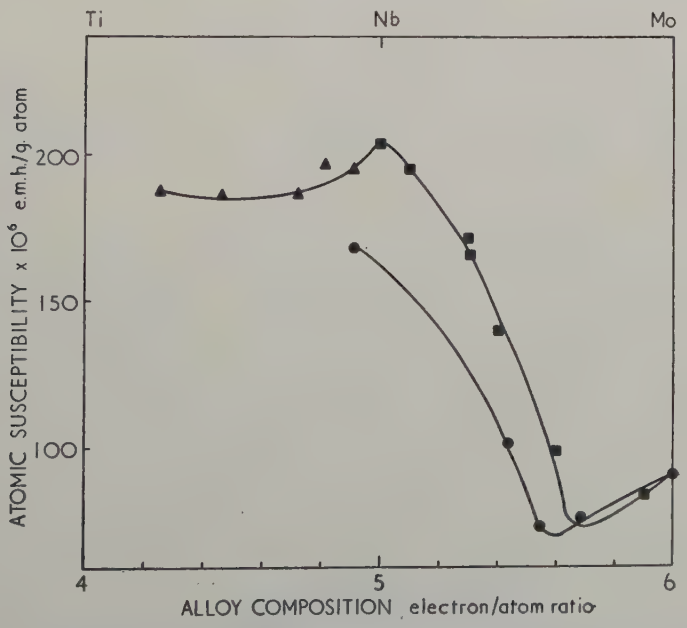

Magnetic susceptibility of body-centred cubic alloys of titanium–niobium ▲, niobium–molybdenum ■, and titanium–molybdenum ● at room temperature.

approached, is becoming increasingly positive in the same composition range. A similar picture of a sub-band filling at an electron/atom ratio of approximately 5·6 electrons emerges from results obtained from the measurement of the low-temperature specific heats of body-centred cubic alloys of the early transition metals of the first long period (Cheng *et al.* 1960).

Fig. 4

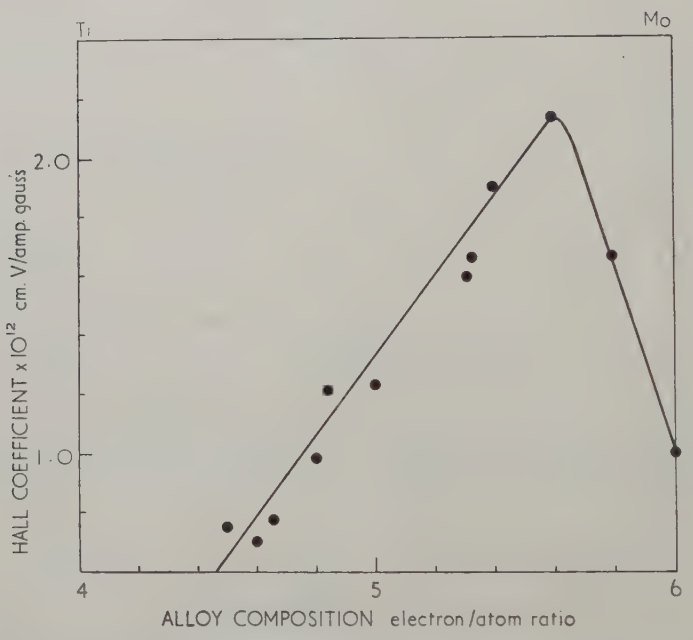

Hall coefficient of body-centred cubic alloys of titanium–molybdenum ● at room temperature, after Grum-Grzhimailo and Gromova 1956.

The form of the curves of magnetic susceptibility and Hall coefficient shown in figs. 3 and 4, together with the results of Cheng *et al.* strongly suggest that, beyond the critical composition of 5·6 electrons per atom, there exists another sub-band, and that the top of the lower sub-band overlaps the bottom of this upper band. In a recent paper (Goodenough 1960), it is proposed that early transition metals with the body-centred cubic structure have a band structure consisting of a partially filled s–p bonding band overlapping a sub-band composed of d-electrons in t_{2g} states. On this model, the alloy having the critical composition of 5·6 electrons per atom would have three electrons per atom in the t_{2g} sub-band and 2·6 electrons per atom in the s–p bonding band. Furthermore, an increase in electron/atom ratio would lead to the filling of localized e_g states. While there are difficulties in reconciling the details

of Goodenough's model with our results, it is evident that this type of approach, in which the d-band of the early transition metals is split into sub-bands, is likely to be extremely productive in attempting to find an explanation for the unusual physical properties of these materials. The question will be discussed in greater detail in later papers when the results of further experiments now in progress become available.

References

Cheng, C. H., Wei, C. T., and Beck, P. A., 1960, *Phys. Rev.*, **120**, 426.
Goodenough, J. B., 1960, *Phys. Rev.*, **120**, 67.
Grum-Grzhimailo, N. V., and Gromova, V. G., 1956, *J. inorg. Chem. Acad. Sci. U.S.S.R.*, **2**, 2426.

Density and Expansivity of Solid Xenon

By A. J. Eatwell and B. L. Smith
Department of Physics, Queen Mary College (University of London), London, E.1

[Received October 17, 1960]

In previous communications, measurements of the densities and expansivities of solid argon (Dobbs *et al.* 1956) and solid krypton (Figgins and Smith 1960) have been reported. We have now determined the lattice parameter of solid xenon between 20° and 120°K using the X-ray method of Debye–Scherrer powder photographs and a bulk density method and have thus derived values of the density and the volume coefficient of expansion.

In the X-ray measurements, polycrystalline xenon was deposited from the vapour in a Perspex tube of 1 mm internal diameter, and all specimens used were free from visible defects. The temperature was kept constant to within 0·04°K at 20°K and to 0·01°K at 90°K. Thus temperature fluctuations could only contribute a negligible error (5×10^{-7} Å) in the values of lattice parameter. 'Spottiness' in the films due to large grain size at the higher temperatures has been much reduced by the introduction of vertical and rotational motion of the cylindrical specimen. Thus, the accuracy quoted for X-ray values at 20°K by Figgins and Smith ($\pm 0{\cdot}001$ Å) now applies to the whole range of working temperatures. The lattice parameter values are not corrected for refraction, this correction being small (Jette and Foote 1935). The xenon used in both experiments was stated by the British Oxygen Company Ltd to be of 99–100% purity, the remainder being krypton. The estimates of lattice parameter made from the bulk density measurements are accurate to within $\pm 0{\cdot}005$ Å.

The results are shown in the figure. It will be seen that there is agreement between the results obtained by the two methods. Our results are in fairly good agreement with the X-ray measurements of Cheesman and Soane (1957), are within the limits of the experimental error of the single value of Simon and Ruhemann (1932) but outside those of the single value of Natta and Nasini (1930). It is of interest to note that a separate sample of gas, also stated to be of 99–100% purity, was used for the X-ray measurement at 60°K.

In the tables, we summarize our results for the density and estimates of the volume coefficient of expansion $\alpha = 1/V\,(\partial V/\partial T)_p$ at rounded temperatures. For convenience the corresponding results previously obtained for argon and krypton are repeated.

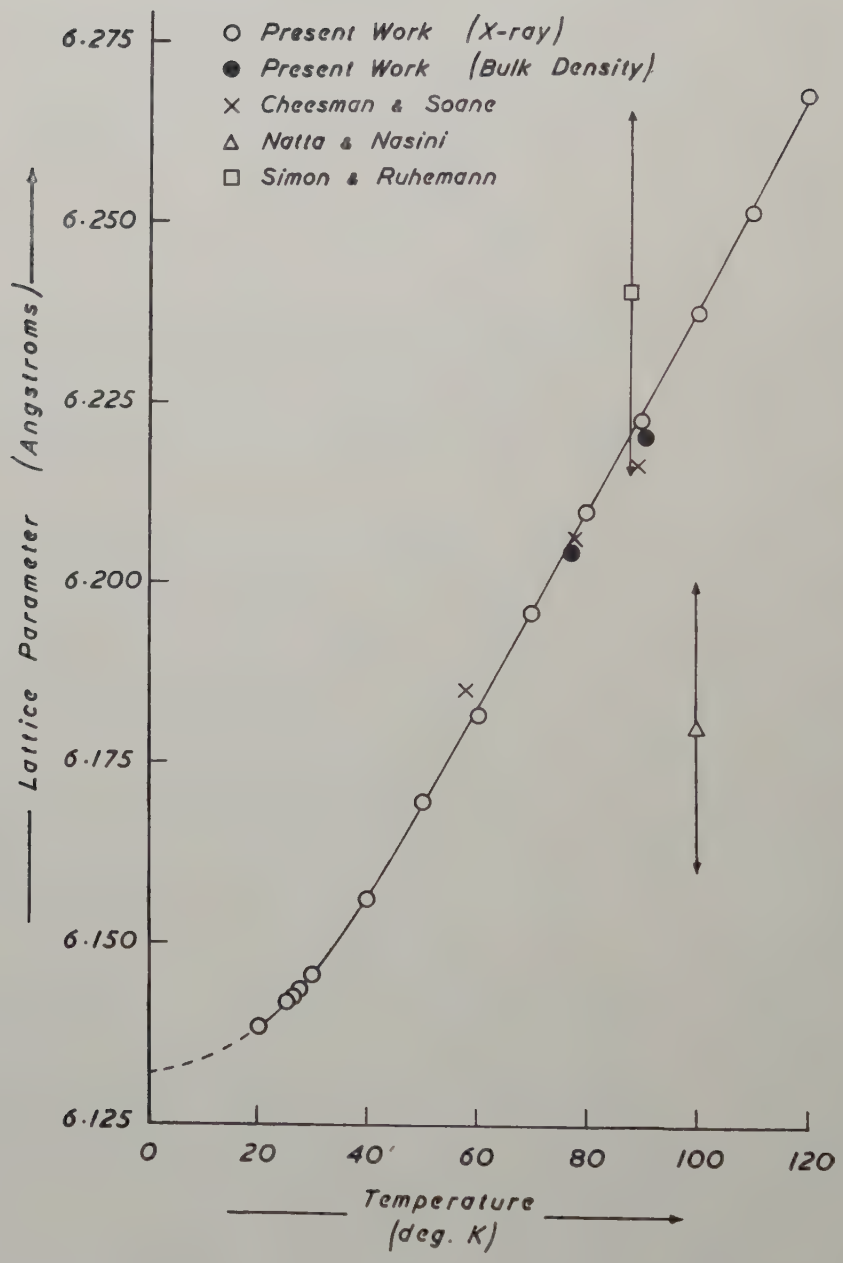
Present Work (X-ray)
Present Work (Bulk Density)
Cheesman & Soane
Natta & Nasini
Simon & Ruhemann
Lattice Parameter (Angstroms)
6.275
6.250
6.225
6.200
6.175
6.150
6.125
0
20
40
60
80
100
120
Temperature (deg. K)

Table 1. Density (g cm^{-3})

T (°K)	20	40	60	80	100	120
Argon	1·764	1·737	1·691	1·636	—	—
Krypton	3·078	3·040	2·988	2·926	—	—
Xenon	3·772	3·736	3·689	3·642	3·593	3·542

Table 2. Volume coefficient of expansion ($\times 10^4$ deg^{-1} C)

T (°K)	20	40	60	80	100	120
Argon	4	12	15	18	—	—
Krypton	4·8	7·7	9·7	11·0	—	—
Xenon	3·0	5·76	6·46	6·65	6·77	6·80

An extrapolation of our curve leads to an estimate at absolute zero of a lattice parameter of 6·13 Å for xenon and a corresponding density of 3·78 g cm^{-3}.

Acknowledgments

We acknowledge the help and advice of Dr. B. F. Figgins, and assistance given by Mr. W. Eagers during the measurements. We are grateful to the D.S.I.R. for the award of studentships to both of us.

References

Cheesman, G. H., and Soane, C. M., 1957, *Proc. phys. Soc. Lond.* B, **70,** 700.
Dobbs, E. R., Figgins, B. F., Jones, G. O., Piercey, D. C., and Riley, D. P., 1956, *Nature, Lond.*, **178,** 483.
Figgins, B. F., and Smith, B. L., 1960, *Phil. Mag.*, **5,** 186.
Jette, E. R., and Foote, F., 1935, *J. chem. Phys.*, **3,** 605.
Natta, G., and Nasini, G., 1930, *Atti. Accad. Lincei. Rend.*, **6,** 11, 1009.
Simon, F., and Ruhemann, B., 1932, *Z. phys. Chem.* B, **15,** 389.

Dislocation Loops and Hardening in Neutron Irradiated Copper

By M. J. Makin, A. D. Whapham and F. J. Minter
Metallurgy Division, A.E.R.E., Harwell

[Received October 17, 1960]

Silcox and Hirsch (1959) using the transmission electron microscope technique have shown that in copper prismatic dislocation loops are formed during neutron irradiation at 35–100°C. The loops increased in diameter with dose and their density could be substantially reduced by annealing for a few minutes at 350°C. They suggested that the loops were vacancy loops similar to those observed in quenched metals, but that they were nucleated by the collapse of vacancy-rich regions in the centre of Brinkman displacement spikes. They further concluded that the lattice hardening formed during irradiation was the stress required for a dislocation to cut through the ' forest ' of loops threading the glide plane. In considering the details of this model certain objections become apparent, notably the difficulty in simultaneously accounting for the very large temperature dependence and the absolute magnitude of the lattice hardening. For these reasons experiments were undertaken to investigate (*a*) the nature of the loops and (*b*) the relation between the loops and the irradiation hardening.

Foils, 0·001 in. thick, of 99·998% copper were irradiated at ~ 27°C in an air-cooled hollow uranium cylinder in the BEPO reactor at Harwell, and were subsequently electropolished in an orthophosphoric acid–water mixture and examined in a Siemens Elmiskop I microscope. The distribution of the number of loops as a function of diameter after various neutron doses is shown in fig. 1. The average diameter of the loops increased during irradiation, showing that individual loops must grow by acquiring mobile defects. Loops can grow therefore only in the temperature range in which the constituent point defects are mobile. In principle it is possible to distinguish whether the loops are formed from platelets of interstitial atoms or vacancies by irradiating at a sufficiently low temperature to immobilize one of these defects. At 27°C it is believed that both interstitial atoms and vacancies are mobile, assuming that the energies of migration are $\sim 0{\cdot}1$ ev for interstitials and $\sim 0{\cdot}7$ ev for vacancies (Holmes *et al.* 1958). Irradiations were therefore carried out at -195°C and the specimens examined on the cold stage of a Siemens microscope keeping the temperature low throughout. Two procedures were adopted. In the first, bulk foils 0·001 in. thick were neutron irradiated ($3{\cdot}1 \times 10^{17}$ fast n cm^{-2}) at -195°C

and then polished in a methyl alcohol–nitric acid bath at $-70°$C. They were washed in methyl alcohol and then ether at $-78°$C and dried *in vacuo* at $-50°$C. Transfer into the microscope specimen holder was performed under liquid nitrogen. In the second procedure previously polished specimens were irradiated at $-195°$C with pile neutrons or with 100 kev alpha particles in an accelerator, care being taken to ensure good thermal contact between the specimen and the cooled support.

Fig. 1

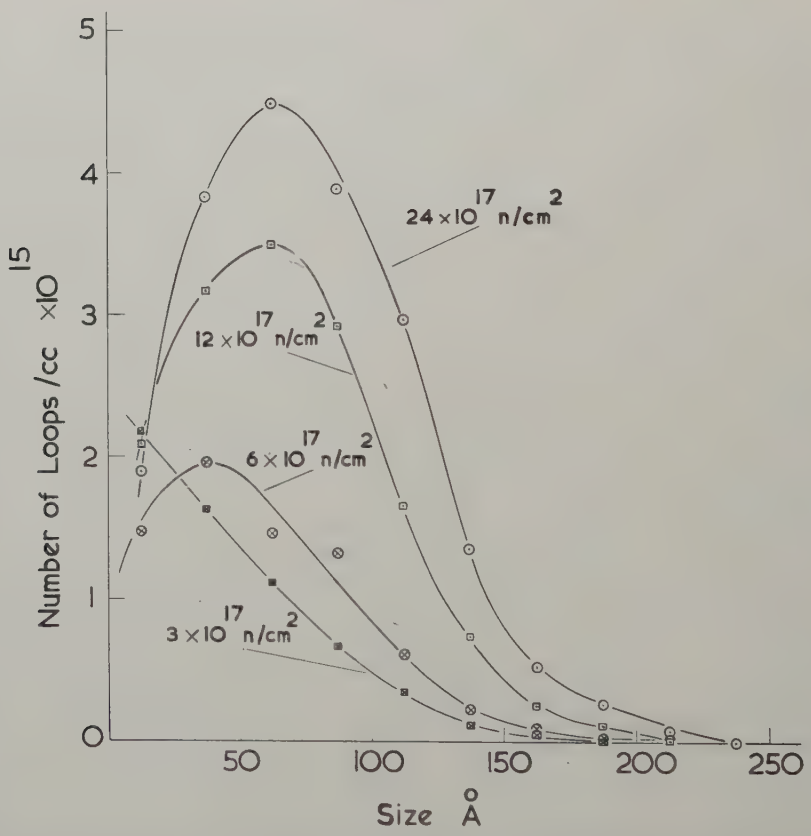

The density of dislocation loops as a function of diameter for neutron doses up to $2{\cdot}4 \times 10^{18}$ fast n cm^{-2}.

As before these specimens were inserted into the cold stage at $-195°$C. This technique eliminates the polishing and washing at $-70°$C and the drying at $-50°$C entailed in the first procedure and enables the specimens to be kept within a few degrees of $-195°$C until they are inside the microscope. The cold stage operates at $\sim -120°$C but at this temperature ice condenses from the microscope vacuum onto the specimen. This

can be removed by the electron beam at a local temperature of $-50°$C and areas could be photographed within one minute of warming to this temperature. In all cases loops were observed immediately the ice cleared (fig. 2†) and no further change occurred even on warming to room temperature. This result virtually eliminates the possibility that the loops are formed from vacancies since these are capable of only 0·1 jumps per minute at $-50°$C assuming that the energy for migration is 0·7 ev. Hence loops are formed below the temperature at which vacancies are mobile and it is inferred therefore that the loops must be formed from interstitial atoms. This conclusion is supported by the observation of Barnes and Mazey (1960) of the growth of the loops in the helium band of alpha irradiated copper on annealing. In this case it is concluded that the loops expand by emitting vacancies (which are absorbed by the helium bubbles) and must therefore be interstitial in character.

The role that the interstitial loops play in the irradiation hardening is shown by experiments in which electron micrographs are compared with the mechanical properties during annealing at 306°C. A large number of polycrystalline tensile test specimens and 0·001 in. foils were irradiated with 2×10^{18} fast n cm^{-2} and annealed at 306°C for various times. The electron micrographs from the annealed foils show two effects : (*a*) the density of loops decreases rapidly with annealing and (*b*) a high density ($1{\cdot}3 \times 10^{16}$ cm^{-3}) of very small (< 25 Å) defects become readily visible (fig. 3). That these defects are different in kind from the loops is indicated by the very large difference in size and also the different response to the grain boundaries. The loops form a wide denuded zone on annealing but the small defects show no appreciable denudation (fig. 4). The small defects are thought to be vacancy clusters formed by the redistribution of the multiple vacancies created in the displacement spikes (Seeger 1958). If the defects observed in the electron microscope are responsible for the hardening the yield stress should be proportional to the square root of the loop density. A plot of the square root of the densities of both loops and small defects versus the yield stress after various anneals (fig. 5) shows that whereas there is no linear relationship between the hardening and the number of large loops, there may well be such a relation between the small defects and the hardening. This suggests that the small defects may be responsible for a large part of the hardening. This is supported by the observation that on mild annealing (i.e. 10–60 min at 306°C) simultaneously with the decrease in density of the large loops and the formation of the small defects there is a large reduction in the temperature sensitivity of the hardening. It is unlikely that this is associated with the decrease in density of the large loops since theoretically these are expected to produce a hardening with a low temperature dependence. It is more reasonable to associate

† Figures 2, 3 and 4 are shown as plates.

the temperature dependence with submicroscopic defects which anneal away to produce the observable small defects. Furthermore, nickel does not show any large loops on irradiation at 35°c (Silcox 1960) although the great similarity in the characteristics of the hardening in this metal to those in copper (Makin and Minter 1960) suggests that the same types of defects are responsible in both.

Fig. 5

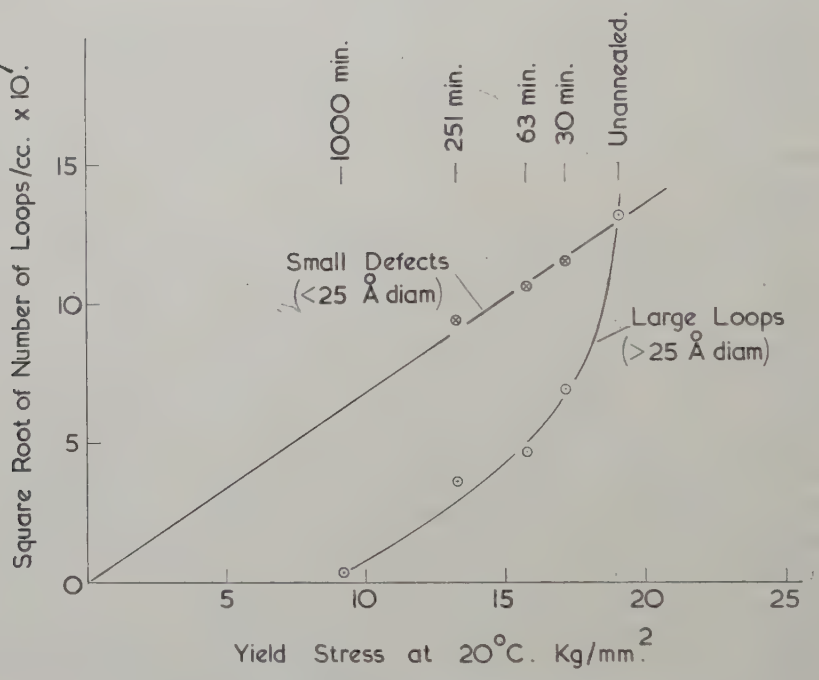

The (defect density)$^{1/2}$ as a function of the yield stress during annealing for both large and small defects.

It is concluded that in copper although the interstitial loops must play some part in the hardening they are unlikely to be the sole cause.

References

Barnes, R. S., and Mazey, D. J., 1960, *Phil. Mag.*, **5**, 1247.

Holmes, D. K., Corbett, J. W., Walker, R. M., Koehler, J. S., and Seitz, F., 1958, *Second Geneva Conf. on Peaceful Uses of Atomic Energy*, **6**, 274.

Makin, M. J., and Minter, F. J., 1960, *Acta Met.*, **8**, 691.

Seeger, A. K., 1958, *Second Geneva Conf. on Peaceful Uses of Atomic Energy*, **6**, 250.

Silcox, J., 1960, "Radiation Damage in Face Centred Cubic Metals", *Proceedings of the European Reg. Conf. on Electron Microscopy, Delft* (to be published).

Silcox, J., and Hirsch, P. B., 1959, *Phil. Mag.*, **4**, 1356.

REVIEWS OF BOOKS

Translation from Russian for Scientists. By C. R. Buxton and H. Sheldon Jackson. (Blackie & Son, 1960.) [Pp. xvii+299.] 30*s.*

A concise survey of Russian grammar is followed by an extensive series of texts drawn from physics, chemistry and engineering. The book provides a valuable introduction to scientific Russian and should enable scientific journals to be read without difficulty. M. G. P.

Magnetic Materials. Third edition. By F. Brailsford. (London : Methuen & Co ; New York : John Wiley & Sons, 1960). [Pp. vii+188.] 16*s.* net.

The study of magnetism and magnetic materials has expanded so enormously since the publication in 1948 of the first edition of this well-known Methuen Monograph that at a recent conference no less than 164 papers on these topics were presented. This new edition nevertheless encompasses many of the advances of the past 12 years in a volume not exceeding unduly that of the earlier one. It should hence continue to be a useful companion to those engaged in the art and practice of magnetic materials. The major addition is a chapter on ferrites, both cubic and hexagonal, appearing here with chapters on iron–silicon, iron–nickel and related alloys as well as on permanent magnet materials. One looks forward to the fourth edition, where, it is hoped, an equally coherent account will be given of the properties of thin films for computer applications, of garnets and of the novel permanent magnet materials, as well as of other substances as yet undreamt of. One despairs, however, of magnetic recording tapes being regarded as respectable enough to be included even in the *n*th edition. E. P. W.

Cartesian Tensors. By G. Temple. (London : Methuen & Co. Ltd., 1960.) [Pp. 92.] 12*s.* 6*d.*

Every physicist needs to know just a little about tensors, and it is not easy to find a good simple account of the elements. Professor Temple has attempted this; for its very existence his book is welcome. Yet it is really a trifle dry—much more suitable for applied mathematicians than ordinary physicists. It is a pity that he has concentrated so much on the representation of vectors and tensors by their components and ignored the advantages, at least for some ways of thought, of conceiving them as geometrical objects which can be symbolized as a whole, in Clarendon Bold type as you might say. The whole theory of the eigenvalues, for example can be flooded with light by the simple analogy of the reduction of a quadric surface to its principal axes. The chapter on spinors also seems very formal and difficult for a beginner. However, it will be useful to know where to refer students for an elegant deviation of the main theorems and their application. J. M. Z.

Progress in Solid Mechanics. Edited by I. N. Sneddon and R. Hill. (The North-Holland Publishing Company, 1960.) [Pp. xii+448.] Price £5 0*s.* 0*d.*

This book is Volume I of a new series of which the aim is to present " review articles of the highest standard which from time to time summarize and unify the most recent work in a particular field or group of fields " in the mechanics of solid continua. It contains the following articles: Viscoelastic waves (S. C. Hunter), Matrices of transmission in beam problems (K. Marguerre), Dynamic expansion of spherical cavities in metals (H. G. Hopkins), General theorems for elastic-plastic solids (W. T. Koiter), Dispersion relations for elastic waves

in bars (W. A. Green), Thermoelasticity: the dynamical theory (P. Chadwick), Continuous distributions of dislocations (B. A. Bilby), Asymmetric problems of the theory of elasticity (R. Muki).

Each writer reviews the work done on his topic up to 1958 and gives a useful list of references. In general the standard of exposition is high, being concise without assuming too much previous knowledge on the part of the reader. The layout of the mathematics is pleasing and easy to read.

This series promises to be of very great value to workers on the mechanics of solids: the North-Holland Publishing Company is to be congratulated on its initiative, and the editors thanked for the excellent start they have made on the task they have set themselves. E. R. L.

Mechanics. Second edition. By K. R. Symon. (Addison-Wesley, 1960.) [Pp. 557.] Price £3 0*s*. 0*d*.

This text-book can be warmly recommended. It is a treatment of classical mechanics with a choice of topics intended to emphasize present-day points of view. The inadequacies of classical mechanics are pointed out, as are the points of connection with relativity and wave mechanics. Only a knowledge of the calculus is assumed; there are adequate accounts of other mathematical techniques such as vector analysis and tensors. The first eight chapters deal with such topics as Newtonian concepts, motion of a particle in three dimensions, rotation about a fixed axis, gravitation, moving coordinate systems and wave motion. The treatment is on the whole too sophisticated for students attending a first University course, although the brighter members of a class would find it very stimulating. The last four chapters deal with a Lagrangian mechanics, inertia and stress tensors, rotation about a point, and small vibrations of a system. The book in fact covers all aspects of classical mechanics for which space is likely to be found in undergraduate courses up to and including the Honours level. A student who, with some guidance, worked through even an appreciable part of this book, would have laid a very solid foundation for study in other branches of physics. There are approximately 360 problems, and answers are given to half of these. The book is clearly written and produced, and for its length it is very reasonably priced. W. C.

Crystal-Structure Analysis. By M. J. Buerger. (New York: John Wiley, Inc., 1960.) [Pp. 668.] Price £7 8*s*. 0*d*.

This book by a distinguished American crystallographer will be in continual use in all laboratories concerned with crystal-structure analysis. It contains a wealth of material, set out clearly at considerable length, and there are many references for further reading. The present volume is intended as a companion volume to the author's *X-ray Crystallography* and *Vector Space and its applications in Crystal Structure Analysis*. The former dealt largely with experimental methods; to some extent the ground is gone over again in the present volume, which does not however overlap to any extent with 'Vector Space'. The book opens with an interesting historical survey, and a discussion of the theory of diffraction by crystals. Subsequent chapters deal with, for example, the measurement and correction of x-ray intensities, examples of crystal structure determinations, the theory of Fourier methods, the reciprocal lattice, methods of phase determination, and accurate structure analysis. The very complete treatment of most topics serves to emphasize some surprising omissions. The author's stated reason for omitting optical analogue methods may or may not be sound, but the fact that intensity statistics is a self-contained topic on which a monograph could be written does not justify its omission from a comprehensive textbook. Most surprising of all for a textbook which, according

to the publishers, sets out to review all the available methods for crystal structure analysis, the word 'neutron' does not even appear in the index. X-ray crystallographers should not be encouraged in their insularity by ignoring the fact that there is now a large and increasing effort devoted to structure determination, particularly of magnetic materials, by neutron diffraction. This is a good book; it could so easily have been a better one. W. C.

Mechanical Waveguides. By Martin Redwood. (London and New York: Pergamon Press, 1960.) [Pp. 300.] Price £2 10*s.* 0*d.*

Many measurements of the velocity and attenuation of ultrasonic waves in fluids and solids have been made in recent years and this book is primarily addressed to researches in this field. It is a mathematical text on elastic wave propagation in lossless media and does not discuss experimental techniques. But it is a timely addition to the literature on elasticity and brings together a large number of results from many different courses.

A useful introduction to the wave equation precedes a detailed account of the reflection of elastic waves at an interface. These interfaces are the boundaries of the 'mechanical waveguides' through which the elastic waves are propagated. A detailed analysis of the propagation of both continuous waves and pulses in fluid and solid waveguides is given. In many cases the sine and cosine solutions of the parallel plate guide are followed by the Bessel function solutions for the cylindrical guide. The analysis refers only to lossless, isotropic media, but includes both the ultrasonic 'narrow bandwidth' pulses and the explosive 'wide bandwidth' pulses studied extensively by Kolsky.

Unfortunately it is not an easy book to read. The text is broken up unnecessarily by the display of the longer equations over many lines and by the inclusion of over thirty pages of 'additional' references, which are not referred to in the text. Some chapters of the book are subdivided *ad infinitum*, so that for example, § 9.2.5 (iii) contains only three sentences. But the author is to be congratulated on including so many different examples of elastic wave propagation in one short book. E. R. D.

Infra-red Methods: Principles and Applications. By G. K. T. Cohn and D. G. Avery. (New York and London: Academic Press, 1960.) [Pp. 203.] Price $6.80.

This book provides a clear and concise introduction to current infra-red techniques and is intended for the research student or worker in allied fields. The first part covers a wide range of topics and has chapters on sources, optical materials, detectors, amplifiers and dispersive systems. The emphasis here is on the underlying theory which is treated concisely and for the most part adequately. The shorter section deals briefly with a few specialized applications and considers calibration of detectors, a prism monochromator, gas analysis and optical pyrometry. The book is well supplied with graphs, diagrams and useful tables, and since the treatment is general, rather than detailed, the authors wisely include at the end of each chapter an excellent list of references.

The only criticism worth mentioning is that the much greater space given to the description of prism spectrometers might suggest that they are technically more important than grating instruments. Since the diffraction grating is rapidly superseding the prism and is, as the authors point out, a cheaper and better dispersive element, the grating spectrometer deserves, if anything, a fuller treatment than the prism instrument. Criticisms other than this would be of minor faults. *Infra-red Methods* is not only an adequate introduction to the subject but also a compact reference book. F. A. J.

BOOK NOTICES

A Degree Physics. Part 1 : The General Properties of Matter. By C. J. Smith. (London : Edward Arnold, Ltd., 1960.) Second edition. [Pp. 732.] £3 3*s*. 0*d*.

Molecular Distillation. By G. Burrows. (Monographs on the Physics and Chemistry of Materials ; General Editors : W. Jackson, H. Fröhlich, N. F. Mott, E. C. Bullard.) (Oxford : Clarendon Press, 1960.) [Pp. 214.] £1 15*s*. 0*d*.

Lectures in Theoretical Physics. Vol. II. Lectures delivered at the Summer Institute for Theoretical Physics, University of Colorado, Boulder, 1959. Edited by W. E. Brittin and B. W. Downs. (New York and London : Interscience Publishers, Inc., 1960.) [Pp. 483.] £3 8*s*. 0*d*.

Crystal Structures. Supplement V. By Ralph W. G. Wyckoff. (New York and London : Interscience Publishers, Inc., 1960.) £10 0*s*. 0*d*.

Advances in Biological and Medical Physics, Vol. VII. Edited by Cornelius A. Tobias and J. H. Lawrence. Assistant editor, Thomas L. Hayes. (New York and London : Academic Press, 1960.) [Pp. 362.] Price $10.00.

Solid State Physics in Electronics and Telecommunications, Vol. 2. Semiconductors, Part 2. Proceedings of an International Conference held in Brussels, June 2–7, 1958. Edited by M. Désirant and J. L. Michiels. (London and New York : Academic Press, 1960.) [Pp. 639.] Price £6 8*s*. 6*d*.

Solid State Physics in Electronics and Telecommunications, Vol. 3. Magnetic and Optical Properties, Part 1. Proceedings of an International Conference held in Brussels, June 2–7, 1958. Edited by M. Désirant and J. L. Michiels. (London and New York : Academic Press, 1960.) [Pp. 557.] Price £6 8*s*. 6*d*.

Growth of Crystals, Vol. 2. Interim reports between the first (1956) and second Conference on Crystal Growth, Institute of Crystallography, Academy of Sciences, USSR. Edited by A. V. Shubnikov and N. N. Sheftal'. Translated from the Russian. (London : Chapman & Hall Ltd. ; New York : Consultants Bureau, Inc., 1959.) [Pp. 178.] Price £6 8*s*. 0*d*.

[*The Editors do not hold themselves responsible for the views expressed by their correspondents.*]

Fig. 2

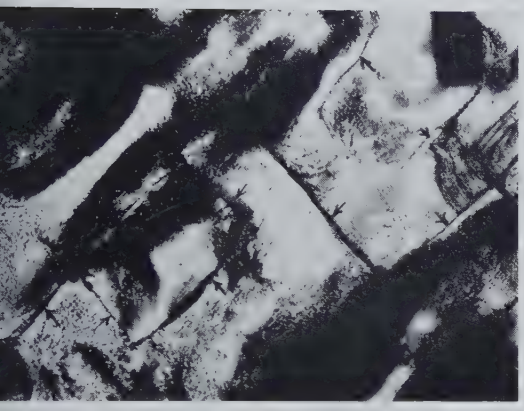

$\times 10^4$ cycles after repolishing at $1{\cdot}75 \times 10^6$ cycles. Fine slip traces produced the mottled effect. Arrows indicate boundaries at ± 45 degrees to the specimen axis which is parallel to the long edge of the figure. Strain $\pm 0{\cdot}092\%$ ($\times 75$).

Fig. 4

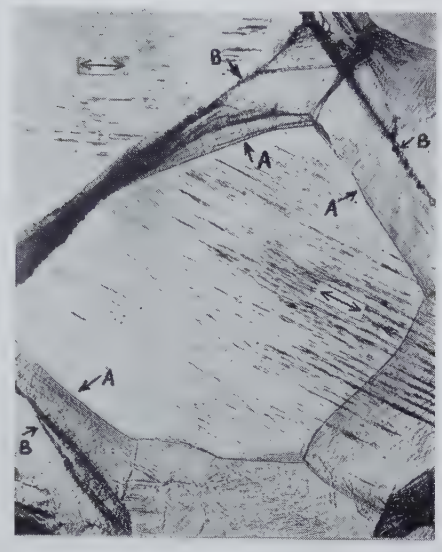

5×10^4 cycles ($\times 75$).

Fig. 5

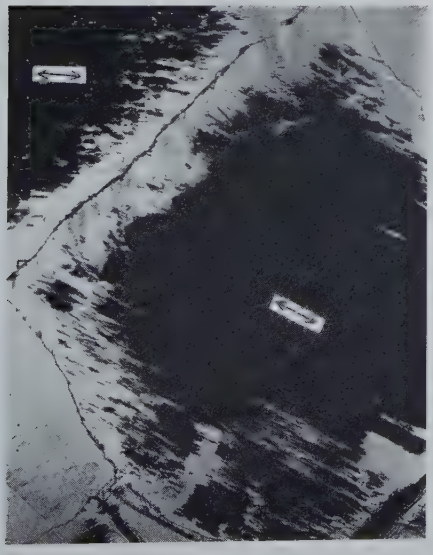

$5{\cdot}30 \times 10^6$ cycles, repolished $7{\cdot}5 \times 10^5$ cycles ($\times 75$).

Fig. 6

$5{\cdot}93 \times 10^6$ cycles, repolished $5{\cdot}30 \times 10^6$ cycles ($\times 75$).

n figs. 4–8 the specimen axis is parallel to the long edge of the figure. In figs. 4–6 the two main systems of slip are indicated by double-headed arrows.

Fig. 7

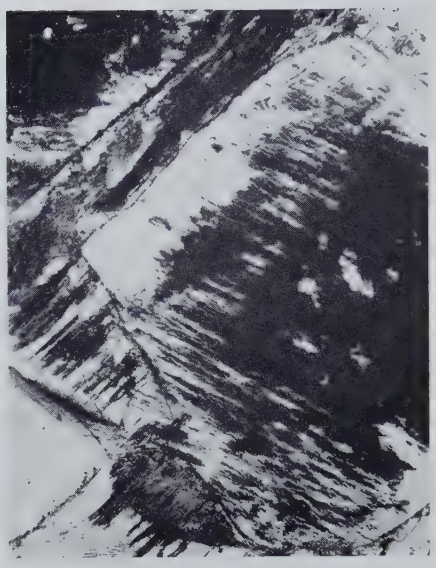

$8{\cdot}0 \times 10^6$ cycles ($\times 75$).

Fig. 8

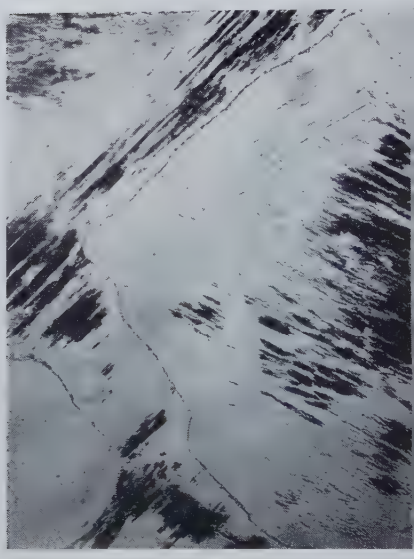

$8{\cdot}50 \times 10^6$ cycles, repolished at $8{\cdot}20 \times 10^6$ cycles ($\times 75$).

Fig. 10

After 10^3 cycles ($\times 75$).

Fig. 11

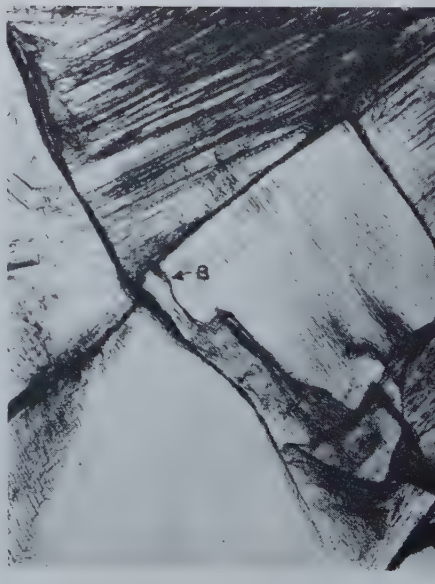

After 2×10^4 cycles ($\times 75$).

Fig. 1

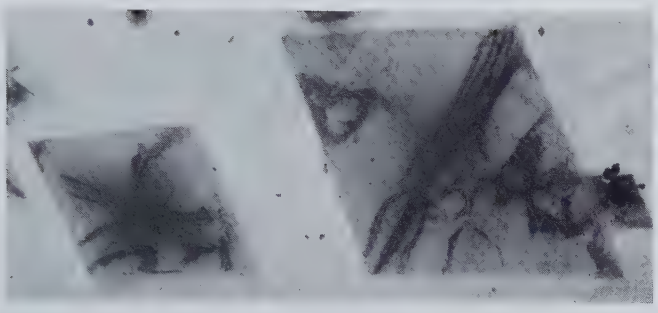

Untreated thin crystal of $n C_{36}H_{74}$. Transmission electron micrograph showing Bragg fringes. $\times 1760$.

Fig. 2

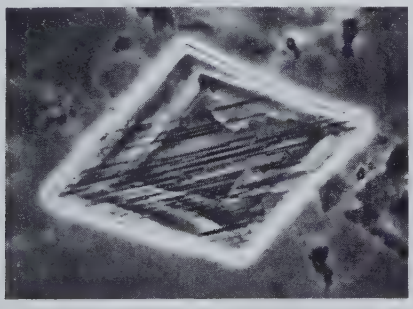

$n C_{36}H_{74}$ crystal with **a** striations. Photomicrograph. $\times 630$.

Fig. 3

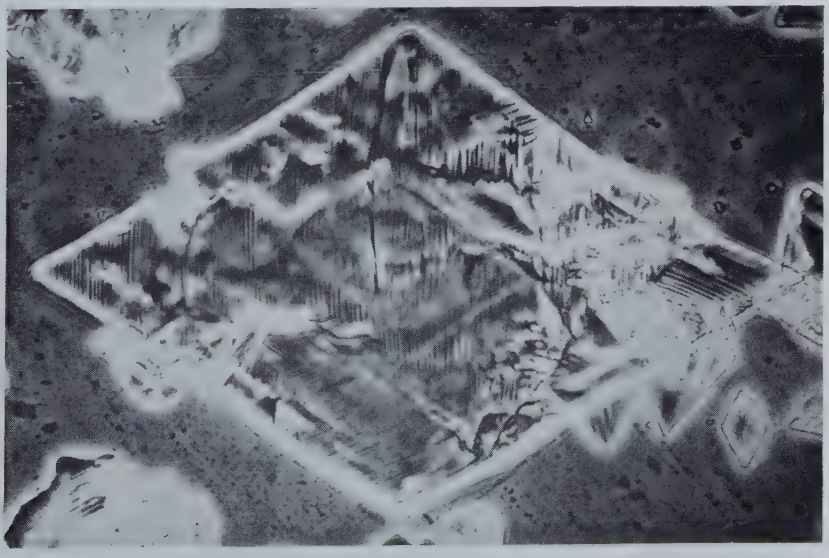

$n C_{36}H_{74}$ crystal with **b** and ⟨110⟩ striations. Photomicrograph. $\times 630$.

Fig. 4

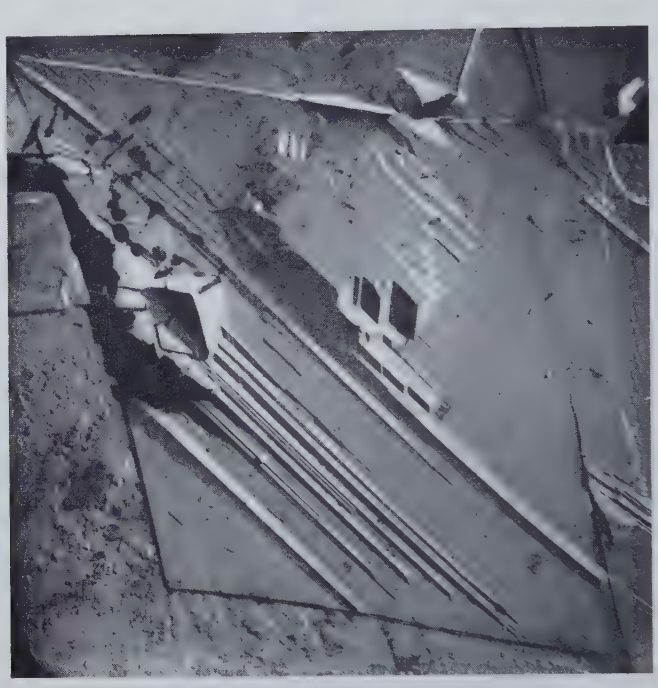

$n C_{36}H_{74}$ crystal with **a** striations. Electron micrograph. Replica. Au–Pd shadowed at ~26°. ×3600.

Fig. 5

Detail of a $n C_{36}H_{74}$ crystal with **a** striations. Electron micrograph. Replica, Au–Pd shadowed at 9°. ×5500.

Fig. 6

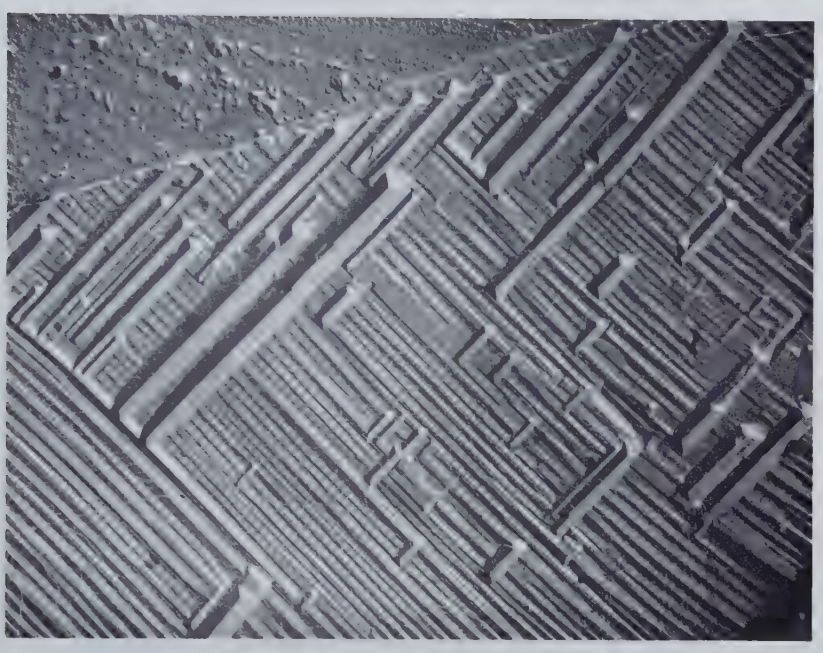

Detail of a $nC_{36}H_{74}$ crystal with **a** (NE–SW) and **b** (NW–SE) striations. Electron micrograph. Replica, Au–Pd shadowed at 12°. ×4300.

Fig. 7

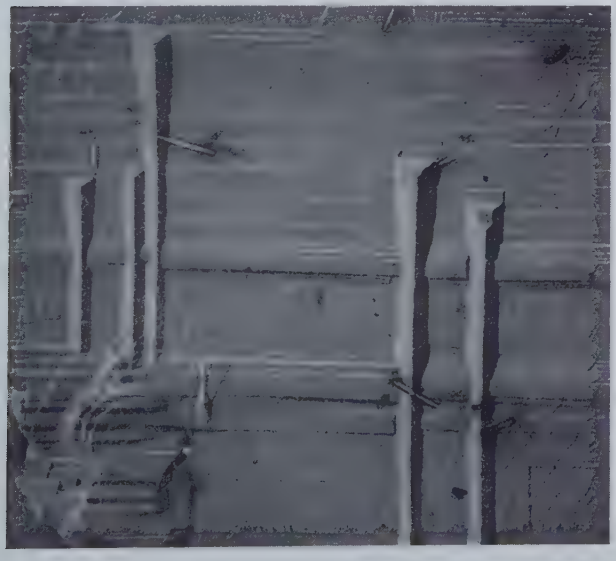

Detail of a $nC_{36}H_{74}$ crystal with **a** (vertical) and **b** (horizontal) striations. Electron micrograph. Replica, Au–Pd shadowed at ~26°. × 8900.

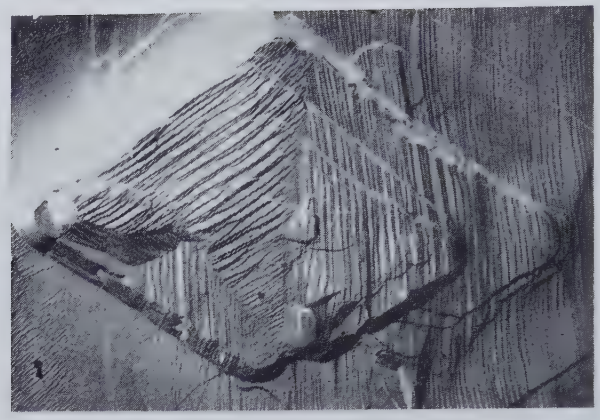

Fig. 8

Central detail of a $nC_{36}H_{74}$ crystal with **b** and ⟨110⟩ striation. Electron micrograph. Replica, Au–Pd shadowed at 10°. ×4600.

Fig. 9

Crystal of a $nC_{30}H_{62}$ with ⟨130⟩ and ⟨110⟩ striation. Electron micrograph. Replica, Au–Pd shadowed at 10°. ×4600.

Fig. 10

Crystals of $nC_{36}H_{74}$ with **a** striation. Transmission electron micrograph showing Bragg extinction contrast. Unshadowed. ×840.

Fig. 11

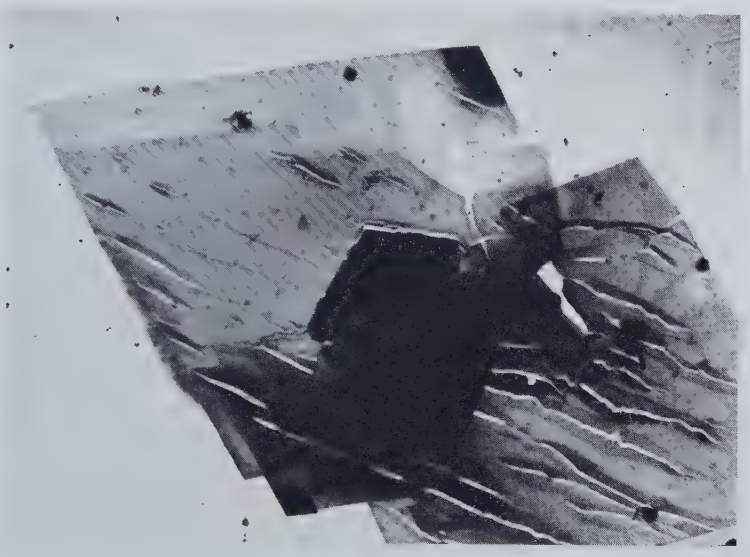

Thin crystals of $n C_{36}H_{74}$ with cracks along the **a** striations. Transmission electron micrograph taken in a hot stage. ×1630.

Fig. 12

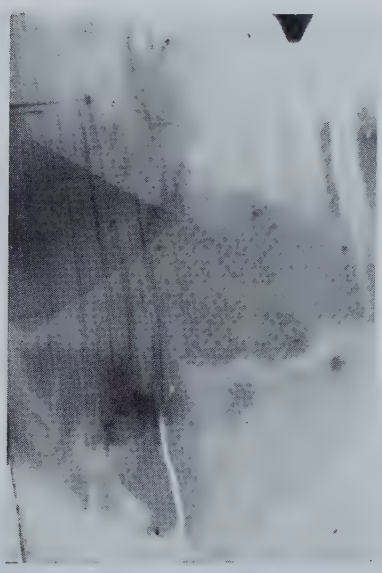

Detail of a crystal of $n C_{36}H_{74}$ with pleat-like **b** striations. Transmission electron micrograph. ×1960.

Fig. 13

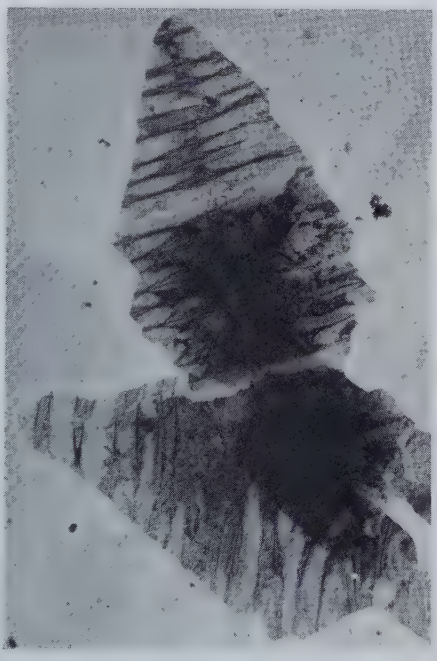

Crystal of $n C_{36}H_{74}$ with **b** striations showing in Bragg extinction contrast. Transmission electron micrograph. ×1850.

Fig. 1

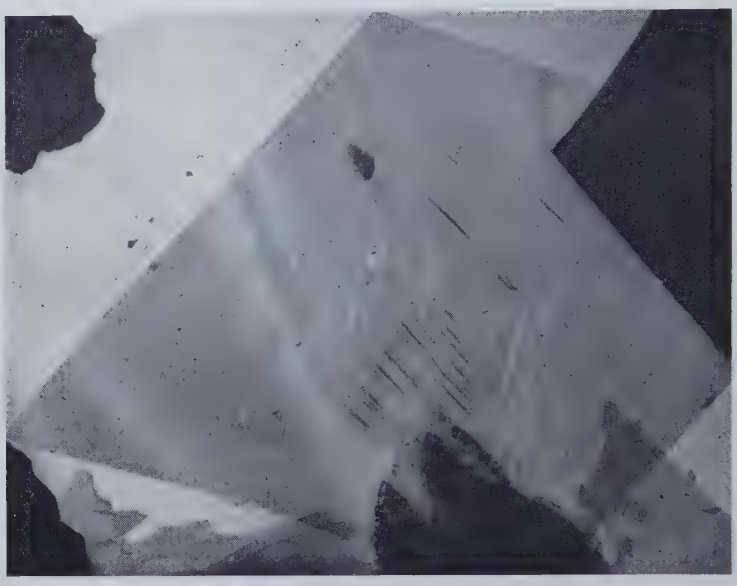

Polyethylene lozenge with Bragg fringes dividing the crystal into four quadrants. Notice the different contrast in opposite pairs of quadrants. Electronmicrograph. (×1800).

Fig. 2

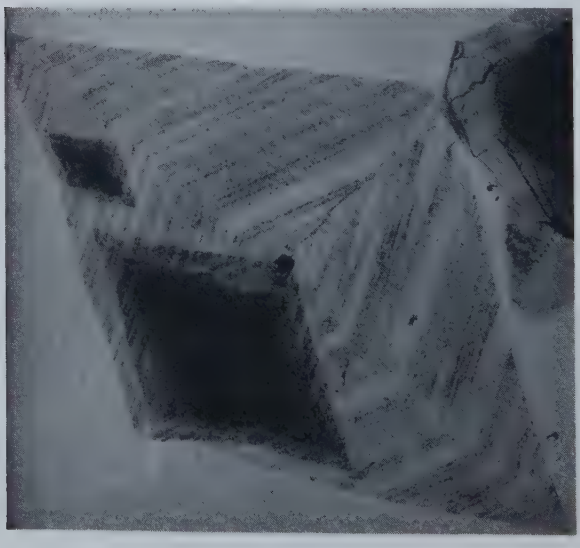

Polyethylene lozenge with rectangular bands shown up by diffraction contrast. Electronmicrograph. (×2500.)

Fig. 3

A central detail of a polyethylene crystal as in fig. 2, showing ridge and pleat striations. Electronmicrograph. Au–Pd shadowed. (×9000.)

Fig. 4

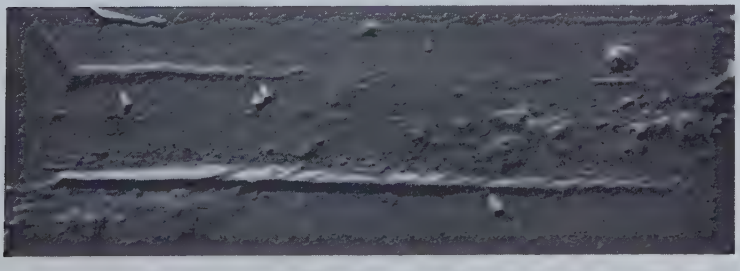

Detail of a crystal as in figs. 2 and 3 showing a regular ridge in a polyethylene crystal. Electronmicrograph. Au–Pd shadowed. (×19 000.)

Fig. 5

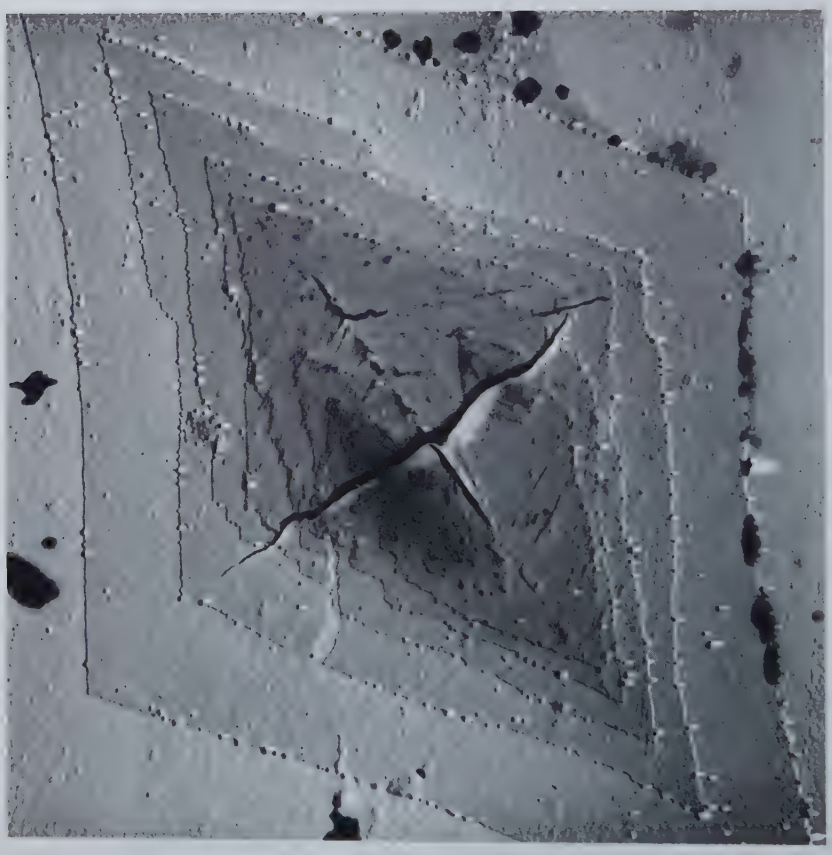

Polyethylene crystal with striations on the upper layers only. Electronmicrograph. Au–Pd shadowed. (×8500.)

Fig. 6

Truncated polyethylene lozenge with **b** ridges in the {100} sectors. Notice the {100} sector boundaries. Electronmicrograph. Au–Pd shadowed. ($\times 8000$.)

Fig. 7

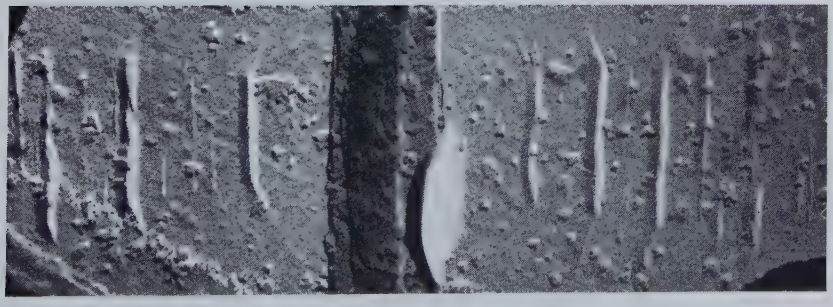

Detail of a truncated polyethylene lozenge with regular ridges along **b** in the {100} sectors. The overgrowth consists of crystals formed at a lower temperature. Electronmicrograph. Au–Pd shadowed. ($\times 23\,000$.)

Fig. 8

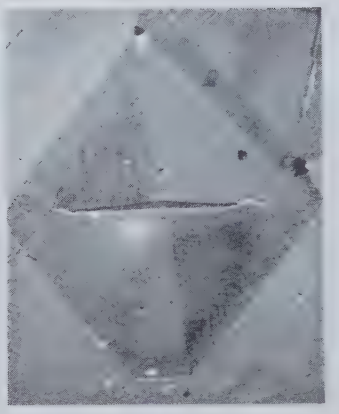

Truncated polyethylene lozenge with two {110} sectors in diffraction constrast. Notice the central triangular fold which is a characteristic feature of this type of lozenge. Electronmicrograph. (×2800.)

Fig. 9

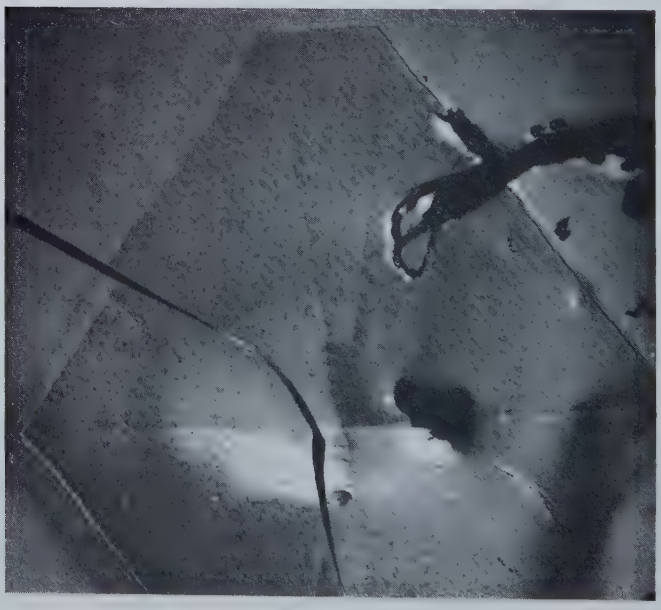

A non-planar polyethylene lozenge prepared so as to avoid a collapse on drying down (see text). Electronmicrograph. Au–Pd shadowed. (×6500.)

Fig. 10

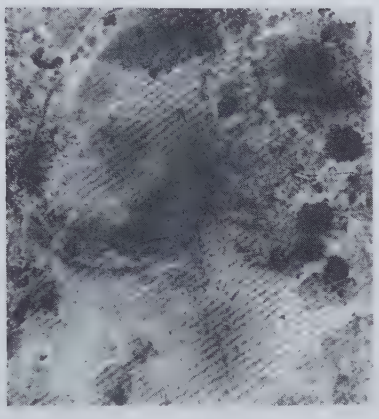

Well-defined fringes in a polyoxymethylene crystal. The contrast is provided mainly by diffraction. Electronmicrograph. (×4500.)

Fig. 11

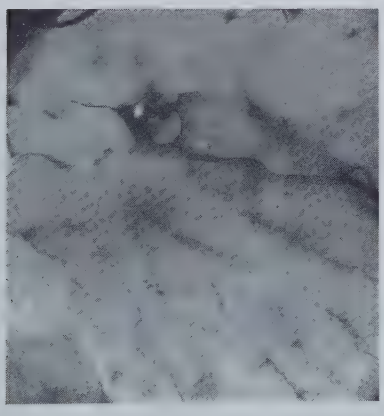

Detail of a crystal as in fig. 10, revealing the underlying morphology causing the fringes. Electronmicrograph. (×4000.)

Fig. 1

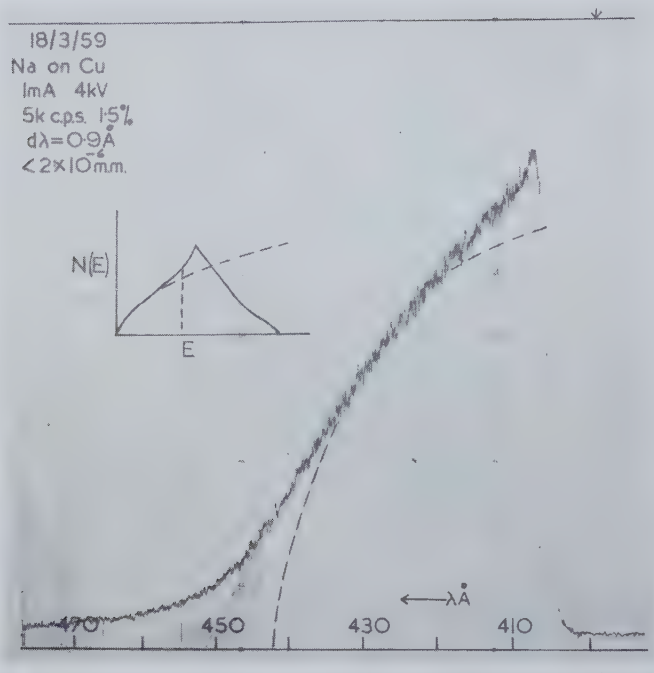

Sodium L_{23} freshly evaporated on to copper. Broken line is for $I(E) \propto E^{1/2}$. Inset is theoretical $N(E)$ vs E curve according to Jones and Mott (1937).

Fig. 2

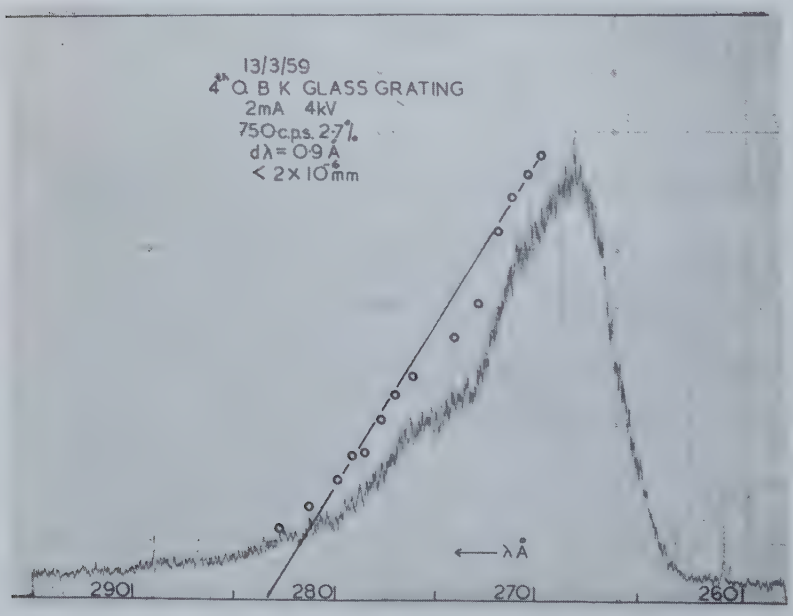

Boron K spectrum from amorphous boron. Plotted points assume $I(E) \propto E^{1/2}$.

Fig. 3

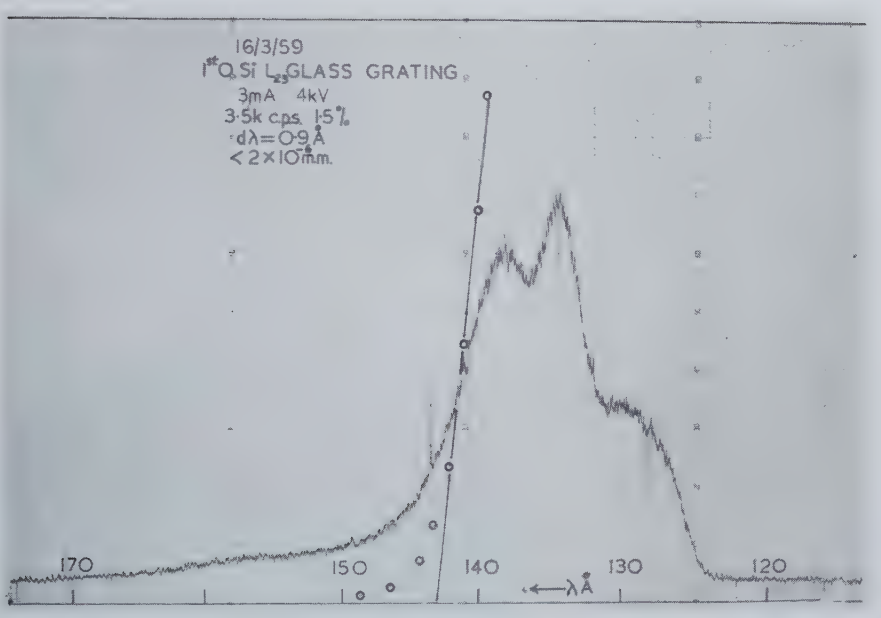

Silicon L_{23} from powdered AR grade Si at red heat. Points plotted for $I(E) \propto E^{1/2}$.

Fig. 4

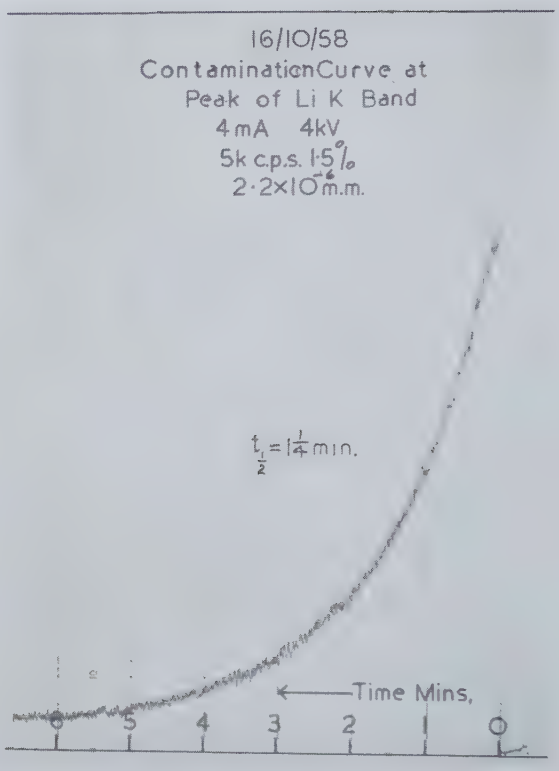

(*a*)

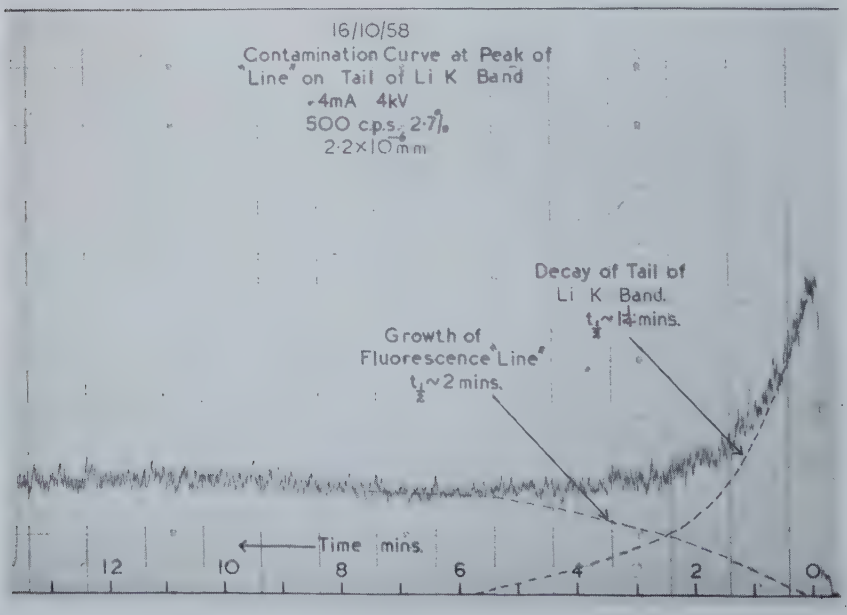

(*b*)

(*a*) Decrease of intensity with time for peak of Li K band.
(*b*) Change of intensity with time at 253 Å (peak of Li Line).

Fig. 4 (*continued*)

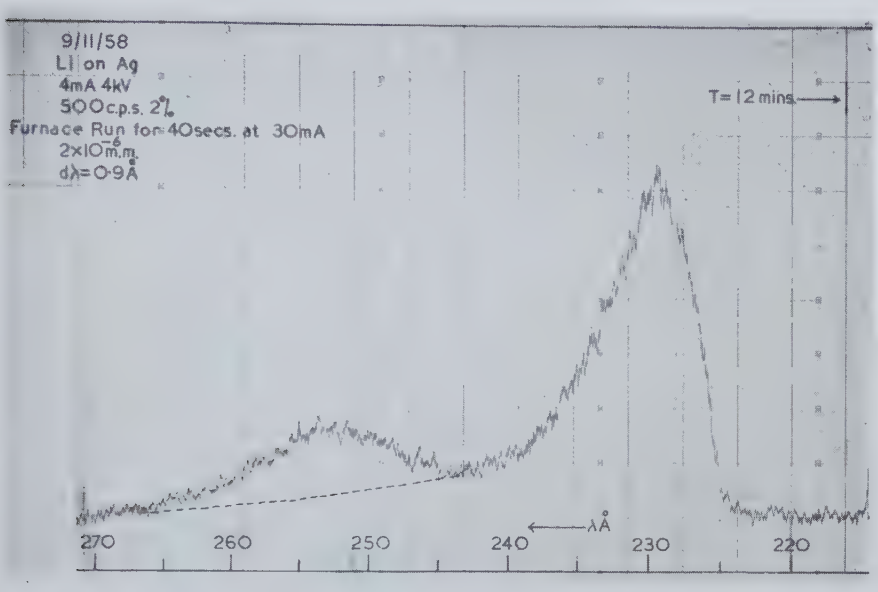

(*c*)

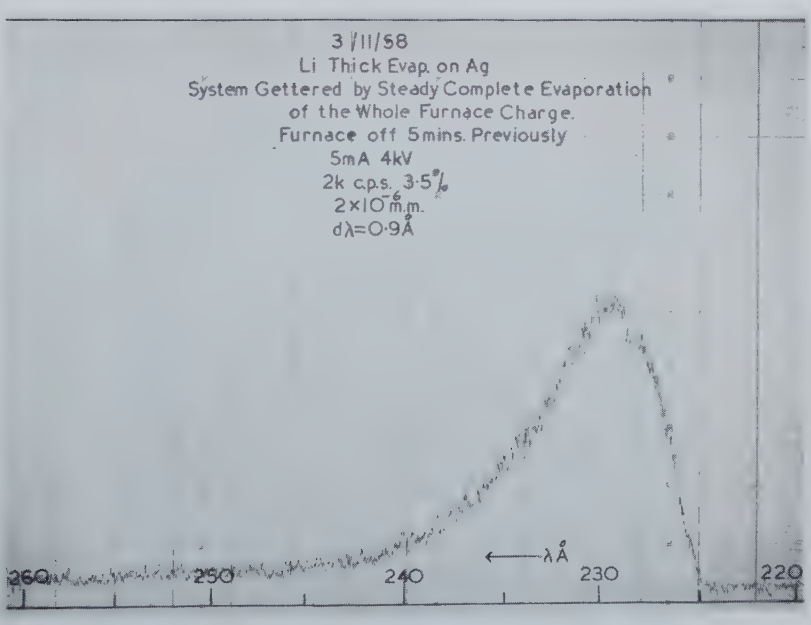

(*d*)

(*c*) Li K band and Li Line, the latter developed to maximum intensity.
(*d*) Li K band with no Li line following heavy evaporation of Li.

Fig. 1

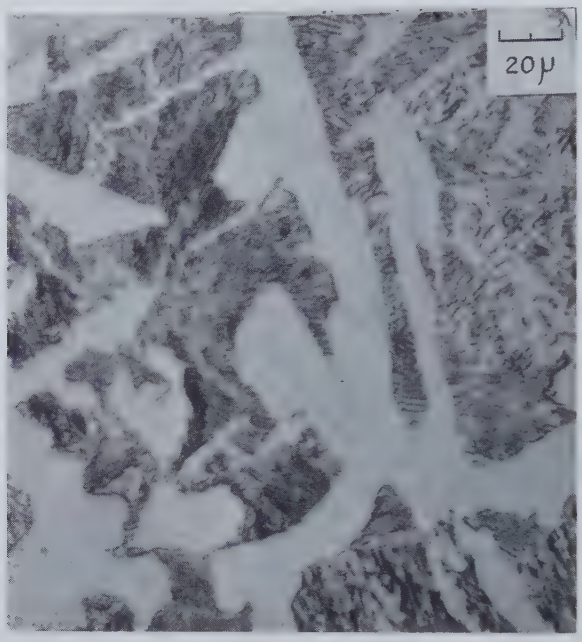

Typical microstructure.

Fig. 3

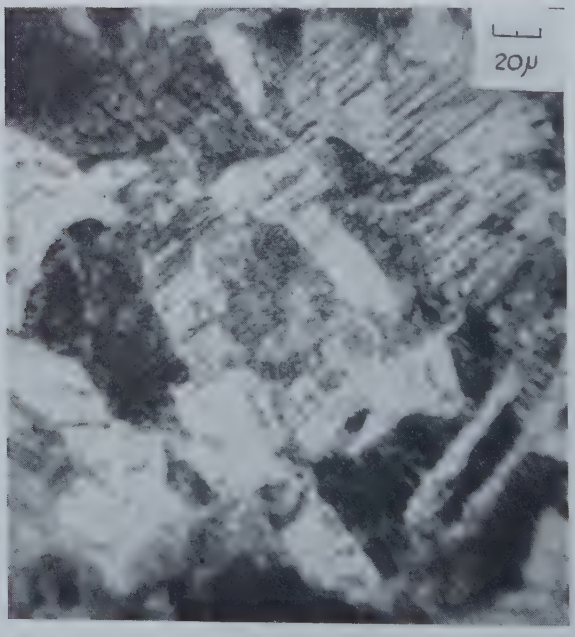

Microstructure after fatiguing showing slip in the ferrite.

Fig. 4

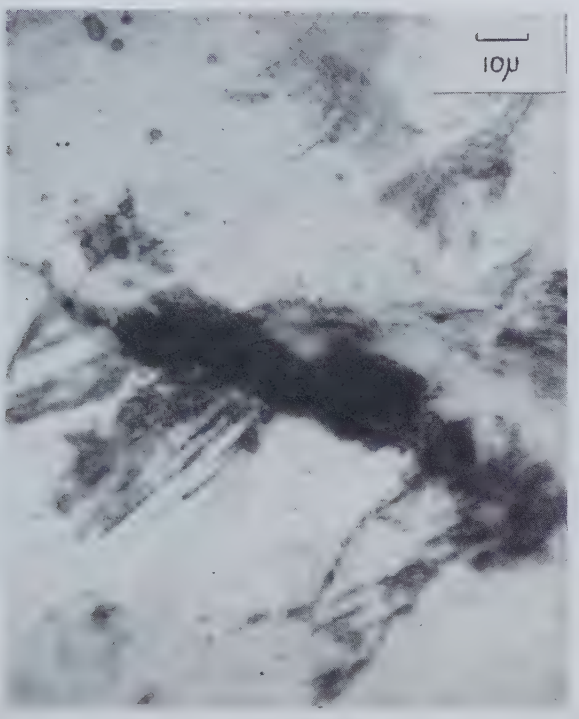

Crack in specimen fatigued in vacuum below the fatigue limit.
The crack was opened by subsequent extension of the specimen.

Fig. 5

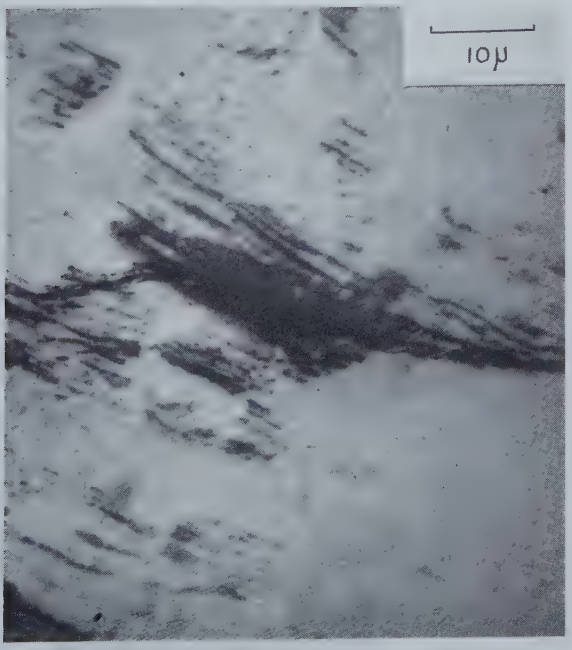

Crack in specimen fatigued in air below the fatigue limit.
The crack was opened by subsequent extension of the specimen.

Fig. 1

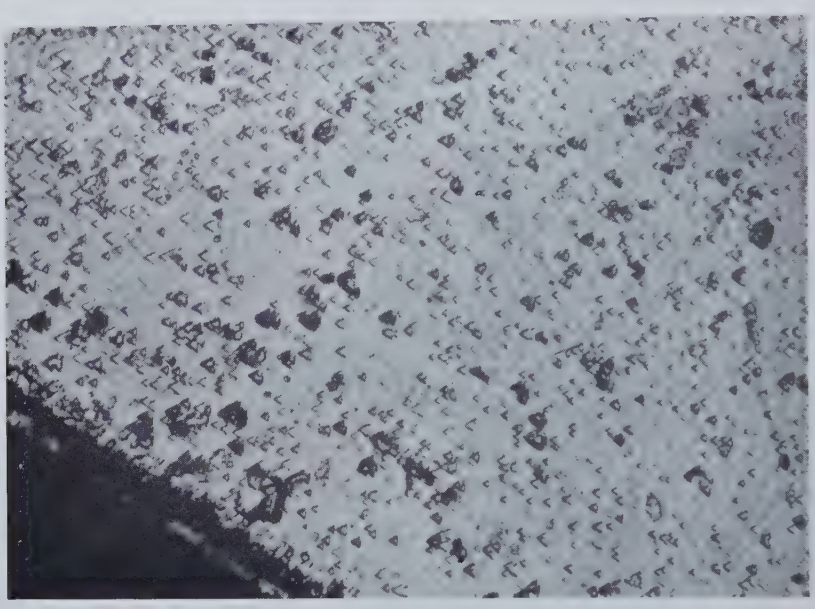

Triangular etch pits in positive orientation on an octahedral face after etching in air at 850°C. ×175.

Fig. 2

Triangular etch pits in negative orientation on an octahedral face after etching in air at 1250°C. ×470.

Fig. 3

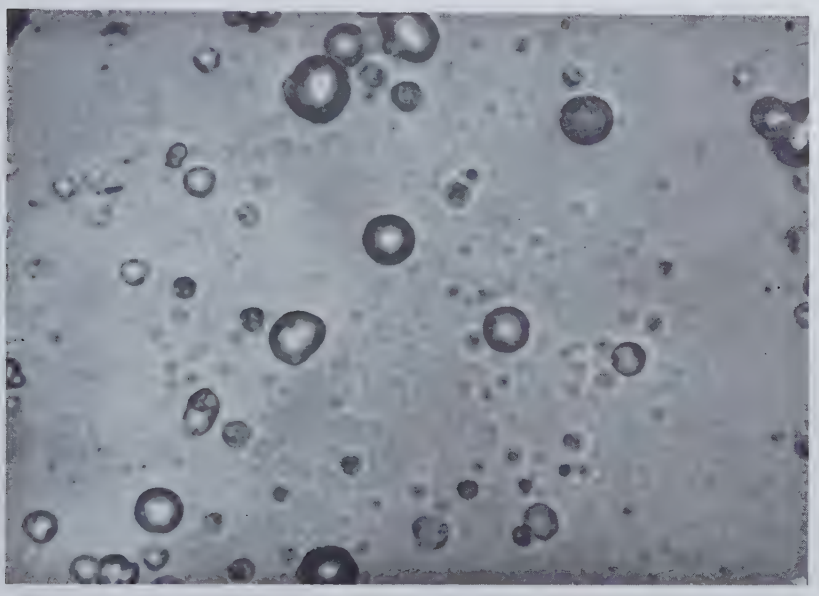

Round pits on octahedral face after heating in air at 950°c. ×875.

Fig. 4

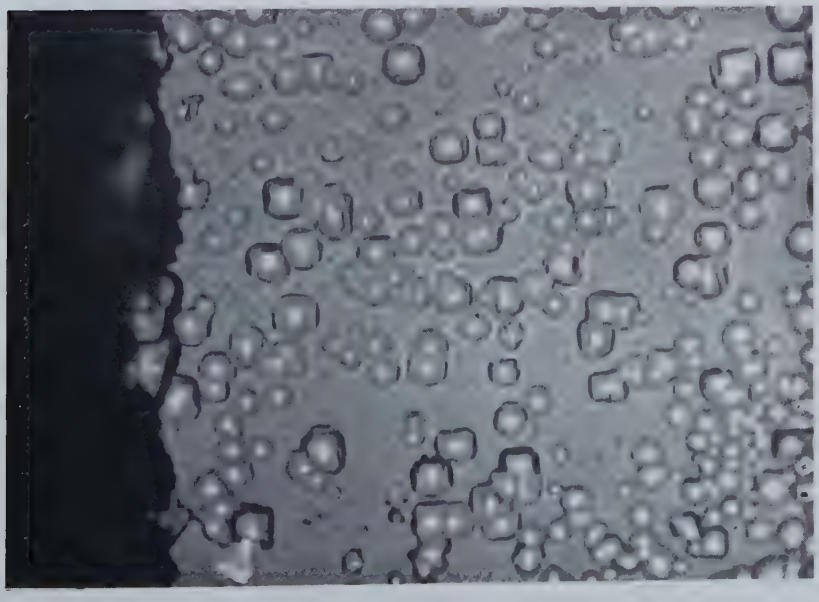

Square pits on cubic face after heating in air at 775°c. ×1500.

Fig. 5

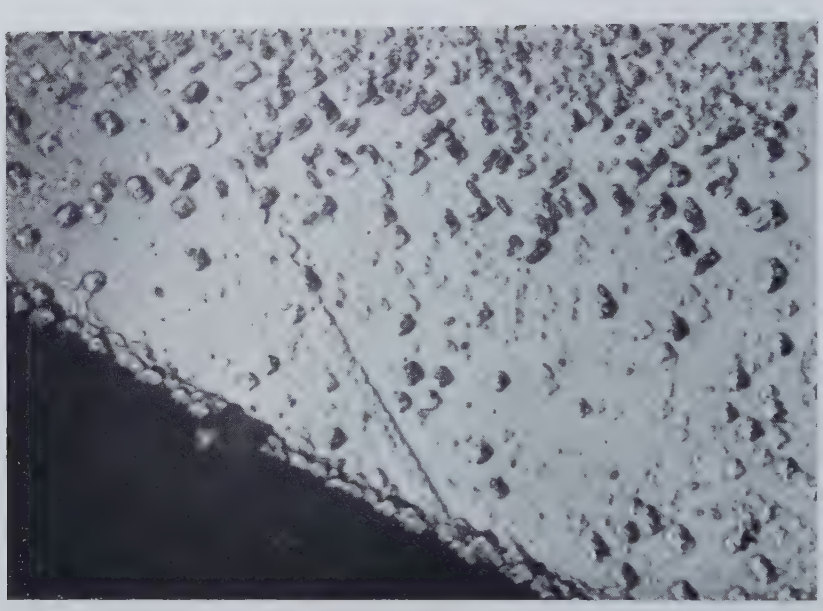

Square pits on cubic face after heating in air at 1400°c. ×470.

Fig. 6

Boat-shaped pits on dodecahedral face after heating in air at 800°c. ×470.

Fig. 7

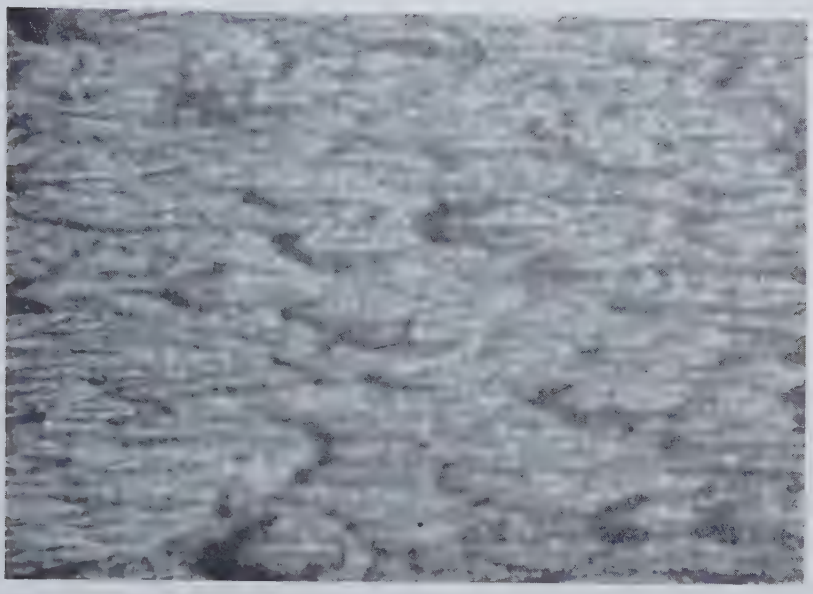

Boat-shaped pit on dodecahedral face after heating in air at 1400°C. ×1500.

Fig. 9

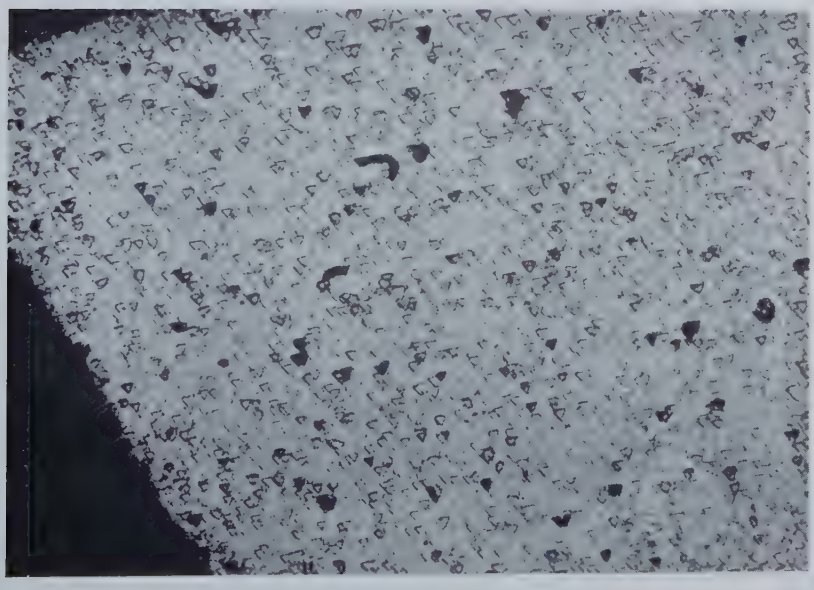

Triangular etch pits on octahedral face in positive orientation after heating in nitrogen, oxygen and water vapour mixture at 850°C. ×175.

Fig. 10

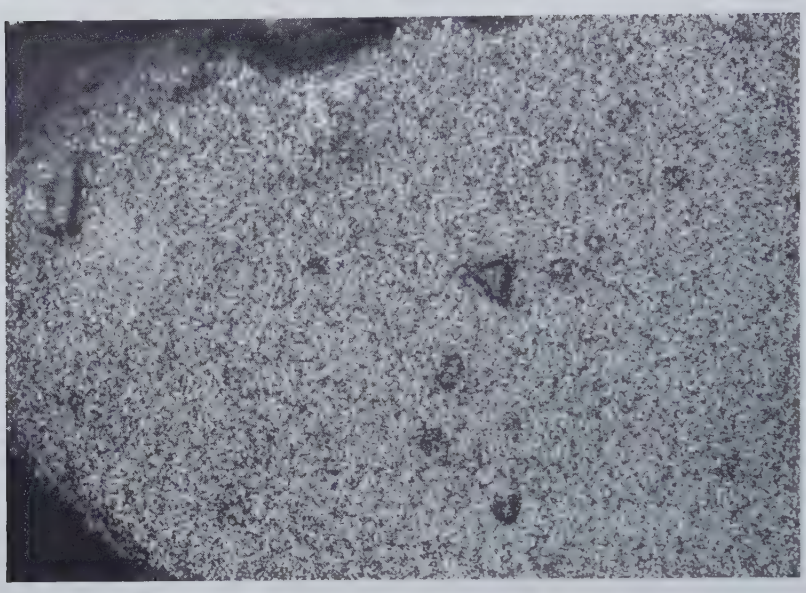

Matt type surface on octahedral face after heating in dry oxygen at 850°C. ×175.

Fig. 11

Triangular etch pits on octahedral face in negative orientation after heating in nitrogen, oxygen and water vapour mixture at 1250°C. ×470.

Fig. 1

Etch pits formed on the (010) face of a crystal of gypsum after treatment for 3 min at 20°C with 1% solution of sodium hexametaphosphate. ×330.

Fig. 2

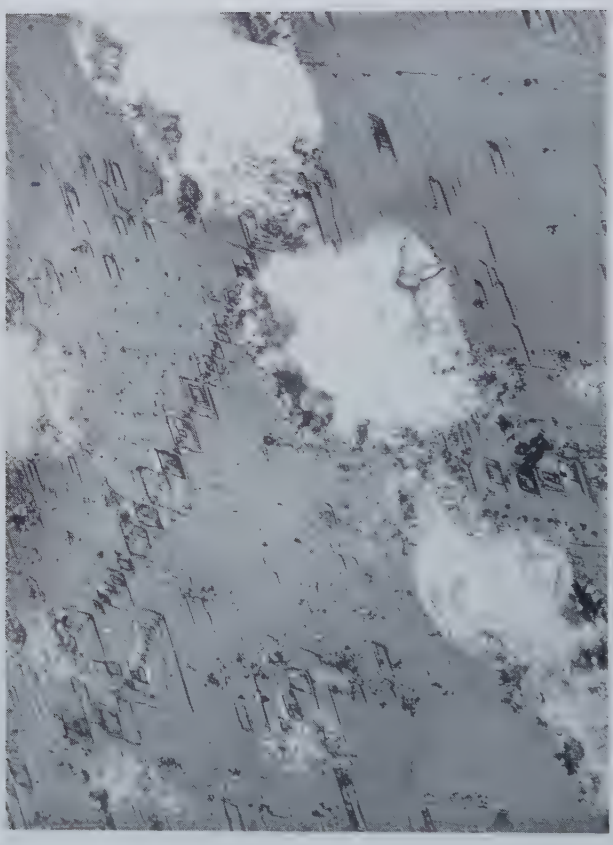

The same field as shown in fig. 1, after several hours in an air oven at 98°C. ×330.

Fig. 3

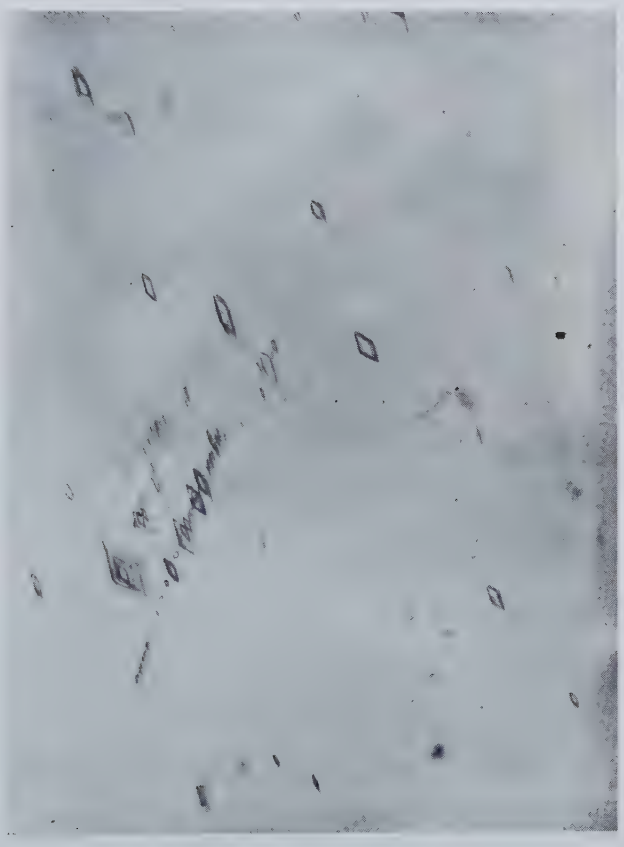

The field shown in fig. 2 after 60 μ had been removed by grinding and the new surface washed with distilled water. $\times 330$.

Fig. 4

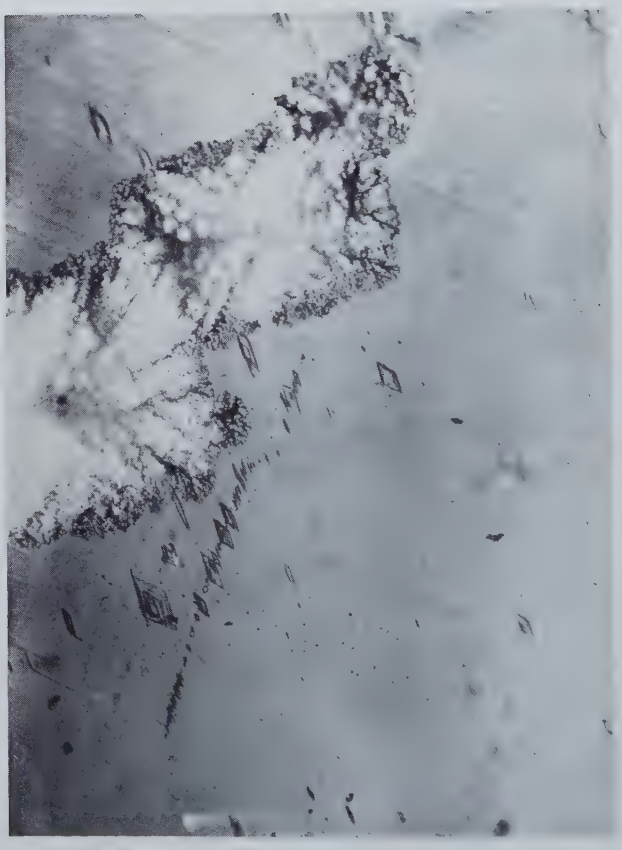

The field as shown in fig. 3 after 4 hours at 98°C. ×330.

Fig. 5

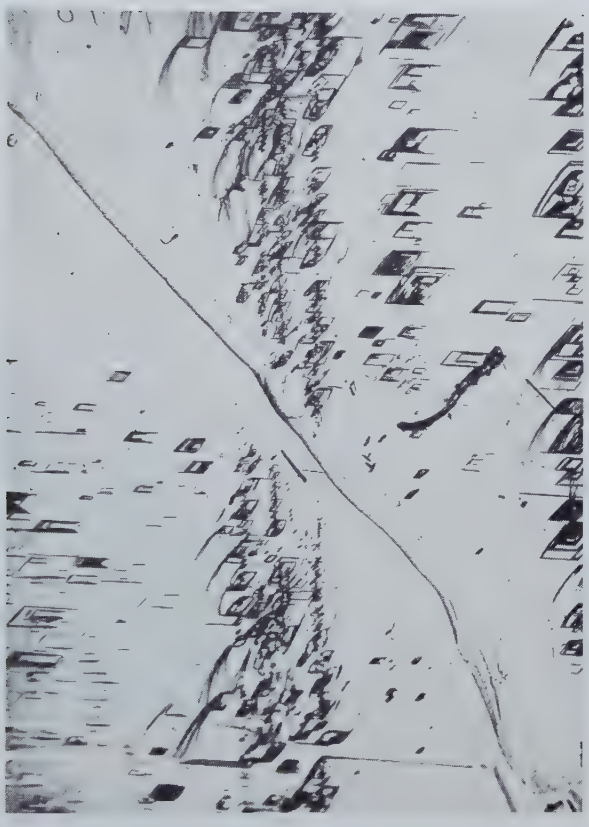

A row of etch pits on the (010) face showing a discontinuity in the region of a cleavage step. ×300.

Fig. 2

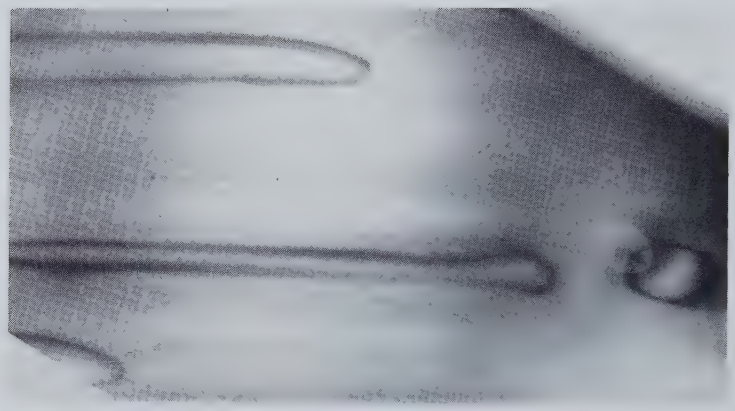

1μ

(*a*)

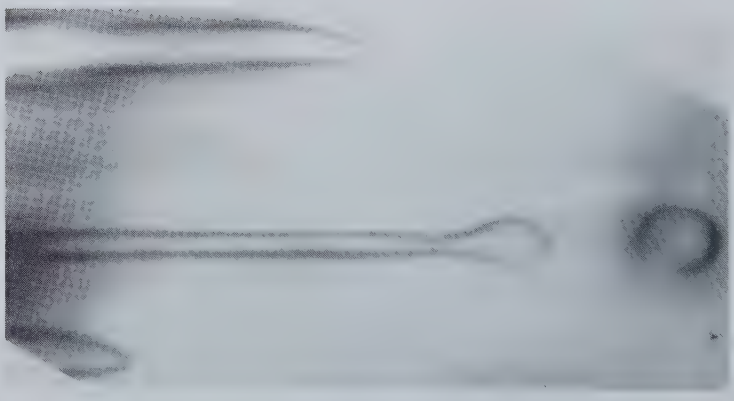

(*b*)

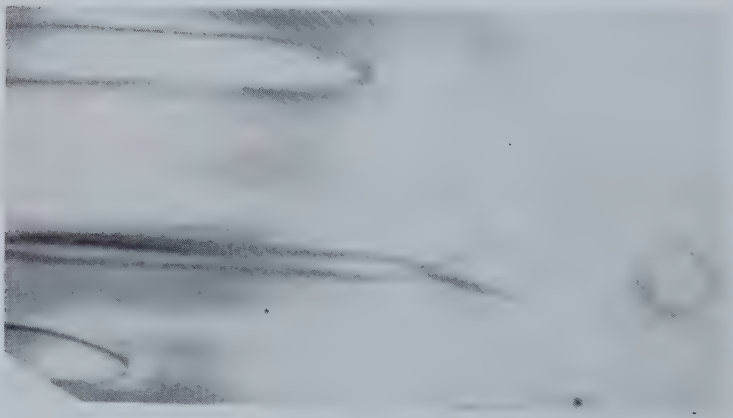

(*c*)

Fig. 2 (*continued*)

(*d*)

(*e*)

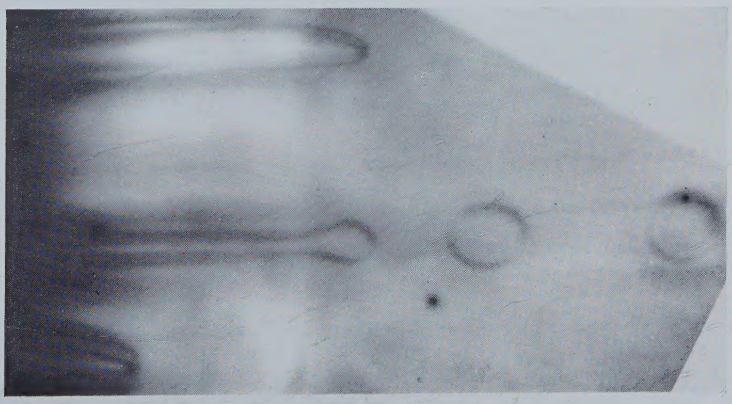

(*f*)

Dislocation loops produced by low temperature pyramidal glide. The successive stages in the process of splitting into circular loops were taken at 20 sec intervals at an estimated temperature of $-40°$ C.

1 μ

99·9999% Aluminium foil, strained in the electron microscope. The axis of tension is vertical in the micrograph. Dislocation movement is from right to left. $\times 10\,000$.

Fig. 2

Dislocation loops in copper irradiated at $-195°$C ($3{\cdot}1 \times 10^{17}$ fast n cm^{-2}) and examined at $-50°$C. ($\times 100\,000$.)

Fig. 3

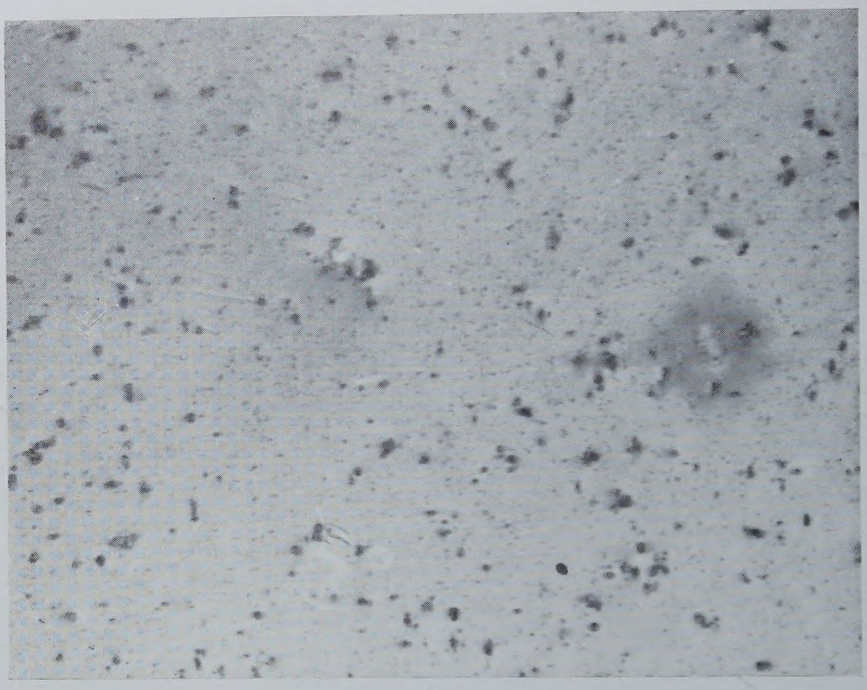

Irradiated copper (2×10^{18} fast n cm^{-2}) annealed at 306°C for 63 min showing small defects and large loops. Foil thinned after annealing. ($\times 100\,000$.)

Fig. 4

As in fig. 3, but showing a zone (3500 Å wide) free of large loops along a grain boundary. The small defects show no denuded zone. ($\times 100\,000$.)